UNITED STATES DISTRICT COURT
FOR THE DISTRICT OF MASSACHUSETTS

PROGENICS PHARMACEUTICALS, INC., and EXINI DIAGNOSTICS AB, Plaintiffs, v. MIM SOFTWARE INC., Defendant.	Civil Action No. **JURY TRIAL DEMANDED**

COMPLAINT

Plaintiffs Progenics Pharmaceuticals, Inc. ("Progenics") and EXINI Diagnostics AB ("EXINI") (collectively, "Plaintiffs") hereby file this Complaint for patent infringement against Defendant MIM Software Inc. ("MIM"), alleging as follows:

NATURE OF THE ACTION

1. This case is about medical imaging technology that enables improved diagnosis and treatment of cancer and other serious diseases. Plaintiffs pioneered techniques to advance the reliability and accuracy of diagnostic imaging tests like computed tomography (CT) scans or positron emission tomography (PET) scans. More specifically, the inventors developed and patented new systems and methods to help physicians more consistently and accurately interpret the images produced by those types of scans.

2. Plaintiffs own numerous patents that claim inventions in the field of medical imaging analysis and interpretation, specifically including U.S. Patent No. 10,665,346 (the "'346 patent), and U.S. Patent No. 10,973,486 (the "'486 patent") (the "Asserted Patents").

3. Through this case, Plaintiffs seek to protect their significant investment in medical imaging technology, which facilitates their commitment to the advancement of disease diagnosis and treatment.

4. In doing so, Plaintiffs aim to redeem the basic principle that Defendant MIM cannot infringe Plaintiffs' patents simply because MIM would prefer not to pay for a license to Plaintiffs' coveted, patented technology.

5. Defendant MIM sells imaging tools for radiation oncology, radiology, and nuclear medicine, including software products like Contour ProtégéAI® and MIM SurePlan™ MRT (the "Infringing Products"), as well as other products like LesionID®, that display scan results to physicians. In 2020, MIM and Plaintiffs began discussing potentially integrating the inventions claimed in the Asserted Patents (amongst other technological advances) into MIM's nuclear imaging software platform. Pursuant to a Confidential Disclosure Agreement signed in 2021, Plaintiffs agreed to explore a possible integration with MIM. In other words, MIM was considering licensing Plaintiffs' patented technology so that the two companies could partner. As part of that effort, Plaintiffs shared their patented inventions with MIM and helped MIM consider how those inventions could improve MIM's software. One of the inventors of the '486 patent (Karl Sjöstrand) even agreed to work with MIM on that project.

6. In October 2022, about two years after the partnership discussions began, Plaintiffs sent MIM a draft Collaboration Agreement. The agreement included a list of Plaintiffs' relevant patents—including the Asserted Patents.

7. Months went by, and Plaintiffs heard nothing back from MIM about the draft Agreement, even though MIM continued to emphasize its interest in incorporating Plaintiffs' patented technology into MIM's software.

8. Clouds gathered around June 2023 when Plaintiffs discovered that MIM had begun publishing articles and website materials about apparently new features included in two MIM products—Contour ProtégéAI® and MIM SurePlan™ MRT (the "Infringing Products"). MIM's publications were and are troubling to Plaintiffs. They plainly show that MIM took the inventions claimed in the Asserted Patents and, instead of licensing the technology from Plaintiffs, simply integrated the inventions into the Infringing Products without Plaintiffs' permission.

9. Making matters worse, MIM relied on Plaintiffs' patented innovations to induce GE HealthCare to acquire MIM in January of this year. Apparently, MIM had been pursuing acquisition by GE HealthCare for months while simultaneously incorporating Plaintiffs' patented inventions into MIM's software.

10. Upon information and belief, MIM disregarded the Asserted Patents after deciding that it was simply more convenient than paying for a license to use them. MIM infringed the Asserted Patents to both improve its software and market itself to its eventual acquirer, GE HealthCare.

11. Plaintiffs thus bring this suit to put a stop to MIM's illegal conduct and obtain compensation for MIM's intentional wrongdoing.

THE PARTIES

12. Plaintiff Progenics is a corporation organized and existing under the laws of the State of Delaware, having its principal place of business at 201 Burlington Road, South Building, Bedford, Massachusetts, 01730. Progenics is an oncology company focused on the development and commercialization of innovative targeted medicines and artificial intelligence to find, fight, and follow cancer.

13. Plaintiff EXINI is a corporation organized and existing under the laws of Sweden, having its principal place of business at Scheelevägen 27, Ideon Science Park, Gateway, 223 70

Lund, Sweden. EXINI develops advanced software for medical image analysis. EXINI's products are developed using unique image analysis derived from expert knowledge in nuclear medicine, image analysis, handling of large databases, and machine learning.

14. Defendant MIM is a corporation organized and existing under the laws of the State of Ohio, having its principal place of business at 25800 Science Park Drive, Suite 180, Cleveland, Ohio, 44122. MIM sells imaging tools for radiation oncology, radiology, nuclear medicine, urology, neuroimaging, and cardiac imaging.

JURISDICTION AND VENUE

15. This action arises under the patent laws of the United States, 35 U.S.C. § 100 *et seq.*, and this Court has jurisdiction over the subject matter of this action under 28 U.S.C. §§ 1331 and 1338(a).

16. This Court has personal jurisdiction over MIM because, upon information and belief, MIM, directly or through its affiliates, develops, manufactures, imports, markets, offers to sell, sells, and/or distributes its software products throughout the United States, including in Massachusetts (including to various renowned Massachusetts-based hospitals and cancer centers, including, upon information and belief, Dana Farber, Massachusetts General Hospital, and Harvard Medical School). MIM, therefore, does business in Massachusetts, derives revenue from conducting business in Massachusetts, and maintains continuous and systematic contacts with Massachusetts. The Court also has personal jurisdiction over MIM because MIM has committed, induced, or contributed to acts of patent infringement in Massachusetts by selling its infringing software products throughout the United States, including in this judicial district.

17. Venue is proper in this district under 28 U.S.C. §§ 1391 and 1400.

FACTUAL BACKGROUND

A. Medical Imaging for Cancer and Other Serious Diseases.

18. One major challenge in treating and managing cancer (and other serious diseases) has long been the difficulty of accurately and consistently interpreting the diagnostic images produced by medical imaging tools.

19. Both anatomical scans (like X-rays or CT) and functional scans (like PET or single-photon emission computed tomography (SPECT)) are valuable tools. But before the inventions claimed in the Asserted Patents, physicians faced major obstacles in using those scans to form a complete and trustworthy picture of a patient's disease.

20. One difficulty was that each type of scan could only capture part of the relevant picture for any given patient. Anatomical scans capture images of the anatomy or structure of organs and tissues within the body (but not the function); functional scans capture the activity and function of those organs or tissues (but not the anatomy/structure). As applied to cancer, an anatomical scan thus cannot reliably detect the activity of a tumor, whereas a functional scan can struggle to differentiate between the organs and tissue surrounding a tumor. Physicians were left to parse two different types of scans to try to piece together the full picture, and this often led to inaccurate or inconsistent diagnoses or treatments.

21. More broadly, the traditional process for interpreting medical imaging—which involved a physician receiving one or more different scan images prepared by a computer—left room for human error. Without any automated integration, mapping, and assessment of those scan results, a physician might misinterpret a PET scan (or a combination of a CT scan and a PET scan) and miss a critical diagnostic insight that could save a patient's life.

22. Plaintiffs' claimed inventions were therefore major advances in overcoming the limitations of medical imaging interpretation, including in the field of (but not limited to) cancer diagnosis and treatment.

B. Plaintiffs' Asserted Patents Claim Major Advances in the Interpretation of Medical Imaging for Cancer and Other Diseases.

23. Plaintiffs spent at least five years and millions of dollars to develop solutions that unlock medical imaging's full potential. Plaintiffs' efforts culminated in the inventions claimed in the Asserted Patents (as well as other patents).

24. Plaintiffs' patented innovations improved the reliability and accuracy of medical imaging interpretation by (amongst other things): (a) using AI algorithms to reliably segment the organs (and lesions) captured in scans; (b) using a two-step segmentation technique to identify and flag organs, lesions, and/or other points of interest on the scan; and (c) creating graphical interfaces that report scan results in a way that benefits from segmentation and two-step segmentation to provide reliable risk insights to help ensure accurate diagnosis and treatment by physicians.

25. U.S. Patent No. 10,665,346 ("the '346 patent"), entitled "Network for Medical Image Analysis, Decision Support System, and Related Graphical User Interface (GUI) Applications," was duly and legally issued by the Patent Office on May 26, 2020, and has not expired. The '346 patent is assigned to Progenics. This patent claims, *inter alia*, a platform and supported graphical user interface (GUI) decision-making tools for use by medical practitioners (and/or their patients) to aid in the process of making decisions about a course of cancer treatment (and/or to track treatment and/or the progress of the disease). A true and correct copy of this patent is attached as Exhibit 1.

26. U.S. Patent No. 10,973,486 ("the '486 patent"), entitled "Systems and Methods for Rapid Neural Network-based Image Segmentation and Radiopharmaceutical Uptake

Determination," was duly and legally issued by the Patent Office on April 13, 2021, and has not expired. The '486 patent is assigned to Progenics and EXINI. This patent claims, *inter alia*, systems and methods that provide for automated analysis of 3D medical images of a patient in order to automatically identify specific 3D volumes within the 3D images that correspond to specific organs and/or tissue. This kind of accurate identification of 3D volumes allows one to determine quantitative metrics that measure uptake of tracers in particular organs/tissues, which can in turn be used to assess disease state in a patient (including, but not limited to, prostate cancer). A true and correct copy of this patent is attached as Exhibit 2.

27. The Asserted Patents generally describe inventions for improving the reliability, usability, and accuracy of medical imaging, including by: (a) using AI algorithms to help segment the 3D image into different organs (or tissues), thus allowing for clearer differentiation of organs, tissues, and lesions, (b) using a two-step segmentation technique, whereby volumes of interest (say, the pelvic region) are first localized within a large and complex 3D image, and are then analyzed by fine-grained segmentation modules, allowing those segmentation modules to efficiently and accurately identify critical organs and tissue regions, such as prostate, in medical images, and/or (c) analyzing scan results to prepare a risk map that analyzes areas of importance of concern for physician and patient review.

28. The inventions claimed in the Asserted Patents improve upon prior art by increasing the reliability, accuracy, and usability of medical imaging for cancer diagnoses and treatment.

29. For example, representative claim 1 of the '346 patent recites:

A network-based system for generating a disease risk map for use as a decision-making support for evaluating risk of cancer or risk of recurrence of cancer, the system comprising:

a processor; and

a memory having instructions stored thereon, wherein the instructions, when executed by the processor, cause the processor to:

(i) access one or more medical images associated with a particular patient from a database;

(ii) perform an analysis of the one or more medical images associated with the particular patient using a machine learning algorithm, to generate the risk map, wherein the risk map comprises a visual representation of tissue overlaid with graphical denotations marking one or more regions of risk of cancer or risk of recurrence of cancer; and

(iii) cause display of risk map via a graphical user interface (GUI) for presentation or review of the risk map by a user,

wherein the analysis of the one or more medical images comprises creation of a 3D image of the one or more regions of risk of cancer or risk of recurrence of cancer overlaid on the one or more medical images, and wherein the 3D image comprises geographic identification of one or more specific tissue region(s) overlaid on the one or more medical images.

30. Representative claim 42 of the ’486 patent recites:

A method for automatically processing 3D images to identify 3D volumes within the 3D images that correspond to a prostate of a subject and determining one or more uptake metrics indicative of radiopharmaceutical uptake therein, the method comprising:

(a) receiving, by a processor of a computing device, a 3D anatomical image of the subject obtained using an anatomical imaging modality, wherein the 3D anatomical image comprises a graphical representation of tissue within a subject, at least a portion of which corresponds to a pelvic region of the subject;

(b) receiving, by the processor, a 3D functional image of the subject obtained using a functional imaging modality, wherein the 3D functional image comprises a plurality of voxels, each representing a particular physical volume within the subject and having an intensity value that represents detected radiation emitted from the particular physical volume, wherein at least a portion of the plurality of voxels of the 3D functional image represent physical volumes within the pelvic region of the subject;

(c) determining, by the processor, using a first module, an initial volume of interest (VOI) within the 3D anatomical image, the initial VOI corresponding to tissue within the pelvic region of the subject and excluding tissue outside the pelvic region of the subject;

(d) identifying, by the processor, using a second module, a prostate volume within the initial VOI corresponding to the prostate of the subject;

(e) determining, by the processor, the one or more uptake metrics using the 3D functional image and the prostate volume identified within the initial VOI of the 3D anatomical image;

MIM Ex1039
MIM Software Inc. v. Progenics Pharmaceuticals, Inc.
Trial IPR2025-00630

(f) causing, by the processor, display of an interactive graphical user interface (GUI) for presentation to the user of a visual representation of the 3D anatomical image and/or the 3D functional image; and

(g) causing, by the processor, graphical rendering of, within the GUI, the 3D anatomical image and/or the 3D functional image as selectable and superimposable layers, such that either can be selected for display and rendered separately, or both selected for display and rendered together by overlaying the 3D anatomical image with the 3D functional image.

31. The inventions of the Asserted Patents address technological limitations of medical imaging interpretation that were not routine or conventional at the time of the invention. A person of ordinary skill in the art reading the Asserted Patents and their claims would understand that (a) the Asserted Patents' disclosures and claims solve specific problems, and (b) the claimed inventions represent significant advances in the technical field.

C. 2020-2022: Plaintiffs and MIM Explore Possible Collaboration Involving the Inventions Claimed in Plaintiffs' Asserted Patents.

32. Upon information and belief, MIM infringed (and is infringing) the Plaintiffs' Asserted Patents because MIM decided—after years of negotiations with Plaintiffs about a possible collaboration—that it wanted to use Plaintiffs' patented inventions without paying for them.

33. Around June 2020, MIM and EXINI (and Plaintiffs' parent company, Lantheus Holdings, Inc.) began discussions about a potential collaboration involving (amongst other things) the inventions claimed by the Asserted Patents. More specifically, MIM was interested in integrating the claimed inventions into MIM's nuclear imaging software.

34. The following year, MIM worked with Karl Sjöstrand at EXINI—who is an inventor on the '486 patent—to explore powering MIM's systems with Plaintiffs' patented algorithms (including the inventions in the Asserted Patents).

35. Reflecting the substantiveness and seriousness of these discussions, the parties entered into a Confidential Disclosure Agreement in October 2021.

36. These discussions continued into 2022, and included giving MIM access to Plaintiffs' systems to review the capabilities and function of Plaintiffs' patented inventions.

37. Around October 2022, Plaintiffs sent MIM a draft Collaboration Agreement.

38. The draft Collaboration Agreement included a list of Plaintiffs' patents that claimed the inventions that the parties had discussed sharing.

39. Both Asserted Patents were on that list, indicating that MIM was considering implementing and using Plaintiffs' patented technology. Plaintiffs, too, were considering a collaboration – *but only* if it agreed to partnership terms.

40. Plaintiffs followed up with MIM a few times in late 2022 and 2023, as Plaintiffs waited to hear back from MIM about the draft Collaboration Agreement.

41. Plaintiffs never heard back.

D. MIM Markets and Sells Infringing Products and Pursues Acquisition by GE HealthCare.

42. Instead, Plaintiffs discovered around June 2023 that MIM was publishing articles, brochures, and website information about the two Infringing Products (Contour ProtégéAI® and MIM SurePlan™ MRT). These materials plainly indicate that the Infringing Products practice the inventions claimed in the Asserted Patents as discussed below.

43. MIM is making, using, offering to sell, and selling products that infringe the Asserted Patents.

44. Not only did MIM develop through imitation, market, and sell the Infringing Products, MIM also benefited from the Infringing Products because (upon information and belief) those products—and Plaintiffs' patented inventions embodied in those Infringing Products—enticed GE HealthCare to acquire MIM. *See* "GE HealthCare Announces Agreement to Acquire MIM Software" (Jan. 8, 2024), *available at*

https://www.gehealthcare.com/about/newsroom/press-releases/ge-healthcare-announces-agreement-to-acquire-mim software.

45. GE HealthCare announced in a recent press release its plan to acquire MIM. In that press release, GE HealthCare emphasized how the inventions claimed by the Asserted Patents—which MIM integrated into the Infringing Products—were a main reason GE HealthCare decided to acquire MIM.

46. The press release states, in relevant part:

> MIM Software's portfolio of innovative imaging solutions provides a variety of beneficial features, including: **the integration of diagnostic images from multiple modalities into treatment plans**; automation to help reduce repetitive tasks and manual interventions; **quantitation and advanced processing in diagnostic imaging** and nuclear medicine to help determine therapy response . . . GE HealthCare expects to integrate MIM Software solutions into its advanced visualizations to facilitate **AI-based segmentation and contouring** as well as dosimetry analysis for patients across their treatment journeys and in the growing fields of radiology, molecular imaging, and radiation oncology.

Id. (emphasis added).

47. The release is replete with references to Plaintiffs' claimed inventions. For example, the reference to "integration of diagnostic images from multiple modalities" is captured, *inter alia*, by claim 42 of the '486 patent, which describes integrating anatomical and functional diagnostic images into the creation of treatment plans. The reference to "quantitation and advanced processing in diagnostic imaging" refers to, *inter alia*, claim 1 of the '346 patent and the use of AI to create tailored risk maps of cancer/disease risk based on analysis of medical images. And the reference to "AI-based segmentation and contouring" refers to the AI-assisted organ segmentation described across multiple claims of the Asserted Patents. All of these GE HealthCare statements indicate that MIM's use of the patented inventions in its software was a key driver of GE HealthCare's decision to acquire MIM.

MIM Ex1039
MIM Software Inc. v. Progenics Pharmaceuticals, Inc.
Trial IPR2025-00630

48. The GE HealthCare press release, however, is not the only public source that reveals MIM's unlawful use of the Asserted Patents in the Infringing Products.

49. MIM publishes information about the Infringing Products on its website, including via product brochures. MIM's website explains that the brochures "[t]ake a closer look at MIM's solutions and products in downloadable PDFs." *See* MIM Brochures, *available at* https://www.mimsoftware.com/literature/brochures (accessed on Jan. 30, 2024).

50. These publications reflect several ways that the Infringing Products practice the inventions claimed by the Asserted Patents.

51. For example, MIM's publications show that the Infringing Products possess each element of representative claim 1 of the '346 patent.

52. The preamble to claim 1 describes "[a] network-based system for generating a disease risk map for use as a decision-making support for evaluating risk of cancer of risk of recurrence of cancer . . ." *See* '346 patent, at col. 35:46-49 (claim 1 preamble). MIM's brochure entitled "Molecular Radiotherapy Dosimetry" describes how the Infringing Products "Deliver AI on Premise or in the Cloud"—in other words, on a "network-based system." *See* "Molecular Radiotherapy Dosimetry" brochure, *available at* https://go.mimsoftware.com/hubfs/00_Website/02_Literature_Case_Studies/Brochures/TD1000-MIM_Nuclear_Medicine_MRT_Brochure-20230608.pdf (accessed on Jan. 30, 2024), at 6. The brochure also describes how the Infringing Products provide a decision-support tool that "allow[s] for effective communication with patients and referring physicians," and for "track[ing] dose across therapy cycles and quickly review tumor progression." *Id*. at 10. A different MIM brochure entitled "Nuclear Imaging and Nuclear Medicine Diagnostic Solutions" describes how the Infringing Products "Empower Clinical Decisions" by "mak[ing]

capturing dosimetry information clinically feasible," and "offer[ing] deep-learning algorithms that expedite the segmentation process." *See* "Nuclear Imaging and Nuclear Medicine Diagnostic Solutions", *available at* https://go.mimsoftware.com/hubfs/_Market/MIM%20General/Brochures/Radiology%20and%20Nuclear%20Medicine/MIM%20Nuclear%20Medicine%20Diagnostic%20Solutions%20Brochure.pdf (accessed Jan. 30, 2024) at 10. These disclosures illustrate that the Infringing Products possess the preamble of claim 1.

53. The Infringing Products also possess the first limitation of claim 1 of the '346 patent[1] because the Infringing Products access scan images for particular patients from an electronic database, and then present those images to clinicians and patients. A MIM brochure, for example, notes how "Contour ProtégéAI for MIM SurePlan MRT has flexible deployment models that allow for easier adoption across any institution." *See* "Molecular Radiotherapy Dosimetry" brochure, *available at* https://go.mimsoftware.com/hubfs/00_Website/02_Literature_Case_Studies/Brochures/TD1000-MIM_Nuclear_Medicine_MRT_Brochure-20230608.pdf (accessed on Jan. 30, 2024) at 6. The brochure also shows an image of a patient scan presented on a screen. *Id*. MIM's website also refers to how MIMcloud can "push and pull images, and easily share studies . . ." *See* MIMCloud, *available at* https://www.mimsoftware.com/remote-access/mimcloud (accessed Jan. 30, 2024).

54. The Infringing Products also possess the second limitation of claim 1 of the '346 patent[2] because MIM SurePlan™ MRT uses Contour ProtégéAI® which, according to a MIM

[1] *See* claim 1(a) ("access[es] one or more medical images associated with a particular patient from a database.").
[2] *See* claim 1(b) ("perform[ing] an analysis of the one or more medical images associated with the particular patient using a machine learning algorithm, to generate a risk map, wherein the risk map comprises a visual representation of tissue overlaid with graphical denotations marking one or more regions of risk of cancer …").

brochure, "segment[s] normal structures with artificial intelligence." *See* "Molecular Radiotherapy Dosimetry" brochure, *available at* https://go.mimsoftware.com/hubfs/00_Website/02_Literature_Case_Studies/Brochures/TD1000-MIM_Nuclear_Medicine_MRT_Brochure-20230608.pdf (accessed on Jan. 30, 2024), at 6; *see also id.* ("Triggered automatically upon image arrival, Contour ProtégéAI and MIM SurePlan MRT uses a neural network for segmenting normal structures on CT images. Results are more accurate than atlas-based approaches so users spend less time editing."). The same brochure also discusses how MIM SurePlan™ MRT uses PET Edge to create a contour of tumor regions that is overlaid on a SPECT/CT image. *Id*.

55. The Infringing Products also possess the third limitation of claim 1 of the '346 patent[3] because, as reflected in the image below from a MIM brochure, MIM SurePlan™ MRT displays the risk map (i.e., tumor segmentation) via a graphical user interface (GUI):

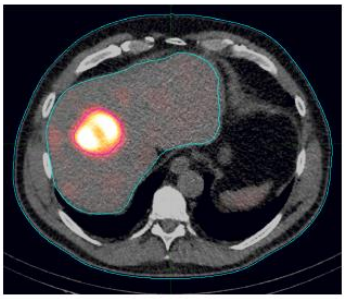

Id. at 7. The same image also reveals that the Infringing Products display normal organ contours and tumor contours overlaid on medical images. *See id*. (blue color outlining an organ, and red

[3] *See* claim 1(c) ("caus[ing] display of the risk map via a graphical user interface (GUI) for presentation or review of the risk map by a user, wherein the analysis of one or more medical images comprises creation of a 3D image of the one or more regions of risk of cancer or risk of recurrence of cancer overlaid on the one or more medical images, and wherein the 3D image comprises geographic identification of one or more specific tissue region(s) overlaid on the one or more medical images").

color outlining a tumor). Another image in the same brochure also shows images of a SPECT/CT with organs and tumors outlined:

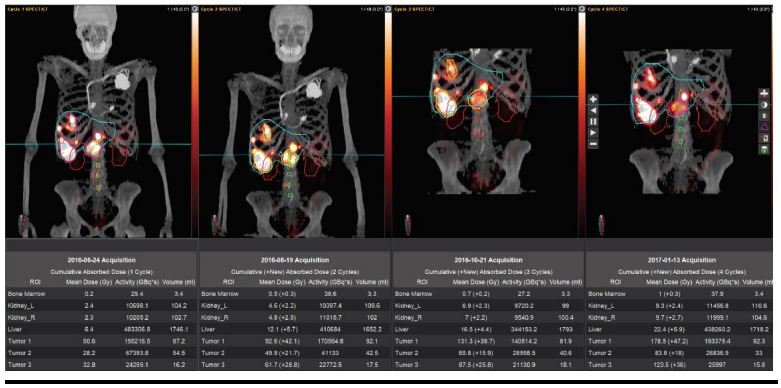

2016-06-24 Acquisition
Cumulative Absorbed Dose (1 Cycle)

ROI	Mean Dose (Gy)	Activity (GBq*s)	Volume (ml)
Bone Marrow	0.2	28.4	3.4
Kidney_L	2.4	10698.1	104.2
Kidney_R	2.3	10209.2	102.7
Liver	6.4	483306.8	1746.1
Tumor 1	50.6	186216.5	87.2
Tumor 2	28.2	67393.8	54.5
Tumor 3	32.8	24259.1	16.2

2016-08-19 Acquisition
Cumulative (+New) Absorbed Dose (2 Cycles)

ROI	Mean Dose (Gy)	Activity (GBq*s)	Volume (ml)
Bone Marrow	0.5 (+0.3)	39.6	3.3
Kidney_L	4.6 (+2.2)	10397.4	109.6
Kidney_R	4.8 (+2.5)	11015.7	102
Liver	12.1 (+5.7)	410584	1652.2
Tumor 1	92.6 (+42.1)	170564.8	92.1
Tumor 2	49.9 (+21.7)	41133	42.5
Tumor 3	61.7 (+28.9)	22772.5	17.5

2016-10-21 Acquisition
Cumulative (+New) Absorbed Dose (3 Cycles)

ROI	Mean Dose (Gy)	Activity (GBq*s)	Volume (ml)
Bone Marrow	0.7 (+0.2)	27.2	3.3
Kidney_L	6.9 (+2.3)	9720.2	99
Kidney_R	7 (+2.2)	9540.9	100.4
Liver	16.5 (+4.4)	344153.2	1793
Tumor 1	131.3 (+38.7)	140514.2	81.9
Tumor 2	65.8 (+15.9)	28958.5	40.6
Tumor 3	87.5 (+25.8)	21130.9	18.1

2017-01-13 Acquisition
Cumulative (+New) Absorbed Dose (4 Cycles)

ROI	Mean Dose (Gy)	Activity (GBq*s)	Volume (ml)
Bone Marrow	1 (+0.3)	37.9	3.4
Kidney_L	9.3 (+2.4)	11456.8	110.6
Kidney_R	9.7 (+2.7)	11999.1	104.8
Liver	22.4 (+5.9)	438260.2	1718.2
Tumor 1	178.8 (+47.2)	193375.4	92.3
Tumor 2	83.8 (+18)	26836.9	33
Tumor 3	123.5 (+36)	25997	15.8

Id. at 10.

56. Turning next to the '486 patent, the Infringing Products also possess all the elements of exemplary claim 42.

57. The preamble to claim 42 describes "[a] method for automatically processing 3D images to identify 3D volumes within the 3D images that correspond to a prostate of a subject and determining one or more uptake metrics indicative of radiopharmaceutical uptake therein . . ." *See* '486 patent, claim 42, preamble. The Infringing Products possess this limitation because: (a) MIM SurePlan™ MRT uses Contour ProtégéAI® to perform organ segmentation (*see* "Molecular Radiotherapy Dosimetry" brochure, *available* at https://go.mimsoftware.com/hubfs/00_Website/02_Literature_Case_Studies/Brochures/TD1000-MIM_Nuclear_Medicine_MRT_Brochure-20230608.pdf (accessed on Jan. 30, 2024), at 6); (b) MIM SurePlan™ MRT provides dose accumulation statistics. *Id*. at 10 ("Dose accumulation runs in the background through MIM Assistant®. Cumulative doses and volume changes across cycles can be reviewed."); and (c) Contour ProtégéAI® segments a variety of organs, including the prostate, listing "Prostate" as one of the "Available Structures for Organ Contouring" (*see* "Contour ProtégéAI+™: Zero-Click AI Auto-Contouring", *available at* https://www.mimsoftware.com/radiation-

oncology/contour-protegeai-plus (accessed on Jan. 30, 2024)). The brochure also refers to how "MIM SurePlan™ MRT has been helping institutions drastically reduce the clinical requirements for dosimetry by including AI-based auto-segmentation and support for quantitative SPECT reconstruction with existing SPECT/CT cameras," with CT providing 3D anatomical images. *See* "Molecular Radiotherapy Dosimetry" brochure, *available* at https://go.mimsoftware.com /hubfs/00_Website/02_Literature_Case_Studies/Brochures/TD1000-MIM_Nuclear_Medicine_ MRT_Brochure-20230608.pdf (accessed on Jan. 30, 2024), at 2.

58. The Infringing Products also possess the first limitation of claim 42 of the '486 patent[4] because, as MIM's brochures proclaim, "MIM SurePlan™ MRT has been helping institutions drastically reduce the clinical requirements for dosimetry by including AI-based auto-segmentation and support for quantitative SPECT reconstruction with existing SPECT/**CT cameras**." *Id*. at 2 (emphasis added). CT cameras provide anatomical images. And, as discussed above, MIM directs that physicians and patients can use the Infringing Products on images relating to the patient's pelvic region. *Supra* at ¶ 57. The Contour ProtégéAI® website lists several applications in the pelvic region, including (but not limited to) the prostate:

[4] *See* claim 42(a) ("receiving, by a processor of a computing device, a 3D anatomical image of the subject obtained using an anatomical imaging modality, wherein the 3D anatomical image comprises a graphical representation of tissue within a subject, at least a portion of which corresponds to a pelvic region of the subject.").

See "Contour ProtégéAI+™: Zero-Click AI Auto-Contouring", *available at* https://www.mimsoftware.com/radiation-oncology/contour-protegeai-plus (accessed on Jan. 30, 2024) (yellow box added).

59. The Infringing Products also possess the second limitation of claim 42 of the '486 patent[5] for the reasons already discussed above. The MIM brochure refers to how "MIM SurePlan™ MRT has been helping institutions drastically reduce the clinical requirements for dosimetry by including AI-based auto-segmentation and support for quantitative SPECT reconstruction with existing SPECT/CT cameras," with CT cameras providing 3D anatomical

[5] *See* claim 42(b) ("receiving, by the processor, a 3D functional image of the subject obtained using a functional imaging modality, wherein the 3D functional image comprises a plurality of voxels, each representing a particular physical volume within the subject and having an intensity value that represents detected radiation emitted from the particular physical volume, wherein at least a portion of the plurality of voxels of the 3D functional image represent physical volumes within the pelvic region of the subject");

MIM Ex1039
MIM Software Inc. v. Progenics Pharmaceuticals, Inc.
Trial IPR2025-00630

images. *See* "Molecular Radiotherapy Dosimetry" brochure, *available* at https://go.mimsoftware.com/hubfs/00_Website/02_Literature_Case_Studies/Brochures/TD1000-MIM_Nuclear_Medicine_MRT_Brochure-20230608.pdf (accessed on Jan. 30, 2024) at 2. SPECT imaging is a 3D functional image. And, as discussed above, the Infringing Products are targeted at multiple applications within the pelvic region. *Supra* at ¶ 57.

60. The Infringing Products also possess the third limitation of claim 42 of the '486 patent[6] because MIM SurePlan™ MRT uses Contour ProtégéAI® to segment normal structures in a CT image. In other words, when Contour ProtégéAI® "detects [the] treatment site to apply correct AI model" as described in the image below, it is determining, using a first module, an initial volume of interest (VOI):

[6] *See* claim 42(c) ("determining, by the processor, using a first module, an initial volume of interest (VOI) within the 3D anatomical image, the initial VOI corresponding to tissue within the pelvic region of the subject and excluding tissue outside the pelvic region of the subject;").

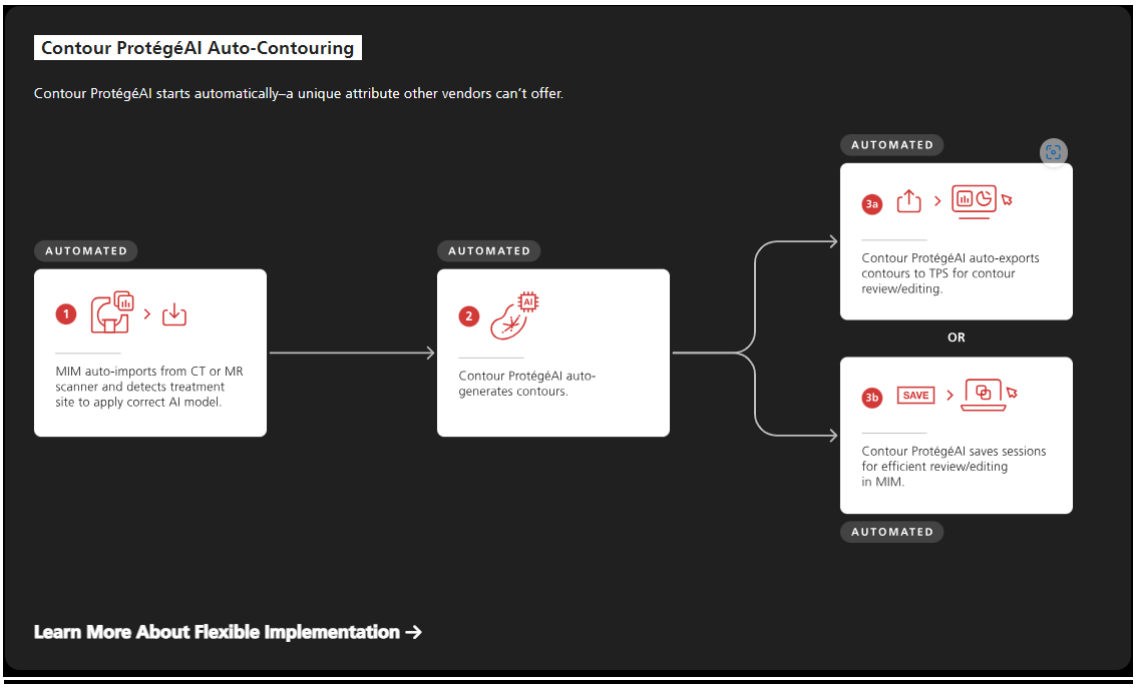

See "Contour ProtégéAI+™: Zero-Click AI Auto-Contouring", *available at* https://www.mimsoftware.com/radiation-oncology/contour-protegeai-plus (accessed on Jan. 30, 2024). As discussed above, Contour ProtégéAI® includes a "Pelvis CT" model for segmenting organs within the pelvic region, i.e., where the initial VOI corresponds to a pelvic region. *Id.*

61. The Infringing Products also possess the fourth limitation of claim 42 of the '486 patent[7] because, when Contour ProtégéAI® uses the "Pelvis CT" model to segment the prostate, *supra* at ¶ 57, it uses a second module to identify a prostate volume within the initial VOI:

[7] *See* claim 42(d) ("identifying, by the processor, using a second module, a prostate volume within the initial VOI corresponding to the prostate of the subject.").

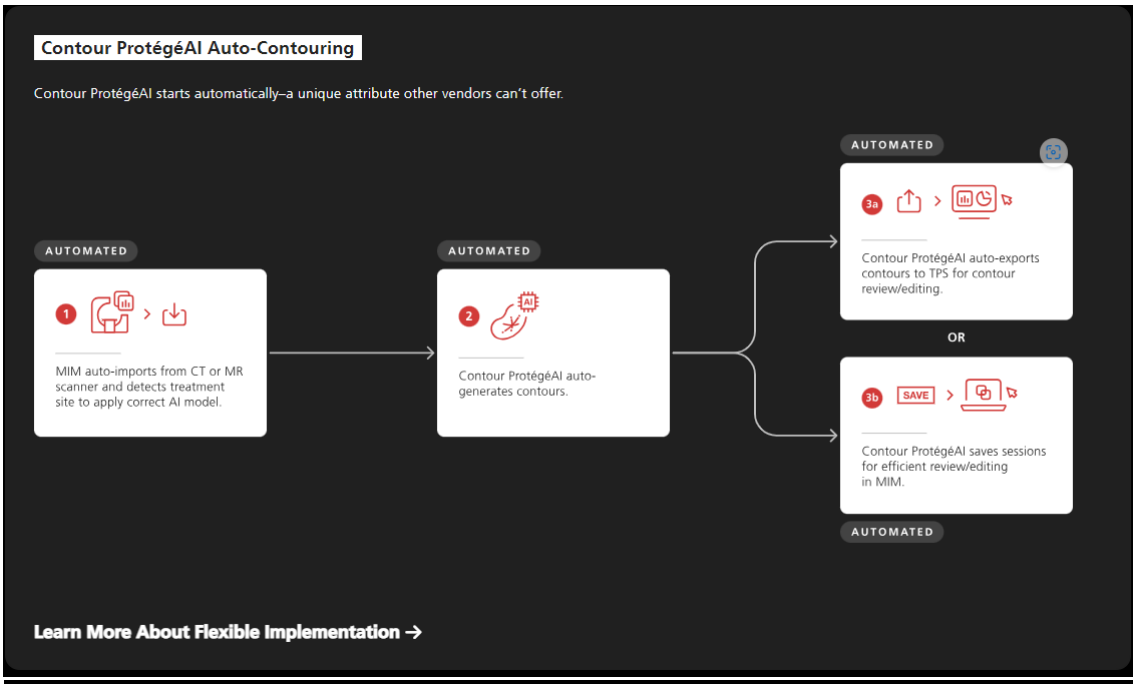

See id. In other words, the left-most box in the image above shows the initial segmentation step (as discussed in the preceding paragraph), and then the reference in the center box to "auto-generat[ing] contours" refers to the Infringing Products' use of the Pelvic CT model to segment the prostate.

62. The Infringing Products also possess the fifth limitation of claim 42 of the '486 patent[8] because, as discussed above, the MIM brochure shows uptake measurements (in bone, kidneys, liver, and tumors):

[8] *See* claim 42(e) ("determining, by the processor, the one or more uptake metrics using the 3D functional image and the prostate volume identified within the initial VOI of the 3D anatomical image,").

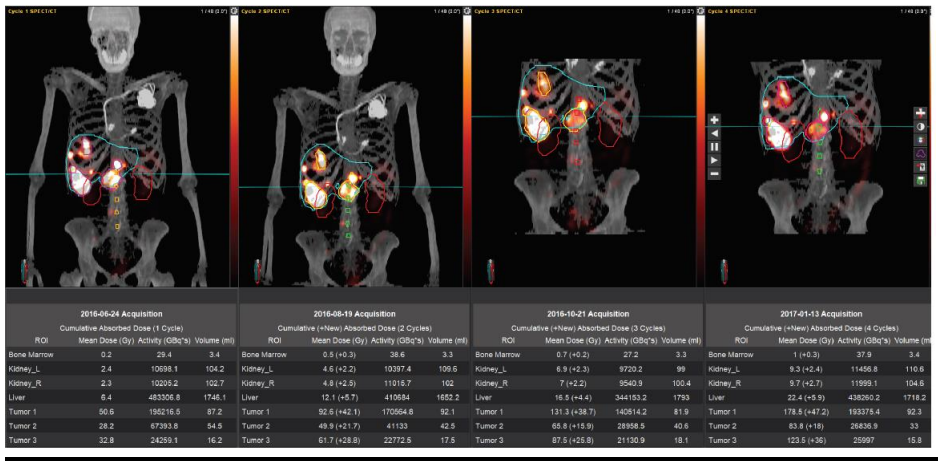

2016-06-24 Acquisition
Cumulative Absorbed Dose (1 Cycle)

ROI	Mean Dose (Gy)	Activity (GBq*s)	Volume (ml)
Bone Marrow	0.2	29.4	3.4
Kidney_L	2.4	10698.1	104.2
Kidney_R	2.3	10205.2	102.7
Liver	6.4	483306.8	1746.1
Tumor 1	50.6	195216.5	87.2
Tumor 2	28.2	67393.8	54.5
Tumor 3	32.8	24259.1	16.2

2016-08-19 Acquisition
Cumulative (+New) Absorbed Dose (2 Cycles)

ROI	Mean Dose (Gy)	Activity (GBq*s)	Volume (ml)
Bone Marrow	0.5 (+0.3)	38.6	3.3
Kidney_L	4.6 (+2.2)	10397.4	109.6
Kidney_R	4.8 (+2.5)	11015.7	102
Liver	12.1 (+5.7)	410684	1652.2
Tumor 1	92.6 (+42.1)	170564.8	92.1
Tumor 2	49.9 (+21.7)	41133	42.5
Tumor 3	61.7 (+28.8)	22772.5	17.5

2016-10-21 Acquisition
Cumulative (+New) Absorbed Dose (3 Cycles)

ROI	Mean Dose (Gy)	Activity (GBq*s)	Volume (ml)
Bone Marrow	0.7 (+0.2)	27.2	3.3
Kidney_L	6.9 (+2.3)	9720.2	99
Kidney_R	7 (+2.2)	9540.9	100.4
Liver	16.5 (+4.4)	344153.2	1793
Tumor 1	131.3 (+38.7)	140514.2	81.9
Tumor 2	65.8 (+15.9)	28958.5	40.6
Tumor 3	87.5 (+25.8)	21130.9	18.1

2017-01-13 Acquisition
Cumulative (+New) Absorbed Dose (4 Cycles)

ROI	Mean Dose (Gy)	Activity (GBq*s)	Volume (ml)
Bone Marrow	1 (+0.3)	37.9	3.4
Kidney_L	9.3 (+2.4)	11456.8	110.6
Kidney_R	9.7 (+2.7)	11999.1	104.6
Liver	22.4 (+5.9)	438260.2	1718.2
Tumor 1	178.5 (+47.2)	193375.4	92.3
Tumor 2	83.8 (+18)	26836.9	33
Tumor 3	123.5 (+36)	25997	15.8

See "Molecular Radiotherapy Dosimetry" brochure, *available at* https://go.mimsoftware.com/hubfs/00_Website/02_Literature_Case_Studies/Brochures/TD1000-MIM_Nuclear_Medicine_MRT_Brochure-20230608.pdf (accessed on Jan. 30, 2024), at 10. As discussed above, Contour ProtégéAI® also includes a specific model that segments these organs, as well as the prostate. *Id*. Therefore, the Infringing Products calculate dose within a prostate volume segmented by the Pelvic CT model of Contour ProtégéAI®.

63. The Infringing Products also possess the sixth limitation of claim 42 of the '486 patent[9] as reflected in the image immediately above, which displays SPECT/CT image overlays, which are, respectively, 3D functional and anatomical images. *See id*.

64. The Infringing Products also possess the seventh limitation of claim 42 of the '486 patent[10] as reflected by the same image above, which shows that SurePlan™ MRT displays SPECT/CT image overlays. *Id*.

[9] *See* claim 42(f) ("causing, by the processor, display of an interactive graphical user interface (GUI) for presentation to the user of a visual representation of the 3D anatomical image and/or the 3D functional image.").

[10] *See* claim 42(g) ("causing, by the processor, graphical rendering of, within the GUI, the 3D anatomical image and/or the 3D functional image as selectable and superimposable layers, such that either can be selected for display and rendered separately, or both selected for display and rendered together by overlaying the 3D anatomical image with the 3D functional image.").

65. MIM has known of the existence of the Asserted Patents. MIM's infringement has been and is willful and in disregard for the Asserted Patents. MIM has no reasonable basis for believing that it has a right to engage in the infringing conduct. As discussed above, MIM and Plaintiffs negotiated for years about a potential collaboration involving MIM purchasing the right to integrate Plaintiffs' patented inventions into MIM's software. During those negotiations, Plaintiffs even sent MIM, upon agreement to do so, a draft Collaboration Agreement that expressly listed the Asserted Patents. Yet, MIM willfully developed, marketed, and sold (and continues to market and sell) the Infringing Products containing Plaintiffs' patented inventions.

66. Plaintiffs have suffered substantial damage (and MIM has unlawfully benefitted) from MIM's infringement of the Asserted Patents. As discussed above, GE HealthCare chose to acquire MIM (rather than enter into a profitable commercial relationship of some kind with Plaintiffs) in large part because of MIM's infringing conduct. *Supra* at ¶¶ 45-46. Plaintiffs have also lost substantial advantage in the market as the only companies permitted to use the claimed inventions, which (as discussed above) represent major breakthroughs in the performance, reliability, and usability of nuclear medicine imaging for cancer and other serious ailments. As a result, Plaintiffs have begun to lose both existing and prospective business to MIM. MIM and Plaintiffs continue to compete for specific customers, and Plaintiffs expect future losses of their existing and prospective business unless MIM ceases its unlawful infringement. Plaintiffs have also lost a licensing and partnership opportunity in view of MIM's actions. Plaintiffs are thus entitled to the full measure of their damages from MIM's infringement, including (without limitation) lost profits, a reasonable royalty, and damages for MIM's willful infringement.

COUNT I: INFRINGEMENT OF U.S. PATENT NO. 10,665,346

67. Plaintiffs repeat and re-allege each of the foregoing paragraphs as if fully set forth herein.

68. MIM has been and is directly and/or indirectly infringing the '346 patent by making, using, selling, or offering for sale in the United States, including within this judicial district, the Infringing Products, in violation of 35 U.S.C. § 271(a).

69. MIM has been and is inducing infringement of the '346 patent by actively and knowingly inducing its customers to use the Infringing Products that embody or use the inventions claimed in the '346 patent, in violation of 35 U.S.C. § 271(b).

70. MIM's infringement has been, and continues to be knowing, intentional, and willful.

71. MIM's infringement of the '346 patent has caused, and will continue to cause, Plaintiffs damages for which Plaintiffs are entitled to compensation pursuant to 35 U.S.C. § 284.

72. MIM's infringement of the '346 patent has caused, and will continue to cause, Plaintiffs immediate and irreparable harm unless such infringing activities are enjoined by this Court pursuant to 35 U.S.C. § 283. Plaintiffs have no adequate remedy at law.

73. This case is exceptional and Plaintiffs are entitled to an award of attorney fees pursuant to 35 U.S.C. § 285.

COUNT II: INFRINGEMENT OF U.S. PATENT NO. 10,973,486

74. Plaintiffs repeat and re-allege each of the foregoing paragraphs as if fully set forth herein.

75. MIM has been and is directly and/or indirectly infringing the '486 patent by making, using, selling, or offering for sale in the United States, including within this judicial district, the Infringing Products, in violation of 35 U.S.C. § 271(a).

76. MIM has been and is inducing infringement of the '486 patent by actively and knowingly inducing its customers to use the Infringing Products that embody or use the inventions claimed in the '346 patent, in violation of 35 U.S.C. § 271(b).

77. MIM's infringement has been, and continues to be knowing, intentional, and willful.

78. MIM's infringement of the '486 patent has caused, and will continue to cause, Plaintiffs damages for which Plaintiffs are entitled to compensation pursuant to 35 U.S.C. § 284.

79. MIM's infringement of the '486 patent has caused, and will continue to cause, Plaintiffs immediate and irreparable harm unless such infringing activities are enjoined by this Court pursuant to 35 U.S.C. § 283. Plaintiffs have no adequate remedy at law.

80. This case is exceptional and Plaintiffs are entitled to an award of attorney fees pursuant to 35 U.S.C. § 285.

PRAYER FOR RELIEF

WHEREFORE, Plaintiffs respectfully request the following relief:

(A) A judgment that MIM has infringed the Asserted Patents;

(B) A judgment that MIM's infringement of the Asserted Patents has been willful;

(C) An award against MIM of damages sufficient to compensate Plaintiffs for MIM's infringement of the Asserted Patents;

(D) An award against MIM of all other damages permitted by 35 U.S.C. § 284, including increased damages up to three times the amount of compensatory damages found;

(E) A declaration that this is an exceptional case and an award against MIM and to Plaintiffs of their reasonable attorneys' fees incurred in this action as provided by 35 U.S.C. § 285;

(F) An order preliminarily and permanently enjoining MIM, and its officers, directors, agents, employees, affiliates, and all others acting in privity or in concert with it, and its parents, subsidiaries, divisions, successors, and assigns from further acts of infringement of the Asserted Patents; and

(G) All such other relief that this Court deems just and proper.

JURY DEMAND

Pursuant to Fed. R. Civ. P. 38(b), Plaintiffs hereby demand a jury trial on all issues triable of right by a jury.

Dated: February 23, 2024

Respectfully submitted,

/s/ Michael H. Bunis

Michael H. Bunis (BBO #566839)
Anita M. C. Spieth (BBO #676302)
John C. Calhoun (BBO #694479)
CHOATE HALL & STEWART LLP
Two International Place
Boston, MA 02110
(617) 248-5000
mbunis@choate.com
aspieth@choate.com
jcalhoun@choate.com

Attorneys for Plaintiffs Progenics Pharmaceuticals, Inc. and EXINI Diagnostics AB.

EXHIBIT 1

US010665346B2

(12) **United States Patent**
Baker

(10) **Patent No.: US 10,665,346 B2**
(45) **Date of Patent: *May 26, 2020**

(54) **NETWORK FOR MEDICAL IMAGE ANALYSIS, DECISION SUPPORT SYSTEM, AND RELATED GRAPHICAL USER INTERFACE (GUI) APPLICATIONS**

(71) Applicant: **Progenics Pharmaceuticals, Inc.**, New York, NY (US)

(72) Inventor: **Mark R. Baker**, New York, NY (US)

(73) Assignee: **Progenics Pharmaceuticals, Inc.**, New York, NY (US)

(*) Notice: Subject to any disclaimer, the term of this patent is extended or adjusted under 35 U.S.C. 154(b) by 0 days.

This patent is subject to a terminal disclaimer.

(21) Appl. No.: **16/718,839**

(22) Filed: **Dec. 18, 2019**

(65) **Prior Publication Data**

US 2020/0126666 A1 Apr. 23, 2020

Related U.S. Application Data

(63) Continuation of application No. 16/418,527, filed on May 21, 2019, which is a continuation of application
(Continued)

(51) **Int. Cl.**
G06Q 10/00 (2012.01)
G06K 9/00 (2006.01)
(Continued)

(52) **U.S. Cl.**
CPC ***G16H 50/20*** (2018.01); ***G01N 33/57434*** (2013.01); ***G16H 15/00*** (2018.01);
(Continued)

(58) **Field of Classification Search**
USPC 382/100, 103, 128–134, 154–158, 162, 382/168, 173, 181, 206, 209, 220, 224,
(Continued)

(56) **References Cited**

U.S. PATENT DOCUMENTS

7,450,747 B2 11/2008 Jabri et al.
7,970,194 B2 6/2011 Kimura
(Continued)

FOREIGN PATENT DOCUMENTS

EP 1426903 A2 6/2004
EP 1508872 A1 2/2005
(Continued)

OTHER PUBLICATIONS

Anand, A. et al., Analytic Validation of the Automated Bone Scan Index as an Imaging Biomarker to Standardize Quantitative Changes in Bone Scans of Patients with Metastatic Prostate Cancer, J. Nucl. Med., 57(1):41-45 (2016).
(Continued)

Primary Examiner — Seyed H Azarian
(74) *Attorney, Agent, or Firm* — Ronen Adato; William R. Haulbrook; Choate, Hall and Stewart LLP

(57) **ABSTRACT**

Described herein is a platform and supported graphical user interface (GUI) decision-making tools for use by medical practitioners and/or their patients, e.g., to aide in the process of making decisions about a course of cancer treatment and/or to track treatment and/or the progress of a disease.

13 Claims, 11 Drawing Sheets

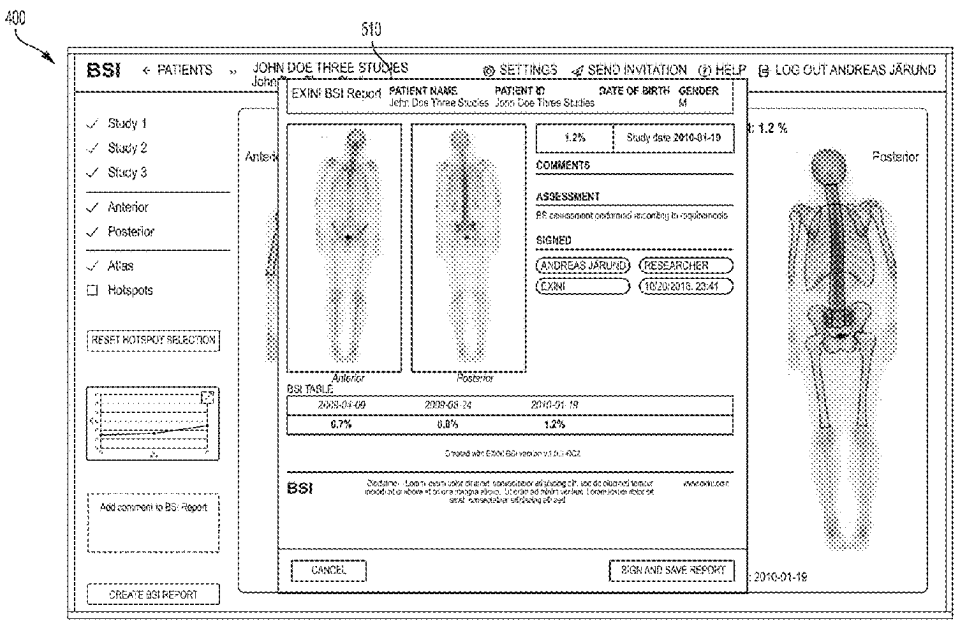

Related U.S. Application Data

No. 15/794,220, filed on Oct. 26, 2017, now Pat. No. 10,340,046.

(60) Provisional application No. 62/413,936, filed on Oct. 27, 2016.

(51) **Int. Cl.**

G16H 50/20	(2018.01)
G16H 30/20	(2018.01)
G16H 30/40	(2018.01)
G16H 50/70	(2018.01)
G16H 50/30	(2018.01)
G16H 15/00	(2018.01)
G01N 33/574	(2006.01)

(52) **U.S. Cl.**
CPC ***G16H 30/20*** (2018.01); ***G16H 30/40*** (2018.01); ***G16H 50/30*** (2018.01); ***G16H 50/70*** (2018.01)

(58) **Field of Classification Search**
USPC 382/232, 254, 286–295, 305, 312; 705/2
See application file for complete search history.

(56) **References Cited**

U.S. PATENT DOCUMENTS

8,211,401	B2	7/2012	Babich et al.	
8,538,166	B2	9/2013	Gordon et al.	
8,705,887	B2	4/2014	Ma et al.	
8,778,305	B2	7/2014	Pomper et al.	
8,855,387	B2	10/2014	Hamadeh et al.	
8,962,799	B2	2/2015	Babich et al.	
9,002,081	B2 *	4/2015	Brown	G06T 7/0014 382/128
RE47,609	E	9/2019	Hamadeh et al.	
2003/0215120	A1	11/2003	Uppaluri et al.	
2006/0062425	A1 *	3/2006	Shen	G06T 15/08 382/100
2007/0081712	A1 *	4/2007	Huang	G06T 7/38 382/128
2007/0081713	A1	4/2007	Jerebko	
2007/0100225	A1	5/2007	Maschke	
2015/0110716	A1	4/2015	Armor	
2015/0331995	A1 *	11/2015	Zhao	G16Z 99/00 705/2
2016/0203263	A1 *	7/2016	Maier	G16H 50/30 705/2
2016/0335395	A1 *	11/2016	Wu	G06F 19/321
2017/0083682	A1 *	3/2017	McNutt	G16H 50/30
2018/0144828	A1	5/2018	Baker	

FOREIGN PATENT DOCUMENTS

WO	WO-9905503	A2	2/1999
WO	WO-2007/062135	A2	5/2007
WO	WO-2009/084995	A1	7/2009
WO	WO-2018/081354	A1	5/2018

OTHER PUBLICATIONS

Anand, A. et al., Automated Bone Scan Index as a quantitative imaging biomarker in metastatic castration-resistant prostate cancer patients being treated with enzalutamide, EJNMMI Research, 6:23, 7 pages (2016).

Anand, A. et al., Translating Prostate Cancer Working Group 2 (PCWG2) Progression Criteria into a Quantitative Response Biomarker in Metastatic Castration Resistant Prostate Cancer (mCRPC), ASCO GU Conference, Poster, presented Feb. 16, 2017.

Anand, A. et al., Translating Prostate Cancer Working Group 2 (PCWG2) progression criteria into a quantitative response biomarker in metastatic castration-resistant prostate cancer (mCRPC), Journal of Clinical Oncology, 35(6):170 (2017).

Armstrong, A. et al., Assessment of the bone scan index in a randomized placebo-controlled trial of tasquinimod in men with metastatic castration-resistant prostate cancer (mCRPC), Urologic Oncology: Seminars and Original Investigations, 32:1308-1316 (2014).

Armstrong, A. et al., Development and validation of a prognostic model for overall survival in chemotherapy-naive men with metastatic castration-resistant prostate cancer (mCRPC) from the phase 3 prevail clinical trial, Journal of Clinical Oncology, 35(Suppl. 6):Abstract 138 (2017).

Armstrong, A. J. et al., Phase 3 prognostic analysis of the automated bone scan index (aBSI) in men with bone-metastatic castration-resistant prostate cancer (CRPC), Meeting Library ASC University, 1 page abstract, (2017).

Belal, S. et al., Association of PET Index quantifying skeletal uptake in NaF PET/CT images with overall survival in prostate cancer patients, ASCO GU 2017, Poster 178, presented Feb. 16, 2017.

Belal, S. et al., PET Index quantifying skeletal uptake in NaF PET/CT images with overall survival in prostate cancer patients, ASCO GU 2017, Abstract (Feb. 13, 2017).

Belal, S. L. et al, 3D skeletal uptake of ^{18}F sodium fluoride in PET/CT images is associate with overall survival in patients with prostate cancer, EJNMMI Research, 7(15):1-8 (2017).

Belal, S.L. et al., Automated evaluation of normal uptake in different skeletal parts in 18F-sodium fluoride (NaF) PET/CT using a new convolutional neural network method, EJNMMI, EANM '17, 44(Suppl 2):S119-S956, Abstract EP-0116 (2017).

Bushberg, J. T. et al., Essential Physics of Medical Imaging, Essential Physics of Medical Imaging, 19.3: p. 581 (table 15-3), p. 713 paragraph 6, section 19.3 and p. 720, (2011).

Dennis, E. et al., Bone Scan Index: A Quantitative Treatment Response Biomarker for Castration-Resistant Metastatic Prostate Cancer, Journal of Clinical Oncology, 30(5):519-524 (2012).

Eiber, M. et al., Prostate Cancer Molecular Imaging Standardized Evaluation (PROMISE): Proposed miTNM Classification for the Interpretation of PSMA-Ligand PET/CT, The Journal of Nuclear Medicine, 59(3):469-478, (2018).

GE Healthcare, SPECT/CT Cameras, retrieved Oct. 25, 2017: <http://www3.gehealthcare.com.sg/en-gb/products/categories/nuclear_medicine/spect-ct_cameras>.

Giesel, F. L. et al., F-18 labelled PSMA-1007: biodistribution, radiation dosimetry and histopathological validation of tumor lesions in prostate cancer patients, Eur. J. Nucl. Med. Mol. Imaging, 44:678-688 (2017).

Goffin, K. E. et al., Phase 2 Study of 99mTc-trofolastat SPECT/CT to identify and localize prostate cancer in intermediate- and high-risk patients undergoing radical prostatectomy and extended pelvic lymph node dissection, Journal of Nuclear Medicine, pp. 1-22 with supplemental data included, (2017).

Guimond, A. et al., Average Brain Models: A Convergence Study, Computer Vision and Image Understanding, 77:192-210 (2000).

Hajnal, J. et al., 4.4 Intensity, Size, and Skew Correction; 7.1 Introduction; 7.2 Methods; 7.3 Image Interpretation—General, In: Medical Image Registration, CRC Press LLC, 80-81:144-148 (2001).

Hiller, S. M. et al., 99mTc-Labeled Small-Molecule Inhibitors of Prostate-Specific Membrane Antigen for Molecular Imaging of Prostate Cancer, Journal of Nuclear Medicine, 54(8):1369-1376 (2013) retrieved Oct. 25, 2017: <http://jnm.snmjournals.org/content/54/8/1369.full>.

Horikoshi, H. et al., Computer-aided diagnosis system for bone scintigrams from Japanese patients: importance of training database, Annals of Nuclear Medicine, 26(8):622-626 (2012).

Huang, J.-H. et al., A Set of Image Processing Algorithms for Computer-Aided Diagnosis in Nuclear Medicine Whole Body Bone Scan Images, IEEE Transactions on Nuclear Science, 54(3):514-522 (2007).

International Search Report, International Application No. PCT/US2017/058418 (Network for Medical Image Analysis, Decision Support System, and Related Graphical User Interface (GUI) Applications, filed Oct. 26, 2017), issued by ISA/European Patent Office, 4 pages, dated Feb. 27, 2018.

(56) **References Cited**

OTHER PUBLICATIONS

Kaboteh R. et al., Progression of bone metastases in patients with prostate cancer—automated detection of new lesions and calculation of bone scan index, EJNMMI Research, 3:64 (2013).
Kaboteh, R. et al., Convolutional neural network based quantification of choline uptake in PET/CT studies is associated with overall survival in patents with prostate cancer, EJNMMI, EANM '17, 44(Suppl 2):S119-S956, Abstract EP-0642 (2017).
Keiss, et al., Prostate-specific membrane antigen and a target for cancer imaging and therapy, The Quarterly Journal of Nuclear Medicine and Molecular Imaging, 59(3):241-268 (2015).
Kikuchi, A. et al., Automated segmentation of the skeleton in whole-body bone scans: influence of difference in atlas, Nuclear Medicine Communications, 33(9):947-953 (2012).
Kinahan, P.E. et al., PET/CT Standardized Update Values (SUVs) in Clinical Practice and Assessing Response to Therapy, Semin Ultrasuond CT MR 31(6):496-505 (2010) retrieved Oct. 25, 2017: <https://www.ncbi.nlm.nih.gov/pmc/articles/PMC3026294/>.
Knutsson, H., and Andersson, M., Morphons: Segmentation using Elastic Canvas and Paint on Priors, IEEE International Conference on Image Processing (ICIP 2005), Genova, Italy, 4 pages. (2005).
Kopka, K. et al., Glu-Ureido-Based Inhibitors of Prostate-Specific Membrane Antigen: Lessons Learned During the Development of a Novel Class of Low-Molecular-Weight Theranostic Radiotracers, The Journal of Nuclear Medicine, 58(9)(Suppl. 2):17S-26S, (2017).
Litjens, G. et al., A survey on deep learning in medical image analysis, Medical Image Analysis, 42:60-88, (2017).
Liu, L. et al., Computer-Aided Detection of Prostate Cancer with MRI: Technology and Applications, Acad Radiol. Author manuscript, 50 pages 2016.
Ma, L. et al., Automatic segmentation of the prostate on CT images using deep learning and multi-atlas fusion, Proc. of SPIE vol. 10133:101332O-1-101332O-9 (2017).
Ma, L. et al., Combining Population and Patient-Specific Characteristics for Prostate Segmentation on 3D CT Images, Proc of SPIE 9784:978427-1-8 (2016).
Ma, L. et al., Random Walk Based Segmentation for the Prostate on 3D Transrectal Ultrasound Images, Proc SPIE Int Soc Opt Eng. Author manuscript, 13 pages (2016).
Mayo Clinic Staff, Choline C-11 PET scan, Overview, Mayo Clinic, 4 pages (2017), retrieved Oct. 25, 2017: <https://www.mayoclinic.org/tests-procedures/choline-c-11-pet-scan/home/ovc-20156994>.
Nakajima, K. et al., Enhanced diagnostic accuracy for quantitative bone scan using an artificial neural network system: a Japanese multi-center database project, EJNMMI Research, 3:83 (2013).
National Cancer Institute, NCI Drug Dictionary: gallium Ga 68-labeled PSMA-11, retrieved Oct. 25, 2017: <https://www.cancer.gov/publications/dictionaries/cancer-drug?cdrid=766400>.
National Cancer Institute, NCI Drug Dictionary: technetium Tc 99m methylene diphosphonate, retrieved Oct. 25, 2017: <https://www.cancer.gov/publications/dictionaries/cancer-drug?cdrid=537722>.
Perera, M. et al., Sensitivity, Specificity, and Predictors of Positive 68Ga-Prostate-specific Membrane Antigen Positron Emission Tomography in Advanced Prostate Cancer: A Systematic Review and Meta-analysis, European Urology, 70(6):926-937 (2016).
Polymeri, E. et al., Analytical validation of an automated method for segmentation of the prostate gland in CT images, EJNMMI, EANM '17, 44(Suppl 2):S119-S956, Abstract EP-0641 (2017).
radiologyinfo.org for Patients, Computed Tomography (CT), retrieved Oct. 25, 2017: <https://www.radiologyinfo.org/en/submenu.cfm?pg=ctscan>.
Rowe, S. P. et al., PET Imaging of prostate-specific membrane antigen in prostate cancer: current state of the art and future challenges, Prostate Cancer and Prostatic Diseases, 1-8 (2016).
Rowe, S. P. et al., PSMA-Based [^{18}F]DCFPyL PET/CT Is Superior to Conventional Imaging for Lesion Detection in Patients with Metastatic Prostate Cancer, Mol Imaging Biol, 18:411-419, (2016).
Sabbatini, P. et al., Prognostic Significance of Extent of Disease in Bone in Patients With Androgen-Independent Prostate Cancer, Journal of Clinical Oncology, 17(3):948-957 (1999).
Sadik, M. et al., 3D prostate gland uptake of 18F-choline—association with overall survival in patients with hormone-naïve prostate cancer, The Journal of Nuclear Medicine, 58(Suppl. 1):Abstract 544 (2017).
Sadik, M. et al., A new computer-based decision-support system for the interpretation of bone scans, Nuclear Medicine Communications, 27(5):417-423 (2006).
Sadik, M. et al., Automated 3D segmentation of the prostate gland in CT images—a first step towards objective measurements of prostate uptake in PET and SPECT images, Journal of Nuclear Medicine, 58(1):1074, (2017).
Sadik, M. et al., Automated quantification of reference levels in liver and mediastinum (blood pool) for the Deauville therapy response classification using FDG-PET/CT in lymphoma patients, EJNMMI, EANM '17, 44(Suppl 2):S119-S956, Abstract EP-0770 (2017).
Sadik, M. et al., Computer-assisted interpretation of planar whole-body bone scans, Journal Nuclear Medicine, 49(12):1958-65, 2008.
Sadik, M. et al., Convolutional neural networks for segmentation of 49 selected bones in CT images show high reproducibility, EJNMMI, EANM '17, 44(Suppl 2):S119-S956, Abstract OP-657 (2017).
Sadik, M. et al., Improved classifications of planar whole-body bone scans using a computer-assisted diagnosis system: a multicenter, multiple-reader, multiple-case study, Journal of Nuclear Medicine, 50(3): 368-75, 2009.
Sadik, M. et al., Variability in reference levels for Deauville classifications applied to lymphoma patients examined with 18F-FDG-PET/CT, EJNMMI, EANM '17, 44(Suppl 2):S119-S956, Abstract EP-0771 (2017).
Sajn, L. et al., Computerized segmentation of whole-body bone scintigrams and its use in automated diagnostics, Computer Methods and Programs in Biomedicine, 80:47-55 (2005).
Salerno, J. et al., Multiparametric magnetic resonance imaging for pre-treatment local staging of prostate cancer: A Cancer Care Ontario clinical practice guideline, Canadian Urological Association Journal, 10(9-10):332-339 (2016).
Sjöstrand K. et al., Statistical regularization of deformation fields for atlas-based segmentation of bone scintigraphy images, MICCAI 5761:664-671 (2009).
Sluimer, I. et al., Toward Automated Segmentation of the Pathological Lung in CT, IEEE Transactions on Medical Imaging, 24(8):1025-1038 (2005).
Tian, Z. et al., A fully automatic multi-atlas based segmentation method for prostate MR images, Proc SPIE Int Soc Opt Eng. Author manuscript, 12 pages (2015).
Tian, Z. et al., A supervoxel-based segmentation method for prostate MR images, Med. Phys., 44(2):558-569 (2017).
Tian, Z. et al., Deep convolutional neural network for prostate MR segmentation, Proc. of SPIE 10135:101351L-1-101351L-6 (2017).
Tian, Z., et al., Superpixel-based Segmentation for 3D Prostate MR Images, IEEE Trans Med Imaging, Author manuscript, 32 pages, (2016).
Ulmert, D. et al., A Novel Automated Platform for Quantifying the Extent of Skeletal Tumour Involvement in Prostate Cancer Patients Using the Bone Scan Index, European Urology, 62(1):78-84 (2012).
Wrangsjo, A. et al., Non-rigid Registration Using Morphons, Proceedings of the 14th Scandinavian Conference on Image Analysis (SCIA '05), pp. 501-510 (2005).
Written Opinion, International Application No. PCT/US2017/058418 (Network for Medical Image Analysis, Decision Support System, and Related Graphical User Interface (GUI) Applications, filed Oct. 26, 2017), issued by ISA/European Patent Office, 9 pages, dated Feb. 27, 2018.
Yin, T.-K., A Computer-Aided Diagnosis for Locating Abnormalities in Bone Scintigraphy by a Fuzzy System With a Three-Step Minimization Approach, IEEE Transactions on Medical Imaging, 23(5):639-654 (2004).

* cited by examiner

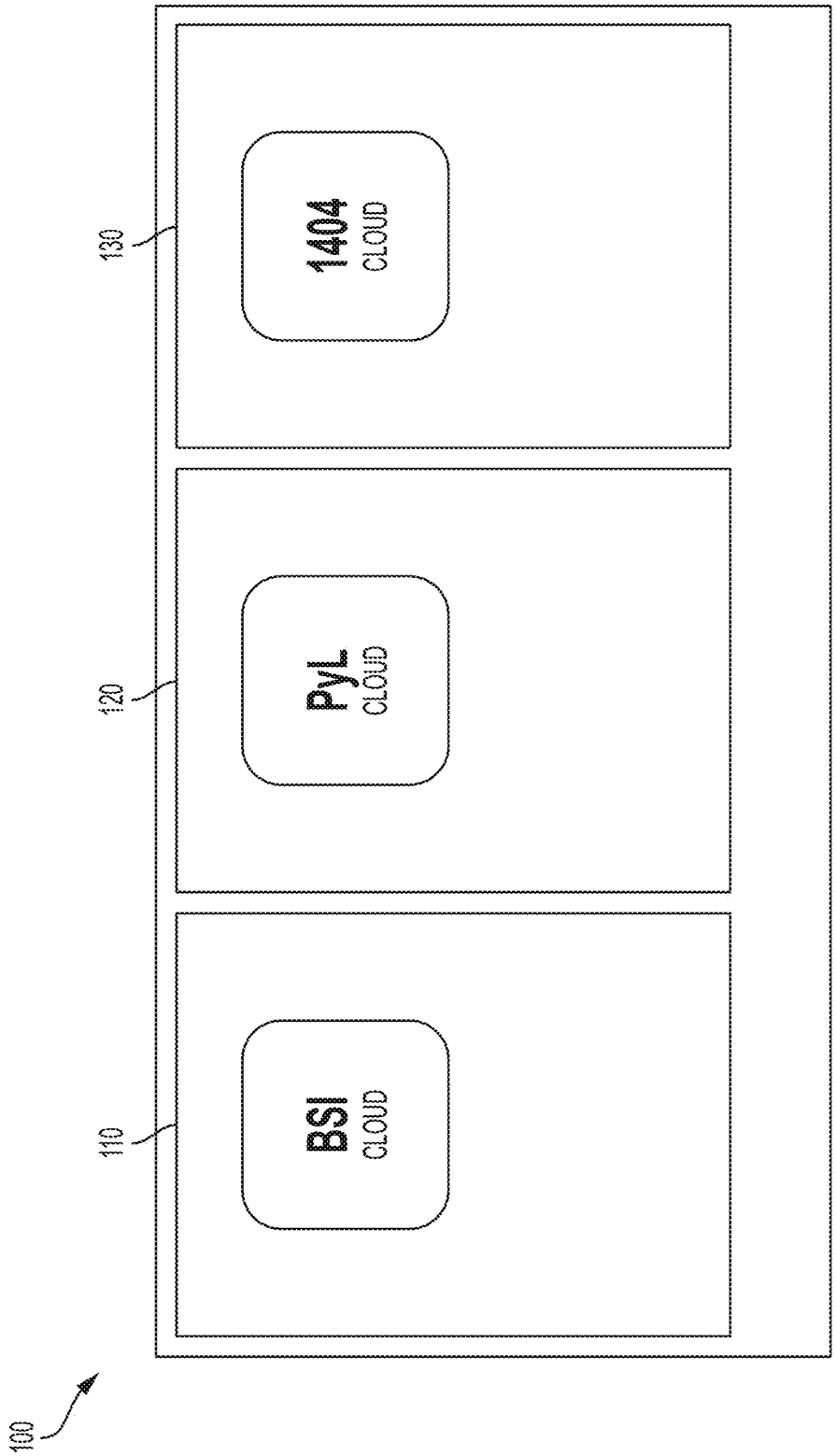

FIG. 1

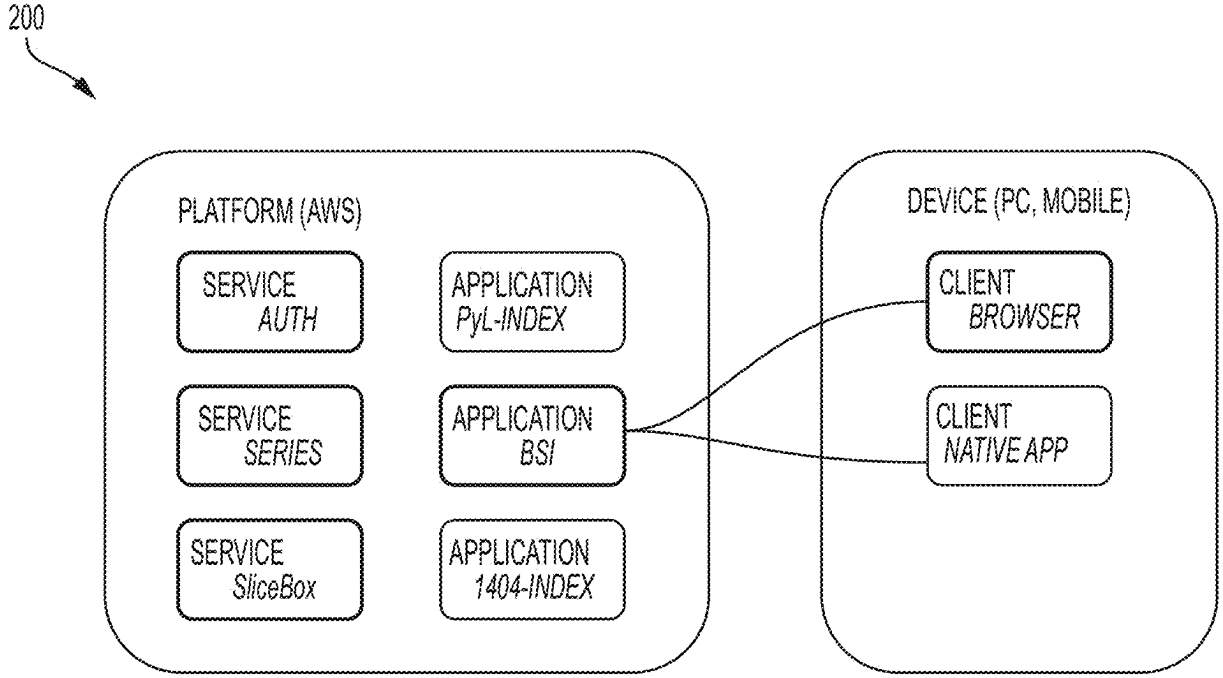
200
PLATFORM (AWS)
SERVICE AUTH
SERVICE SERIES
SERVICE SliceBox
APPLICATION PyL-INDEX
APPLICATION BSI
APPLICATION 1404-INDEX
DEVICE (PC, MOBILE)
CLIENT BROWSER
CLIENT NATIVE APP

FIG. 2

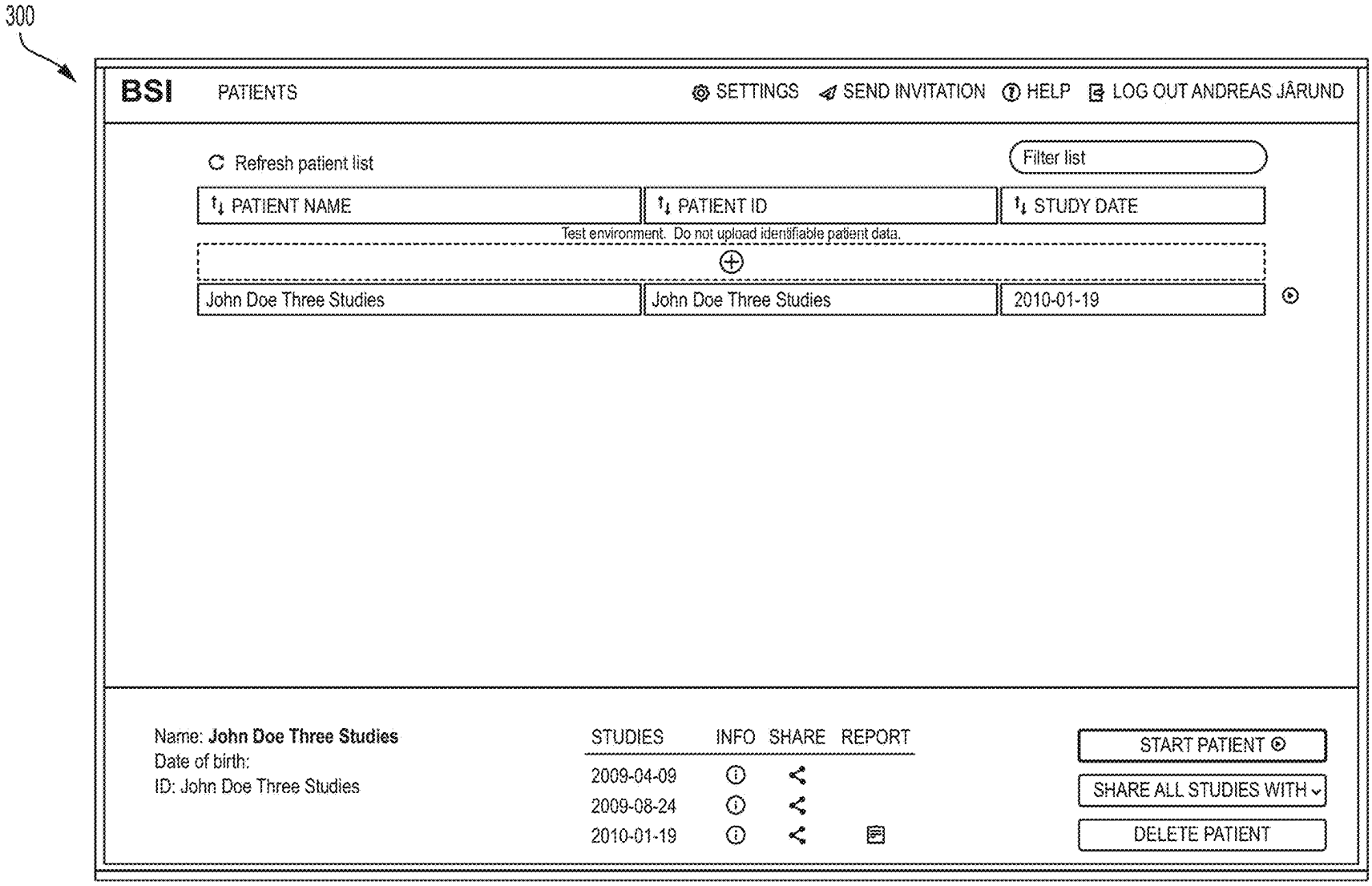
300
BSI
PATIENTS
SETTINGS
SEND INVITATION
HELP
LOG OUT ANDREAS JÅRUND
Refresh patient list
Filter list
PATIENT NAME
PATIENT ID
STUDY DATE
Test environment. Do not upload identifiable patient data.
John Doe Three Studies
John Doe Three Studies
2010-01-19
Name: John Doe Three Studies
Date of birth:
ID: John Doe Three Studies
STUDIES
INFO
SHARE
REPORT
2009-04-09
2009-08-24
2010-01-19
START PATIENT
SHARE ALL STUDIES WITH
DELETE PATIENT

FIG. 3

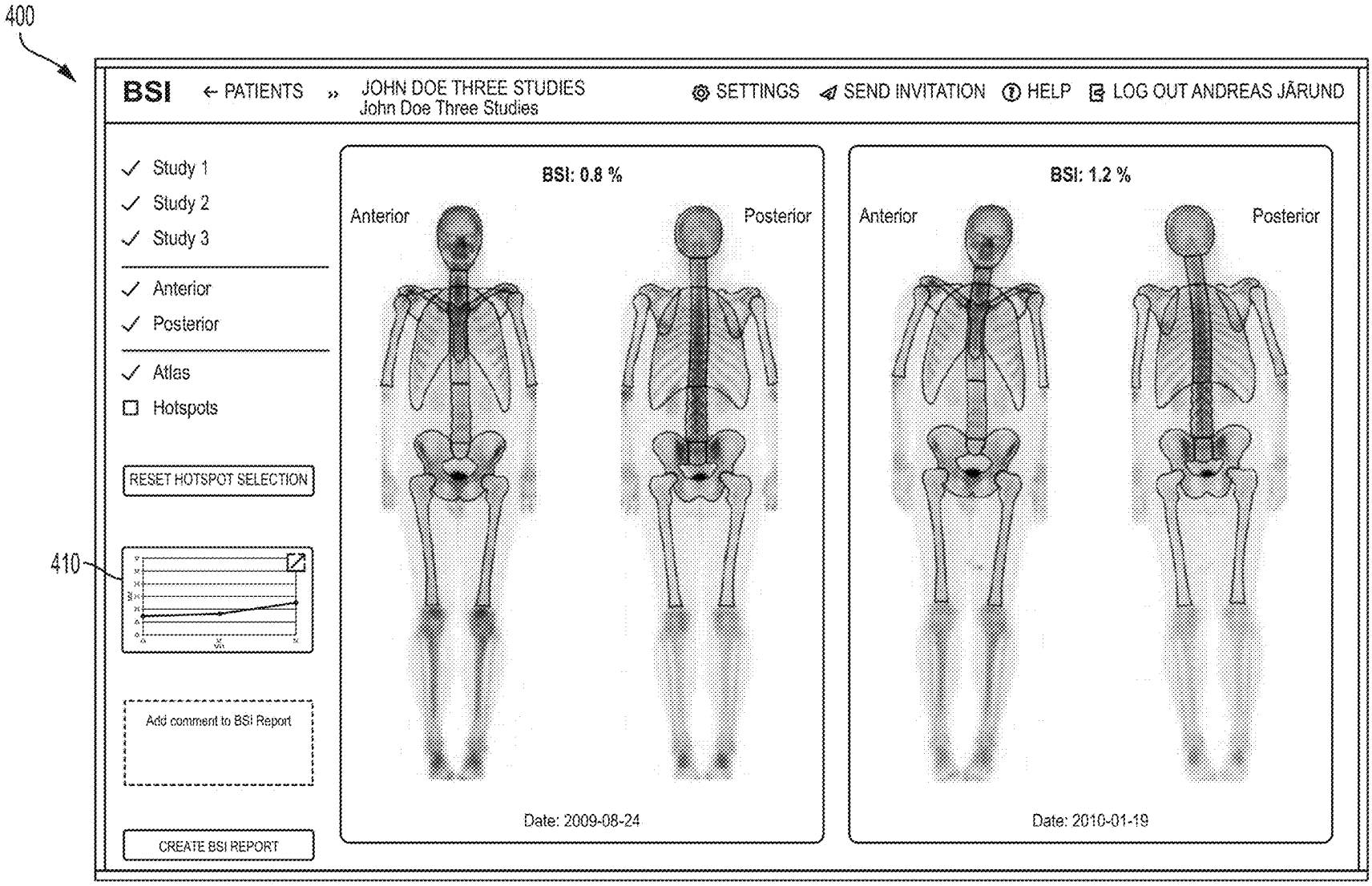
400
BSI
← PATIENTS
JOHN DOE THREE STUDIES
John Doe Three Studies
SETTINGS
SEND INVITATION
HELP
LOG OUT ANDREAS JÄRUND
Study 1
Study 2
Study 3
Anterior
Posterior
Atlas
Hotspots
RESET HOTSPOT SELECTION
410
Add comment to BSI Report
CREATE BSI REPORT
BSI: 0.8 %
Anterior
Posterior
Date: 2009-08-24
BSI: 1.2 %
Anterior
Posterior
Date: 2010-01-19

FIG. 4

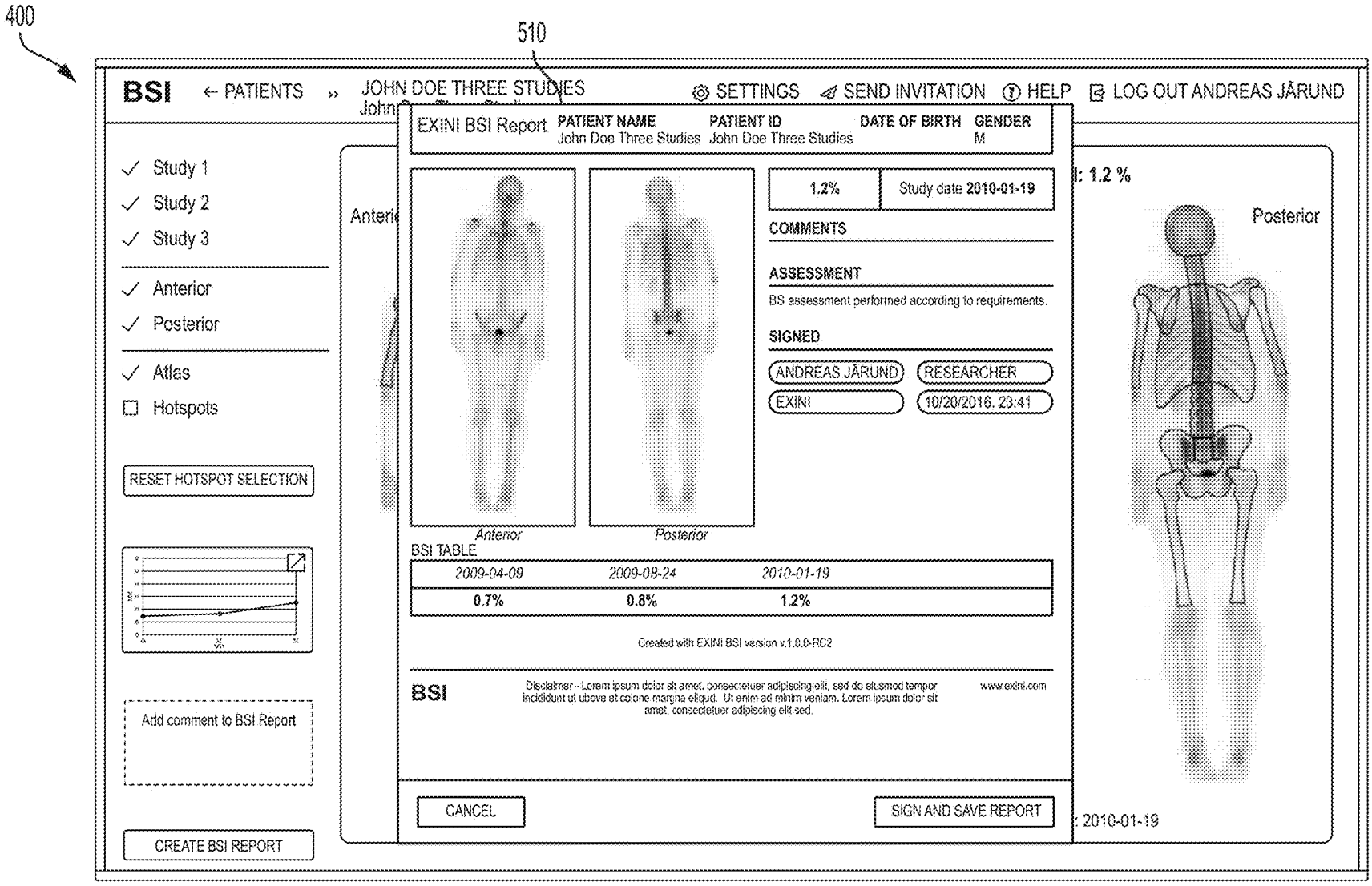
400
510
BSI
← PATIENTS
JOHN DOE THREE STUDIES
SETTINGS
SEND INVITATION
HELP
LOG OUT ANDREAS JÄRUND
Study 1
Study 2
Study 3
Anterior
Posterior
Atlas
Hotspots
RESET HOTSPOT SELECTION
Add comment to BSI Report
CREATE BSI REPORT
EXINI BSI Report
PATIENT NAME
John Doe Three Studies
PATIENT ID
John Doe Three Studies
DATE OF BIRTH
GENDER
M
1.2%
Study date 2010-01-19
COMMENTS
ASSESSMENT
BS assessment performed according to requirements.
SIGNED
ANDREAS JÄRUND
RESEARCHER
EXINI
10/20/2016, 23:41
Anterior
Posterior
BSI TABLE
2009-04-09
2009-08-24
2010-01-19
0.7%
0.8%
1.2%
Created with EXINI BSI version v.1.0.0-RC2
BSI
Disclaimer - Lorem ipsum dolor sit amet, consectetuer adipiscing elit, sed do eiusmod tempor incididunt ut ubove et colone magna eliqud. Ut enim ad minim veniam. Lorem ipsum dolor sit amet, consectetuer adipiscing elit sed.
www.exini.com
CANCEL
SIGN AND SAVE REPORT
1.2 %
Posterior
2010-01-19

FIG. 5

(I) RECEIVING AND STORING SETS OF MEDICAL IMAGES IN A DATABASE

(II) ACCESSING ONE OR MORE OF THE MEDICAL IMAGES FOR TRANSMISSION TO THE USER FOR DISPLAY ON A USER COMPUTING DEVICE

(III) AUTOMATICALLY ANALYZING, BY THE PROCESSOR, THE MEDICAL IMAGES TO COMPUTE A RISK INDEX (E.G., BSI) AND/OR TO GENERATE A RISK MAP

(IV) GENERATING A RADIOLOGIST REPORT FOR A PATIENT ACCORDING TO THE PATIENT IMAGES AND/OR RISK INDEX/ RISK MAP

(V) APPLYING A MACHINE LEARNING ALGORITHM TO UPDATE A PROCESS FOR THE AUTOMATIC ANALYSIS OF FUNCTION (III)

FIG. 6

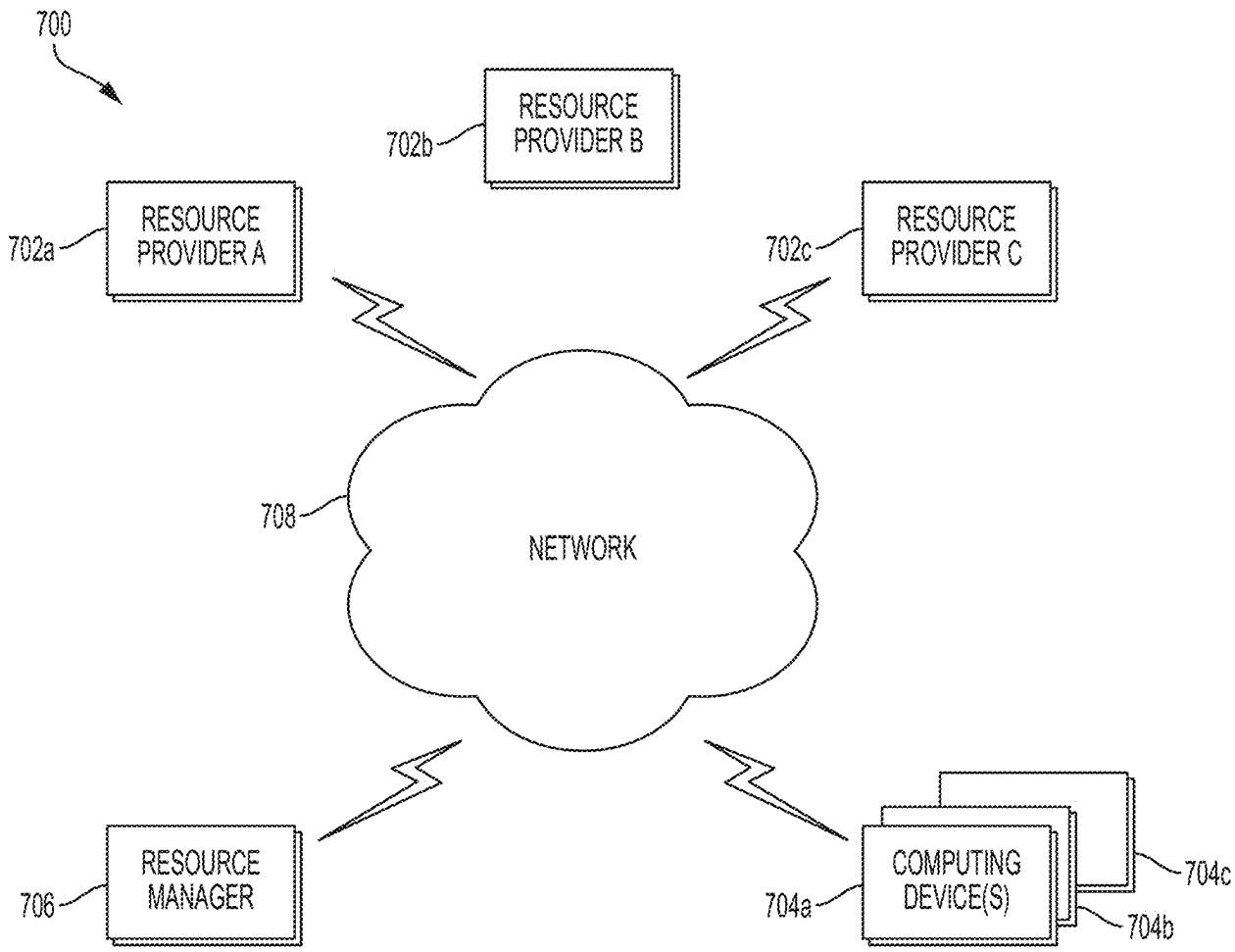
700
RESOURCE PROVIDER B
702b
RESOURCE PROVIDER A
702a
RESOURCE PROVIDER C
702c
708
NETWORK
RESOURCE MANAGER
706
COMPUTING DEVICE(S)
704a
704b
704c

FIG. 7

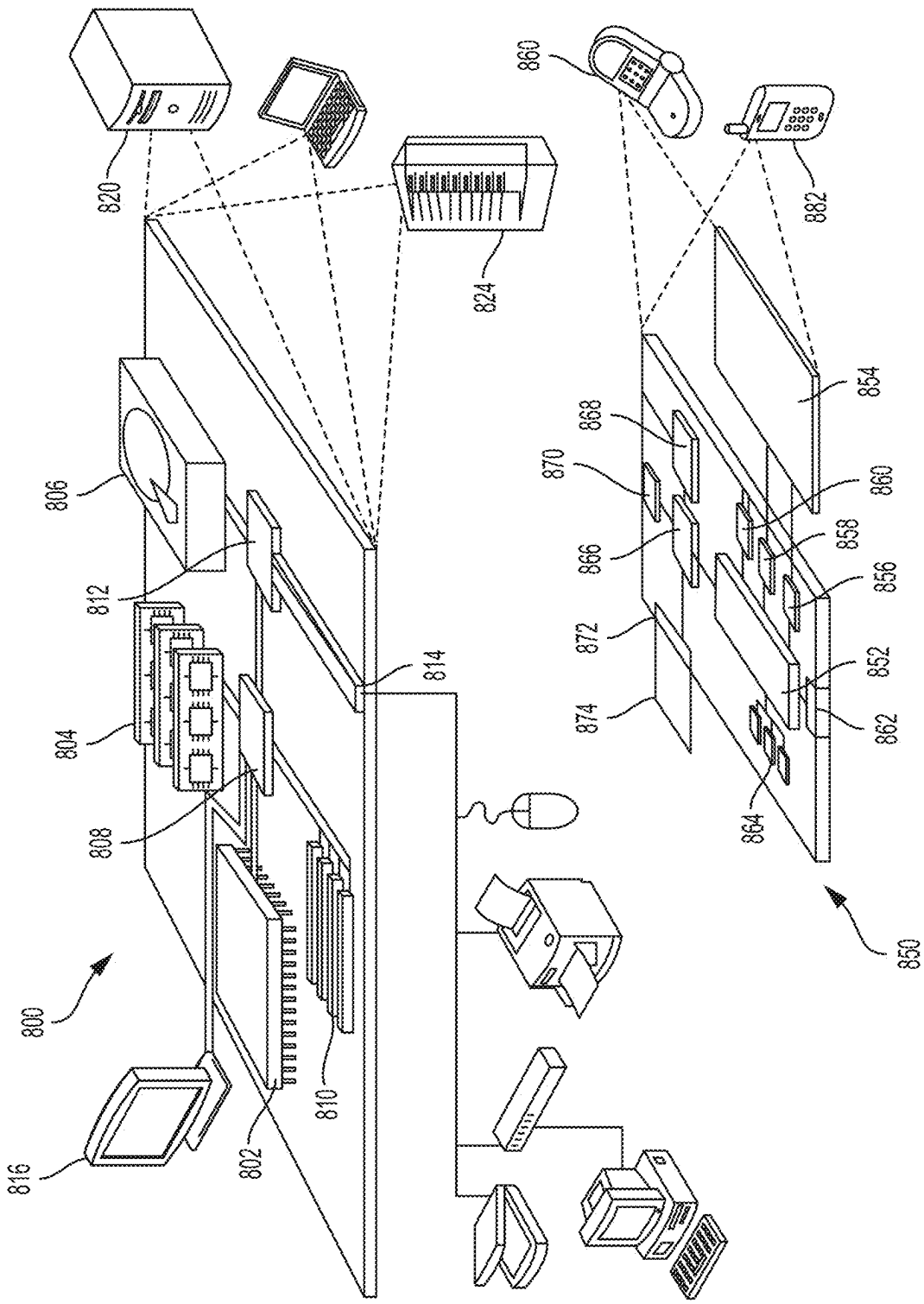
800
802
804
806
808
810
812
814
816
820
824
850
852
854
856
858
860
862
864
866
868
870
872
874
882

FIG. 8

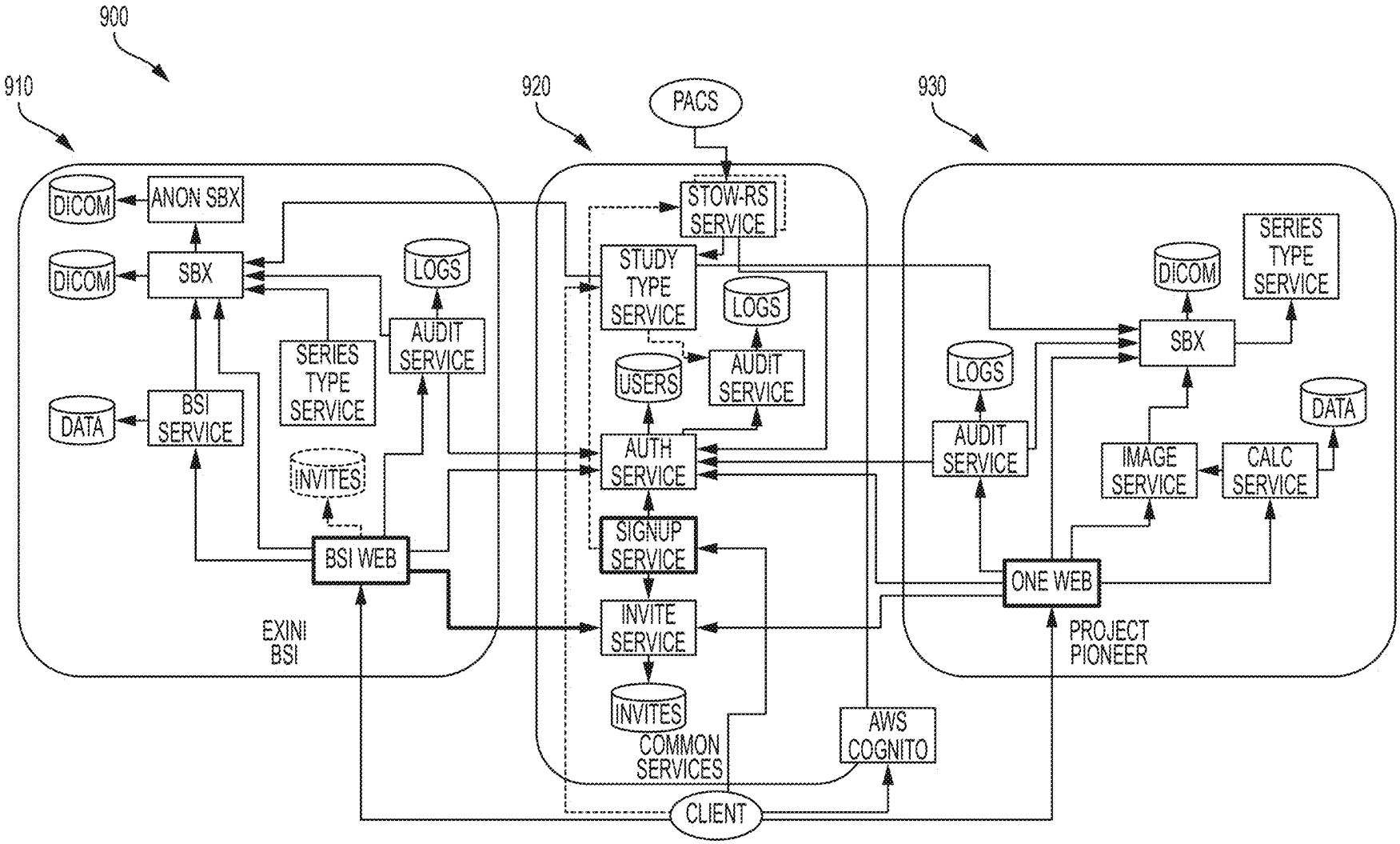
900
910
920
930
PACS
DICOM
ANON SBX
DICOM
SBX
DATA
BSI SERVICE
LOGS
AUDIT SERVICE
SERIES TYPE SERVICE
INVITES
BSI WEB
EXINI BSI
STOW-RS SERVICE
STUDY TYPE SERVICE
LOGS
USERS
AUDIT SERVICE
AUTH SERVICE
SIGNUP SERVICE
INVITE SERVICE
INVITES
COMMON SERVICES
AWS COGNITO
CLIENT
LOGS
AUDIT SERVICE
DICOM
SERIES TYPE SERVICE
SBX
DATA
IMAGE SERVICE
CALC SERVICE
ONE WEB
PROJECT PIONEER

FIG. 9

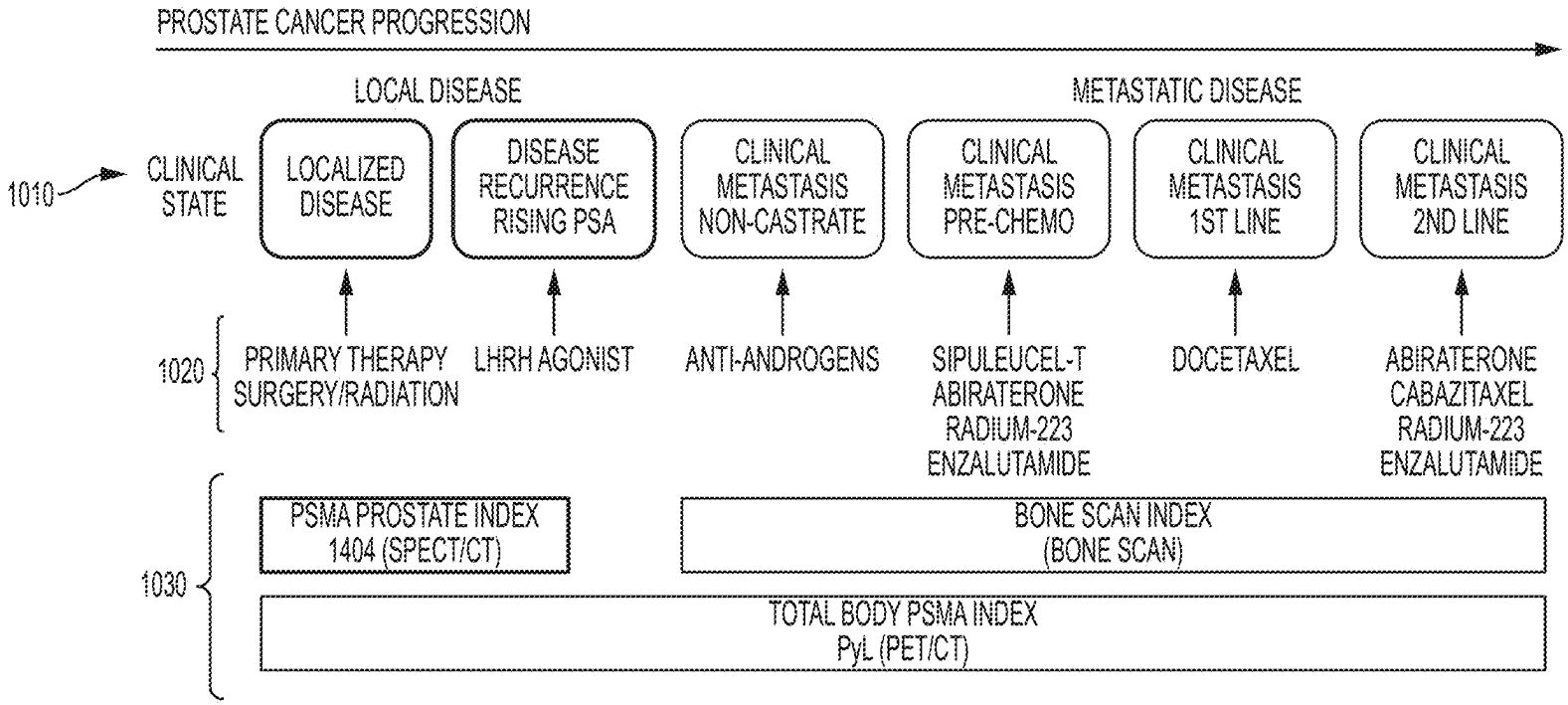
PROSTATE CANCER PROGRESSION
LOCAL DISEASE
METASTATIC DISEASE
1010
CLINICAL STATE
LOCALIZED DISEASE
DISEASE RECURRENCE RISING PSA
CLINICAL METASTASIS NON-CASTRATE
CLINICAL METASTASIS PRE-CHEMO
CLINICAL METASTASIS 1ST LINE
CLINICAL METASTASIS 2ND LINE
1020
PRIMARY THERAPY SURGERY/RADIATION
LHRH AGONIST
ANTI-ANDROGENS
SIPULEUCEL-T ABIRATERONE RADIUM-223 ENZALUTAMIDE
DOCETAXEL
ABIRATERONE CABAZITAXEL RADIUM-223 ENZALUTAMIDE
1030
PSMA PROSTATE INDEX 1404 (SPECT/CT)
BONE SCAN INDEX (BONE SCAN)
TOTAL BODY PSMA INDEX PyL (PET/CT)

FIG. 10

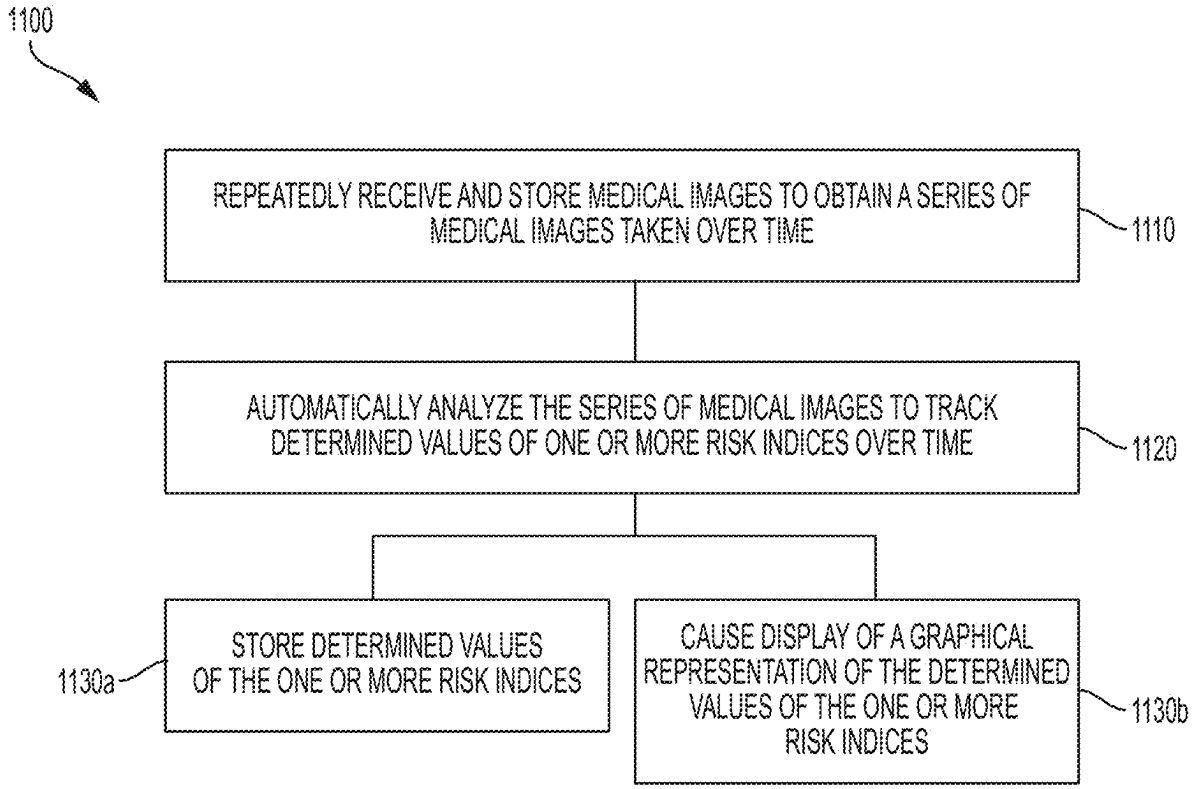
1100
REPEATEDLY RECEIVE AND STORE MEDICAL IMAGES TO OBTAIN A SERIES OF MEDICAL IMAGES TAKEN OVER TIME
1110
AUTOMATICALLY ANALYZE THE SERIES OF MEDICAL IMAGES TO TRACK DETERMINED VALUES OF ONE OR MORE RISK INDICES OVER TIME
1120
STORE DETERMINED VALUES OF THE ONE OR MORE RISK INDICES
1130a
CAUSE DISPLAY OF A GRAPHICAL REPRESENTATION OF THE DETERMINED VALUES OF THE ONE OR MORE RISK INDICES
1130b

FIG. 11

NETWORK FOR MEDICAL IMAGE ANALYSIS, DECISION SUPPORT SYSTEM, AND RELATED GRAPHICAL USER INTERFACE (GUI) APPLICATIONS

CROSS REFERENCE TO RELATED APPLICATIONS

This application is a continuation of U.S. application Ser. No. 16/418,527, filed May 21, 2019, which is a continuation of U.S. application Ser. No. 15/794,220, filed Oct. 26, 2017 (now U.S. Pat. No. 10,340,046, issued Jul. 2, 2019), which claims the benefit of U.S. Provisional Application 62/413,936, filed on Oct. 27, 2016, the content of each of which are hereby incorporated by reference herein in their entirety.

TECHNICAL FIELD

This invention relates generally to systems and methods for creation, analysis, and/or presentation of medical image data. More particularly, in certain embodiments, the invention relates to a cloud-based platform and supported GUI decision-making tools for use by medical practitioners and/or their patients, e.g., to aide in the process of making decisions about a course of cancer treatment and/or to track treatment and/or the progress of a disease.

BACKGROUND

Targeted image analysis involves the use of radiolabeled small molecules that bind to specific receptors, enzymes and proteins in the body that are altered during the evolution of disease. After administration to a patient, these molecules circulate in the blood until they find their intended target. The bound radiopharmaceutical remains at the site of disease, while the rest of the agent clears from the body. The radioactive portion of the molecule serves as a beacon so that an image may be obtained depicting the disease location and concentration using commonly available nuclear medicine cameras, known as single-photon emission computerized tomography (SPECT) or positron emission tomography (PET) cameras, found in most hospitals throughout the world. Physicians can then use this information to determine the presence and the extent of disease in a patient. The physician can use this information to provide a recommended course of treatment to the patient and to track the progression of disease.

There are a variety of software-based analytical techniques available for analysis and enhancement of PET and SPECT images that can be used by a radiologist or physician. There are also a number of radiopharmaceuticals available for imaging particular kinds of cancer. For example, the small molecule diagnostic 1404 targets the extracellular domain of prostate specific membrane antigen (PSMA), a protein amplified on the surface of >95% of prostate cancer cells and a validated target for the detection of primary and metastatic prostate cancer. 1404 is labeled with technetium-99m, a gamma-emitter isotope that is widely available, relatively inexpensive, facilitates efficient preparation, and has spectrum characteristics attractive for nuclear medicine imaging applications.

Another example radiopharmaceutical is PyL™ (also known as [^{18}F]DCFPyL), which is a clinical-stage, fluorinated PSMA-targeted PET imaging agent for prostate cancer. A proof-of-concept study published in the April 2015 issue of the Journal of Molecular Imaging and Biology demonstrated that PET imaging with PyL™ showed high

levels of PyL™ uptake in sites of putative metastatic disease and primary tumors, suggesting the potential for high sensitivity and specificity in detecting prostate cancer.

An oncologist may use images from a targeted PET or SPECT study of a patient as input in her assessment of whether the patient has a particular disease, e.g., prostate cancer, what stage of the disease is evident, what the recommended course of treatment (if any) would be, whether surgical intervention is indicated, and likely prognosis. The oncologist may use a radiologist report in this assessment. A radiologist report is a technical evaluation of the PET or SPECT images prepared by a radiologist for a physician who requested the imaging study and includes, for example, the type of study performed, the clinical history, a comparison between images, the technique used to perform the study, the radiologist's observations and findings, as well as overall impressions and recommendations the radiologist may have based on the imaging study results. A signed radiologist report is sent to the physician ordering the study for the physician's review, followed by a discussion between the physician and patient about the results and recommendations for treatment.

Thus, the process involves having a radiologist perform an imaging study on the patient, analyzing the images obtained, creating a radiologist report, forwarding the report to the requesting physician, having the physician formulate an assessment and treatment recommendation, and having the physician communicate the results, recommendations, and risks to the patient. The process may also involve repeating the imaging study due to inconclusive results, or ordering further tests based on initial results.

If an imaging study shows that the patient has a particular disease or condition (e.g., cancer), the physician discusses various treatment options, including surgery, as well as risks of doing nothing or adopting a watchful waiting or active surveillance approach, rather than having surgery.

There are limitations associated with this process, both from the perspective of the physician and from the perspective of the patient. While the radiologist's report is certainly helpful, the physician must ultimately rely on her experience in formulating an assessment and recommendation for her patient. Furthermore, the patient must place a great deal of trust in his physician. The physician may show the patient his PET/SPECT images and may tell the patient a numerical risk associated with various treatment options or likelihood of a particular prognosis, but the patient may very well struggle to make sense of this information. Moreover, the patient's family will likely have questions, particularly if cancer is diagnosed but the patient opts not to have surgery. The patient and/or his family members may search online for supplemental information and may become misinformed about risks of the diagnosed condition. A difficult ordeal may become more traumatic.

Thus, there remains a need for systems and methods for improved analysis of medical imaging studies and communication of those results, diagnoses, prognoses, treatment recommendations, and associated risks to a patient.

SUMMARY OF THE INVENTION

Presented herein is a cloud-based platform and supported graphical user interface (GUI) decision-making tools for use by medical practitioners and/or their patients, e.g., to aide in the process of making decisions about a course of cancer treatment and/or to track treatment and/or the progress of a disease.

For example, presented herein is a network-based (e.g., cloud-based) support platform allowing multiple users to store, access, analyze, and/or provide feedback regarding a given set of image data for a patient; platform supports software tools for automated analysis of targeted PET/SPECT/or other image(s), generation of radiologist reports, and application of machine learning algorithms to update process by which images are analyzed (e.g. updating segmentation and/or classification routines based on growing image database). In certain embodiments, the targeted PET/SPECT image(s) may be obtained using PyL™ and/or 1404 as the radiopharmaceutical(s). In certain embodiments, multiple (accredited) users can access the information, e.g., to weigh in on data interpretation.

Also presented herein is a software tool (e.g., mobile app) featuring a graphical user interface (GUI) element with controls for adjusting presentation of a 3D risk image corresponding to a patient organ (and/or other tissue) for comparison with reference images (e.g., for use in communication of results to patient as a decision-making support). For example, the tool may be supported by the network-based support platform above. This tool can provides an easily-understood, user-friendly, interactive, controllable pictorial display to communicate information about a patient's condition to the patient (and/or to the physician, or to the patient's family with the patient's permission). For example, a patient for whom a risk of cancer is detected can display a map indicating areas and/or degrees of risk and can compare this risk map with those of others for whom a given course of treatment is recommended. For instance, this tool can help a patient in his decision whether or not to have surgery (e.g., for a detected risk of prostate cancer). The patient can visually compare his risk map with a map representing a typical risk-level for which surgery would be recommended, below which it may be reasonable to opt not to have surgery and engage in watchful waiting or active surveillance. Thus, a low-risk patient who is told by his physician that he has a non-zero risk of cancer may find comfort in a visual, controllable comparison between his situation and that of someone (e.g., where the reference to which the patient's risk situation is compared can be tuned for age, weight, and/or other risk factors of the patient).

In one aspect, the invention is directed to a network-based (e.g., cloud based) decision support system comprising: a processor (e.g., of a network or Internet host server); and a memory having instructions stored thereon, wherein the instructions, when executed by the processor, cause the processor to perform one or more of functions (i) to (v) as follows: (i) receive and store medical images [e.g., comprising one or more of the following: targeted PET images, targeted SPECT images, computed tomography (CT) images, magnetic resonance (MR) images, ultrasound (US) images, gamma camera (i.e. scintillation camera) images, and combinations, fusions, or derivatives of any of the above] in a database [e.g., wherein the targeted PET/SPECT/gamma camera image(s) are obtained using one or more radiopharmaceuticals (e.g., [18F]DCFPyL and/or 1404 and/or a composition comprising technetium 99m, {e.g., technetium 99m methylenediphosphonate (^{99m}Tc MDP)}), and/or wherein the medical images are obtained using non-radioactive agents or no agents], each medical image associated with a particular patient; (ii) access one or more of the medical images and/or related data associated with a particular patient from the database upon user request (e.g., following automated verification that the user is properly credentialed for receiving the requested images and/or data) for transmission to the user for display on a user computing device; (iii) automatically analyze one or more of the medical images [e.g., to generate a risk index (e.g., BSI) and/or a risk map, e.g., a visual representation (e.g., 3D representation) of tissue (e.g., an organ or other part of the body) with graphical denotations (e.g., texture- or color-coding) marking regions of risk of current disease or risk of recurrence of disease, e.g., cancer, e.g., wherein the risk map is displayed as an overlay of the PET/SPECT/CT/MRI/US/combined/derived/fused image of the tissue, or is in place of the image of the tissue]; (iv) generate a radiologist report for a patient according to one or more of the medical images for the patient; and (v) apply a machine learning algorithm to update a process for automatically analyzing one or more of the medical images using accumulated image data in the database [e.g., wherein the automatic analysis of the one or more medical images in (iii) and/or (v) above comprises any one or more of (a) to (d) as follows: (a) automated fusion of the (e.g., PET, SPECT, CT, Mill, and/or US) image(s) of the tissue; (b) geographic identification of one or more organs, organ structures, sub-organs, organ regions, and/or other regions of the imaged tissue of the patient and production of a 3D image of the geographically identified tissue with PET, SPECT, CT, MM, and/or US data overlaid; (c) computation of risk information comprising one or more risk indices, a risk field, or a risk map using data from the database, the image(s) of the tissue, and/or the 3D image in (b); and (d) use of the risk information computed in (c) (e.g., and data from the database) to produce a 3D risk picture for the patient].

In certain embodiments, the medical images in the database comprise a series of medical images of a first patient taken over time (e.g., over the course of multiple visits to one or more doctors), and wherein the instructions cause the processor to determine a value of at least a first risk index for each medical image of the series, thereby tracking determined values of at least the first risk index for the first patient over time.

In certain embodiments, the medical images comprise a single-photon emission computerized tomography (SPECT) scan of a first patient obtained (e.g., to identify one or more hotspots) following administration to the first patient of an imaging agent comprising 1404 labeled with ^{99m}Tc, and a computed tomography (CT) scan (e.g., to identify anatomical features) of the first patient, wherein the instructions cause the processor to overlay the SPECT scan with the CT scan to create a composite image (SPECT-CT) of the first patient.

In certain embodiments, the medical images comprise a positron emission tomography (PET) scan of a first patient obtained (e.g., to identify one or more hotspots) following administration to the first patient of an imaging agent comprising [18F]DCFPyL (DCFPyL labeled with ^{18}F), and a CT scan of the first patient, wherein the instructions cause the processor to overlay the PET scan with the CT scan to create a composite image (PET-CT) of the first patient.

In certain embodiments, the medical images comprise a whole-body scan (e.g., including anterior and posterior views) of a first patient made with a gamma camera following administration to the first patient of an imaging agent comprising technetium 99m methylenediphosphonate (^{99m}Tc MDP).

In certain embodiments, the medical images comprise a composite image of a first patient, the composite image comprising a CT scan overlaid with a nuclear medicine image (e.g., a SPECT scan; e.g., a PET scan) obtained at substantially the same time as the CT scan and following administration to the first patient of an imaging agent

comprising a Prostate Specific Membrane Antigen (PSMA) binding agent comprising (e.g., labelled with) a radionuclide, and the instructions cause the processor to automatically analyze the composite image by: (a) using the composite image to geographically identify a 3D boundary for each of one or more regions of imaged tissue [e.g., organs (e.g., a prostate; e.g., a liver; e.g., lungs or a lung; e.g., lymph nodes), organ structures, sub-organs, organ regions, and/or other regions (e.g., one or more particular bones; e.g., a skeletal region of the patient), e.g., regions of interest] within the nuclear medicine image (e.g., such that portions of the nuclear medicine image falling within and/or outside of the 3D boundaries can be differentiated from each other); and (c) computing (i) a value of each of one or more risk indices and/or (ii) a risk map using the nuclear medicine image with the identified 3D boundaries of the one or more region(s).

In certain embodiments, the instructions cause the processor to, for at least one risk index of the one or more risk indices, compute the value of the risk index by: determining, for each of the one or more regions, a corresponding cancerous tissue level within the region based on intensity values of the nuclear medicine image within the 3D boundary of the region (e.g., by identifying within the nuclear medicine image, a plurality of hotspots within the 3D boundary of the region and computing a total number of and/or a total volume of the identified hotspots); and computing the value of the risk index based on the determined cancerous tissue levels within the one or more regions.

In certain embodiments, the nuclear medicine image is a SPECT scan.

In certain embodiments, the imaging agent comprises a metal chelated to the PSMA binding agent, and wherein the metal is the radionuclide [e.g., wherein the metal is a radioisotope of technetium (Tc) (e.g., wherein the metal is technetium-99m (^{99m}Tc)); e.g., wherein the metal is a radioisotope of rhenium (Re) (e.g., wherein the metal is rhenium-188 (^{188}Re); e.g., wherein the metal is rhenium-186 (^{86}Re)); e.g., wherein the metal is a radioisotope of yttrium (Y) (e.g., wherein the metal is ^{90}Y); e.g., wherein the metal is a radioisotope of lutetium (Lu)(e.g., wherein the metal is ^{177}Lu); e.g., wherein the metal is a radioisotope of gallium (Ga) (e.g., wherein the metal is ^{68}Ga; e.g., wherein the metal is ^{67}Ga); e.g., wherein the metal is a radioisotope of indium (e.g., ^{111}In); e.g., wherein the metal is a radioisotope of copper (Cu) (e.g., wherein the metal is ^{67}Cu].

In certain embodiments, the imaging agent comprises ^{99m}Tc-MIP-1404.

In certain embodiments, the nuclear medicine image is a PET scan.

In certain embodiments, the radionuclide is a radioisotope of a halogen [e.g., a radioisotope of fluorine (e.g., ^{18}F); e.g., a radioisotope of iodine (e.g., ^{123}I; e.g., ^{124}I; e.g., ^{125}I; e.g., ^{126}I; e.g., ^{131}I); e.g., a radioisotope of bromine (e.g., ^{75}Br; e.g., ^{76}Br; e.g., ^{77}Br; e.g., ^{80}Br; e.g., ^{80m}Br; e.g., ^{82}Br; e.g., ^{83}Br), e.g., a radioisotope of astatine (e.g., ^{211}At)].

In certain embodiments, the imaging agent comprises [18F]DCFPyL (DCFPyL labeled with ^{18}F).

In certain embodiments, the radionuclide is a radioisotope of gallium (Ga) (e.g., ^{68}Ga).

In certain embodiments, the medical images comprise a nuclear medicine image (e.g., a whole-body scan made with a gamma camera) of a first patient following administration to the first patient of an imaging agent comprising a radionuclide (e.g., ^{99m}Tc)(e.g., wherein the imaging agent comprises ^{99m}Tc MDP), wherein the instructions cause the processor to automatically analyze the nuclear medicine image by: (a) geographically identifying a boundary (e.g., a 2D boundary; e.g., a 3D boundary) for each of one or more regions of imaged tissue [e.g., organs (e.g., a prostate; e.g., a liver; e.g., lungs or a lung; e.g., lymph nodes), organ structures, sub-organs, organ regions, and/or other regions (e.g., one or more particular bones; e.g., a skeletal region of the patient), e.g., regions of interest] within the nuclear medicine image (e.g., such that portions of the nuclear medicine image falling within and/or outside of the boundaries can be differentiated from each other); and (c) computing (i) a value of each of one or more risk indices and/or (ii) a risk map using the nuclear medicine image with the identified boundaries of the one or more region(s).

In certain embodiments, the instructions cause the processor to, for at least one risk index of the one or more risk indices, compute the value of the risk index by: determining, for each of the one or more regions, a corresponding cancerous tissue level within the region based on intensity values of the nuclear medicine image within the boundary of the region (e.g., by identifying within the nuclear medicine image, a plurality of hotspots within the boundary of the region and computing a total number of and/or a total volume of the identified hotspots); and computing the value of the risk index based on the determined cancerous tissue levels within the one or more regions.

In certain embodiments, the system is a cloud-based system.

In certain embodiments, the processor is a processor of one or more network or Internet host servers.

In another aspect, the invention is directed to a method comprising any one or more of (i) to (v) as follows: (i) receiving and storing, by a processor of a server computing device (e.g., received over a network from a client computing device) medical images [e.g., comprising one or more of the following: targeted PET images, targeted SPECT images, computed tomography (CT) images, magnetic resonance (MR) images, ultrasound (US) images, gamma camera (i.e. scintillation camera) images, and combinations, fusions, or derivatives of any of the above] in a database [e.g., wherein the targeted PET/SPECT/gamma camera image(s) are obtained using one or more radiopharmaceuticals, e.g., [18F]DCFPyL and/or 1404 and/or a composition comprising technetium 99m, e.g., technetium 99m methylenediphosphonate (^{99m}Tc MDP), and/or wherein the medical images are obtained using non-radioactive agents or no agents], each medical image associated with a particular patient; (ii) accessing, by the processor, one or more of the medical images and/or related data associated with a particular patient from the database upon user request (e.g., following automated verification that the user is properly credentialed for receiving the requested images and/or data) for transmission to the user for display on a user computing device; (iii) automatically analyzing, by the processor, one or more of the medical images[e.g., to generate a risk map, e.g., a visual representation (e.g., 3D representation) of tissue (e.g., an organ or other part of the body) with graphical denotations (e.g., texture- or color-coding) marking regions of risk of current disease or risk of recurrence of disease, e.g., cancer, e.g., wherein the risk map is displayed as an overlay of the PET/SPECT/CT/MRI/US/combined/derived/fused image of the tissue, or is in place of the image of the tissue]; (iv) generating, by the processor, a radiologist report for a patient according to one or more of the medical images for the patient; and (v) applying, by the processor, a machine learning algorithm to update a process for automatically analyzing one or more of the medical images using accumulated image data in the database, [e.g., wherein the

automatically analyzing the one or more medical images in (iii) and/or (v) above comprises any one or more of (a) to (d) as follows: (a) automatically fusing the (e.g., PET, SPECT, CT, Mill, and/or US) image(s) of the tissue; (b) geographically identifying one or more organs, organ structures, sub-organs, organ regions, and/or other regions of the imaged tissue of the patient and production of a 3D image of the geographically identified tissue with PET, SPECT, CT, MM, and/or US data overlaid; (c) computing risk information comprising one or more risk indices, a risk field, or a risk map using data from the database, the image(s) of the tissue, and/or the 3D image in (b); and (d) using the risk information computed in (c) (e.g., and data from the database) to produce a 3D risk picture for the patient].

In certain embodiments, the medical images in the database comprise a series of medical images of a first patient taken over time (e.g., over the course of multiple visits to one or more doctors), and wherein the method comprises determining a value of at least a first risk index for each medical image of the series, thereby tracking determined values of at least the first risk index over time.

In certain embodiments, the receiving and storing of the medical images comprises repeatedly receiving and storing, over time, a plurality of medical images of the first patient, each obtained at a different time (e.g., at a different visit to one or more doctors), to obtain the series of medical images of the first patient.

In certain embodiments, the medical images comprise a single-photon emission computerized tomography (SPECT) scan of a first patient obtained (e.g., to identify one or more hotspots) following administration to the first patient of an imaging agent comprising 1404 labeled with ^{99m}Tc, and a computed tomography (CT) scan (e.g., to identify anatomical features) of the first patient, wherein the method comprises overlaying the SPECT scan with the CT scan to create a composite image (SPECT-CT) of the first patient.

In certain embodiments, the medical images comprises a positron emission tomography (PET) scan of a first patient obtained following administration to the first patient of an imaging agent comprising [18F]DCFPyL (DCFPyL labeled with ^{18}F), and a CT scan of the first patient, wherein the method comprises overlaying the PET scan with the CT scan to create a composite image (PET-CT) of the first patient.

In certain embodiments, the medical images comprise a whole-body scan (e.g., including anterior and posterior views) of a first patient made with a gamma camera following administration to the first patient of an imaging agent comprising technetium 99m methylenediphosphonate (^{99m}Tc MDP).

In certain embodiments, the medical images comprise a composite image of a first patient, the composite image comprising a CT scan overlaid with a nuclear medicine image (e.g., a SPECT scan; e.g., a PET scan) acquired at substantially the same time and following administration to the first patient of an imaging agent comprising a Prostate Specific Membrane Antigen (PSMA) binding agent comprising a radionuclide, wherein the method comprises automatically analyzing the composite image by: (a) using the composite image to geographically identify a 3D boundary for each of one or more regions of imaged tissue [e.g., organs (e.g., a prostate; e.g., a liver; e.g., lungs or a lung; e.g., lymph nodes), organ structures, sub-organs, organ regions, and/or other regions (e.g., one or more particular bones; e.g., a skeletal region of the patient), e.g., regions of interest] within the nuclear medicine image (e.g., such that portions of the nuclear medicine image falling within and/or outside of the 3D boundaries can be differentiated from each other); and (c) computing (i) a value of each of one or more risk indices and/or a (ii) risk map using the nuclear medicine image with the identified 3D boundaries of the one or more region(s).

In certain embodiments, step (c) comprises, for at least one risk index of the one or more risk indices, computing the value of the risk index by: determining, for each of the one or more regions, a corresponding cancerous tissue level within the region based on intensity values of the nuclear medicine image within the 3D boundary of the region (e.g., by identifying within the nuclear medicine image, a plurality of hotspots within the 3D boundary of the region and computing a total number of and/or a total volume of the identified hotspots); and computing the value of the risk index based on the determined cancerous tissue levels within the one or more regions.

In certain embodiments, the nuclear medicine image is a SPECT scan.

In certain embodiments, the imaging agent comprises a metal chelated to the PSMA binding agent, and wherein the metal is the radionuclide [e.g., wherein the metal is a radioisotope of technetium (Tc) (e.g., wherein the metal is technetium-99m (^{99m}Tc)); e.g., wherein the metal is a radioisotope of rhenium (Re) (e.g., wherein the metal is rhenium-188 (^{188}Re); e.g., wherein the metal is rhenium-186 (^{86}Re)); e.g., wherein the metal is a radioisotope of yttrium (Y) (e.g., wherein the metal is ^{90}Y); e.g., wherein the metal is a radioisotope of lutetium (Lu)(e.g., wherein the metal is ^{177}Lu); e.g., wherein the metal is a radioisotope of gallium (Ga) (e.g., wherein the metal is ^{68}Ga; e.g., wherein the metal is ^{67}Ga); e.g., wherein the metal is a radioisotope of indium (e.g., ^{111}In); e.g., wherein the metal is a radioisotope of copper (Cu) (e.g., wherein the metal is ^{67}Cu)].

In certain embodiments, the imaging agent comprises ^{99m}Tc-MIP-1404.

In certain embodiments, the nuclear medicine image is a PET scan.

In certain embodiments, the radionuclide is a radioisotope of a halogen [e.g., a radioisotope of fluorine (e.g., ^{18}F); e.g., a radioisotope of iodine (e.g., ^{123}I; e.g., ^{124}I; e.g., ^{125}I; e.g., ^{126}I; e.g., ^{131}I); e.g., a radioisotope of bromine (e.g., ^{75}Br; e.g., ^{76}Br; e.g., ^{77}Br; e.g., ^{80}Br; e.g., ^{80m}Br; e.g., ^{82}Br; e.g., ^{83}Br), e.g., a radioisotope of astatine (e.g., ^{211}At)].

In certain embodiments, the imaging agent comprises [18F]DCFPyL (DCFPyL labeled with ^{18}F).

In certain embodiments, the radionuclide is a radioisotope of gallium (Ga)(e.g., ^{68}Ga)

In certain embodiments, the medical images comprise a nuclear medicine image (e.g., a whole-body scan made with a gamma camera) of a first patient obtained following administration to the first patient of an imaging agent comprising a radionuclide (e.g., ^{99m}Tc)(e.g., wherein the imaging agent comprises ^{99m}Tc MDP), wherein the method comprises automatically analyzing the nuclear medicine image by: (a) geographically identifying a boundary (e.g., a 2D boundary; e.g., a 3D boundary) for each of one or more regions of imaged tissue [e.g., organs (e.g., a prostate; e.g., a liver; e.g., lungs or a lung; e.g., lymph nodes), organ structures, sub-organs, organ regions, and/or other regions (e.g., one or more particular bones; e.g., a skeletal region of the patient), e.g., regions of interest] within the nuclear medicine image (e.g., such that portions of the nuclear medicine image falling within and/or outside of the 3D boundaries can be differentiated from each other); and (c) computing (i) a value of each of one or more risk indices and/or (ii) a risk map using the nuclear medicine image with the identified boundaries of the one or more region(s).

In certain embodiments, step (c) comprises, for at least one risk index of the one or more risk indices, computing the value of the risk index by: determining, for each of the one or more regions, a corresponding cancerous tissue level within the region based on intensity values of the nuclear medicine image within the boundary of the region (e.g., by identifying within the nuclear medicine image, a plurality of hotspots within the 3D boundary of the region and computing a total number of and/or a total volume of the identified hotspots); and computing the value of the risk index based on the determined cancerous tissue levels within the one or more regions.

In certain embodiments, the processor is a processor of a cloud-based system.

In certain embodiments, the processor is a processor of one or more network or Internet host servers.

In another aspect, the invention is directed to a system comprising: a processor (e.g., of a network or Internet host server or of a portable computing device); and a memory having instructions stored thereon, wherein the instructions, when executed by the processor, cause the processor to generate and cause display of an interactive graphical user interface (GUI) element (e.g., cause display of the GUI element on a laptop computer or on a remote computing device, e.g., via a mobile app), the GUI element having user-selectable and/or user-adjustable graphical controls (e.g., slider bars, option buttons, text bars, drop-down boxes, windows, animations, and/or any other GUI widget) for selecting and/or adjusting a digital presentation of a 3D risk picture of a patient for comparison with reference images (e.g., for use in communication of results to patient as a decision-making support) caused to be displayed by the processor (e.g., wherein the reference images displayed to the user or presented for selection by the user are tunable according to one or more predetermined variables associated with the patient, e.g., patient age, time since diagnosis, prior treatment, and/or future treatment).

In certain embodiments, the interactive GUI element is produced from medical images of the patient [e.g., comprising one or more of the following: targeted PET images, targeted SPECT images, magnetic resonance (MR) images, ultrasound (US) images, gamma camera (i.e. scintillation camera) images, and combinations, fusions, or derivatives of any of the above] and/or other images or information (e.g., other images received and stored in the database of the network-based decision support system of any of the aspects and/or embodiments described herein).

In another aspect, the invention is directed to a method for tracking prostate cancer progression and treatment efficacy over time, for one or more patient(s), the method comprising: (a) repeatedly receiving and storing in a database, over time, by a processor of a computing device (e.g., a server computing device), a plurality of medical images for each of the one or more patient(s) to obtain, for each of the one or more patient(s), a series of medical images taken over time (e.g., over the course of multiple visits to one or more doctors); (b) for each of the one or more patient(s), automatically analyzing, by the processor, the series of medical images for the patient to determine values of one or more risk indices [e.g., the values of the one or more risk indices corresponding to numeric values indicative of prostate cancer state and/or progression in the patient (e.g., numeric values identifying a particular cancer stage; e.g., numeric values corresponding to a determined overall survival rate for the patient)] for each medical image of the series, thereby tracking determined values of the one or more risk indices over a course prostate cancer progression and treatment for the patient; and (c) for each of the one or more patient(s), storing, by the processor, the determined values of the one or more risk indices for the patient for further processing and/or causing, by the processor, display of a graphical representation of the determined values of the one or more risk indices for the patient (e.g., causing display of a graph showing variation in the determined values of the one or more risk indices for the patient over time).

In certain embodiments, the series of medical images for a particular patient of the one or more patient(s) comprises: (i) a first image subseries comprising one or more medical images obtained using a first nuclear imaging modality (e.g., SPECT scans; e.g., composite SPECT-CT images) each following administration to the particular patient of a first radiopharmaceutical (e.g., ^{99m}Tc-MIP-1404) (e.g., wherein the first radiopharmaceutical facilitates imaging of localized disease, e.g., localized prostate cancer); and (ii) a second image subseries comprising one or more medical images obtained using a second nuclear imaging modality (e.g., PET scans; e.g., composite PET-CT images; e.g., whole-body scans) each following administration to the particular patient of a second radiopharmaceutical (e.g., [18F]DCF-PyL; e.g., ^{99m}Tc MDP) (e.g., wherein the second radiopharmaceutical facilitates imaging of metastatic disease, e.g., metastatic prostate cancer), such that the values of the one or more risk indices determined in step (b) for the particular patient comprise a first subseries of values of a first risk index determined by automated analysis of the first image subseries and a second subseries of values of a second risk index determined by automated analysis of the second image subseries.

In certain embodiments, the medical images of first image subseries are obtained over a first period of time, when prostate cancer of the particular patient is localized (e.g., substantially localized to a prostate of the particular patient), and the medical images of the second image subseries are obtained over a second period of time, when prostate cancer of the particular patient is metastatic (e.g., having spread to regions of the patient outside of the prostate).

In certain embodiments, the first image subseries comprises one or more composite SPECT-CT image(s), each composite SPECT-CT image comprising a CT scan overlaid with a SPECT scan acquired at substantially the same time; the second image subseries comprises one or more composite PET-CT image(s), each composite PET-CT image comprising a CT scan overlaid with a PET scan acquired at substantially the same time; and step (b) comprises: automatically analyzing each of the one or more composite SPECT-CT images by: using the composite SPECT-CT image to geographically identify a 3D boundary of a prostate region (e.g., corresponding to a prostate of the patient) within the SPECT scan of the composite SPECT-CT image (e.g., such that portions of the nuclear medicine image falling within and/or outside of the 3D boundary of the prostate region can be differentiated from each other); and computing a value of the first risk index using the SPECT scan with the identified 3D boundary of the prostate region (e.g., computed based on a region of the SPECT scan corresponding to the identified 3D boundary of the prostate region); and automatically analyzing each of the one or more composite PET-CT images by: using the composite PET-CT image to geographically identify a 3D boundary of one or more metastatic regions within the PET scan of the composite PET-CT image, the one or metastatic regions including regions corresponding to patient tissue locations outside of the prostate [e.g., organs (e.g., a prostate; e.g., a liver; e.g., lungs or a lung; e.g., lymph nodes), organ structures, sub-

organs, organ regions, and/or other regions (e.g., one or more particular bones; e.g., a skeletal region corresponding to the patient's skeleton), e.g., regions of interest] (e.g., such that portions of the PET imaging scan falling within and/or outside of the 3D boundaries of the one or more metastatic region(s) can be differentiated from each other); and computing a value of the second risk index using the PET scan with the identified 3D boundaries of the one or more metastatic region(s).

In certain embodiments, the first image subseries comprises one or more composite SPECT-CT image(s), each composite SPECT-CT image comprising a CT scan overlaid with a SPECT scan acquired at substantially the same time; the second image subseries comprises one or more whole-body scan(s); and step (b) comprises: automatically analyzing each of the one or more composite SPECT-CT images by: using the composite SPECT-CT image to geographically identify a 3D boundary of a prostate region (e.g., corresponding to a prostate of the patient) within the SPECT scan of the composite SPECT-CT image (e.g., such that portions of the nuclear medicine image falling within and/or outside of the 3D boundary of the prostate region can be differentiated from each other); and computing a value of the first risk index using the SPECT scan with the identified 3D boundary of the prostate region (e.g., computed based on a region of the SPECT scan corresponding to the identified 3D boundary of the prostate region); and automatically analyzing each of the one or more whole-body scan(s) by: geographically identifying a boundary of one or more metastatic regions within the whole-body scan, the one or metastatic regions including regions corresponding to patient tissue locations outside of the prostate [(e.g., one or more particular bones; e.g., a skeletal region corresponding to the patient's skeleton), e.g., regions of interest] (e.g., such that portions of the whole-body scan falling within and/or outside of the boundaries of the one or more metastatic region(s) can be differentiated from each other); and computing a value of the second risk index using the PET scan with the identified 3D boundaries of the one or more metastatic region(s).

In another aspect, the invention is directed to a system for tracking prostate cancer progression and treatment efficacy over time, for one or more patient(s), the system comprising: a processor (e.g., of a network or Internet host server); and a memory having instructions stored thereon, wherein the instructions, when executed by the processor, cause the processor to: (a) repeatedly receive and store in a database, over time, a plurality of medical images for each of the one or more patient(s) to obtain, for each of the one or more patient(s), a series of medical images taken over time (e.g., over the course of multiple visits to one or more doctors); (b) for each of the one or more patient(s), automatically analyze the series of medical images for the patient to determine values of one or more risk indices [e.g., the values of the one or more risk indices corresponding to numeric values indicative of prostate cancer state and/or progression in the patient (e.g., numeric values identifying a particular cancer stage; e.g., numeric values corresponding to a determined overall survival rate for the patient)] for each medical image of the series, thereby tracking determined values of the one or more risk indices over a course prostate cancer progression and treatment for the patient; and (c) for each of the one or more patient(s), store the determined values of the one or more risk indices for the patient for further processing and/or cause display of a graphical representation of the determined values of the one or more risk indices for the patient (e.g., causing display of a graph showing variation in the determined values of the one or more risk indices for the patient over time).

In certain embodiments, the series of medical images for a particular patient of the one or more patient(s) comprises: (i) a first image subseries comprising one or more medical images obtained using a first nuclear imaging modality (e.g., SPECT scans; e.g., composite SPECT-CT images) each following administration to the particular patient of a first radiopharmaceutical (e.g., ^{99m}Tc-MIP-1404) (e.g., wherein the first radiopharmaceutical facilitates imaging of localized disease, e.g., localized prostate cancer); and (ii) a second image subseries comprising one or more medical images obtained using a second nuclear imaging modality (e.g., PET scans; e.g., composite PET-CT images; e.g., whole-body scans) each following administration to the particular patient of a second radiopharmaceutical (e.g., [18F]DCF-PyL; e.g., ^{99m}Tc MDP) (e.g., wherein the second radiopharmaceutical facilitates imaging of metastatic disease, e.g., metastatic prostate cancer), such that the values of the one or more risk indices determined in step (b) for the particular patient comprise a first subseries of values of a first risk index determined by automated analysis of the first image subseries and a second subseries of values of a second risk index determined by automated analysis of the second image subseries.

In certain embodiments, the medical images of first image subseries are obtained over a first period of time, when prostate cancer of the particular patient is localized (e.g., substantially localized to a prostate of the particular patient), and the medical images of the second image subseries are obtained over a second period of time, when prostate cancer of the particular patient is metastatic (e.g., having spread to regions of the patient outside of the prostate).

In certain embodiments, the first image subseries comprises one or more composite SPECT-CT image(s), each composite SPECT-CT image comprising a CT scan overlaid with a SPECT scan acquired at substantially the same time; the second image subseries comprises one or more composite PET-CT image(s), each composite PET-CT image comprising a CT scan overlaid with a PET scan acquired at substantially the same time; and the instructions cause the processor to, at step (b): automatically analyze each of the one or more composite SPECT-CT images by: using the composite SPECT-CT image to geographically identify a 3D boundary of a prostate region (e.g., corresponding to a prostate of the patient) within the SPECT scan of the composite SPECT-CT image (e.g., such that portions of the nuclear medicine image falling within and/or outside of the 3D boundary of the prostate region can be differentiated from each other); and computing a value of the first risk index using the SPECT scan with the identified 3D boundary of the prostate region (e.g., computed based on a region of the SPECT scan corresponding to the identified 3D boundary of the prostate region); and automatically analyze each of the one or more composite PET-CT images by: using the composite PET-CT image to geographically identify a 3D boundary of one or more metastatic regions within the PET scan of the composite PET-CT image, the one or metastatic regions including regions corresponding to patient tissue locations outside of the prostate [e.g., organs (e.g., a prostate; e.g., a liver; e.g., lungs or a lung; e.g., lymph nodes), organ structures, sub-organs, organ regions, and/or other regions (e.g., one or more particular bones; e.g., a skeletal region corresponding to the patient's skeleton), e.g., regions of interest] (e.g., such that portions of the PET imaging scan falling within and/or outside of the 3D boundaries of the one or more metastatic region(s) can be differentiated from each other); and computing a value of the second risk index using the PET scan with the identified 3D boundaries of the one or more metastatic region(s).

In certain embodiments, the first image subseries comprises one or more composite SPECT-CT image(s), each composite SPECT-CT image comprising a CT scan overlaid with a SPECT scan acquired at substantially the same time; the second image subseries comprises one or more whole-body scan(s); and the instructions cause the processor to, at

step (b): automatically analyze each of the one or more composite SPECT-CT images by: using the composite SPECT-CT image to geographically identify a 3D boundary of a prostate region (e.g., corresponding to a prostate of the patient) within the SPECT scan of the composite SPECT-CT image (e.g., such that portions of the nuclear medicine image falling within and/or outside of the 3D boundary of the prostate region can be differentiated from each other); and computing a value of the first risk index using the SPECT scan with the identified 3D boundary of the prostate region (e.g., computed based on a region of the SPECT scan corresponding to the identified 3D boundary of the prostate region); and automatically analyze each of the one or more whole-body scan(s) by: geographically identifying a boundary of one or more metastatic regions within the whole-body scan, the one or metastatic regions including regions corresponding to patient tissue locations outside of the prostate [(e.g., one or more particular bones; e.g., a skeletal region corresponding to the patient's skeleton), e.g., regions of interest] (e.g., such that portions of the whole-body scan falling within and/or outside of the boundaries of the one or more metastatic region(s) can be differentiated from each other); and computing a value of the second risk index using the PET scan with the identified 3D boundaries of the one or more metastatic region(s).

Embodiments described with respect to one aspect of the invention may be, applied to another aspect of the invention (e.g., features of embodiments described with respect to one independent claim, e.g., a method claim, are contemplated to be applicable to other embodiments of other independent claims, e.g., a system claim, and vice versa).

BRIEF DESCRIPTION OF THE DRAWINGS

The foregoing and other objects, aspects, features, and advantages of the present disclosure will become more apparent and better understood by referring to the following description taken in conjunction with the accompanying drawings, in which:

FIG. **1** is a screenshot of a graphical user interface (GUI) showing mobile app icons for three cloud-based services, according to illustrative embodiments.

FIG. **2** is a schematic showing the relationship between a platform and a computing device (e.g., personal computer or mobile computing device, e.g., smart phone) running an application, according to illustrative embodiments of the invention.

FIG. **3** is a screenshot of a GUI window in the BSI Cloud application (displayed to a user) that allows a user to enter information about a patient and upload and/or access medical images for the patient, e.g., series of images obtained over a period of time, according to an illustrative embodiment.

FIG. **4** is a screenshot of a GUI window in the BSI Cloud application showing representative full body gamma camera images showing hotspots automatically identified by the system, with corresponding overall computed BSI values for a particular image set obtained at a given time, according to an illustrative embodiment.

FIG. **5** is a screenshot of a GUI window in the BSI Cloud application showing an automatically or semi-automatically generated radiologist report, which can be signed and dated by a radiologist, according to an illustrative embodiment.

FIG. **6** is a block diagram showing a set of functionalities offered by the a cloud-based platform and supported graphical user interface (GUI) decision-making tools described herein, according to an illustrative embodiment.

FIG. **7** is a block diagram of an exemplary cloud computing environment, used in certain embodiments.

FIG. **8** is a block diagram of an example computing device and an example mobile computing device used in certain embodiments.

FIG. **9** is block diagram of an example architecture for implementing the cloud based platform described herein, according to an illustrative embodiment.

FIG. **10** is a schematic showing stages of prostate cancer progression, along with various therapies and diagnostic imaging modalities appropriate for various disease states, according to an illustrative embodiment.

FIG. **11** is a block flow diagram of a process for tracking prostate cancer progression and treatment efficacy over time, according to an illustrative embodiment.

The features and advantages of the present disclosure will become more apparent from the detailed description set forth below when taken in conjunction with the drawings, in which like reference characters identify corresponding elements throughout. In the drawings, like reference numbers generally indicate identical, functionally similar, and/or structurally similar elements.

DETAILED DESCRIPTION

It is contemplated that systems, devices, methods, and processes of the claimed invention encompass variations and adaptations developed using information from the embodiments described herein. Adaptation and/or modification of the systems, devices, methods, and processes described herein may be performed by those of ordinary skill in the relevant art.

Throughout the description, where articles, devices, and systems are described as having, including, or comprising specific components, or where processes and methods are described as having, including, or comprising specific steps, it is contemplated that, additionally, there are articles, devices, and systems of the present invention that consist essentially of, or consist of, the recited components, and that there are processes and methods according to the present invention that consist essentially of, or consist of, the recited processing steps.

It should be understood that the order of steps or order for performing certain action is immaterial so long as the invention remains operable. Moreover, two or more steps or actions may be conducted simultaneously.

The mention herein of any publication, for example, in the Background section, is not an admission that the publication serves as prior art with respect to any of the claims presented herein. The Background section is presented for purposes of clarity and is not meant as a description of prior art with respect to any claim.

Headers are provided for the convenience of the reader—the presence and/or placement of a header is not intended to limit the scope of the subject matter described herein.

A. Medical Imaging Modalities, Associated Radiopharmaceuticals, and Computed Risk Indices

FIG. **1** shows mobile app icons **100** for three cloud-based services, according to illustrative embodiments. As described in the following, the cloud-based services of the platform described herein provide for processing and analysis of medical images in a fully automated fashion and/or in combination with a user interaction (e.g., in a semi-automated fashion). The medical images include nuclear medicine images, obtained using a nuclear imaging modality such as whole-body scans with a gamma camera, Positron Emission Tomography (PET) scans, and Single-Photon Emission Tomography (SPECT) scans.

In certain embodiments, nuclear medicine images use imaging agents comprising radiopharmaceuticals. Nuclear medicine images are obtained following administration of a radiopharmaceutical to a patient, and provide information

regarding the distribution of the radiopharmaceutical within the patient. Radiopharmaceuticals are compounds that comprise a radionuclide.

As used herein, "radionuclide" refers to a moiety comprising a radioactive isotope of at least one element. Exemplary suitable radionuclides include but are not limited to those described herein. In some embodiments, a radionuclide is one used in positron emission tomography (PET). In some embodiments, a radionuclide is one used in single-photon emission computed tomography (SPECT). In some embodiments, a non-limiting list of radionuclides includes ^{99m}Tc, ^{64}Cu, ^{67}Ga, ^{68}Ga, ^{186}Re, ^{188}Re, ^{1535}m, ^{177}Lu, ^{67}Cu, ^{123}I, ^{124}I, ^{125}I, ^{126}I, ^{131}I, ^{11}C, ^{13}N, ^{15}O, ^{18}F, ^{153}Sm, ^{166}Ho, ^{177}Lu, ^{149}Pm, ^{90}Y, ^{213}Bi, ^{103}Pd, ^{109}Pd, ^{159}Gd, ^{140}La, ^{198}Au, ^{199}Au, ^{169}Yb, ^{175}Yb, ^{165}Dy, ^{166}Dy, ^{105}Rh, ^{111}Ag, ^{89}Zr, ^{225}Ac, ^{82}Rb, ^{75}Br, ^{76}Br, ^{77}Br, ^{80}Br, ^{80m}Br, ^{82}Br, ^{83}Br, ^{211}At and ^{192}Ir.

As used herein, the term "radiopharmaceutical" refers to a compound comprising a radionuclide. In certain embodiments, radiopharmaceuticals are used for diagnostic and/or therapeutic purposes. In certain embodiments, radiopharmaceuticals include small molecules that are labeled with one or more radionuclide(s), antibodies that are labeled with one or more radionuclide(s), and antigen-binding portions of antibodies that are labeled with one or more radionuclide(s).

Nuclear medicine images (e.g., PET scans; e.g., SPECT scans; e.g., whole-body scans; e.g. composite PET-CT images; e.g., composite SPECT-CT images) detect radiation emitted from the radionuclides of radiopharmaceuticals to form an image. The distribution of a particular radiopharmaceutical within a patient may be determined by biological mechanisms such as blood flow or perfusion, as well as by specific enzymatic or receptor binding interactions. Different radiopharmaceuticals may be designed to take advantage of different biological mechanisms and/or particular specific enzymatic or receptor binding interactions and thus, when administered to a patient, selectively concentrate within particular types of tissue and/or regions within the patient. Greater amounts of radiation are emitted from regions within the patient that have higher concentrations of radiopharmaceutical than other regions, such that these regions appear brighter in nuclear medicine images. Accordingly, intensity variations within a nuclear medicine image can be used to map the distribution of radiopharmaceutical within the patient. This mapped distribution of radiopharmaceutical within the patient can be used to, for example, infer the presence of cancerous tissue within various regions of the patient's body.

For example, upon administration to a patient, technetium 99m methylenediphosphonate (^{99m}Tc MDP) selectively accumulates within the skeletal region of the patient, in particular at sites with abnormal osteogenesis associated with malignant bone lesions. The selective concentration of radiopharmaceutical at these sites produces identifiable hotspots—localized regions of high intensity in nuclear medicine images. Accordingly, presence of malignant bone lesions associated with metastatic prostate cancer can be inferred by identifying such hotspots within a whole-body scan of the patient. As described in the following, risk indices that correlate with patient overall survival and other prognostic metrics indicative of disease state, progression, treatment efficacy, and the like, can be computed based on automated analysis of intensity variations in whole-body scans obtained following administration of ^{99m}Tc MDP to a patient. In certain embodiments, other radiopharmaceuticals can also be used in a similar fashion to ^{99m}Tc MDP.

In certain embodiments, the particular radiopharmaceutical used depends on the particular nuclear medicine imaging modality used. For example ^{18}F sodium fluoride (NaF) also accumulates in bone lesions, similar to ^{99m}Tc MDP, but can be used with PET imaging. In certain embodiments, PET imaging may also utilize a radioactive form of the vitamin choline, which is readily absorbed by prostate cancer cells.

In certain embodiments, radiopharmaceuticals that selectively bind to particular proteins or receptors of interest—particularly those whose expression is increased in cancerous tissue may be used. Such proteins or receptors of interest include, but are not limited to tumor antigens, such as CEA, which is expressed in colorectal carcinomas, Her2/neu, which is expressed in multiple cancers, BRCA 1 and BRCA 2, expressed in breast and ovarian cancers; and TRP-1 and -2, expressed in melanoma.

For example, human prostate-specific membrane antigen (PSMA) is upregulated in prostate cancer, including metastatic disease. PSMA is expressed by virtually all prostate cancers and its expression is further increased in poorly differentiated, metastatic and hormone refractory carcinomas. Accordingly, radiopharmaceuticals corresponding to PSMA binding agents (e.g., compounds that a high affinity to PSMA) labelled with one or more radionuclide(s) can be used to obtain nuclear medicine images of a patient from which the presence and/or state of prostate cancer within a variety of regions (e.g., including, but not limited to skeletal regions) of the patient can be assessed. In certain embodiments, nuclear medicine images obtained using PSMA binding agents are used to identify the presence of cancerous tissue within the prostate, when the disease is in a localized state. In certain embodiments, nuclear medicine images obtained using radiopharmaceuticals comprising PSMA binding agents are used to identify the presence of cancerous tissue within a variety of regions that include not only the prostate, but also other organs and tissue regions such as lungs, lymph nodes, and bones, as is relevant when the disease is metastatic.

In particular, upon administration to a patient, radionuclide labelled PSMA binding agents selectively accumulate within cancerous tissue, based on their affinity to PSMA. In a similar manner to that described above with regard to ^{99m}Tc MDP, the selective concentration of radionuclide labelled PSMA binding agents at particular sites within the patient produces detectable hotspots in nuclear medicine images. As PSMA binding agents concentrate within a variety of cancerous tissues and regions of the body expressing PSMA, localized cancer within a prostate of the patient and/or metastatic cancer in various regions of the patient's body can be detected, and evaluated. As described in the following, risk indices that correlate with patient overall survival and other prognostic metrics indicative of disease state, progression, treatment efficacy, and the like, can be computed based on automated analysis of intensity variations in nuclear medicine images obtained following administration of a PSMA binding agent radiopharmaceutical to a patient.

A variety of radionuclide labelled PSMA binding agents may be used as radiopharmaceutical imaging agents for nuclear medicine imaging to detect and evaluate prostate cancer. In certain embodiments, the particular radionuclide labelled PSMA binding agent that is used depends on factors such as the particular imaging modality (e.g., PET; e.g., SPECT) and the particular regions (e.g., organs) of the patient to be imaged. For example, certain radionuclide labelled PSMA binding agents are suited for PET imaging, while others are suited for SPECT imaging. For example, certain radionuclide labelled PSMA binding agents facilitate imaging a prostate of the patient, and are used primarily when the disease is localized, while others facilitate imaging organs and regions throughout the patient's body, and are useful for evaluating metastatic prostate cancer.

A variety of PSMA binding agents and radionuclide labelled versions thereof are described in U.S. Pat. Nos. 8,778,305, 8,211,401, and 8,962,799, each of which are incorporated herein by reference in their entireties.

A.i PET Imaging Radionuclide Labelled PSMA Binding Agents

In certain embodiments, the radionuclide labelled PSMA binding agent is a radionuclide labelled PSMA binding agent appropriate for PET imaging.

In certain embodiments, the radionuclide labelled PSMA binding agent comprises [18F]DCFPyL (also referred to as PyL™; also referred to as DCFPyL-18F):

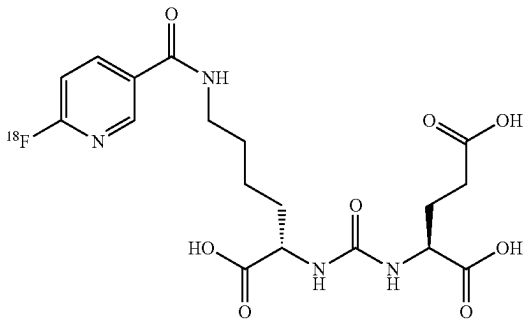

[18F]DCFPyL,

or a pharmaceutically acceptable salt thereof.

In certain embodiments, the radionuclide labelled PSMA binding agent comprises [18F]DCFBC:

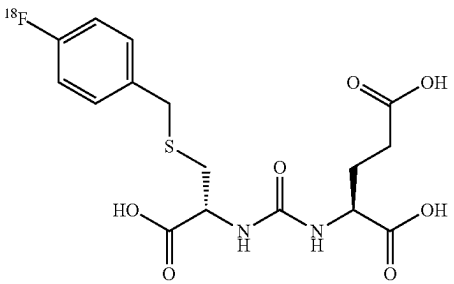

[18F]DCFBC,

or a pharmaceutically acceptable salt thereof.

In certain embodiments, the radionuclide labelled PSMA binding agent comprises ^{68}Ga-PSMA-HBED-CC (also referred to as ^{68}Ga-PSMA-11):

^{68}Ga-PSMA-HBED-CC,

or a pharmaceutically acceptable salt thereof.

In certain embodiments, the radionuclide labelled PSMA binding agent comprises PSMA-617:

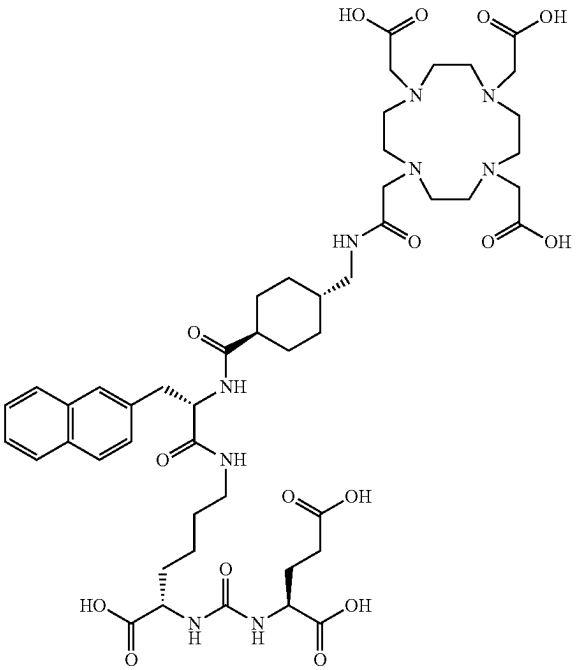

PSMA-617,

or a pharmaceutically acceptable salt thereof. In certain embodiments, the radionuclide labelled PSMA binding agent comprises ^{68}Ga-PSMA-617, which is PSMA-617 labelled with ^{68}Ga, or a pharmaceutically acceptable salt thereof. In certain embodiments, the radionuclide labelled PSMA binding agent comprises ^{177}Lu-PSMA-617, which is PSMA-617 labelled with ^{177}Lu, or a pharmaceutically acceptable salt thereof.

In certain embodiments, the radionuclide labelled PSMA binding agent comprises PSMA-I&T:

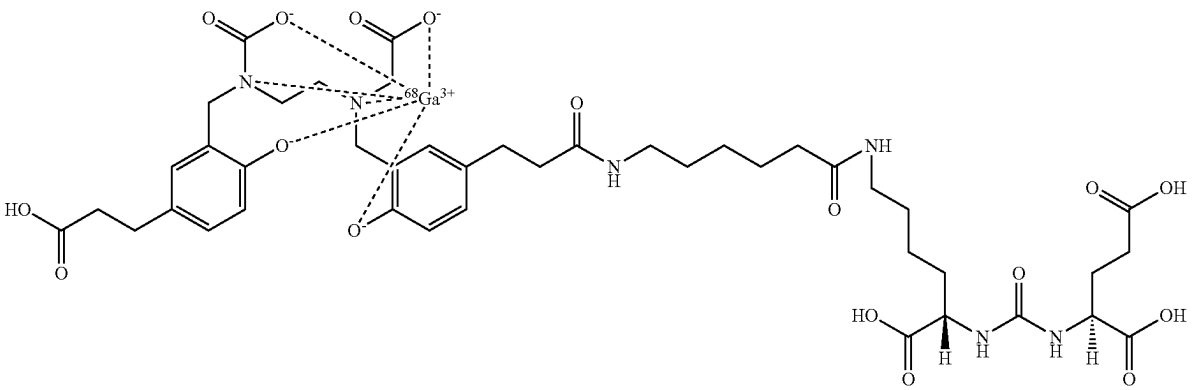

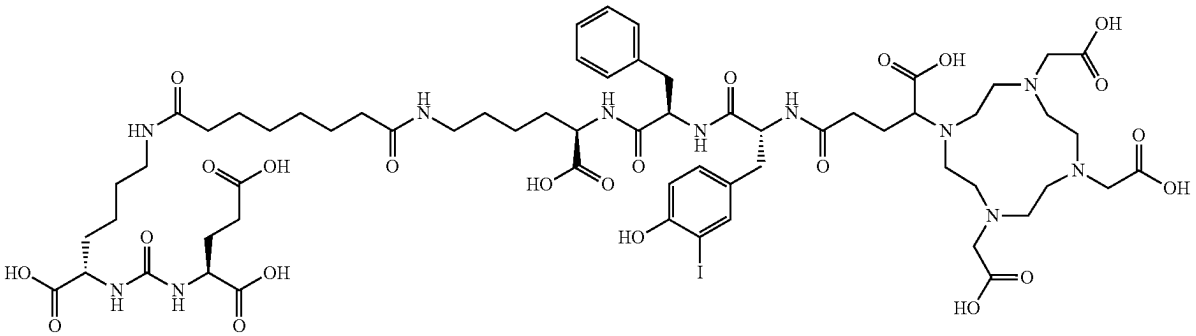

PSMA-I&T,

or a pharmaceutically acceptable salt thereof. In certain embodiments, the radionuclide labelled PSMA binding agent comprises ^{68}Ga-PSMA-I&T, which is PSMA-I&T labelled with ^{68}Ga, or a pharmaceutically acceptable salt thereof.

In certain embodiments, the radionuclide labelled PSMA binding agent comprises PSMA-1007:

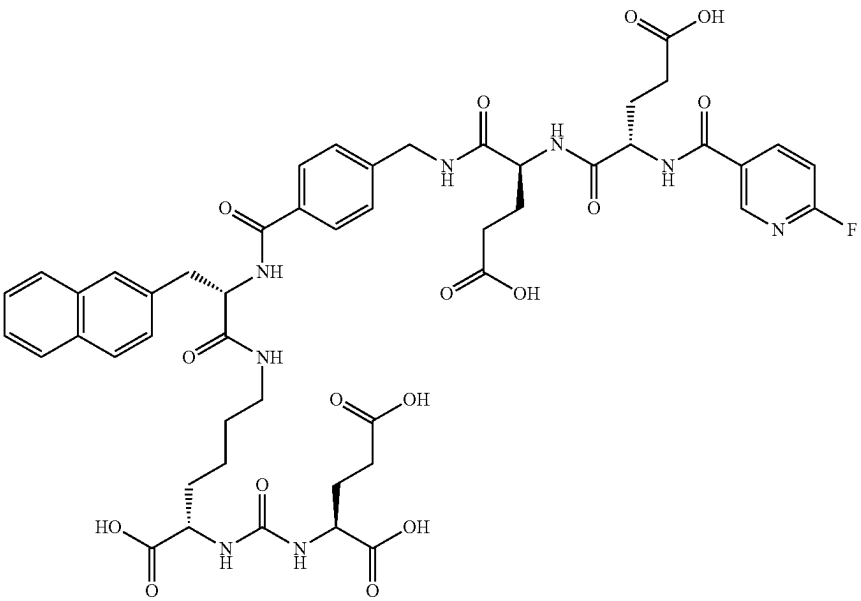

PSMA-1007,

or a pharmaceutically acceptable salt thereof. In certain embodiments, the radionuclide labelled PSMA binding agent comprises ^{18}F-PSMA-1007, which is PSMA-1007 labelled with ^{18}F, or a pharmaceutically acceptable salt thereof.

A.ii SPECT Imaging Radionuclide Labelled PSMA Binding Agents

In certain embodiments, the radionuclide labelled PSMA binding agent is a radionuclide labelled PSMA binding agent appropriate for SPECT imaging.

In certain embodiments, the radionuclide labelled PSMA binding agent comprises 1404 (also referred to as MIP-1404):

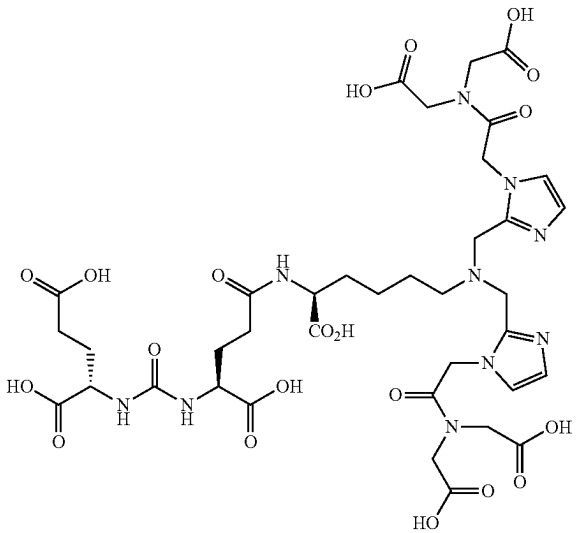

1404,

or a pharmaceutically acceptable salt thereof.

In certain embodiments, the radionuclide labelled PSMA binding agent comprises 1405 (also referred to as MIP-1405):

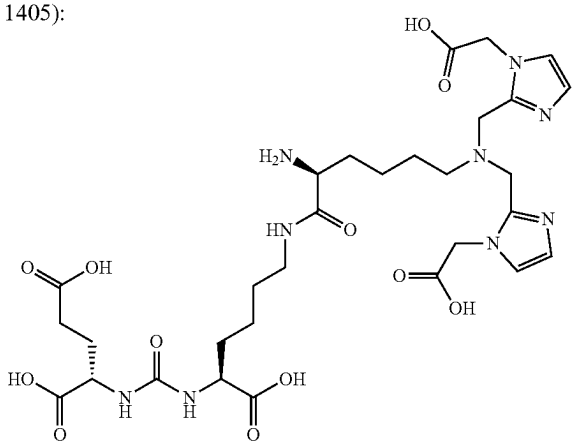

1405,

or a pharmaceutically acceptable salt thereof.

In certain embodiments, the radionuclide labelled PSMA binding agent comprises 1427 (also referred to as MIP-1427):

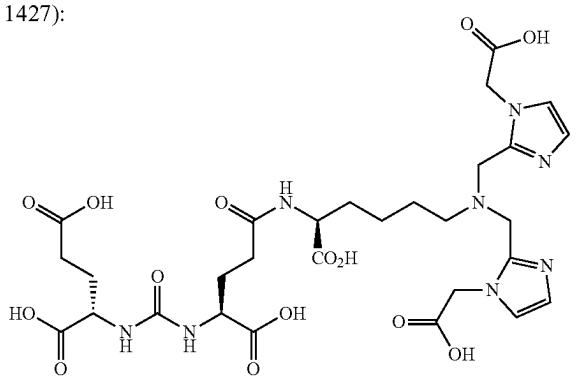

1427,

or a pharmaceutically acceptable salt thereof.

In certain embodiments, the radionuclide labelled PSMA binding agent comprises 1428 (also referred to as MIP-1428):

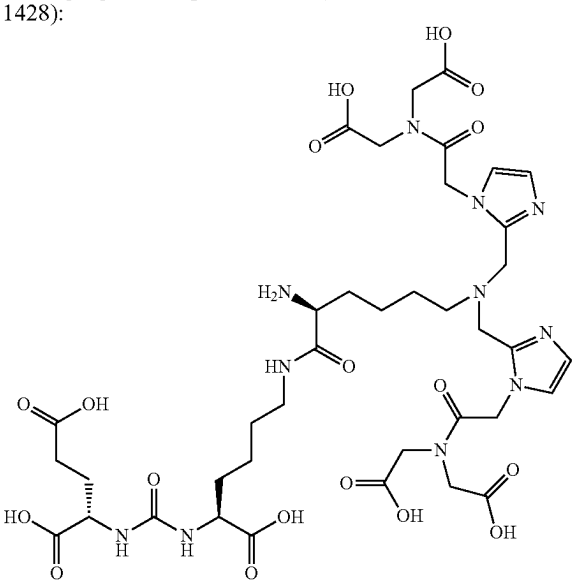

1428,

or a pharmaceutically acceptable salt thereof.

In certain embodiments, the PSMA binding agent is labelled with a radionuclide by chelating it to a radioisotope of a metal [e.g., a radioisotope of technetium (Tc) (e.g., technetium-99m (^{99m}Tc)); e.g., a radioisotope of rhenium (Re) (e.g., rhenium-188 (^{188}Re); e.g., rhenium-186 (^{186}Re)); e.g., a radioisotope of yttrium (Y) (e.g., ^{90}Y); e.g., a radioisotope of lutetium (Lu) (e.g., ^{177}Lu); e.g., a radioisotope of gallium (Ga) (e.g., ^{68}Ga; e.g., ^{67}Ga); e.g., a radioisotope of indium (e.g., ^{111}In); e.g., a radioisotope of copper (Cu) (e.g., ^{67}Cu)].

In certain embodiments, **1404** is labelled with a radionuclide (e.g., chelated to a radioisotope of a metal). In certain embodiments, the radionuclide labelled PSMA binding agent comprises ^{99m}Tc-MIP-1404, which is 1404 labelled with (e.g., chelated to) ^{99m}Tc:

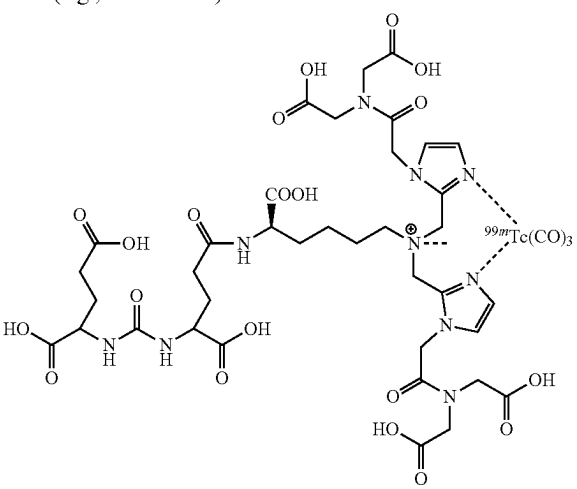

^{99m}Tc-MIP-1404,

or a pharmaceutically acceptable salt thereof. In certain embodiments, 1404 may be chelated to other metal radioisotopes [e.g., a radioisotope of rhenium (Re) (e.g., rhenium-188 (^{188}Re); e.g., rhenium-186 (^{186}Re)); e.g., a radioisotope of yttrium (Y) (e.g., ^{90}Y); e.g., a radioisotope of lutetium

(Lu)(e.g., ^{177}Lu); e.g., a radioisotope of gallium (Ga) (e.g., ^{68}Ga; e.g., ^{67}Ga); e.g., a radioisotope of indium (e.g., ^{111}In); e.g., a radioisotope of copper (Cu) (e.g., ^{67}Cu)] to form a compound having a structure similar to the structure shown above for ^{99m}Tc-MIP-1404, with the other metal radioisotope substituted for ^{99m}Tc.

In certain embodiments, **1405** is labelled with a radionuclide (e.g., chelated to a radioisotope of a metal). In certain embodiments, the radionuclide labelled PSMA binding agent comprises ^{99m}Tc-MIP-1405, which is 1405 labelled with (e.g., chelated to)^{99m}Tc:

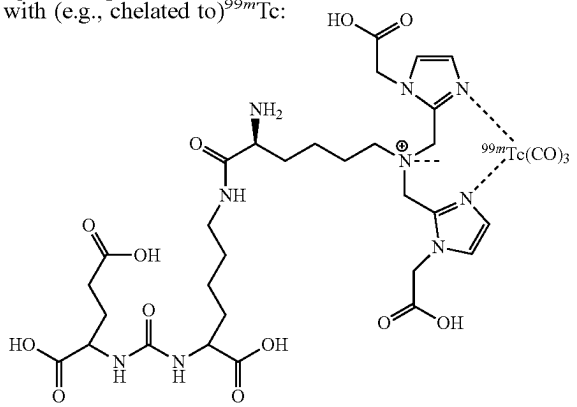

^{99m}Tc-MIP-1405,

or a pharmaceutically acceptable salt thereof. In certain embodiments, 1405 may be chelated to other metal radioisotopes [e.g., a radioisotope of rhenium (Re) (e.g., rhenium-188 (^{188}Re); e.g., rhenium-186 (^{186}Re)); e.g., a radioisotope of yttrium (Y) (e.g., ^{90}Y); e.g., a radioisotope of lutetium (Lu) (e.g., ^{177}Lu); e.g., a radioisotope of gallium (Ga) (e.g., ^{68}Ga; e.g., ^{67}Ga); e.g., a radioisotope of indium (e.g., ^{111}In); e.g., a radioisotope of copper (Cu) (e.g., ^{67}Cu)] to form a compound having a structure similar to the structure shown above for ^{99m}Tc-MIP-1405, with the other metal radioisotope substituted for ^{99m}Tc.

In certain embodiments, 1427 is labelled with (e.g., chelated to) a radioisotope of a metal, to form a compound according to the formula below:

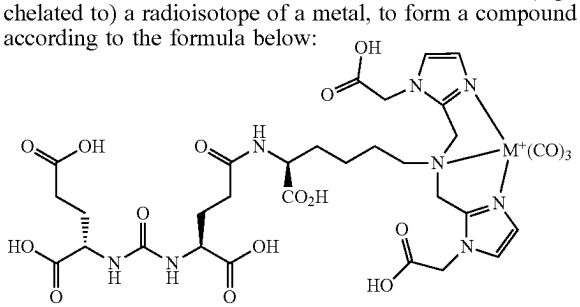

1427 chelated to a metal,

or a pharmaceutically acceptable salt thereof, wherein M is a metal radioisotope [e.g., a radioisotope of technetium (Tc) (e.g., technetium-99m (^{99m}Tc)); e.g., a radioisotope of rhenium (Re) (e.g., rhenium-188 (^{188}Re); e.g., rhenium-186 (^{186}Re)); e.g., a radioisotope of yttrium (Y) (e.g., ^{90}Y); e.g., a radioisotope of lutetium (Lu)(e.g., ^{177}Lu); e.g., a radioisotope of gallium (Ga) (e.g., ^{68}Ga; e.g., ^{67}Ga); e.g., a radioisotope of indium (e.g., In); e.g., a radioisotope of copper (Cu) (e.g., ^{67}Cu)] with which 1427 is labelled.

In certain embodiments, 1428 is labelled with (e.g., chelated to) a radioisotope of a metal, to form a compound according to the formula below:

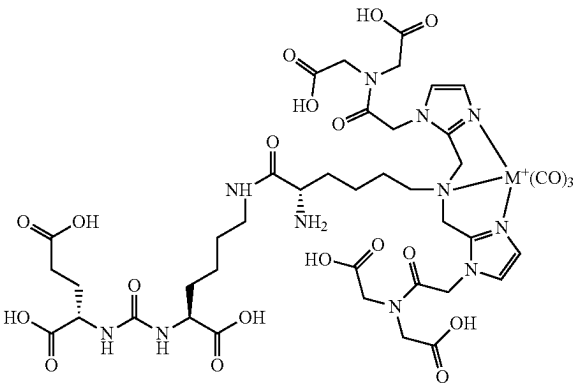

1428 chelated to a metal,

or a pharmaceutically acceptable salt thereof, wherein M is a metal radioisotope [e.g., a radioisotope of technetium (Tc) (e.g., technetium-99m (^{99m}Tc)); e.g., a radioisotope of rhenium (Re) (e.g., rhenium-188 (^{188}Re); e.g., rhenium-186 (^{186}Re)); e.g., a radioisotope of yttrium (Y) (e.g., ^{90}Y); e.g., a radioisotope of lutetium (Lu)(e.g., ^{177}Lu); e.g., a radioisotope of gallium (Ga) (e.g., ^{68}Ga; e.g., ^{67}Ga); e.g., a radioisotope of indium (e.g., In); e.g., a radioisotope of copper (Cu) (e.g., ^{67}Cu)] with which 1428 is labelled.

In certain embodiments, the radionuclide labelled PSMA binding agent comprises PSMA I&S:

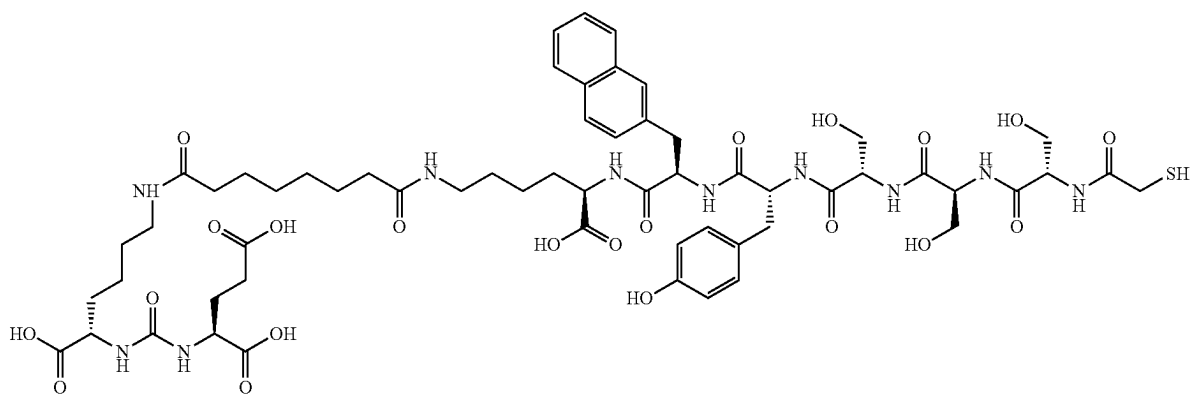

MIM Ex1039
MIM Software Inc. v. Progenics Pharmaceuticals, Inc.
Trial IPR2025-00630

PSMA I& S,

or a pharmaceutically acceptable salt thereof. In certain embodiments, the radionuclide labelled PSMA binding agent comprises ^{99m}Tc-PSMA I&S, which is PSMA I&S labelled with ^{99m}Tc, or a pharmaceutically acceptable salt thereof.

A.iii Whole-Body Bone Scans

Turning to FIG. **1**, BSI Cloud **130** refers to a cloud-based decision support system that implements BSI values. BSI refers to bone scan index, which is a value computed from a method for detecting skeletal lesions from whole-body scanning (and anterior and posterior views) with a gamma camera following administration of the radionuclide technetium 99m methylenediphosphonate (^{99m}Tc MDP). Further explanation of BSI is provided, for example, in U.S. Pat. No. 8,855,387, which is incorporated herein by reference in its entirety, as well as in U.S. patent application Ser. No. 15/282,422, filed Sep. 30, 2016, which is incorporated herein by reference in its entirety.

In particular, BSI is computed from whole-body scans by segmenting anterior and posterior views of the whole-body scan of the patient to geographically identify boundaries of regions within the views that correspond to various portions of the patient's skeleton. Segmentation of the patient's skeleton can be performed using a variety of approaches, such as the Active Shape Model-based approach and the atlas image registration approach (which registers the anterior and posterior views of a whole body scan with reference anterior and posterior views of a reference whole body scan that have already been segmented (referred to as an atlas image)) described in U.S. Pat. No. 8,855,387. Other approaches, based on machine learning techniques (e.g., artificial neural networks (ANNs); e.g., convolutional neural networks (CNNs)) may also be used.

The BSI value is computed based on the intensity values of whole-body scan within the identified boundaries of the various skeletal regions. As discussed above, hotspots that correspond to localized regions of high intensity within the views (anterior and/or posterior views) of the whole-body scan can be detected. Hotspots may be detected and/or classified as corresponding to cancerous lesions (e.g., metastases) using a variety of approaches, including, as described in U.S. Pat. No. 8,855,387, machine learning techniques such as ANNs.

Hotspots corresponding to cancerous tissue lesions within the patient's skeleton, once detected, can be used to determine a risk index that provides a measure of disease state for the patient. For example, cancerous tissue levels within one or more regions, such as particular bones and/or the overall skeletal region, can be determined based on features of detected hotspots (e.g., detected hotspots classified as metastases). For example, a cancerous tissue level within a region (e.g., a particular bone; e.g., the overall skeletal region) may be determined based on (e.g., as a function of) a total number of detected hotspots within the region, a total volume of detected hotspots within the region, an average intensity of detected hotspots, a maximal intensity of detected hotspots, and the like, as well as combinations thereof. Properties of the one or more regions, such as their area or volume may also be used. For example, a total number and/or total volume of detected hotspots may be normalized (e.g., divided) by a volume and/or area of the region in which they are detected. A risk index may be determined based on the determined cancerous tissue levels within one or more regions, directly, e.g., as the cancerous tissue level within a single region, or determined from cancerous tissue levels in multiple regions (e.g., as an average; e.g., as a scaled sum; e.g., as a ratio; etc.), or even using machine learning approaches.

For example, the BSI value is a risk index that is a numeric value that quantifies the fraction of the total skeleton of the patient that is involved by cancerous tissue (e.g., tumors), based on the detected hotspots. The BSI value can be compared between different patients, and used as an objective measure of disease state and risk for a particular patient. Notably, since BSI is computed in an automated fashion, variability due to human factors such as radiologist interpretation of images is avoided.

Moreover, a variety of actionable information can be obtained from a patient's BSI value. For example, BSI can be correlated with prognostic values that provide a measure of disease state, progression, life expectancy (e.g., overall survival), treatment efficacy, and the like for the patient. Accordingly, a patient's BSI value can be used and tracked over time (e.g., over the course of multiple visits to one or more doctors) to provide them or their physician with an objective metric of what state their cancer is in, how fast it is progressing, what their outlook is, and whether one or more particular treatments are proving effective.

A.iv Positron Emission Tomography (PET) Scans

PyL Cloud **120** refers to a cloud-based system that uses medical images obtained with the agent PyL™, which is DCFPyL labeled with ^{18}F ([18F]DCFPyL). The patient, after injection of the imaging agent, receives a positron emission tomography (PET) scan to identify hot spots, and a CT scan. Further information about the PyL™ imaging agent is provided above, and, for example, in U.S. Pat. No. 8,778,305, which is incorporated herein by reference in its entirety.

In certain embodiments, the PET scan and the CT scan are combined as a composite image comprising the CT scan overlaid with the PET scan. As used herein, overlaying one image (e.g., a CT scan) with another (e.g., a PET scan) refers to establishing a mapping between coordinates and/or pixels or voxels of the two images that that represent the same physical locations (e.g., within the patient). CT scans provide accurate anatomical information in the form of detailed three-dimensional (3D) images of internal organs, bones, soft tissue, and blood vessels. Accordingly, 3D boundaries of specific regions of imaged tissue can be accurately identified by analysis of CT scans. For example, automated segmentation of CT scans can be performed to identify 3D boundaries of specific organs (e.g., a prostate, lymph nodes, a lung or lungs), sub-organs, organ regions, as well as other regions of imaged tissue, such as particular bones and an overall skeletal region of the patient. Automated segmentation of CT scans can be accomplished via a variety of approaches, include machine learning techniques [e.g., ANN-based approaches (including, e.g., convolutional neural networks (CNNs))], atlas image registration, and combinations thereof. In certain embodiments, manual segmentation of CT images can also be utilized, alone or in combination with automated segmentation approaches (e.g., to refine 3D boundaries identified via automated segmentation; e.g., to provide an initial starting point for an automated segmentation approach).

Once the 3D boundaries of various regions are identified within a CT scan of a composite image, by virtue of the mapping between the CT scan and PET scan of the composite image, the identified 3D boundaries can be transferred to the PET image. Accordingly, regions of the PET image falling within and/or outside of the identified 3D boundaries can be accurately identified.

In certain embodiments, composite images comprising CT scans overlaid with PET scans are obtained using dedicated PET-CT scanner instruments common in many hospitals, and are uploaded as medical images to the cloud-based platform described herein. In certain embodiments, a PET scan and a corresponding CT scan are obtained separately (but at substantially the same time), and uploaded to the cloud-based platform described herein. In such cases, the separately obtained PET and CT scans can be automatically fused to create a composite image.

In certain embodiments, once the 3D boundaries of the various regions are identified within the PET scan, one or more risk indices can be computed in a similar fashion to that described above with regard to BSI. In particular, in certain embodiments, intensity values of the PET scan in relation to (e.g., within and/or outside of) the 3D boundaries of the identified regions can be used to determine levels of cancerous tissue within the identified regions, e.g., based on features of detected hotspots (e.g., detected hotspots corresponding to metastases). Risk indices can then be computed based on the determined cancerous tissue levels. For example, hotspots within the PET scan can be identified, and, based on features such as their size, number, and distribution with respect to the identified regions, used to compute one or more risk indices. As with BSI, risk indices determined from PET scans can be correlated with prognostic values and tracked over time (e.g., over the course of multiple visits to one or more doctors) to provide patients or their physician with an objective metric of what state their cancer is in, how fast it is progressing, what their outlook is, and whether one or more particular treatments are proving effective. The approaches described herein with regard to PET imaging using PyL™ as a radiopharmaceutical can be applied to a variety of other radiopharmaceuticals, such as those described above, including, without limitation NaF, radioisotopes of choline, and any of the PSMA binding agents described in section A.i above.

A.v Single-Photon Emission Computerized Tomography (SPECT) Scans

1404 Cloud **130** refers to a cloud-based system that uses medical images obtained with the agent ^{99m}Tc-MIP-1404, which, as described above, is 1404 labeled with Tc^{99m}. After injection of the imaging agent, the patient receives a single-photon emission computerized tomography (SPECT) scan, e.g., to identify hot spots, and a computed tomography (CT) scan, e.g., to identify anatomical features. These images are overlaid to make a composite image (SPECT/CT). Further information about ^{99m}Tc-MIP-1404 imaging agent is provided above, and, for example, in U.S. Pat. Nos. 8,211,401 and 8,962,799, both of which are incorporated herein by reference in their entireties.

SPECT and CT scans can be analyzed in a manner similar to that described above with respect to PET and CT scans, in order to determine one or more risk indices. In particular, as with PET and CT scans, the SPECT scan and the CT scan can be combined in a composite image in which the CT scan is overlaid with the SPECT scan—a composite SPECT-CT image. As with composite PET-CT images, composite SPECT-CT images may be directly received as medical images by the cloud-based platform described herein (e.g., having been obtained via dedicated SPECT-CT imager in a hospital), or may be created by the cloud-based platform following receipt of separate SPECT scans and CT scans.

Similar to PET-CT images, 3D boundaries of various regions of imaged tissue can be identified within the SPECT image by virtue of the overlay with the CT image of the composite image. Intensity variations within the SPECT image, in relation to the 3D boundaries can be used to compute one or more risk indices. As with the approaches for computing risk indices from composite PET-CT images, this may comprise determine levels of cancerous tissue within the identified regions, for example by detecting hotspots within the 3D boundaries of the identified regions. Such risk indices can be correlated with prognostic values and tracked over time (e.g., over the course of multiple visits to one or more doctors) to provide patients or their physician with an objective metric of what state their cancer is in, how fast it is progressing, what their outlook is, and whether one or more particular treatments are proving effective. The approaches described herein with regard to SPECT imaging using ^{99m}Tc-MIP-1404 as a radiopharmaceutical can be applied to a variety of other radiopharmaceuticals, such as those described above, including, without limitation, any of the PSMA binding agents described in section A.ii above

B. Platform Services and Computing Device Components

FIG. **2** is a schematic **200** showing the relationship between a platform and a computing device (e.g., personal computer or mobile computing device, e.g., smart phone) running an application, according to illustrative embodiments of the invention. The platform performs various services, for example, user authentication ("Auth"), image and other data storage ("SliceBox), and the like—many more services than those shown may be provided. The applications may have both a platform component and a device component (e.g., native app on the client device).

FIG. **9** shows an example architecture **900** for implementing the cloud-based platform described herein, and providing various services such as the BSI Cloud, PyL Cloud, and 1404 Cloud services described above. The architecture shown in FIG. **9** can be used to implement the platform described herein on a variety of datacenters, including publicly available datacenters. The datacenter provides infrastructure in the form of servers and networks and provides services for e.g. networking, messaging, authentication, logging and storage. The architecture **900** for the platform uses a series of functional units with limited scope referred to as microservices. Each microservice handles an isolated set of tasks such as image storage, calculation of a risk index, identification of medical image type, and other tasks. Services (e.g., microservices) can communicate with each other using standard protocols such as Hypertext Transfer Protocol (HTTP). Organizing the platform into a network of microservices, as shown in the architecture **900** of FIG. **9**, allows for parts of the platform to be scaled individually to meet high demand and to ensure minimal downtime.

In certain embodiments, such an architecture allows for components to be improved or replaced without affecting other parts of the platform. The example architecture **900** shown in FIG. **9** includes a set **920** of microservices that that are common to two or more applications in the platform. The left **910** and right **930** panels show microservices in two applications. The microservice network shown in the left panel **910** implements a version of the BSI Cloud service, as described above, and provides for calculation of an automated BSI index (aBSI), which is a risk index derived from automated analysis of whole-body scans obtained with a gamma camera. The microservice network shown in the right panel **930** implements a version of the 1404 Cloud service, as described above, and provides for automated calculation of a SPECT index, which is a risk index derived from automated analysis of composite SPECT-CT images.

C. Image Collection, Analysis, and Result Presentation

FIG. **3** is a GUI window **300** in the BSI Cloud application (displayed to a user) that allows a user to enter information about a patient and upload and/or access medical images for the patient, e.g., series of images obtained over a period of time.

FIG. **4** is a GUI window **400** in the BSI Cloud application showing representative full body gamma camera images showing hotspots automatically identified by the system, with corresponding overall computed BSI values for a particular image set obtained at a given time. A graph **410** at left shows how the BSI value has changed over time (increase) for this particular patient.

FIG. **5** is a GUI window in the BSI Cloud application showing an automatically or semi-automatically generated radiologist report **510**, which can be signed and dated by a radiologist. In certain embodiments, the automatically identified hotspots may be adjusted by the radiologist (or other medical practitioner attending to the patient), with the change(s) reflected in the report. For example, an identified hotspot may be deactivated by the radiologist, or a new hotspot may be activated by the radiologist, such changes possibly affecting the computed BSI value, displayed in the report.

FIG. **6** is a block flow diagram of an illustrative network-based (e.g., cloud based) decision support system, according to an illustrative embodiment of the invention. FIG. **6** shows various functions that may be performed by the cloud based services described herein. These include: (i) receiving and storing sets of medical images in a database; (ii) accessing one or more of the medical images for transmission to the user for display on a user computing device; (iii) automatically analyzing, by the processor, the medical images to compute a risk index (e.g., BSI) and/or to generate a risk map; (iv) generating a radiologist report for a patient according to the patient images and/or risk index/risk map; and applying a machine learning algorithm to update a process for the automatic analysis of function (iii).

FIG. **10** is a schematic showing clinical stages **1010** of prostate cancer progression, along with various therapies **1020** and diagnostic imaging modalities **1030** appropriate for various disease states. As shown in the schematic, depending on the clinical state of a patient's prostate cancer, different imaging modalities and/or different radiopharmaceuticals may be appropriate. Similarly, different risk indices computed based on different imaging modalities and/or different radiopharmaceuticals may most appropriate, depending on the state of the patient's prostate cancer.

For example, in certain embodiments, when a patient either has, or is suspected of having prostate cancer in a localized state, composite SPECT-CT imaging may be used. SPECT scans of composite SPECT-CT images used for evaluation of localized prostate cancer can be obtained following administration of a particular radiopharmaceutical, such as ^{99m}Tc-MIP-1404, that facilitates imaging of localized prostate cancer. Any of the SPECT-CT images themselves, derivatives thereof, and risk indices computed from the SPECT-CT images can be used, accordingly, to assess risk, disease state, progression, treatment efficacy and the like for localized prostate cancer.

In certain embodiments, when a patient has or is suspected of having metastatic prostate cancer, that has metastasized outside of the prostate, other imaging techniques may be used. For example, whole-body scans obtained following administration of ^{99m}Tc-MDP can be used to assess tumor burden in a patient's skeleton. As discussed above, BSI values computed from whole-body scans can be used to assess risk, disease state, progression, treatment efficacy and the like when a patient's prostate cancer has metastasized to their skeleton. In certain embodiments, certain imaging modalities and/or radiopharmaceuticals can be used for evaluate of prostate cancer in both localized and metastatic states. For example, as illustrated in FIG. **10**, PET-CT imaging can be used for evaluating prostate cancer in both localized and metastatic states. As shown in the figure, such PET-CT images may be obtained using an appropriate radiopharmaceutical, such as PyL™, that facilitates imaging of both localized and metastatic prostate cancer.

In certain embodiments, the cloud-based platform facilitates evaluating prostate cancer progression and treatment efficacy over time. For example, as shown in the example process **1100** of the block flow diagram of FIG. **11**, in certain embodiments medical images of a particular patient are repeatedly received and stored over time **1110**, over the course of multiple visits to one or more doctors and/or clinical specialists (e.g., radiologists) by the patient. In this manner, a series of medical images for the patient are obtained. The series of medical images can be automatically analyzed to determine values of one or more risk indices, so as to track changes in the determined values over time **1120**. The determined risk index values may be stored **1130***a* (e.g., for further processing). In certain embodiments, the process causes a graphical representation of the determined risk index values, such as a graph, to be displayed (e.g., on a user computing device; e.g., via a web-based portal) **1130***b*.

Notably, by virtue of the capability of the cloud-based platform described herein to receive, store, and analyze a variety of different medical image types, such as composite SPECT-CT images, whole-body scans, and composite PET-CT images, the medical images need not be of the same type.

For example, a first subseries of medical images may be obtained using a first imaging modality and a first radiopharmaceutical, such as SPECT-CT imaging with ^{99m}Tc-MIP-1404, when the patient's prostate cancer is in a localized state. If the patient's prostate cancer progresses to a metastatic state, a second subseries of images may comprise images obtained via a different, second imaging modality and/or a different, second radiopharmaceutical. For example, the second subseries of medical images may be PET-CT images obtained using PyL™ For example, the second subseries of medical images may be whole-body scans obtained using ^{99m}Tc-MDP.

Risk indices can be computed for the first image subseries and for the second image subseries to provide a unified picture of the patient's prostate cancer progression and treatment over time. This approach can be performed for multiple patients, not only for decision making purposes with regard to each patient's disease progression and particular course of treatment, but also in the context of clinical trials, for example to compare efficacy of a particular treatment with others or a control.

D. Computer System and Network Environment

FIG. **7** shows an illustrative network environment **700** for use in the methods and systems described herein. In brief overview, referring now to FIG. **7**, a block diagram of an exemplary cloud computing environment **700** is shown and described. The cloud computing environment **700** may include one or more resource providers **702***a*, **702***b*, **702***c* (collectively, **702**). Each resource provider **702** may include computing resources. In some implementations, computing resources may include any hardware and/or software used to process data. For example, computing resources may include hardware and/or software capable of executing

algorithms, computer programs, and/or computer applications. In some implementations, exemplary computing resources may include application servers and/or databases with storage and retrieval capabilities. Each resource provider **702** may be connected to any other resource provider **702** in the cloud computing environment **700**. In some implementations, the resource providers **702** may be connected over a computer network **708**. Each resource provider **702** may be connected to one or more computing device **704***a*, **704***b*, **704***c* (collectively, **704**), over the computer network **708**.

The cloud computing environment **700** may include a resource manager **706**. The resource manager **706** may be connected to the resource providers **702** and the computing devices **704** over the computer network **708**. In some implementations, the resource manager **706** may facilitate the provision of computing resources by one or more resource providers **702** to one or more computing devices **704**. The resource manager **706** may receive a request for a computing resource from a particular computing device **704**. The resource manager **706** may identify one or more resource providers **702** capable of providing the computing resource requested by the computing device **704**. The resource manager **706** may select a resource provider **702** to provide the computing resource. The resource manager **706** may facilitate a connection between the resource provider **702** and a particular computing device **704**. In some implementations, the resource manager **706** may establish a connection between a particular resource provider **702** and a particular computing device **704**. In some implementations, the resource manager **706** may redirect a particular computing device **704** to a particular resource provider **702** with the requested computing resource.

FIG. **8** shows an example of a computing device **800** and a mobile computing device **850** that can be used in the methods and systems described in this disclosure. The computing device **800** is intended to represent various forms of digital computers, such as laptops, desktops, workstations, personal digital assistants, servers, blade servers, mainframes, and other appropriate computers. The mobile computing device **850** is intended to represent various forms of mobile devices, such as personal digital assistants, cellular telephones, smart-phones, and other similar computing devices. The components shown here, their connections and relationships, and their functions, are meant to be examples only, and are not meant to be limiting.

The computing device **800** includes a processor **802**, a memory **804**, a storage device **806**, a high-speed interface **808** connecting to the memory **804** and multiple high-speed expansion ports **810**, and a low-speed interface **812** connecting to a low-speed expansion port **814** and the storage device **806**. Each of the processor **802**, the memory **804**, the storage device **806**, the high-speed interface **808**, the high-speed expansion ports **810**, and the low-speed interface **812**, are interconnected using various busses, and may be mounted on a common motherboard or in other manners as appropriate. The processor **802** can process instructions for execution within the computing device **800**, including instructions stored in the memory **804** or on the storage device **806** to display graphical information for a GUI on an external input/output device, such as a display **816** coupled to the high-speed interface **808**. In other implementations, multiple processors and/or multiple buses may be used, as appropriate, along with multiple memories and types of memory. Also, multiple computing devices may be connected, with each device providing portions of the necessary operations (e.g., as a server bank, a group of blade servers, or a multi-processor system). Thus, as the term is used herein, where a plurality of functions are described as being performed by "a processor", this encompasses embodiments wherein the plurality of functions are performed by any number of processors (one or more) of any number of computing devices (one or more). Furthermore, where a function is described as being performed by "a processor", this encompasses embodiments wherein the function is performed by any number of processors (one or more) of any number of computing devices (one or more) (e.g., in a distributed computing system).

The memory **804** stores information within the computing device **800**. In some implementations, the memory **804** is a volatile memory unit or units. In some implementations, the memory **804** is a non-volatile memory unit or units. The memory **804** may also be another form of computer-readable medium, such as a magnetic or optical disk.

The storage device **806** is capable of providing mass storage for the computing device **800**. In some implementations, the storage device **806** may be or contain a computer-readable medium, such as a floppy disk device, a hard disk device, an optical disk device, or a tape device, a flash memory or other similar solid state memory device, or an array of devices, including devices in a storage area network or other configurations. Instructions can be stored in an information carrier. The instructions, when executed by one or more processing devices (for example, processor **802**), perform one or more methods, such as those described above. The instructions can also be stored by one or more storage devices such as computer- or machine-readable mediums (for example, the memory **804**, the storage device **806**, or memory on the processor **802**).

The high-speed interface **808** manages bandwidth-intensive operations for the computing device **800**, while the low-speed interface **812** manages lower bandwidth-intensive operations. Such allocation of functions is an example only. In some implementations, the high-speed interface **808** is coupled to the memory **804**, the display **816** (e.g., through a graphics processor or accelerator), and to the high-speed expansion ports **810**, which may accept various expansion cards (not shown). In the implementation, the low-speed interface **812** is coupled to the storage device **806** and the low-speed expansion port **814**. The low-speed expansion port **814**, which may include various communication ports (e.g., USB, Bluetooth®, Ethernet, wireless Ethernet) may be coupled to one or more input/output devices, such as a keyboard, a pointing device, a scanner, or a networking device such as a switch or router, e.g., through a network adapter.

The computing device **800** may be implemented in a number of different forms, as shown in the figure. For example, it may be implemented as a standard server **820**, or multiple times in a group of such servers. In addition, it may be implemented in a personal computer such as a laptop computer **822**. It may also be implemented as part of a rack server system **824**. Alternatively, components from the computing device **800** may be combined with other components in a mobile device (not shown), such as a mobile computing device **850**. Each of such devices may contain one or more of the computing device **800** and the mobile computing device **850**, and an entire system may be made up of multiple computing devices communicating with each other.

The mobile computing device **850** includes a processor **852**, a memory **864**, an input/output device such as a display **854**, a communication interface **866**, and a transceiver **868**, among other components. The mobile computing device **850** may also be provided with a storage device, such as a

micro-drive or other device, to provide additional storage. Each of the processor **852**, the memory **864**, the display **854**, the communication interface **866**, and the transceiver **868**, are interconnected using various buses, and several of the components may be mounted on a common motherboard or in other manners as appropriate.

The processor **852** can execute instructions within the mobile computing device **850**, including instructions stored in the memory **864**. The processor **852** may be implemented as a chipset of chips that include separate and multiple analog and digital processors. The processor **852** may provide, for example, for coordination of the other components of the mobile computing device **850**, such as control of user interfaces, applications run by the mobile computing device **850**, and wireless communication by the mobile computing device **850**.

The processor **852** may communicate with a user through a control interface **858** and a display interface **856** coupled to the display **854**. The display **854** may be, for example, a TFT (Thin-Film-Transistor Liquid Crystal Display) display or an OLED (Organic Light Emitting Diode) display, or other appropriate display technology. The display interface **856** may comprise appropriate circuitry for driving the display **854** to present graphical and other information to a user. The control interface **858** may receive commands from a user and convert them for submission to the processor **852**. In addition, an external interface **862** may provide communication with the processor **852**, so as to enable near area communication of the mobile computing device **850** with other devices. The external interface **862** may provide, for example, for wired communication in some implementations, or for wireless communication in other implementations, and multiple interfaces may also be used.

The memory **864** stores information within the mobile computing device **850**. The memory **864** can be implemented as one or more of a computer-readable medium or media, a volatile memory unit or units, or a non-volatile memory unit or units. An expansion memory **874** may also be provided and connected to the mobile computing device **850** through an expansion interface **872**, which may include, for example, a SIMM (Single In Line Memory Module) card interface. The expansion memory **874** may provide extra storage space for the mobile computing device **850**, or may also store applications or other information for the mobile computing device **850**. Specifically, the expansion memory **874** may include instructions to carry out or supplement the processes described above, and may include secure information also. Thus, for example, the expansion memory **874** may be provided as a security module for the mobile computing device **850**, and may be programmed with instructions that permit secure use of the mobile computing device **850**. In addition, secure applications may be provided via the SIMM cards, along with additional information, such as placing identifying information on the SIMM card in a non-hackable manner.

The memory may include, for example, flash memory and/or NVRAM memory (non-volatile random access memory), as discussed below. In some implementations, instructions are stored in an information carrier and, when executed by one or more processing devices (for example, processor **852**), perform one or more methods, such as those described above. The instructions can also be stored by one or more storage devices, such as one or more computer- or machine-readable mediums (for example, the memory **864**, the expansion memory **874**, or memory on the processor **852**). In some implementations, the instructions can be received in a propagated signal, for example, over the transceiver **868** or the external interface **862**.

The mobile computing device **850** may communicate wirelessly through the communication interface **866**, which may include digital signal processing circuitry where necessary. The communication interface **866** may provide for communications under various modes or protocols, such as GSM voice calls (Global System for Mobile communications), SMS (Short Message Service), EMS (Enhanced Messaging Service), or MMS messaging (Multimedia Messaging Service), CDMA (code division multiple access), TDMA (time division multiple access), PDC (Personal Digital Cellular), WCDMA (Wideband Code Division Multiple Access), CDMA2000, or GPRS (General Packet Radio Service), among others. Such communication may occur, for example, through the transceiver **868** using a radio-frequency. In addition, short-range communication may occur, such as using a Bluetooth®, Wi-Fi™, or other such transceiver (not shown). In addition, a GPS (Global Positioning System) receiver module **870** may provide additional navigation- and location-related wireless data to the mobile computing device **850**, which may be used as appropriate by applications running on the mobile computing device **850**.

The mobile computing device **850** may also communicate audibly using an audio codec **860**, which may receive spoken information from a user and convert it to usable digital information. The audio codec **860** may likewise generate audible sound for a user, such as through a speaker, e.g., in a handset of the mobile computing device **850**. Such sound may include sound from voice telephone calls, may include recorded sound (e.g., voice messages, music files, etc.) and may also include sound generated by applications operating on the mobile computing device **850**.

The mobile computing device **850** may be implemented in a number of different forms, as shown in the figure. For example, it may be implemented as a cellular telephone **880**. It may also be implemented as part of a smart-phone **882**, personal digital assistant, or other similar mobile device.

Various implementations of the systems and techniques described here can be realized in digital electronic circuitry, integrated circuitry, specially designed ASICs (application specific integrated circuits), computer hardware, firmware, software, and/or combinations thereof. These various implementations can include implementation in one or more computer programs that are executable and/or interpretable on a programmable system including at least one programmable processor, which may be special or general purpose, coupled to receive data and instructions from, and to transmit data and instructions to, a storage system, at least one input device, and at least one output device.

These computer programs (also known as programs, software, software applications or code) include machine instructions for a programmable processor, and can be implemented in a high-level procedural and/or object-oriented programming language, and/or in assembly/machine language. As used herein, the terms machine-readable medium and computer-readable medium refer to any computer program product, apparatus and/or device (e.g., magnetic discs, optical disks, memory, Programmable Logic Devices (PLDs)) used to provide machine instructions and/or data to a programmable processor, including a machine-readable medium that receives machine instructions as a machine-readable signal. The term machine-readable signal refers to any signal used to provide machine instructions and/or data to a programmable processor.

To provide for interaction with a user, the systems and techniques described here can be implemented on a com-

puter having a display device (e.g., a CRT (cathode ray tube) or LCD (liquid crystal display) monitor) for displaying information to the user and a keyboard and a pointing device (e.g., a mouse or a trackball) by which the user can provide input to the computer. Other kinds of devices can be used to provide for interaction with a user as well; for example, feedback provided to the user can be any form of sensory feedback (e.g., visual feedback, auditory feedback, or tactile feedback); and input from the user can be received in any form, including acoustic, speech, or tactile input.

The systems and techniques described here can be implemented in a computing system that includes a back end component (e.g., as a data server), or that includes a middleware component (e.g., an application server), or that includes a front end component (e.g., a client computer having a graphical user interface or a Web browser through which a user can interact with an implementation of the systems and techniques described here), or any combination of such back end, middleware, or front end components. The components of the system can be interconnected by any form or medium of digital data communication (e.g., a communication network). Examples of communication networks include a local area network (LAN), a wide area network (WAN), and the Internet.

The computing system can include clients and servers. A client and server are generally remote from each other and typically interact through a communication network. The relationship of client and server arises by virtue of computer programs running on the respective computers and having a client-server relationship to each other. In some implementations, the modules and/or services (e.g. cloud based services, such as BSI Cloud **110**, PyL Cloud **120**, 1404 Cloud **130**; e.g., any of the microservices described herein) described herein can be separated, combined or incorporated into single or combined modules and/or services. The modules and/or services depicted in the figures are not intended to limit the systems described herein to the software architectures shown therein

While the invention has been particularly shown and described with reference to specific preferred embodiments, it should be understood by those skilled in the art that various changes in form and detail may be made therein without departing from the spirit and scope of the invention as defined by the appended claims.

What is claimed is:

1. A network-based system for generating a disease risk map for use as a decision-making support for evaluating risk of cancer or risk of recurrence of cancer, the system comprising:

a processor; and

a memory having instructions stored thereon, wherein the instructions, when executed by the processor, cause the processor to:

(i) access one or more medical images associated with a particular patient from a database;

(ii) perform an analysis of the one or more medical images associated with the particular patient using a machine learning algorithm, to generate the risk map, wherein the risk map comprises a visual representation of tissue overlaid with graphical denotations marking one or more regions of risk of cancer or risk of recurrence of cancer; and

(iii) cause display of the risk map via a graphical user interface (GUI) for presentation or review of the risk map by a user,

wherein the analysis of the one or more medical images comprises creation of a 3D image of the one or more regions of risk of cancer or risk of recurrence of cancer overlaid on the one or more medical images, and wherein the 3D image comprises geographic identification of one or more specific tissue region(s) overlaid on the one or more medical images.

2. The system of claim **1**, wherein the one or more medical images comprise one or more magnetic resonance images (MRIs).

3. The system of claim **1**, wherein the one or more medical images comprise (i) one or more PET/CT image(s) or (ii) one or more SPECT/CT image(s).

4. The system of claim **1**, wherein the visual representation of tissue is at least a portion of one of the one or more medical images of the particular patient.

5. The system of claim **1**, wherein the cancer is prostate cancer.

6. The system of claim **1**, wherein the visual representation of tissue comprises a visual representation of bone.

7. The system of claim **1**, wherein the one or more specific tissue region(s) comprise one or more members selected from the group consisting of organs, organ structures, sub-organs, and organ regions.

8. The system of claim **1**, wherein the one or more specific tissue region(s) comprise one or more particular bones.

9. The system of claim **1**, wherein the instructions cause the processor to generate a radiologist report for the particular patient based at least in part on the analysis of the one or more medical images.

10. The system of claim **9**, wherein the radiologist report comprises the one or more medical images and the risk map.

11. The system of claim **9**, wherein the radiologist report comprises one or more reference images or reference risk maps.

12. The system of claim **1**, wherein the instructions cause the processor to apply a machine learning algorithm to update a process for automatically analyzing the one or more medical images using accumulated image data in the database.

13. A method for generating a disease risk map for use as a decision-making support for evaluating risk of cancer or risk of recurrence of cancer, the method comprising:

(i) accessing, by a processor, one or more medical images associated with a particular patient from a database;

(ii) automatically analyzing, by the processor, using a machine learning algorithm, the one or more medical images to generate the risk map, wherein the risk map comprises a visual representation of tissue overlaid with graphical denotations marking one or more regions of risk of cancer or risk of recurrence of cancer; and

(iii) causing, by the processor, display of the risk map via a graphical user interface (GUI) for presentation or review of the risk map by a user,

wherein step (ii) comprises creation of a 3D image of the one or more regions of risk of cancer or risk of recurrence of cancer overlaid on the one or more medical images, and wherein the 3D image comprises geographic identification of one or more specific tissue region(s) overlaid on the one or more medical images.

* * * * *

EXHIBIT 2

US010973486B2

(12) **United States Patent**
Sjöstrand et al.

(10) **Patent No.: US 10,973,486 B2**
(45) **Date of Patent: Apr. 13, 2021**

(54) **SYSTEMS AND METHODS FOR RAPID NEURAL NETWORK-BASED IMAGE SEGMENTATION AND RADIOPHARMACEUTICAL UPTAKE DETERMINATION**

(71) Applicants: **Progenics Pharmaceuticals, Inc.**, New York, NY (US); **EXINI Diagnostics AB**, Lund (SE)

(72) Inventors: **Karl Vilhelm Sjöstrand**, New York, NY (US); **Jens Filip Andreas Richter**, Lund (SE); **Kerstin Elsa Maria Johnsson**, Lund (SE); **Erik Konrad Gjertsson**, Lund (SE)

(73) Assignees: **Progenics Pharmaceuticals, Inc.**, New York, NY (US); **EXINI Diagnostics AB**, Lund (SE)

(*) Notice: Subject to any disclaimer, the term of this patent is extended or adjusted under 35 U.S.C. 154(b) by 259 days.

(21) Appl. No.: **16/003,006**

(22) Filed: **Jun. 7, 2018**

(65) **Prior Publication Data**

US 2019/0209116 A1 Jul. 11, 2019

Related U.S. Application Data

(60) Provisional application No. 62/614,935, filed on Jan. 8, 2018.

(51) **Int. Cl.**
G06K 9/46 (2006.01)
A61B 6/00 (2006.01)
(Continued)

(52) **U.S. Cl.**
CPC ***A61B 6/5217*** (2013.01); ***A61B 6/037*** (2013.01); ***A61B 6/465*** (2013.01); ***A61B 6/466*** (2013.01);
(Continued)

(58) **Field of Classification Search**
CPC A61B 6/037; A61B 6/465; A61B 6/466; A61B 6/467; A61B 6/50; A61B 6/5217;
(Continued)

(56) **References Cited**

U.S. PATENT DOCUMENTS

7,450,747 B2 11/2008 Jabri et al.
7,751,605 B2 7/2010 Gündel et al.
(Continued)

FOREIGN PATENT DOCUMENTS

CN 101528267 A 9/2009
CN 102361594 A 2/2012
(Continued)

OTHER PUBLICATIONS

Cha, Kenny H., et al. "Urinary bladder segmentation in CT urography using deep-learning convolutional neural network and level sets." Medical physics 43.4 (2016): 1882-1896. (Year: 2016).*
(Continued)

Primary Examiner — Nirav G Patel
(74) *Attorney, Agent, or Firm* — William R. Haulbrook; Ronen Adato; Choate, Hall & Stewart LLP

(57) **ABSTRACT**

Presented herein are systems and methods that provide for automated analysis of three-dimensional (3D) medical images of a subject in order to automatically identify specific 3D volumes within the 3D images that correspond to specific organs and/or tissue. In certain embodiments, the accurate identification of one or more such volumes can be used to determine quantitative metrics that measure uptake of radiopharmaceuticals in particular organs and/or tissue regions. These uptake metrics can be used to assess disease state in a subject, determine a prognosis for a subject, and/or determine efficacy of a treatment modality.

55 Claims, 83 Drawing Sheets
(30 of 83 Drawing Sheet(s) Filed in Color)

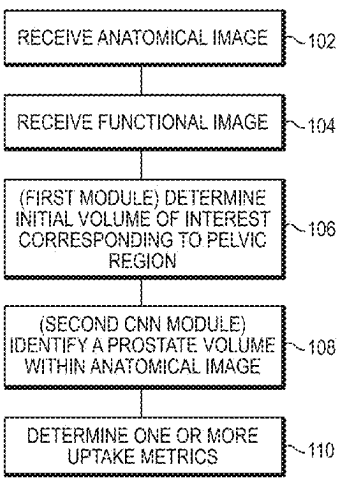

(51) **Int. Cl.**

G06T 7/00	(2017.01)
G06T 5/30	(2006.01)
A61B 6/03	(2006.01)
A61K 51/04	(2006.01)
G06T 15/08	(2011.01)
G06T 7/143	(2017.01)
G06T 7/11	(2017.01)
G06N 3/08	(2006.01)
G06F 3/0484	(2013.01)
G06N 3/04	(2006.01)

(52) **U.S. Cl.**

CPC ***A61B 6/467*** (2013.01); ***A61B 6/50*** (2013.01); ***A61B 6/5223*** (2013.01); ***A61B 6/5229*** (2013.01); ***A61B 6/5258*** (2013.01); ***A61K 51/0478*** (2013.01); ***G06K 9/4647*** (2013.01); ***G06T 5/30*** (2013.01); ***G06T 7/0012*** (2013.01); ***G06T 7/0014*** (2013.01); ***G06T 7/11*** (2017.01); ***G06T 7/143*** (2017.01); ***G06T 15/08*** (2013.01); *G06F 3/04842* (2013.01); *G06K 2209/051* (2013.01); *G06N 3/04* (2013.01); *G06N 3/0454* (2013.01); *G06N 3/08* (2013.01); *G06T 2200/24* (2013.01); *G06T 2207/10081* (2013.01); *G06T 2207/10088* (2013.01); *G06T 2207/10104* (2013.01); *G06T 2207/10108* (2013.01); *G06T 2207/20081* (2013.01); *G06T 2207/30008* (2013.01); *G06T 2207/30081* (2013.01); *G06T 2207/30096* (2013.01)

(58) **Field of Classification Search**

CPC ... A61B 6/5223; A61B 6/5229; A61B 6/5258; A61K 51/0478; G06F 3/04842; G06K 2209/051; G06K 9/00201; G06K 9/4647; G06K 9/6271; G06N 3/04; G06N 3/0454; G06N 3/08; G06N 3/082; G06T 15/08; G06T 2200/24; G06T 2207/10081; G06T 2207/10088; G06T 2207/10104; G06T 2207/10108; G06T 2207/20081; G06T 2207/30008; G06T 2207/30081; G06T 2207/30096; G06T 5/30; G06T 7/0012; G06T 7/0014; G06T 7/11; G06T 7/143

See application file for complete search history.

(56) **References Cited**

U.S. PATENT DOCUMENTS

7,935,055	B2	5/2011	Burckhardt
7,970,194	B2	6/2011	Kimura
8,211,401	B2	7/2012	Babich et al.
8,467,856	B2	6/2013	Renisch et al.
8,538,166	B2	9/2013	Gordon et al.
8,705,887	B2	4/2014	Ma et al.
8,778,305	B2	7/2014	Pomper et al.
8,855,387	B2	10/2014	Hamadeh et al.
8,962,799	B2	2/2015	Babich et al.
9,002,081	B2	4/2015	Brown
9,710,915	B2	7/2017	Firouzian et al.
9,721,340	B2	8/2017	Gillies et al.
10,223,610	B1	3/2019	Akselrod-Ballin et al.
10,311,971	B2	6/2019	Opfer et al.
10,339,653	B2	7/2019	Gillies et al.
10,340,044	B2	7/2019	Yao et al.
10,340,046	B2	7/2019	Baker
RE47,609	E	9/2019	Hamadeh et al.
10,600,184	B2	3/2020	Golden et al.
10,665,346	B2	5/2020	Baker
10,748,652	B2	8/2020	Yao et al.
10,762,993	B2	9/2020	Baker
2003/0215120	A1	11/2003	Uppaluri et al.
2005/0281381	A1	12/2005	Guendel
2006/0062425	A1	3/2006	Shen et al.
2006/0064396	A1	3/2006	Wei et al.
2007/0081712	A1	4/2007	Huang et al.
2007/0081713	A1	4/2007	Jerebko
2007/0100225	A1	5/2007	Maschke
2007/0115204	A1	5/2007	Budz et al.
2008/0027315	A1	1/2008	McGinnis
2009/0309874	A1	12/2009	Salganicoff et al.
2010/0215581	A1	8/2010	Hoffmann
2011/0063288	A1	3/2011	Valadez
2011/0255763	A1	10/2011	Bogoni et al.
2012/0123253	A1	5/2012	Renisch et al.
2013/0038707	A1	2/2013	Cunningham et al.
2013/0211231	A1	8/2013	Sundarapandian et al.
2013/0281841	A1	10/2013	Everett et al.
2015/0110716	A1	4/2015	Armor
2015/0331995	A1	11/2015	Zhao et al.
2016/0203263	A1	7/2016	Maier et al.
2016/0335395	A1	11/2016	Wu et al.
2017/0083682	A1	3/2017	McNutt et al.
2018/0144828	A1	5/2018	Baker
2018/0259608	A1	9/2018	Golden et al.
2018/0360402	A1	12/2018	Carmi
2019/0038239	A1	2/2019	Flohr et al.
2019/0105009	A1	4/2019	Siemionow et al.
2019/0388049	A1	12/2019	Gupta et al.
2020/0027559	A1	1/2020	Baker
2020/0051238	A1	2/2020	El Harouni et al.
2020/0074634	A1	3/2020	Kecskemethy et al.
2020/0085382	A1	3/2020	Taerum et al.
2020/0126666	A1	4/2020	Baker
2020/0193594	A1	6/2020	Georgescu et al.
2020/0193603	A1	6/2020	Golden et al.
2020/0245960	A1	8/2020	Richter et al.
2020/0337658	A1	10/2020	Sjostrand et al.
2020/0342600	A1	10/2020	Sjostrand et al.
2020/0357521	A1	11/2020	Baker

FOREIGN PATENT DOCUMENTS

EP	1426903	A2	6/2004
EP	1508872	A1	2/2005
WO	WO-9905503	A2	2/1999
WO	WO-2007/062135	A2	5/2007
WO	WO-2009/084995	A1	7/2009
WO	WO-2011/077303	A1	6/2011
WO	WO-2018/081354	A1	5/2018
WO	WO-2019/103912	A2	5/2019
WO	WO-2019/136349	A2	7/2019
WO	WO-2020/144134	A1	7/2020
WO	WO-2020/146032	A1	7/2020
WO	WO-2020/190821	A1	9/2020
WO	WO-2020/219620	A1	10/2020

OTHER PUBLICATIONS

Santos-Cuevas, Clara, et al. "99mTc-labeled PSMA inhibitor: Biokinetics and radiation dosimetry in healthy subjects and imaging of prostate cancer tumors in patients." Nuclear Medicine and Biology 52 (2017): 1-6. (Year: 2017).*

Ciernik, I. Frank, et al. "3D-segmentation of the 18F-choline PET signal for target volume definition in radiation therapy of the prostate." Technology in cancer research & treatment 6.1 (2007): 23-30. (Year: 2007).*

Gjertsson, K., Segmentation in Skeletal Scintigraphy Images using Convolutional Neural Networks, Master's Theses in Mathematical Sciences, pp. 39-58, (2017), <https://lup.lub.lu.se/student-papers/search/publication/8916406>. Retrieved on Feb. 24, 2020.

Sjöstrand, K., et al., Automated detection and quantification of Prostatic PSMA uptake in SPECT/CT using a Deep Learning Algorithm for Segmentation of Pelvic Anatomy, The Journal of Nuclear Medicine, 59(1):p. 30, (2018).

Anand, A. et al., Analytic Validation of the Automated Bone Scan Index as an Imaging Biomarker to Standardize Quantitative Changes in Bone Scans of Patients with Metastatic Prostate Cancer, J. Nucl. Med., 57(1):41-45 (2016).

(56) **References Cited**

OTHER PUBLICATIONS

Anand, A. et al., Automated Bone Scan Index as a quantitative imaging biomarker in metastatic castration-resistant prostate cancer patients being treated with enzalutamide, EJNMMI Research, 6:23, 7 pages (2016).
Anand, A. et al., Translating Prostate Cancer Working Group 2 (PCWG2) Progression Criteria into a Quantitative Response Biomarker in Metastatic Castration Resistant Prostate Cancer (mCRPC), ASCO GU Conference, Poster, presented Feb. 16, 2017.
Anand, A. et al., Translating Prostate Cancer Working Group 2 (PCWG2) progression criteria into a quantitative response biomarker in metastatic castration-resistant prostate cancer (mCRPC), Journal of Clinical Oncology, 35(6):170 (2017).
Armstrong, A. et al., Assessment of the bone scan index in a randomized placebo-controlled trial of tasquinimod in men with metastatic castration-resistant prostate cancer (mCRPC), Urologic Oncology: Seminars and Original Investigations, 32:1308-1316 (2014).
Armstrong, A. et al., Development and validation of a prognostic model for overall survival in chemotherapy-naive men with metastatic castration-resistant prostate cancer (mCRPC) from the phase 3 prevail clinical trial, Journal of Clinical Oncology, 35(Suppl. 6):Abstract 138 (2017).
Armstrong, A. J. et al., Phase 3 prognostic analysis of the automated bone scan index (aBSI) in men with bone-metastatic castration-resistant prostate cancer (CRPC), Meeting Library ASC University. 1 page abstract, (2017).
Belal, S. et al., Association of PET Index quantifying skeletal uptake in NaF PET/CT images with overall survival in prostate cancer patients, ASCO GU 2017, Poster 178, presented Feb. 16, 2017.
Belal, S. et al., PET Index quantifying skeletal uptake in NaF PET/CT images with overall survival in prostate cancer patients, ASCO GU 2017, Abstract (Feb. 13, 2017).
Belal, S. L. et al, 3D skeletal uptake of ^{18}F sodium fluoride in PET/CT images is associate with overall survival in patients with prostate cancer, EJNMMI Research, 7(15):1-8 (2017).
Belal, S.L. et al., Automated evaluation of normal uptake in different skeletal parts in 18F-sodium fluoride (NaF) PET/CT using a new convolutional neural network method, EJNMMI, EANM '17, 44(Suppl 2):S119-S956, Abstract EP-0116 (2017).
Bushberg, J. T. et al., Essential Physics of Medical Imaging, Essential Physics of Medical Imaging, 19.3: p. 581 (table 15-3), p. 713 paragraph 6, section 19.3 and p. 720, (2011).
Dennis, E. et al., Bone Scan Index: A Quantitative Treatment Response Biomarker for Castration-Resistant Metastatic Prostate Cancer, Journal of Clinical Oncology. 30(5):519-524 (2012).
GE Healthcare, SPECT/CT Cameras, retrieved Oct. 25, 2017: <http://www3.gehealthcare.com.sg/en-gb/products/categories/nuclear_medicine/spect-ct_cameras>.
Giesel, F. L. et al., F-18 labelled PSMA-1007: biodistribution, radiation dosimetry and histopathological validation of tumor lesions in prostate cancer patients, Eur. J. Nucl. Med. Mol. Imaging, 44:678-688 (2017).
Goffin, K. E. et al., Phase 2 study of ^{99m}Tc-trofolastat SPECT/CT to identify and localize prostate cancer in intermediate- and high-risk patients undergoing radical prostatectomy and extended pelvic lymph node dissection, J. Nucl. Med., 27 pages. (2017).
Goffin, K. E. et al., Phase 2 Study of 99mTc-trofolastat SPECT/CT to identify and localize prostate cancer in intermediate- and high-risk patients undergoing radical prostatectomy and extended pelvic lymph node dissection, Journal of Nuclear Medicine, pp. 1-22 with supplemental data included, (2017).
Guimond, A. et al., Average Brain Models: A Convergence Study, Computer Vision and Image Understanding, 77:192-210 (2000).
Hajnal, J. et al., 4.4 Intensity, Size, and Skew Correction; 7.1 Introduction; 7.2 Methods; 7.3 Image Interpretation—General, In: Medical Image Registration, CRC Press LLC, 80-81:144-148 (2001).
Hiller, S. M. et al., 99mTc-Labeled Small-Molecule Inhibitors of Prostate-Specific Membrane Antigen for Molecular Imaging of Prostate Cancer, Journal of Nuclear Medicine, 54(8):1369-1376 (2013) retrieved Oct. 25, 2017: <http://jnm.snmjournals.org/content/54/8/1369.full>.
Horikoshi, H. et al., Computer-aided diagnosis system for bone scintigrams from Japanese patients: importance of training database, Annals of Nuclear Medicine, 26(8):622-626 (2012).
Huang, J.-H. et al., A Set of Image Processing Algorithms for Computer-Aided Diagnosis in Nuclear Medicine Whole Body Bone Scan Images, IEEE Transactions on Nuclear Science, 54(3):514-522 (2007).
Kaboteh R. et al., Progression of bone metastases in patients with prostate cancer—automated detection of new lesions and calculation of bone scan index, EJNMMI Research, 3:64 (2013).
Kaboteh, R. et al., Convolutional neural network based quantification of choline uptake in PET/CT studies is associated with overall survival in patents with prostate cancer, EJNMMI. EANM '17, 44(Suppl 2):S119-S956, Abstract EP-0642 (2017).
Keiss, et al., Prostate-specific membrane antigen and a target for cancer imaging and therapy, The Quarterly Journal of Nuclear Medicine and Molecular Imaging, 59(3):241-268 (2015).
Kikuchi, A. et al., Automated segmentation of the skeleton in whole-body bone scans: influence of difference in atlas, Nuclear Medicine Communications, 33(9):947-953 (2012).
Kinahan, P.E. et al., PET/CT Standardized Update Values (SUVs) in Clinical Practice and Assessing Response to Therapy, Semin Ultrasuond CT MR 31(6):496-505 (2010) retrieved Oct. 25, 2017: <https://www.ncbi.nlm.nih.gov/pmc/articles/PMC3026294/>.
Knutsson, H., and Andersson, M., Morphons: Segmentation using Elastic Canvas and Paint on Priors, IEEE International Conference on Image Processing (ICIP 2005), Genova, Italy, 4 pages (2005).
Kopka, K. et al., Glu-Ureido-Based Inhibitors of Prostate-Specific Membrane Antigen: Lessons Learned During the Development of a Novel Class of Low-Molecular-Weight Theranostic Radiotracers, The Journal of Nuclear Medicine, 58(9)(Suppl. 2):17S-26S, (2017).
Liu, L. et al., Computer-Aided Detection of Prostate Cancer with MRI: Technology and Applications, Acad Radiol. Author manuscript, 50 pages 2016.
Ma, L. et al., Automatic segmentation of the prostate on CT images using deep learning and multi-atlas fusion, Proc. of SPIE vol. 10133:101332O-1-101332O-9 (2017).
Ma, L. et al., Combining Population and Patient-Specific Characteristics for Prostate Segmentation on 3D CT Images, Proc of SPIE 9784:978427-1-8 (2016).
Ma, L. et al., Random Walk Based Segmentation for the Prostate on 3D Transrectal Ultrasound Images, Proc SPIE Int Soc Opt Eng. Author manuscript, 13 pages (2016).
Mayo Clinic Staff, Choline C-11 PET scan, Overview, Mayo Clinic, 4 pages (2017), retrieved Oct. 25, 2017: <https://www.mayoclinic.org/tests-procedures/choline-c-11-pet-scan/home/ovc-20156994>.
Nakajima, K. et al., Enhanced diagnostic accuracy for quantitative bone scan using an artificial neural network system: a Japanese multi-center database project, EJNMMI Research, 3:83 (2013).
National Cancer Institute, NCI Drug Dictionary: gallium Ga 68-labeled PSMA-11, retrieved Oct. 25, 2017: <https://www.cancer.gov/publications/dictionaries/cancer-drug?cdrid=766400>.
National Cancer Institute, NCI Drug Dictionary: technetium Tc 99m methylene diphosphonate, retrieved Oct. 25, 2017: <https://www.cancer.gov/publications/dictionaries/cancer-drug?cdrid=537722>.
Perera, M. et al., Sensitivity, Specificity, and Predictors of Positive 68Ga-Prostate-specific Membrane Antigen Positron Emission Tomography in Advanced Prostate Cancer: A Systematic Review and Meta-analysis, European Urology, 70(6):926-937 (2016).
Polymeri, E. et al., Analytical validation of an automated method for segmentation of the prostate gland in CT images, EJNMMI, EANM '17, 44(Suppl 2):S119-S956, Abstract EP-0641 (2017).
radiologyinfo.org for Patients, Computed Tomography (CT), retrieved Oct. 25, 2017: <https://www.radiologyinfo.org/en/submenu.cfm?pg=ctscan>.
Rowe, S. P. et al., PET Imaging of prostate-specific membrane antigen in prostate cancer: current state of the art and future challenges, Prostate Cancer and Prostatic Diseases, 1-8 (2016).

(56) **References Cited**

OTHER PUBLICATIONS

Sabbatini, P. et al., Prognostic Significance of Extent of Disease in Bone in Patients With Androgen-Independent Prostate Cancer, Journal of Clinical Oncology, 17(3):948-957 (1999).
Sadik, M. et al., 3D prostate gland uptake of 18F-choline—association with overall survival in patients with hormone-naïve prostate cancer, The Journal of Nuclear Medicine, 58(Suppl. 1):Abstract 544 (2017).
Sadik, M. et al., A new computer-based decision-support system for the interpretation of bone scans, Nuclear Medicine Communications. 27(5):417-423 (2006).
Sadik, M. et al., Automated 3D segmentation of the prostate gland in CT images—a first step towards objective measurements of prostate uptake in PET and SPECT images, Journal of Nuclear Medicine, 58(1) (2017).
Sadik, M. et al., Automated quantification of reference levels in liver and mediastinum (blood pool) for the Deauville therapy response classification using FDG-PET/CT in lymphoma patients, EJNMMI, EANM '17, 44(Suppl 2):S119-S956, Abstract EP-0770 (2017).
Sadik, M. et al., Computer-assisted interpretation of planar whole-body bone scans, Journal Nuclear Medicine, 49(12):1958-65, 2008.
Sadik, M. et al., Convolutional neural networks for segmentation of 49 selected bones in CT images show high reproducibility, EJNMMI, EANM '17, 44(Suppl 2):S119-S956, Abstract OP-657 (2017).
Sadik, M. et al., Improved classifications of planar whole-body bone scans using a computer-assisted diagnosis system: a multicenter, multiple-reader, multiple-case study, Journal of Nuclear Medicine, 50(3): 368-75, 2009.
Sadik, M. et al., Variability in reference levels for Deauville classifications applied to lymphoma patients examined with 18F-FDG-PET/CT, EJNMMI, EANM '17, 44(Suppl 2):S119-S956, Abstract EP-0771 (2017).
Sajn, L. et al., Computerized segmentation of whole-body bone scintigrams and its use in automated diagnostics, Computer Methods and Programs in Biomedicine, 80:47-55 (2005).
Salerno, J. et al., Multiparametric magnetic resonance imaging for pre-treatment local staging of prostate cancer: A Cancer Care Ontario clinical practice guideline, Canadian Urological Association Journal, 10(9-10):332-339 (2016).
Sjöstrand K. et al., Statistical regularization of deformation fields for atlas-based segmentation of bone scintigraphy images, MICCAI 5761:664-671 (2009).
Sluimer, I. et al., Toward Automated Segmentation of the Pathological Lung in CT, IEEE Transactions on Medical Imaging, 24(8):1025-1038 (2005).
Tian, Z. et al., A fully automatic multi-atlas based segmentation method for prostate MR images, Proc SPIE Int Soc Opt Eng. Author manuscript, 12 pages (2015).
Tian, Z. et al., A supervoxel-based segmentation method for prostate MR images, Med. Phys., 44(2):558-569 (2017).
Tian, Z. et al., Deep convolutional neural network for prostate MR segmentation, Proc. of SPIE 10135:101351L-1-101351L-6 (2017).
Tian, Z., et al., Superpixel-based Segmentation for 3D Prostate MR Images, IEEE Trans Med Imaging, Author manuscript, 32 pages, (2016).
Ulmert, D. et al., A Novel Automated Platform for Quantifying the Extent of Skeletal Tumour Involvement in Prostate Cancer Patients Using the Bone Scan Index, European Urology, 62(1):78-84 (2012).
Wrangsjo, A. et al., Non-rigid Registration Using Morphons, Proceedings of the 14th Scandinavian Conference on Image Analysis (SCIA '05), pp. 501-510 (2005).
Yin, T.-K., A Computer-Aided Diagnosis for Locating Abnormalities in Bone Scintigraphy by a Fuzzy System With a Three-Step Minimization Approach, IEEE Transactions on Medical Imaging, 23(5):639-654 (2004).
Litjens, G. et al., A survey on deep learning in medical image analysis, Medical Image Analysis, 42:60-88, (2017).
Partial Search Report and Provisional Opinion, International Application No. PCT/US2019/012486 (Systems and Methods for Rapid Neural Network-Based Image Segmentation and Radiopharmaceutical Uptake Determination, filed Jan. 7, 2019), issued by ISA/European Patent Office, 16 pages, dated May 7, 2019.
Rowe, S. P. et al., PSMA-Based [^{18}F]DCFPyL PET/CT is Superior to Conventional Imaging for Lesion Detection in Patients with Metastatic Prostate Cancer, Mol Imaging Biol, 18:411-419, (2016).
Eiber, M. et al., Prostate Cancer Molecular Imaging Standardized Evaluation (PROMISE): Proposed miTNM Classification for the Interpretation of PSMA-Ligand PET/CT, The Journal of Nuclear Medicine, 59(3):469-478, (2018).
International Search Report, International Application No. PCT/US2019/012486 (Systems and Methods for Rapid Neural Network-Based Image Segmentation and Radiopharmaceutical Uptake Determination, filed Jan. 7, 2019), issued by ISA/European Patent Office, 6 pages, dated Jul. 2, 2019.
Written Opinion, International Application No. PCT/US2019/012486 (Systems and Methods for Rapid Neural Network-Based Image Segmentation and Radiopharmaceutical Uptake Determination, filed Jan. 7, 2019), issued by ISA/European Patent Office, 13 pages, dated Jul. 2, 2019.
American College of Radiology (ACR) and the Society for Pediatric Radiology (SPR), ACR-SPR Practice Parameter for the Performance of Skeletal Scintigraphy (Bone Scan), Resolution 28, (2013-Revused2017), available from: http://www.acr.org.
Anand, A. et al., A Pre-Analytical Validation Study of Automated Bone Scan Index: Effect on Accuracy and Reproducibility Due to the Procedural Variabilities in Bone Scan Image Acquisition. J Nucl Med. Jul. 21, 2016. [Epub ahead of print].
Armstrong, A. J. et al., Phase 3 Assessment of the Automated Bone Scan Index as a Prognostic Imaging Biomarker of Overall Survival in Men with Metastatic Castration-Resistant Prostate Cancer: A Secondary Analysis of a Randomized Clinical Trial. JAMA Oncology 4:944-951, (2018).
Bai, P. et. al., Body region localization in whole-body low-dose CT images of PET/CT scans using virtual landmarks, Medical Physics Wiley USA, 46(3): 1286-1299 (2019).
Bombardieri, E. et al., Bone scintigraphy: procedure guidelines for tumour imaging, Eur J. Nucl. Med. Mol. Imaging, 30:BP99-BP106, (2003).
Brynolfsson, J., et. al., Deep Learning based urinary bladder segmentation using 18FDCFPyL (PyL-PSMA) PET/CT images, EPS-145, European Association of Nuclear Medicine, (2020), <http://link.springer.com/article/10.1007/s00259-020-04988-4>. Retrieved Sep. 18, 2020.
Brynolfsson, J., et. al., Deep Learning-Enabled comprehensive detection and quantification of 18FDCFPyL (PyL-PSMA) PET/CT, OP-548, European Association of Nuclear Medicine, (2020), <http://link.springer.com/article/10.1007/s00259-020-04988-4>. Retrieved Sep. 18, 2020.
Dertat, A., Applied Depp Learning—Part 4: Convolutional Neural Networks, Towards Data Science,<http://towardsdatascience.com/applied-deep-learning-part-4-convolutional-neural-networks-584bc134c1e2> (2017).
Gjertsson, K., et. al., A Novel Automated Deep Learning Algorithm for Segmentation of the Skeleton in Low-Dose CT for [(18)F] DCFPyL PET/CT Hybrid Imaging in Patients with Metastatic Prostate Cancer, Annual Congress of the European Association of Nuclear Medicine Oct. 12-16, 2019 Barcelona, Spain. Eur J Nucl Med Mol Imaging 46 (Suppl 1), S1-S952 (2019). Abstract EP-0823, p. S765.
Johnsson, K., et. al., miPSMA Index: Comprehensive and Automated Quantification of 18F-DCFPyL (PyL-PSMA) PET/CT for Prostate Cancer Staging, J Nucl Med., 61: (Supplement 1): 1435, (2020).
Lin, T.Y. et. al., Feature Pyramid Networks for object detection, FAIR, (2016), <https://arxiv.org/abs/1612.03144v1>.
Meyer, A., et. al., Deep learning algorithm improves identification of men with low-risk prostate cancer using PSMA targeted 99mTc-MIP-1404 SPECT/CT, Journal of Clinical Oncology, 37:(15), (2019).
Nickols, N.G., et. al., A deep learning algorithm to predict coexisting metastatic disease using intraprostatic [F18]DCFPYL PSMA image alone in veterans with prostate cancer, Journal of Clinical Oncology 38, (Supplement 6), 2020.

(56) **References Cited**

OTHER PUBLICATIONS

Ohlsson, M., et. al., Automated decision support for bone scintigraphy, Computer-based medical systems, pp. 1-6, (2009).
Pouliot, F., et. al., Prospective evaluation of a Novel Deep Learning Algorithm (PSMA-AI) in the assessment of 99mTc-MIP-1404 SPECT/CT in patients with low or intermediate risk prostate cancer, Annual Congress of the European Association of Nuclear Medicine Oct. 12-16, 2019 Barcelona, Spain. Eur J Nucl Med Mol Imaging 46 (Suppl 1), S1-S952 (2019). Abstract EP-0804, p. S765.
Ren, S., et. al., Faster R-CNN: Towards Real-Time Object Detection with Region Proposal Networks, (2015), <http://image-net.org/challenges/LSVRC/2015/results>.
Ronneberger, O., et. al., U-Net: Convolutional Networks for Biomedical Image Segmentation, Springer International Publishing, (2015), <http://lmb.informatik.uni-freiburg.de/>. Retrieved on Nov. 18, 2015.
Sjostrand, K., et. al., Automated Assessment of Prostatic PSMA Expression in SPECT/CT using Deep Convolutional Neural Networks—A Prospectively Planned Retrospective Analysis of Phase 3 Study MIP-1404-3301, The Journal of Nuclear Medicine, 60 (Supplement 1): Abstract 401, (2019).

* cited by examiner

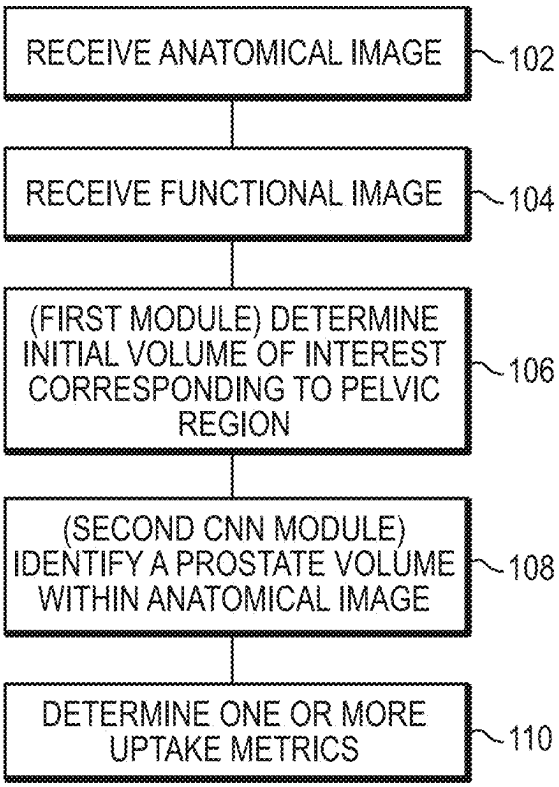
RECEIVE ANATOMICAL IMAGE
102
RECEIVE FUNCTIONAL IMAGE
104
(FIRST MODULE) DETERMINE INITIAL VOLUME OF INTEREST CORRESPONDING TO PELVIC REGION
106
(SECOND CNN MODULE) IDENTIFY A PROSTATE VOLUME WITHIN ANATOMICAL IMAGE
108
DETERMINE ONE OR MORE UPTAKE METRICS
110

FIG. 1

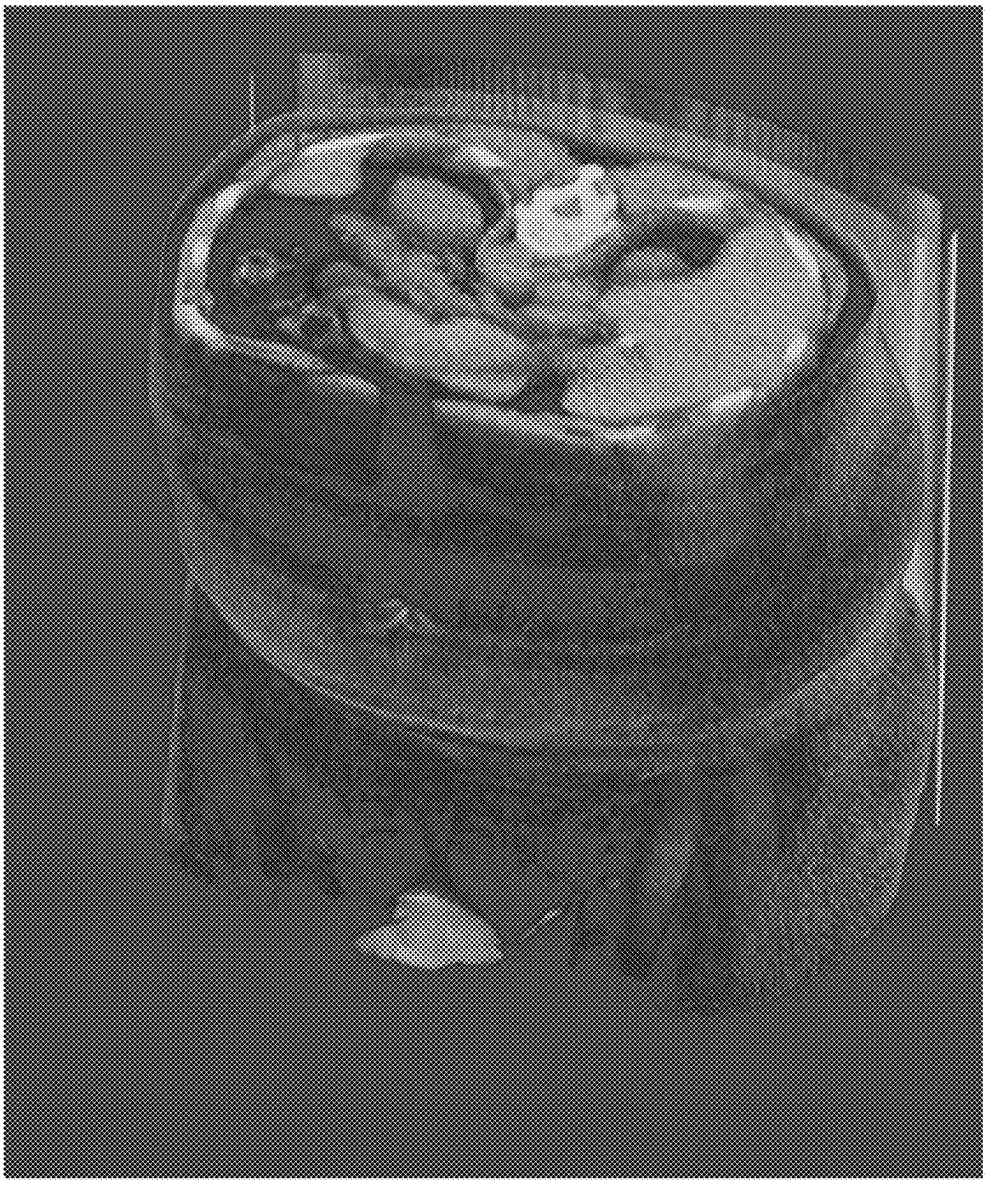

FIG. 2A

FIG. 2B

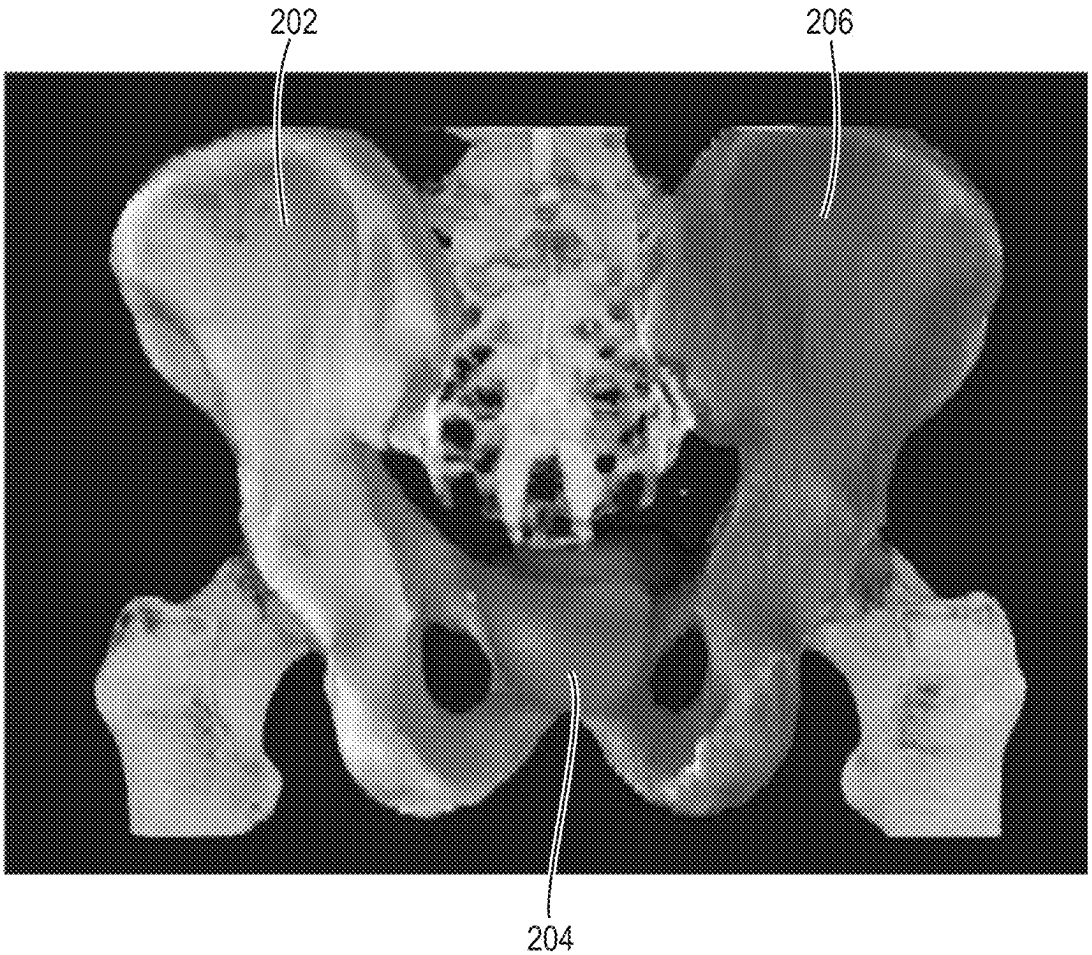

FIG. 2C

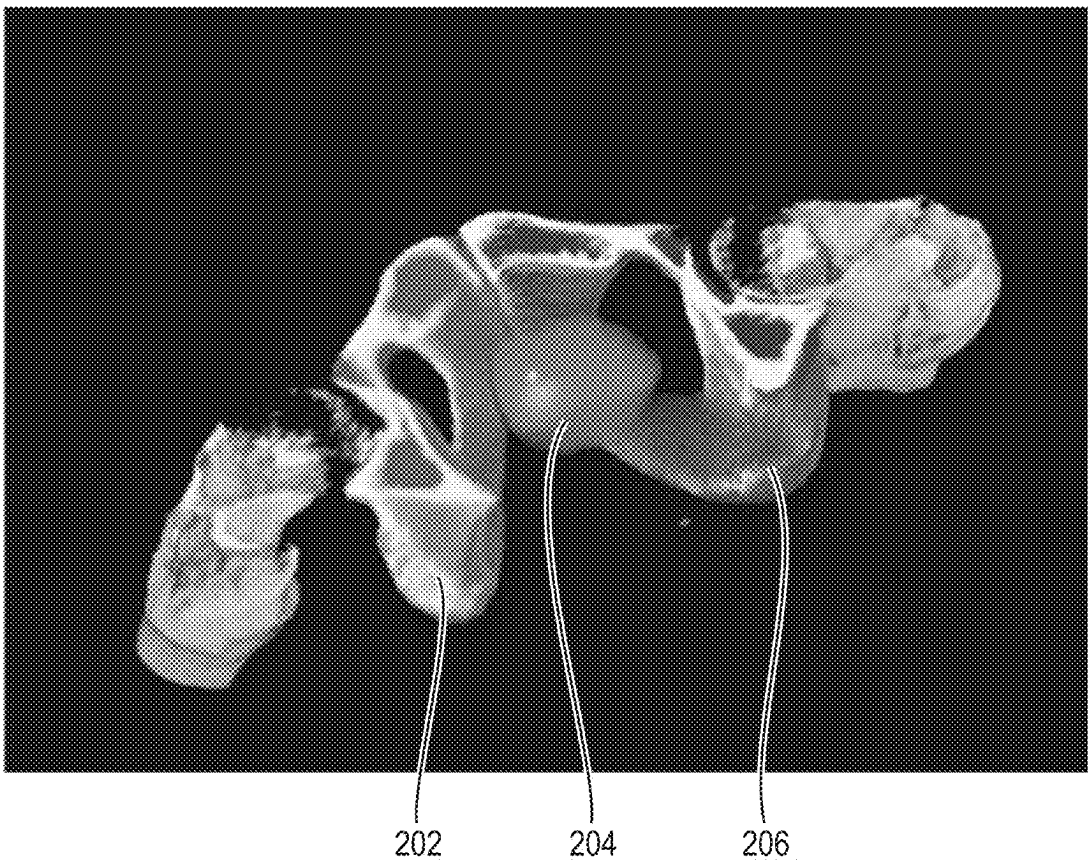

FIG. 2D

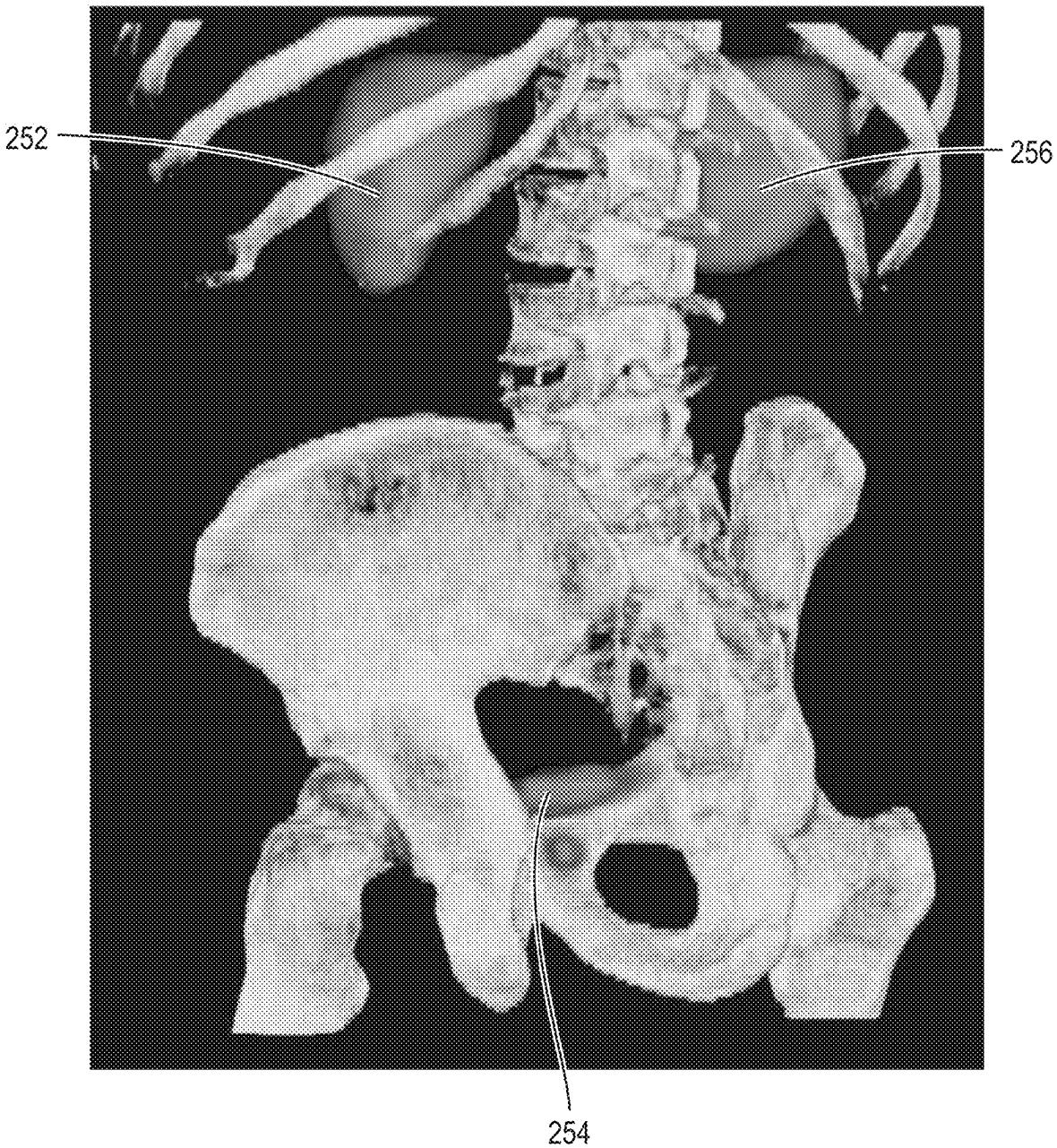

FIG. 2E

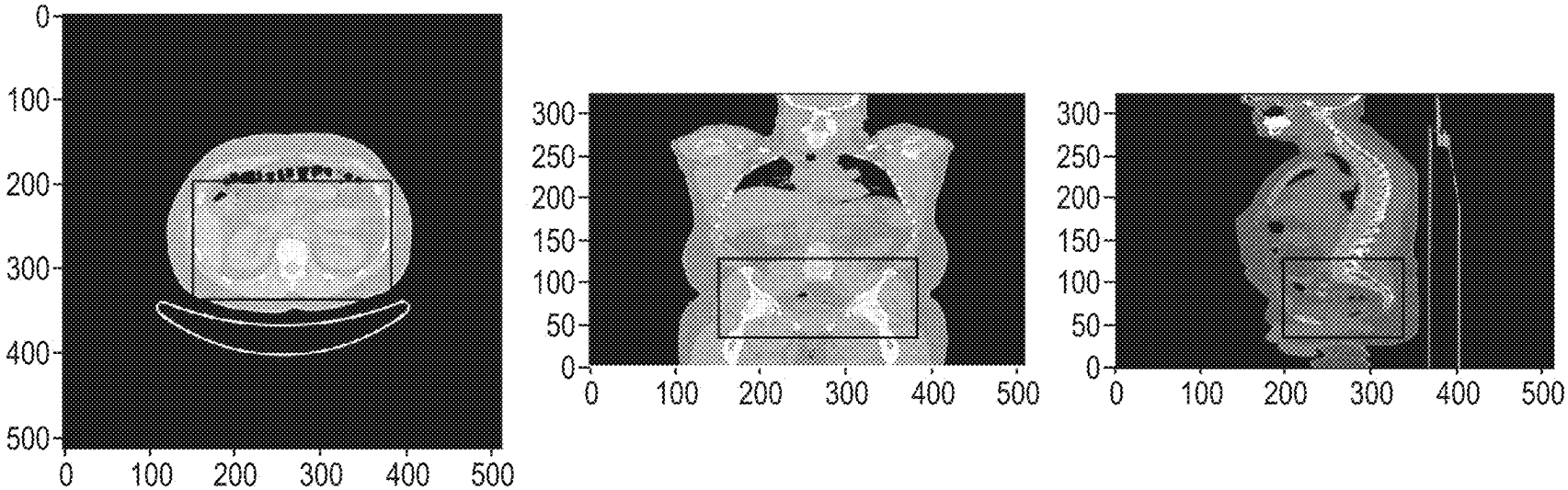
0
100
200
300
400
500
0 100 200 300 400 500
300
250
200
150
100
50
0
0 100 200 300 400 500
300
250
200
150
100
50
0
0 100 200 300 400 500

FIG. 3A

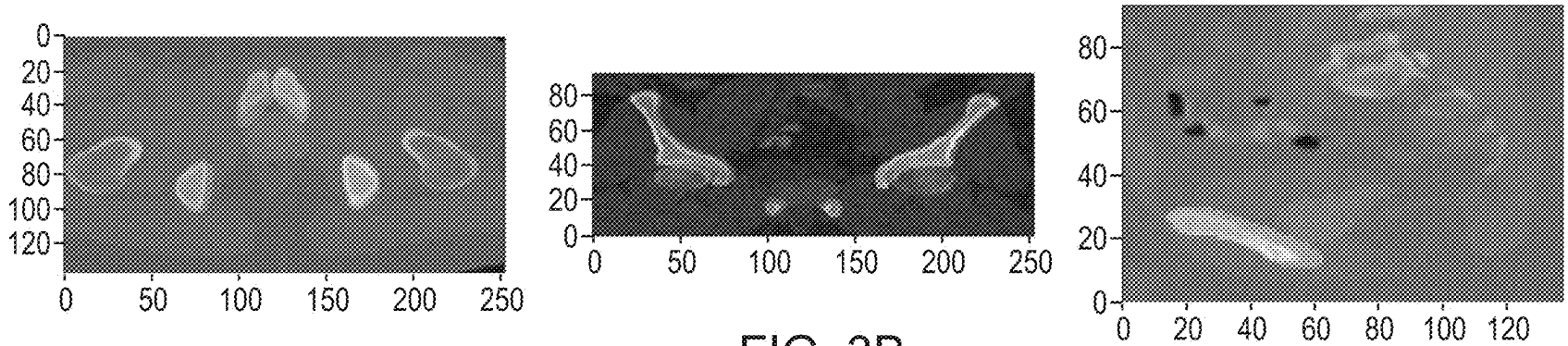
0
20
40
60
80
100
120
0 50 100 150 200 250
80
60
40
20
0
0 50 100 150 200 250
80
60
40
20
0
0 20 40 60 80 100 120

FIG. 3B

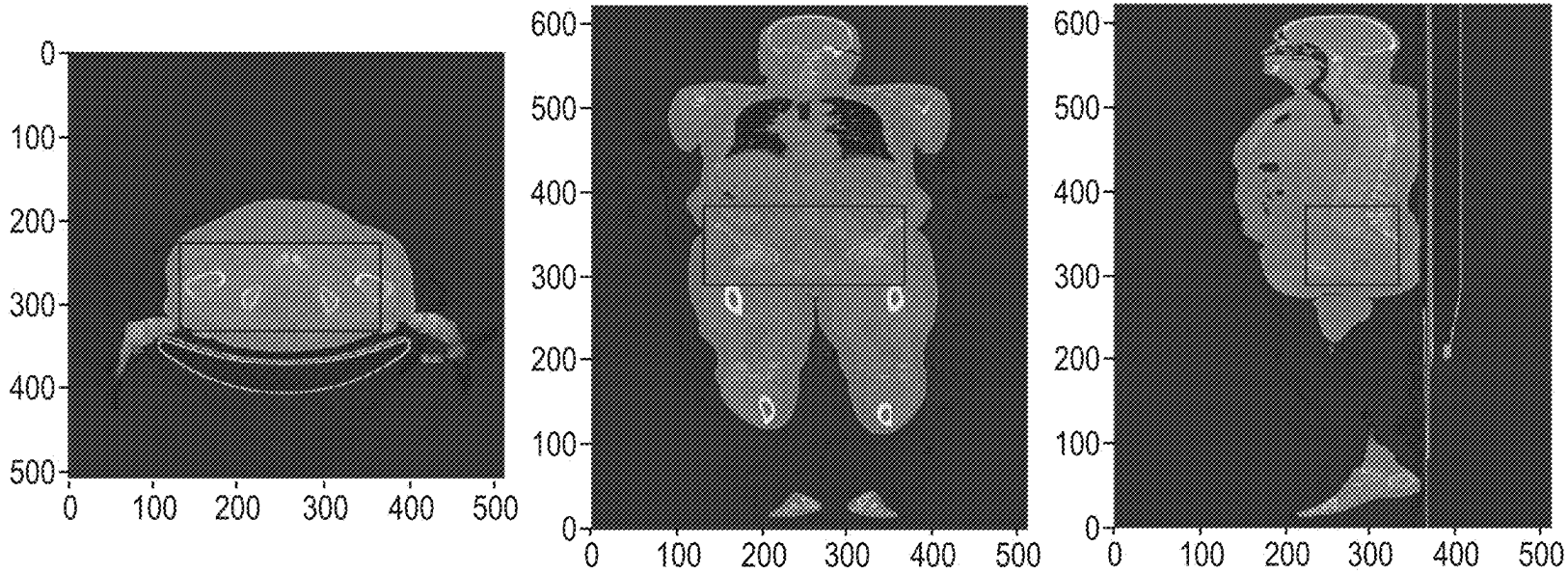
0
100
200
300
400
500
0 100 200 300 400 500
600
500
400
300
200
100
0
0 100 200 300 400 500
600
500
400
300
200
100
0
0 100 200 300 400 500

FIG. 4A

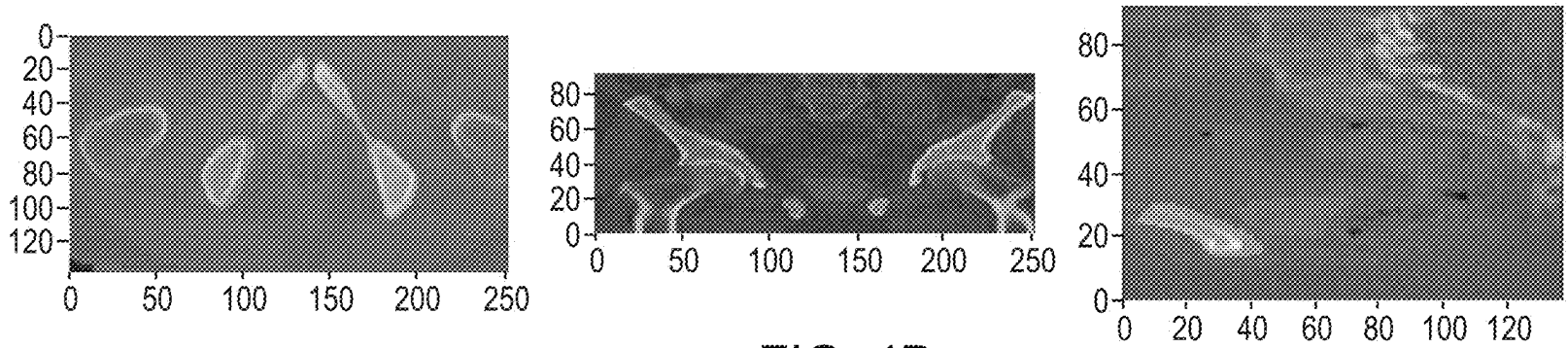
0
20
40
60
80
100
120
0 50 100 150 200 250
80
60
40
20
0
0 50 100 150 200 250
80
60
40
20
0
0 20 40 60 80 100 120

FIG. 4B

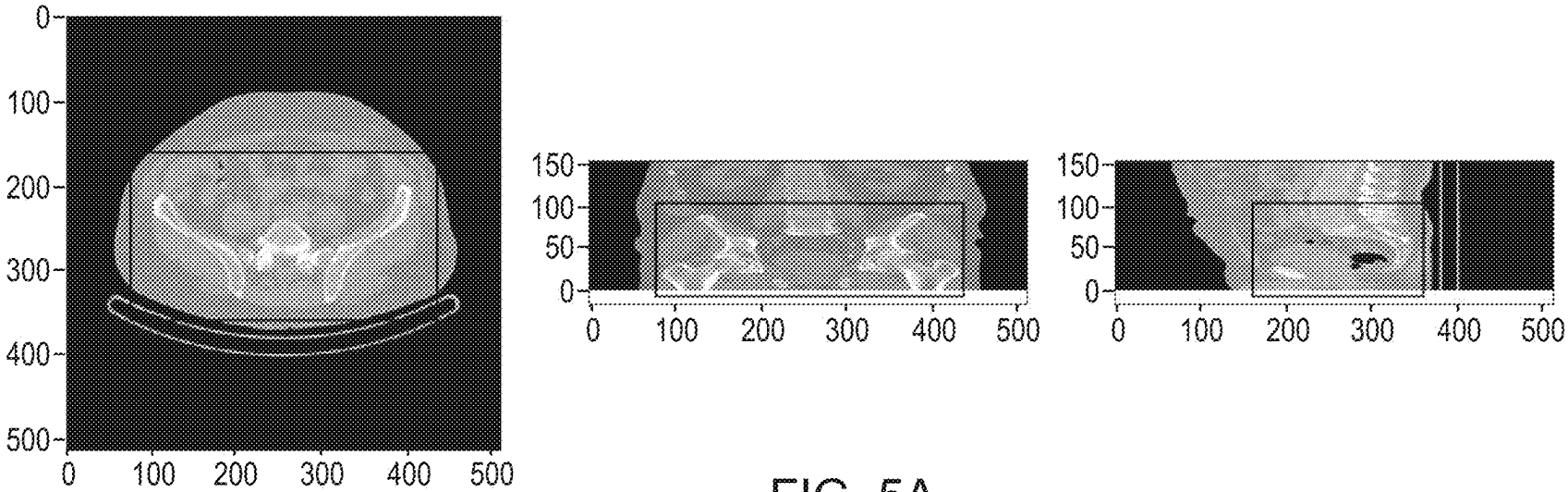
0
100
200
300
400
500
0 100 200 300 400 500
150
100
50
0
0 100 200 300 400 500
150
100
50
0
0 100 200 300 400 500

FIG. 5A

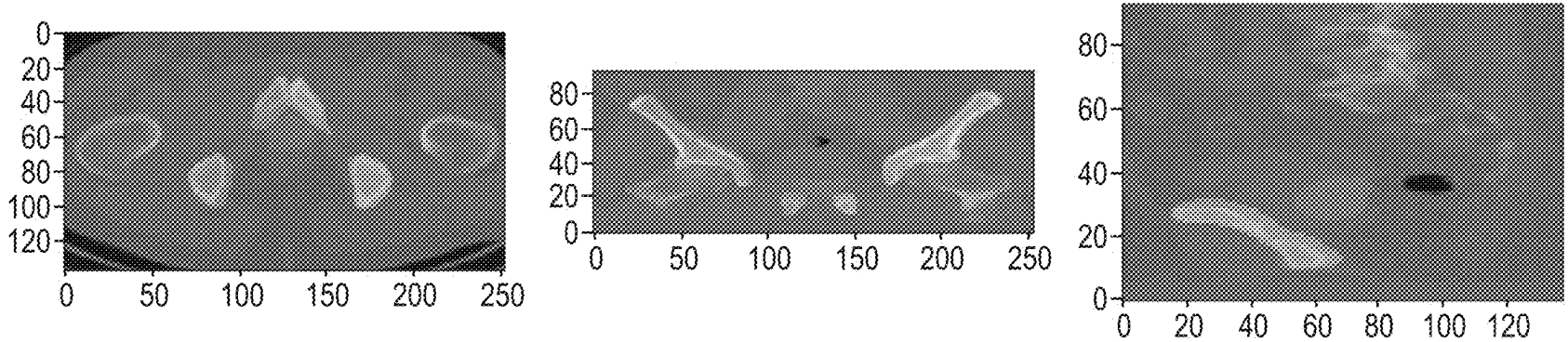
0
20
40
60
80
100
120
0 50 100 150 200 250
80
60
40
20
0
0 50 100 150 200 250
80
60
40
20
0
0 20 40 60 80 100 120

FIG. 5B

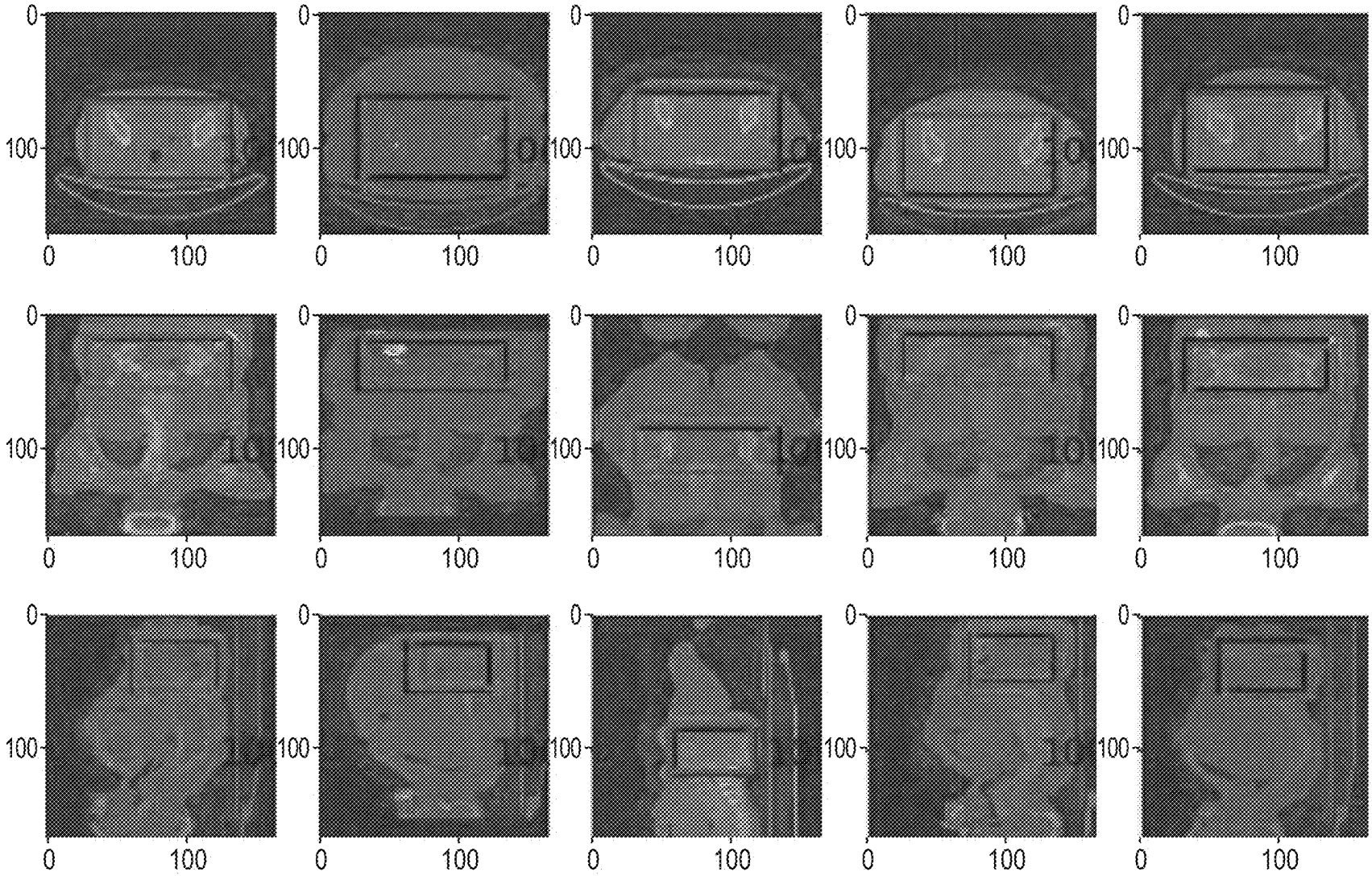

FIG. 6A

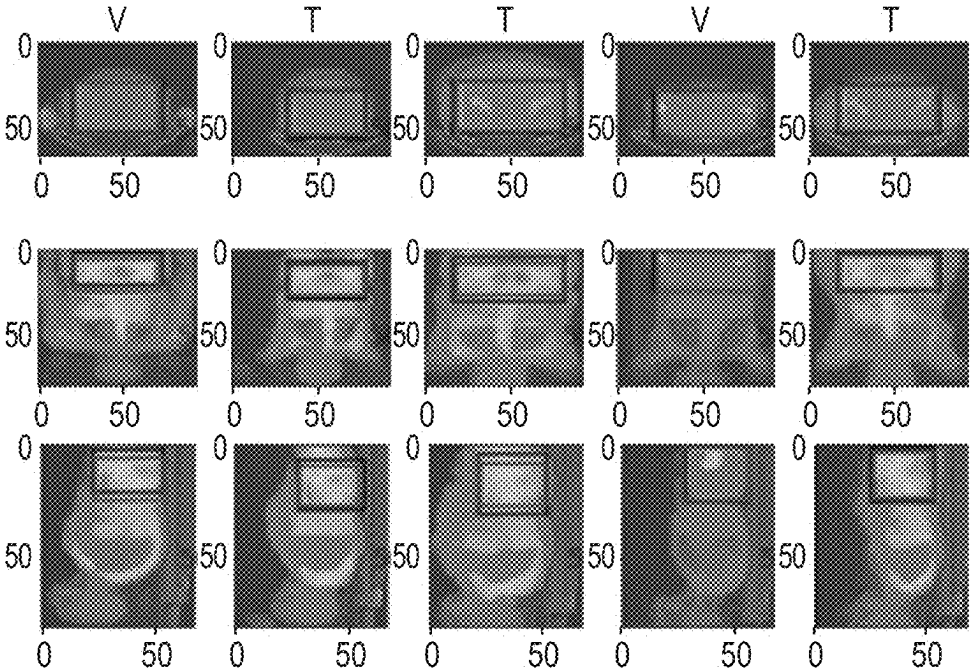

TRAD. LOCALIZATION
(MEDIAN CROP SIZE = 94 x 130 x 221)

FIG. 6B

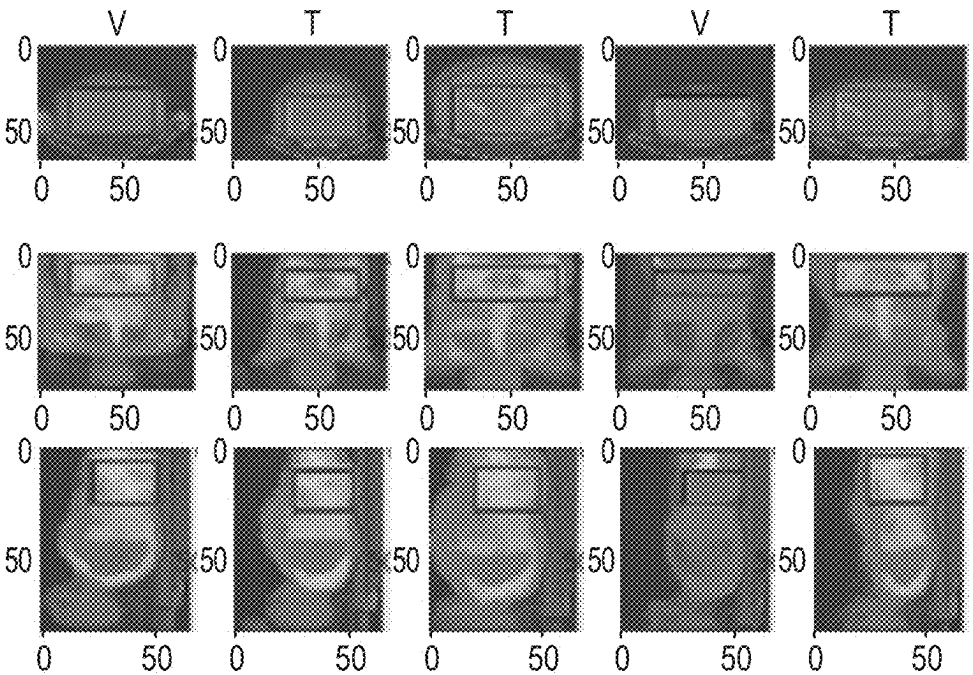

TRAD. LOCALIZATION
(MEDIAN CROP SIZE = 74 x 116 x 205)

FIG. 6C

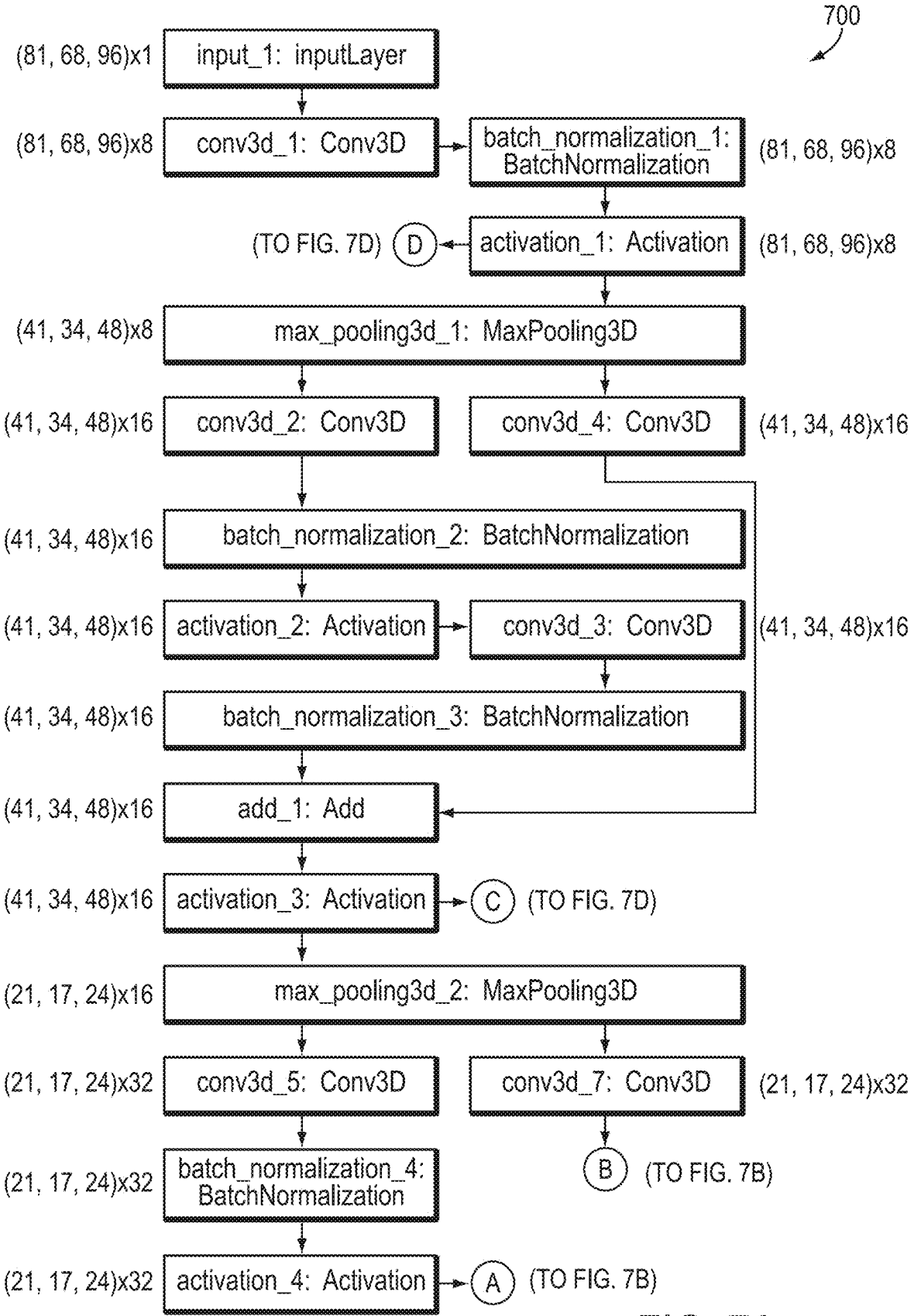
700
(81, 68, 96)x1
input_1: inputLayer
(81, 68, 96)x8
conv3d_1: Conv3D
batch_normalization_1: BatchNormalization
(81, 68, 96)x8
(TO FIG. 7D)
D
activation_1: Activation
(81, 68, 96)x8
(41, 34, 48)x8
max_pooling3d_1: MaxPooling3D
(41, 34, 48)x16
conv3d_2: Conv3D
conv3d_4: Conv3D
(41, 34, 48)x16
(41, 34, 48)x16
batch_normalization_2: BatchNormalization
(41, 34, 48)x16
activation_2: Activation
conv3d_3: Conv3D
(41, 34, 48)x16
(41, 34, 48)x16
batch_normalization_3: BatchNormalization
(41, 34, 48)x16
add_1: Add
(41, 34, 48)x16
activation_3: Activation
C
(TO FIG. 7D)
(21, 17, 24)x16
max_pooling3d_2: MaxPooling3D
(21, 17, 24)x32
conv3d_5: Conv3D
conv3d_7: Conv3D
(21, 17, 24)x32
(21, 17, 24)x32
batch_normalization_4: BatchNormalization
B
(TO FIG. 7B)
(21, 17, 24)x32
activation_4: Activation
A
(TO FIG. 7B)

FIG. 7A

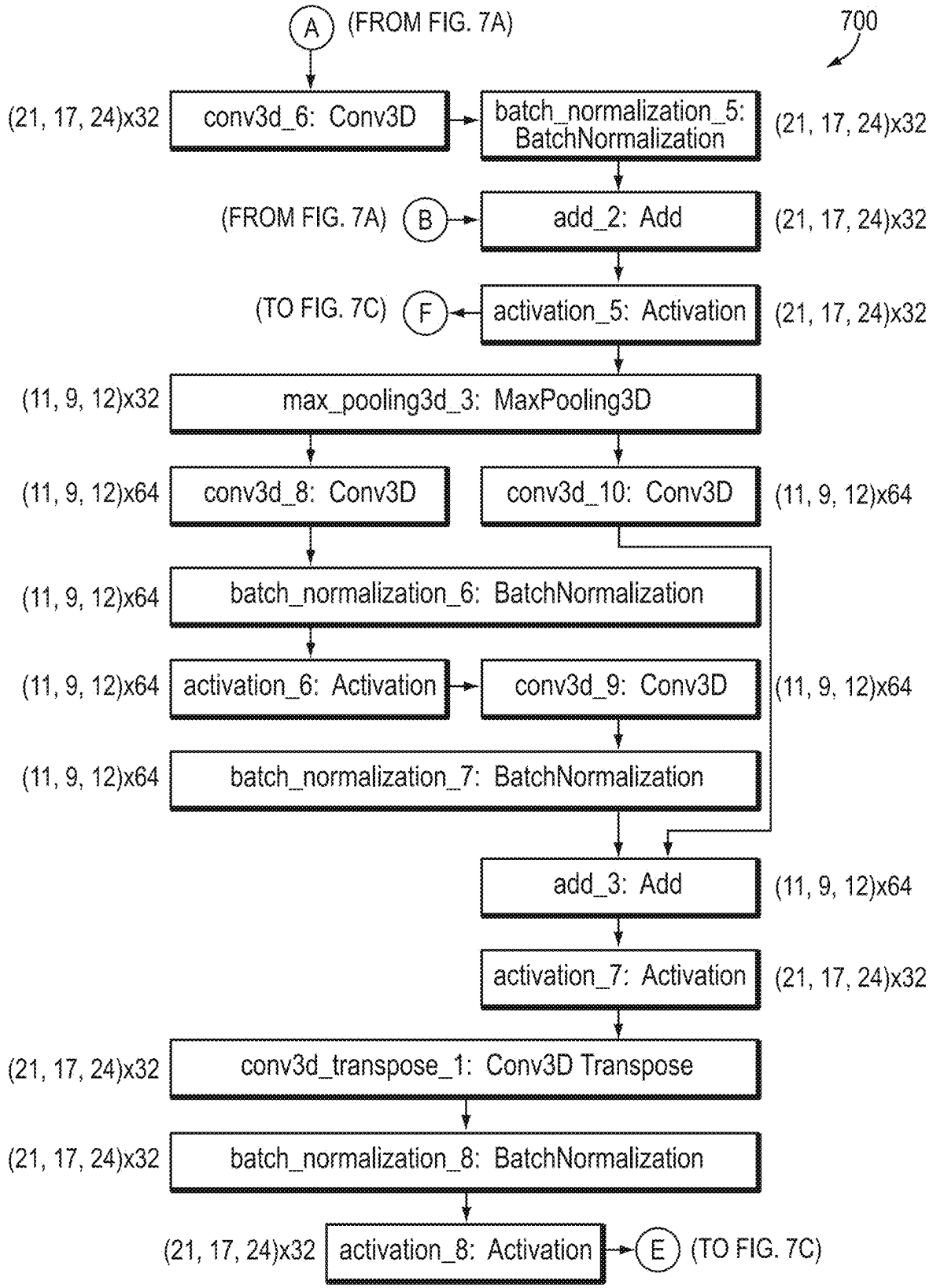
A
(FROM FIG. 7A)
700
(21, 17, 24)x32
conv3d_6: Conv3D
batch_normalization_5: BatchNormalization
(21, 17, 24)x32
(FROM FIG. 7A)
B
add_2: Add
(21, 17, 24)x32
(TO FIG. 7C)
F
activation_5: Activation
(21, 17, 24)x32
(11, 9, 12)x32
max_pooling3d_3: MaxPooling3D
(11, 9, 12)x64
conv3d_8: Conv3D
conv3d_10: Conv3D
(11, 9, 12)x64
(11, 9, 12)x64
batch_normalization_6: BatchNormalization
(11, 9, 12)x64
activation_6: Activation
conv3d_9: Conv3D
(11, 9, 12)x64
(11, 9, 12)x64
batch_normalization_7: BatchNormalization
add_3: Add
(11, 9, 12)x64
activation_7: Activation
(21, 17, 24)x32
(21, 17, 24)x32
conv3d_transpose_1: Conv3D Transpose
(21, 17, 24)x32
batch_normalization_8: BatchNormalization
(21, 17, 24)x32
activation_8: Activation
E
(TO FIG. 7C)

FIG. 7B

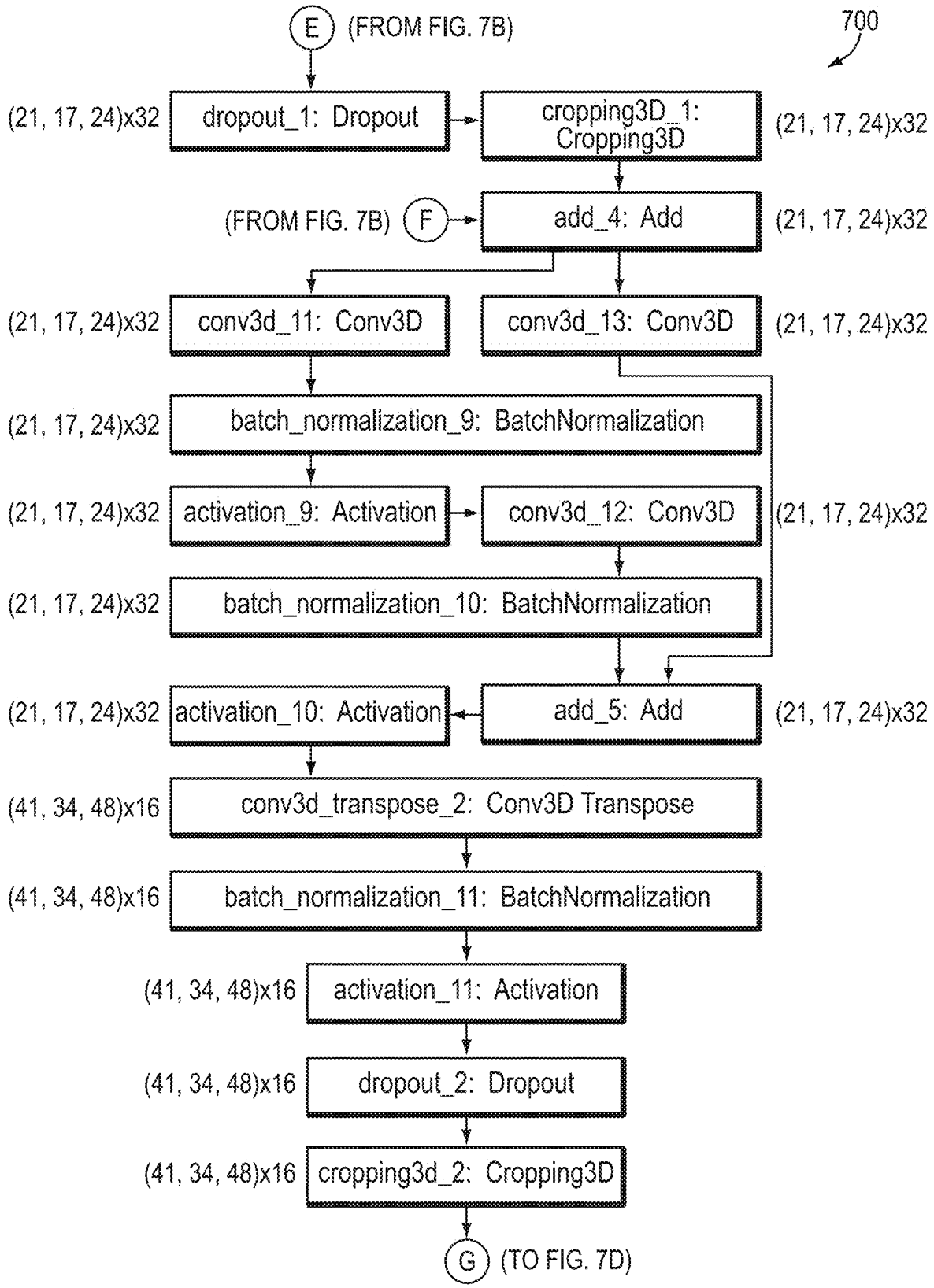
E
(FROM FIG. 7B)
700
(21, 17, 24)x32
dropout_1: Dropout
cropping3D_1: Cropping3D
(21, 17, 24)x32
(FROM FIG. 7B)
F
add_4: Add
(21, 17, 24)x32
(21, 17, 24)x32
conv3d_11: Conv3D
conv3d_13: Conv3D
(21, 17, 24)x32
(21, 17, 24)x32
batch_normalization_9: BatchNormalization
(21, 17, 24)x32
activation_9: Activation
conv3d_12: Conv3D
(21, 17, 24)x32
(21, 17, 24)x32
batch_normalization_10: BatchNormalization
(21, 17, 24)x32
activation_10: Activation
add_5: Add
(21, 17, 24)x32
(41, 34, 48)x16
conv3d_transpose_2: Conv3D Transpose
(41, 34, 48)x16
batch_normalization_11: BatchNormalization
(41, 34, 48)x16
activation_11: Activation
(41, 34, 48)x16
dropout_2: Dropout
(41, 34, 48)x16
cropping3d_2: Cropping3D
G
(TO FIG. 7D)

FIG. 7C

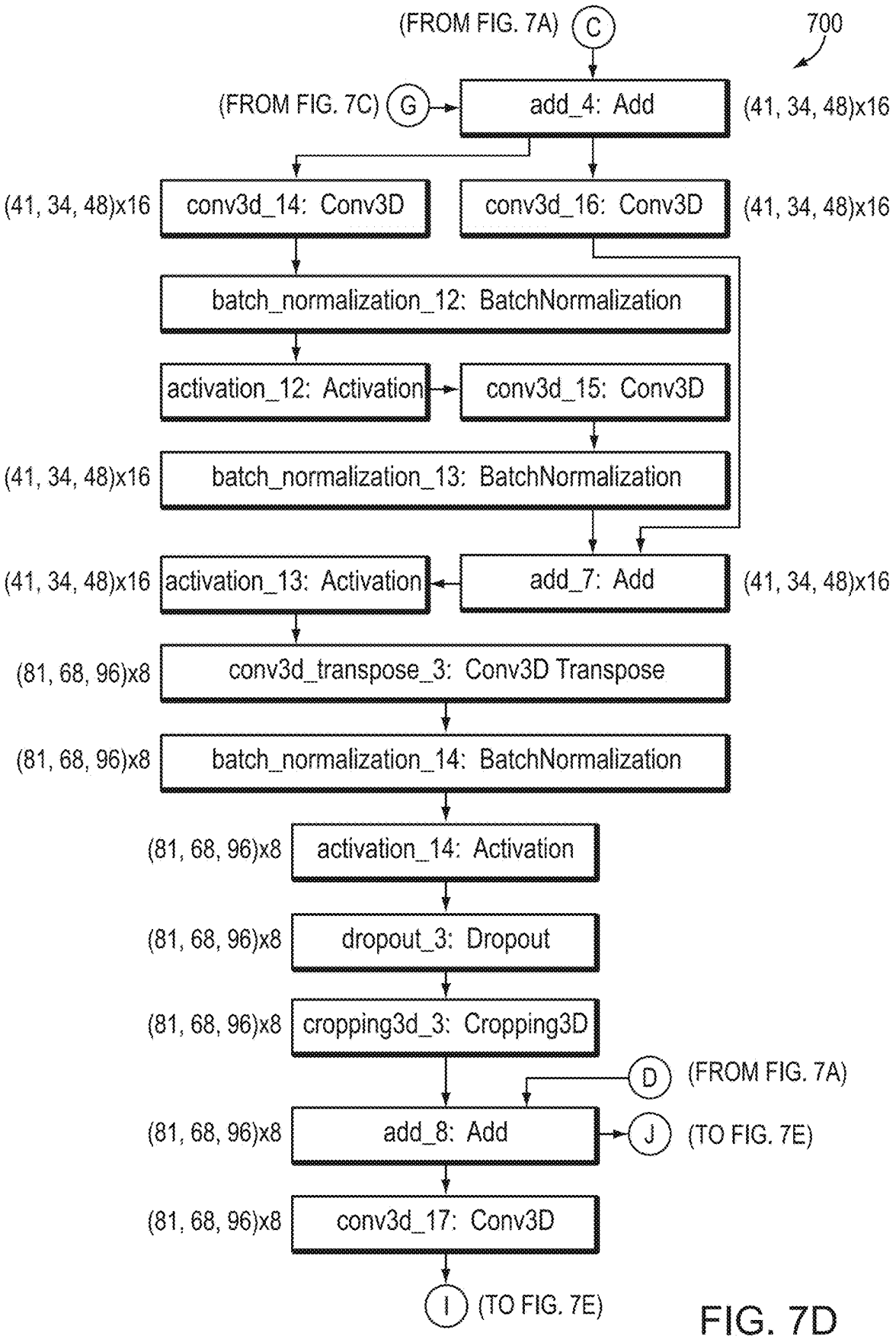
(FROM FIG. 7A)
C
700
(FROM FIG. 7C)
G
add_4: Add
(41, 34, 48)x16
(41, 34, 48)x16
conv3d_14: Conv3D
conv3d_16: Conv3D
(41, 34, 48)x16
batch_normalization_12: BatchNormalization
activation_12: Activation
conv3d_15: Conv3D
(41, 34, 48)x16
batch_normalization_13: BatchNormalization
(41, 34, 48)x16
activation_13: Activation
add_7: Add
(41, 34, 48)x16
(81, 68, 96)x8
conv3d_transpose_3: Conv3D Transpose
(81, 68, 96)x8
batch_normalization_14: BatchNormalization
(81, 68, 96)x8
activation_14: Activation
(81, 68, 96)x8
dropout_3: Dropout
(81, 68, 96)x8
cropping3d_3: Cropping3D
D
(FROM FIG. 7A)
(81, 68, 96)x8
add_8: Add
J
(TO FIG. 7E)
(81, 68, 96)x8
conv3d_17: Conv3D
I
(TO FIG. 7E)

FIG. 7D

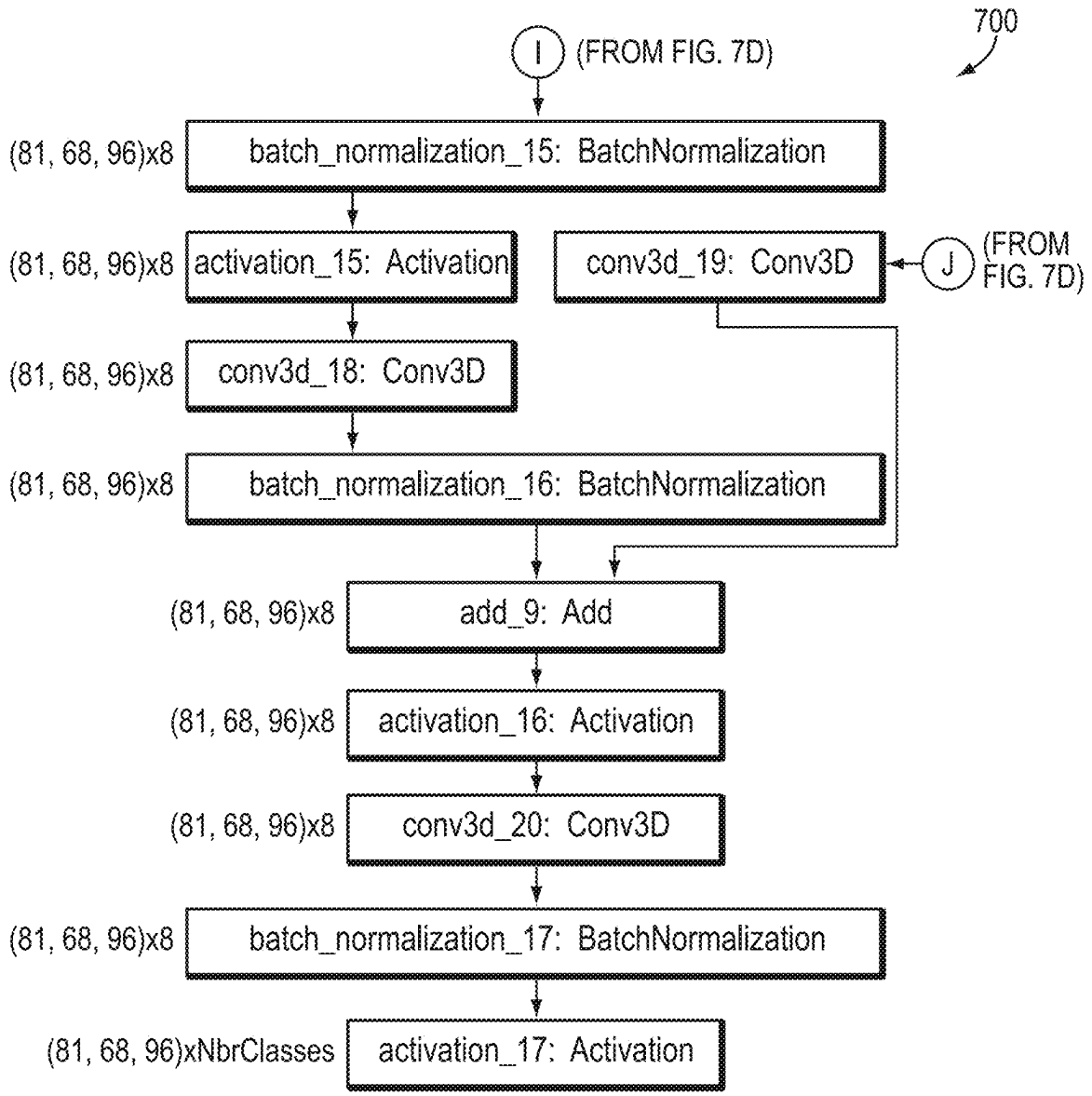
700
I
(FROM FIG. 7D)
(81, 68, 96)x8
batch_normalization_15: BatchNormalization
(81, 68, 96)x8
activation_15: Activation
conv3d_19: Conv3D
J
(FROM FIG. 7D)
(81, 68, 96)x8
conv3d_18: Conv3D
(81, 68, 96)x8
batch_normalization_16: BatchNormalization
(81, 68, 96)x8
add_9: Add
(81, 68, 96)x8
activation_16: Activation
(81, 68, 96)x8
conv3d_20: Conv3D
(81, 68, 96)x8
batch_normalization_17: BatchNormalization
(81, 68, 96)xNbrClasses
activation_17: Activation

FIG. 7E

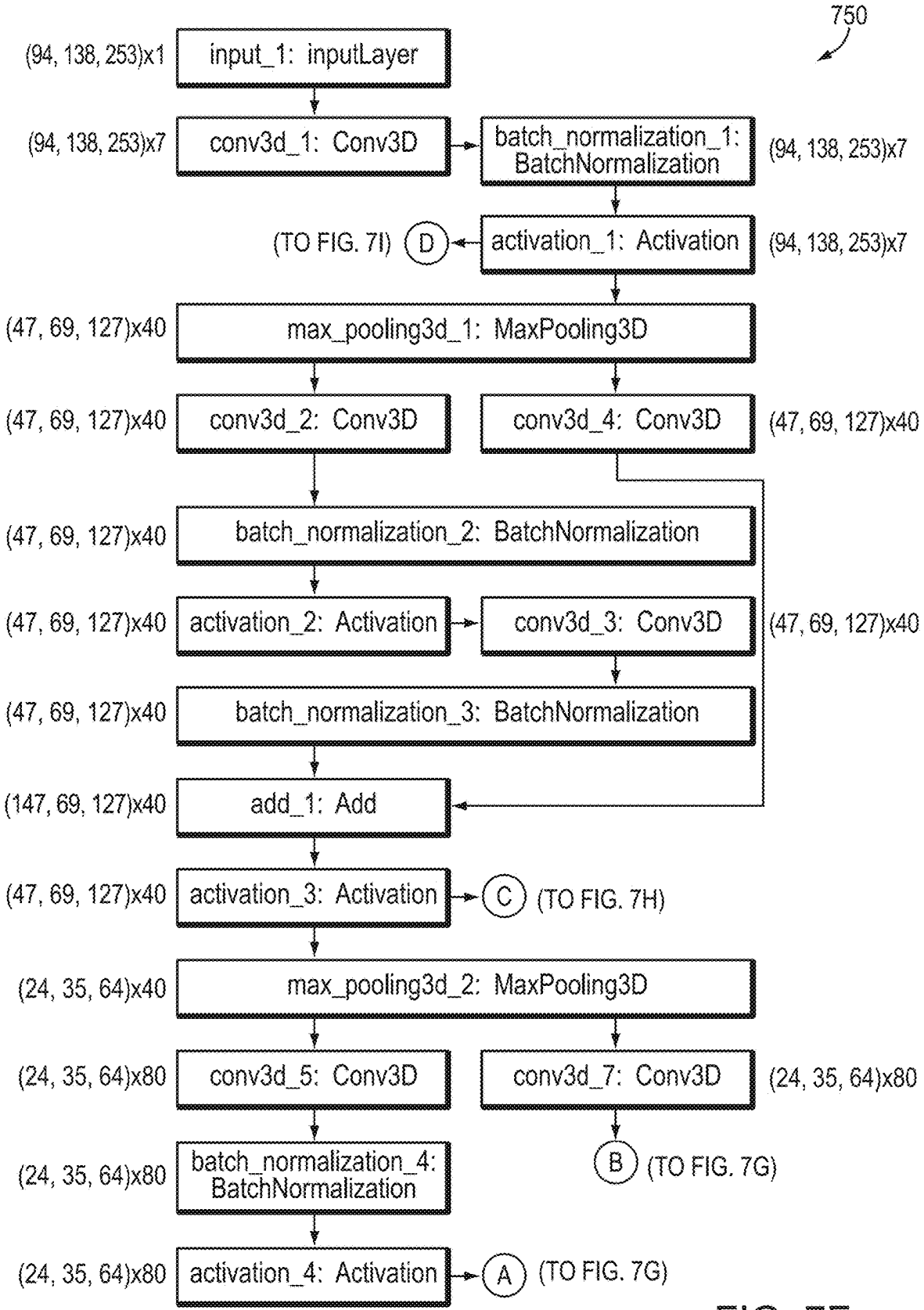
750
(94, 138, 253)x1
input_1: inputLayer
(94, 138, 253)x7
conv3d_1: Conv3D
batch_normalization_1: BatchNormalization
(94, 138, 253)x7
(TO FIG. 7I)
D
activation_1: Activation
(94, 138, 253)x7
(47, 69, 127)x40
max_pooling3d_1: MaxPooling3D
(47, 69, 127)x40
conv3d_2: Conv3D
conv3d_4: Conv3D
(47, 69, 127)x40
(47, 69, 127)x40
batch_normalization_2: BatchNormalization
(47, 69, 127)x40
activation_2: Activation
conv3d_3: Conv3D
(47, 69, 127)x40
(47, 69, 127)x40
batch_normalization_3: BatchNormalization
(147, 69, 127)x40
add_1: Add
(47, 69, 127)x40
activation_3: Activation
C
(TO FIG. 7H)
(24, 35, 64)x40
max_pooling3d_2: MaxPooling3D
(24, 35, 64)x80
conv3d_5: Conv3D
conv3d_7: Conv3D
(24, 35, 64)x80
(24, 35, 64)x80
batch_normalization_4: BatchNormalization
B
(TO FIG. 7G)
(24, 35, 64)x80
activation_4: Activation
A
(TO FIG. 7G)

FIG. 7F

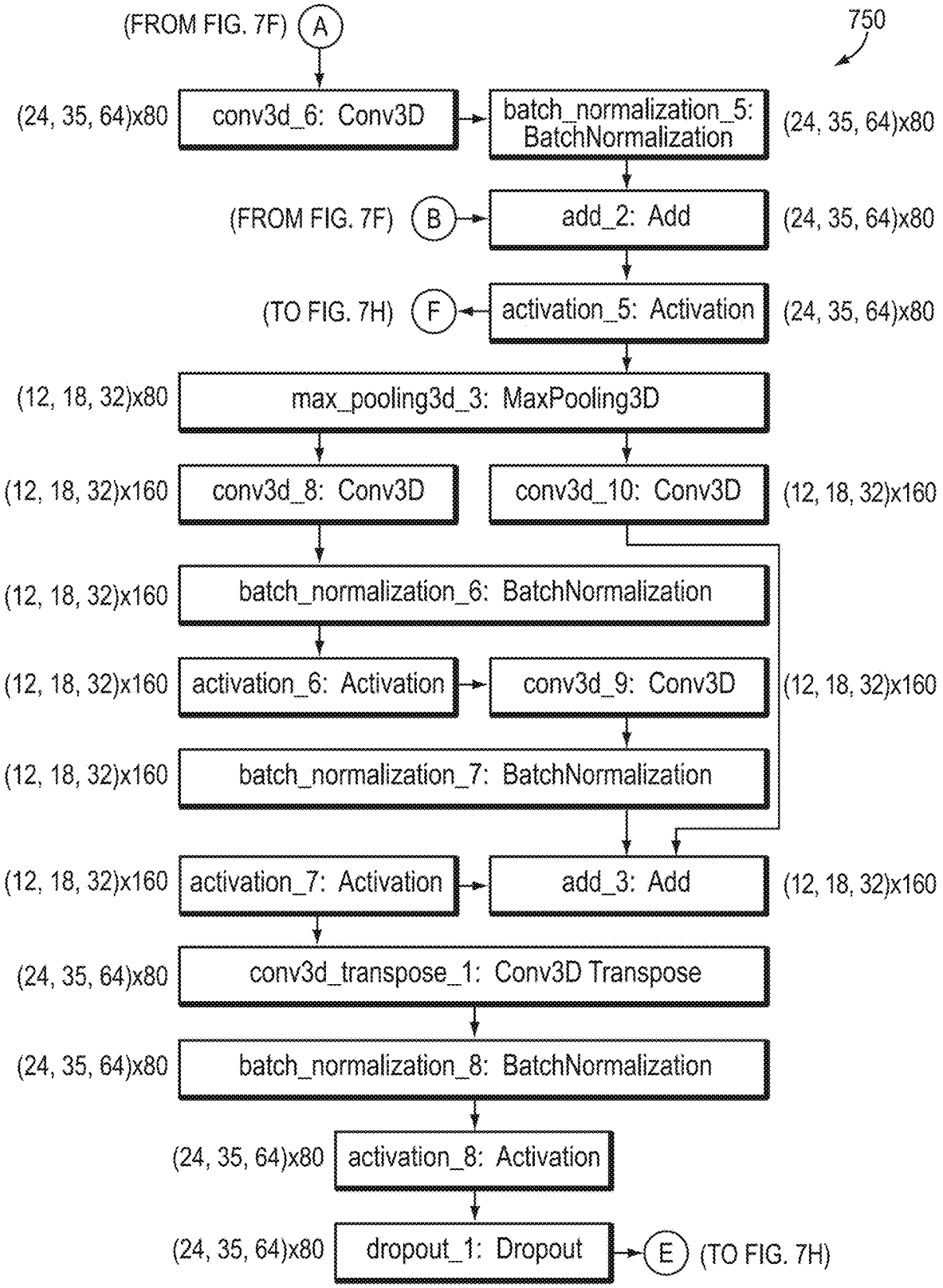
(FROM FIG. 7F) A
750
(24, 35, 64)x80
conv3d_6: Conv3D
batch_normalization_5: BatchNormalization
(24, 35, 64)x80
(FROM FIG. 7F) B
add_2: Add
(24, 35, 64)x80
(TO FIG. 7H) F
activation_5: Activation
(24, 35, 64)x80
(12, 18, 32)x80
max_pooling3d_3: MaxPooling3D
(12, 18, 32)x160
conv3d_8: Conv3D
conv3d_10: Conv3D
(12, 18, 32)x160
(12, 18, 32)x160
batch_normalization_6: BatchNormalization
(12, 18, 32)x160
activation_6: Activation
conv3d_9: Conv3D
(12, 18, 32)x160
(12, 18, 32)x160
batch_normalization_7: BatchNormalization
(12, 18, 32)x160
activation_7: Activation
add_3: Add
(12, 18, 32)x160
(24, 35, 64)x80
conv3d_transpose_1: Conv3D Transpose
(24, 35, 64)x80
batch_normalization_8: BatchNormalization
(24, 35, 64)x80
activation_8: Activation
(24, 35, 64)x80
dropout_1: Dropout
E
(TO FIG. 7H)

FIG. 7G

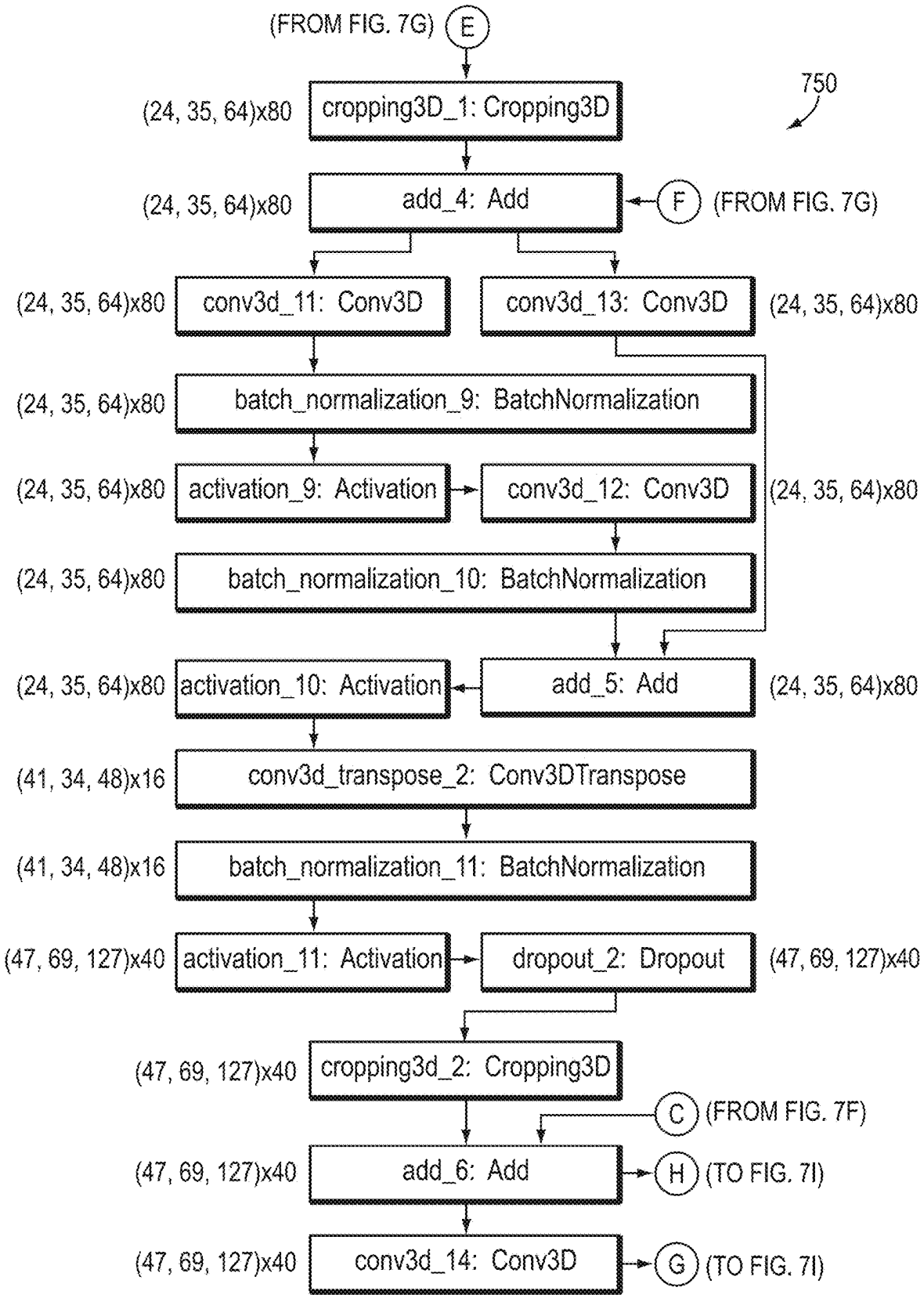
(FROM FIG. 7G) E
750
(24, 35, 64)x80
cropping3D_1: Cropping3D
(24, 35, 64)x80
add_4: Add
F (FROM FIG. 7G)
(24, 35, 64)x80
conv3d_11: Conv3D
conv3d_13: Conv3D
(24, 35, 64)x80
(24, 35, 64)x80
batch_normalization_9: BatchNormalization
(24, 35, 64)x80
activation_9: Activation
conv3d_12: Conv3D
(24, 35, 64)x80
(24, 35, 64)x80
batch_normalization_10: BatchNormalization
(24, 35, 64)x80
activation_10: Activation
add_5: Add
(24, 35, 64)x80
(41, 34, 48)x16
conv3d_transpose_2: Conv3DTranspose
(41, 34, 48)x16
batch_normalization_11: BatchNormalization
(47, 69, 127)x40
activation_11: Activation
dropout_2: Dropout
(47, 69, 127)x40
(47, 69, 127)x40
cropping3d_2: Cropping3D
C (FROM FIG. 7F)
(47, 69, 127)x40
add_6: Add
H (TO FIG. 7I)
(47, 69, 127)x40
conv3d_14: Conv3D
G (TO FIG. 7I)

FIG. 7H

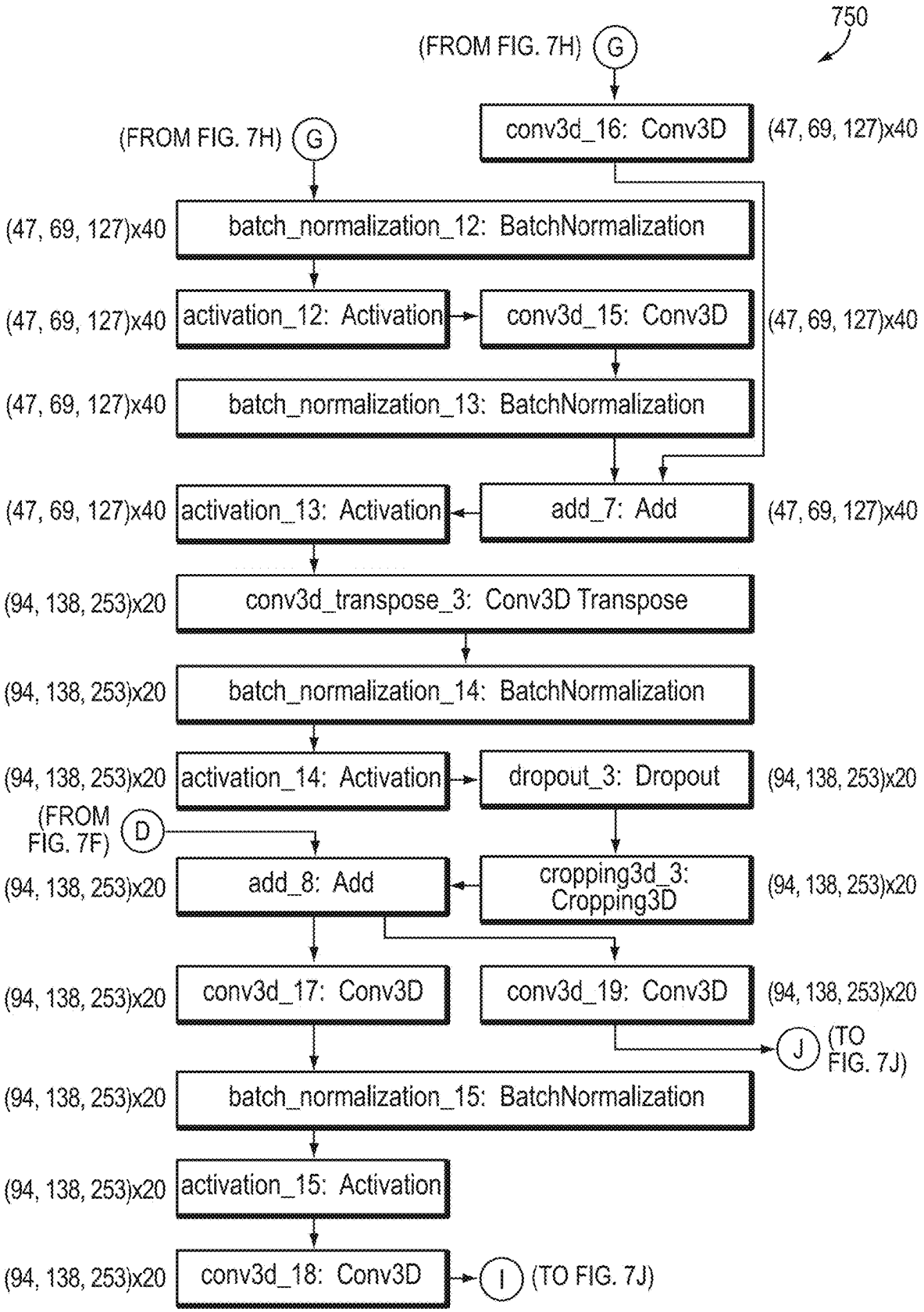
750
(FROM FIG. 7H) G
conv3d_16: Conv3D
(47, 69, 127)x40
(FROM FIG. 7H) G
(47, 69, 127)x40
batch_normalization_12: BatchNormalization
(47, 69, 127)x40
activation_12: Activation
conv3d_15: Conv3D
(47, 69, 127)x40
(47, 69, 127)x40
batch_normalization_13: BatchNormalization
(47, 69, 127)x40
activation_13: Activation
add_7: Add
(47, 69, 127)x40
(94, 138, 253)x20
conv3d_transpose_3: Conv3D Transpose
(94, 138, 253)x20
batch_normalization_14: BatchNormalization
(94, 138, 253)x20
activation_14: Activation
dropout_3: Dropout
(94, 138, 253)x20
(FROM FIG. 7F) D
(94, 138, 253)x20
add_8: Add
cropping3d_3: Cropping3D
(94, 138, 253)x20
(94, 138, 253)x20
conv3d_17: Conv3D
conv3d_19: Conv3D
(94, 138, 253)x20
J (TO FIG. 7J)
(94, 138, 253)x20
batch_normalization_15: BatchNormalization
(94, 138, 253)x20
activation_15: Activation
(94, 138, 253)x20
conv3d_18: Conv3D
I (TO FIG. 7J)

FIG. 7I

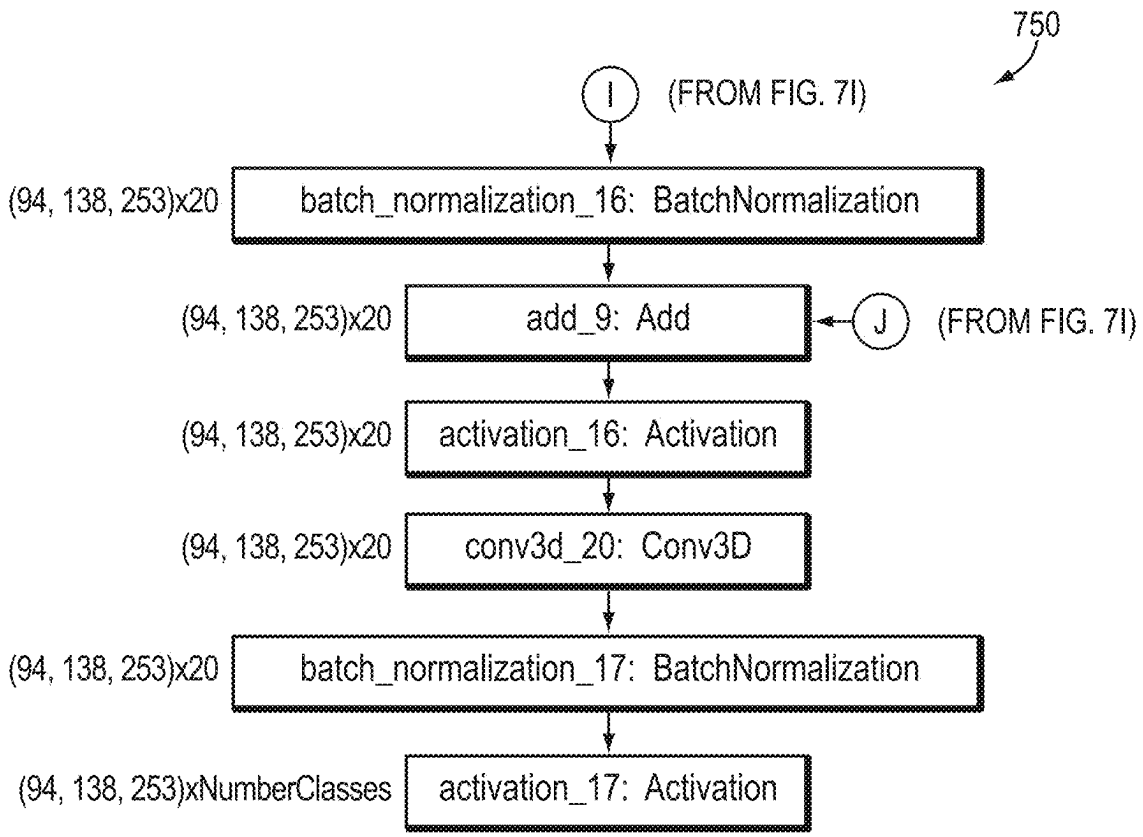
750
I
(FROM FIG. 7I)
(94, 138, 253)x20
batch_normalization_16: BatchNormalization
(94, 138, 253)x20
add_9: Add
J
(FROM FIG. 7I)
(94, 138, 253)x20
activation_16: Activation
(94, 138, 253)x20
conv3d_20: Conv3D
(94, 138, 253)x20
batch_normalization_17: BatchNormalization
(94, 138, 253)xNumberClasses
activation_17: Activation

FIG. 7J

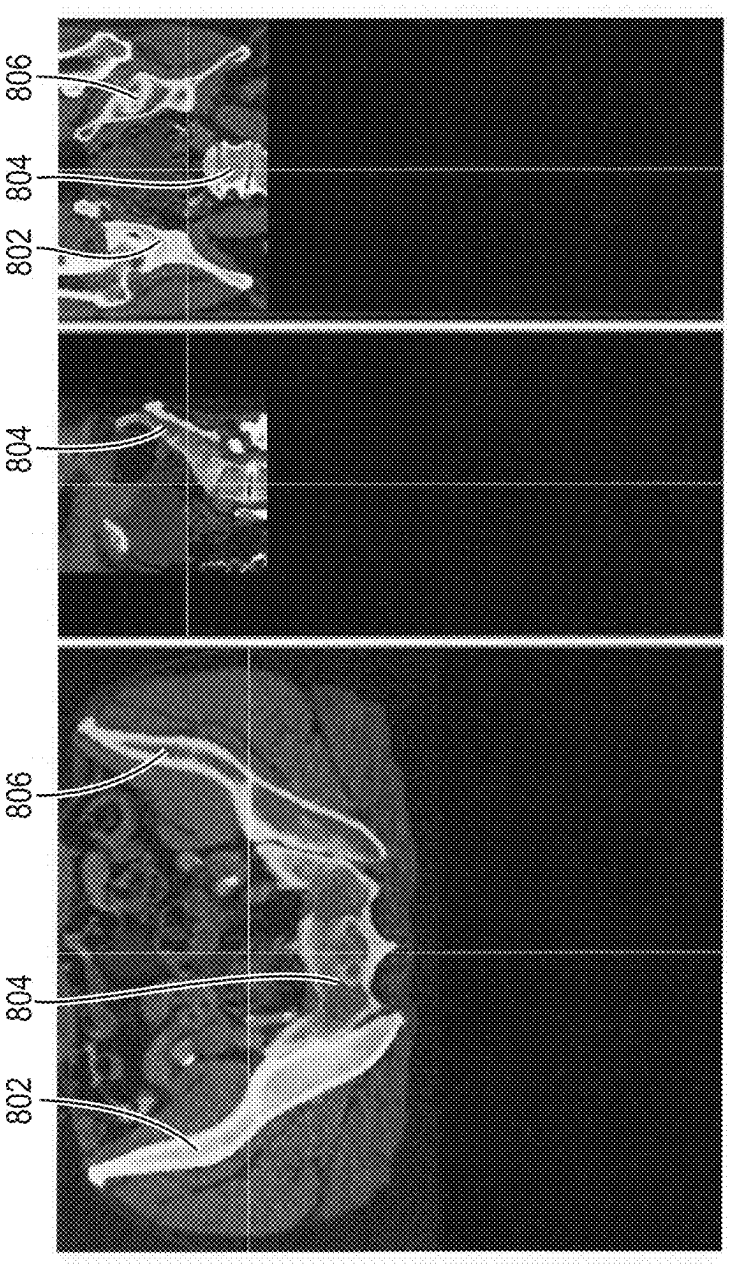

FIG. 8A

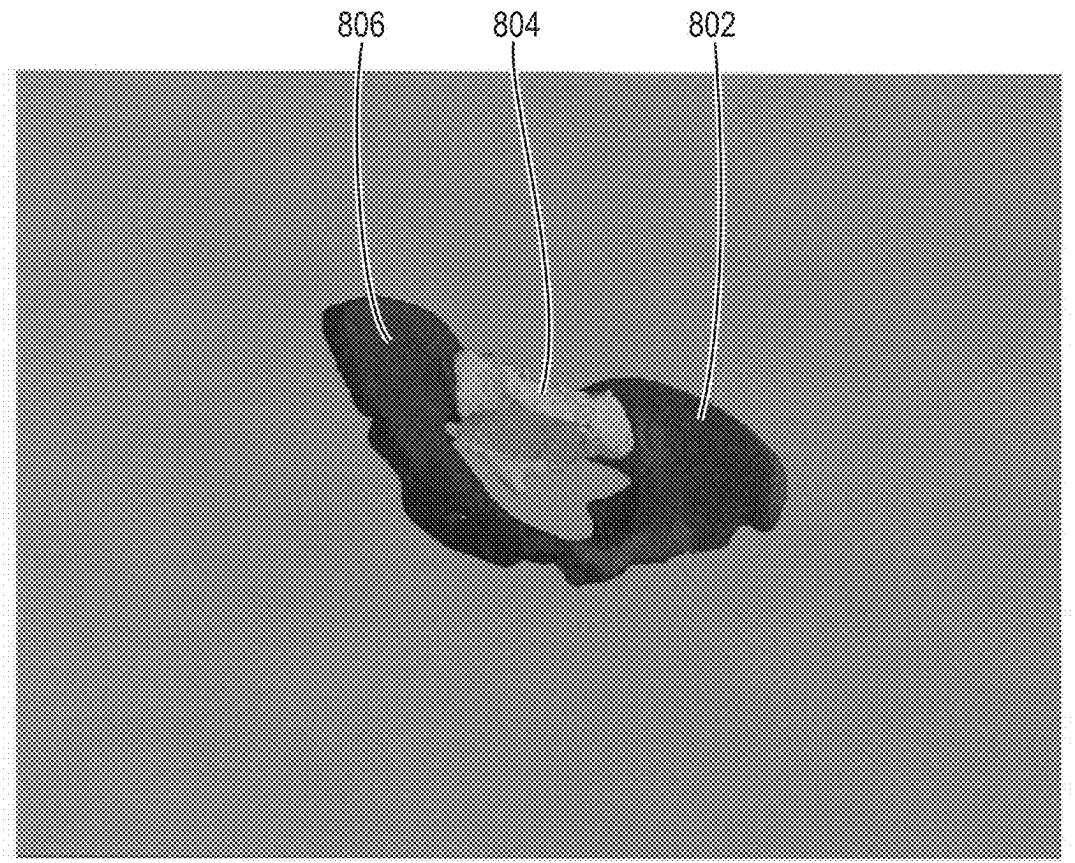

FIG. 8B

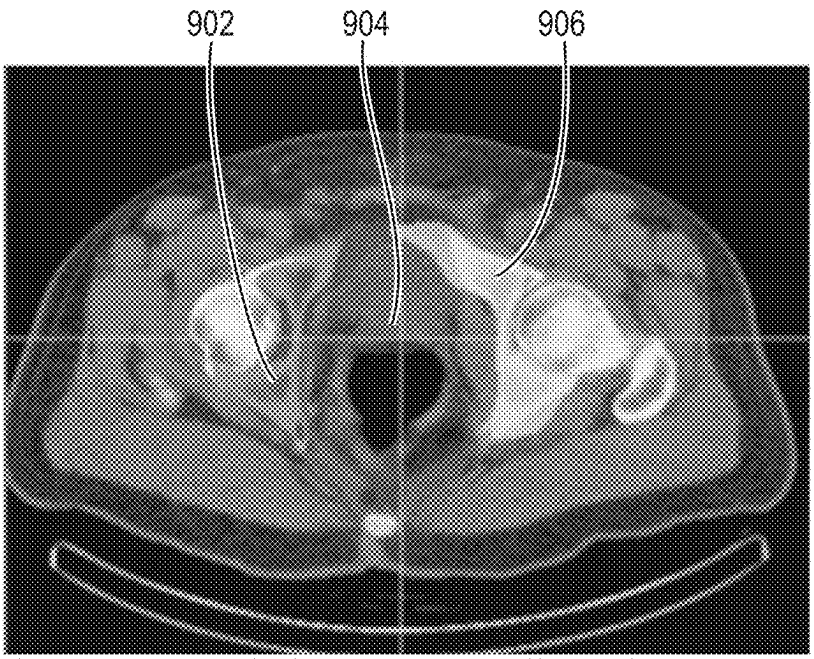

FIG. 9A

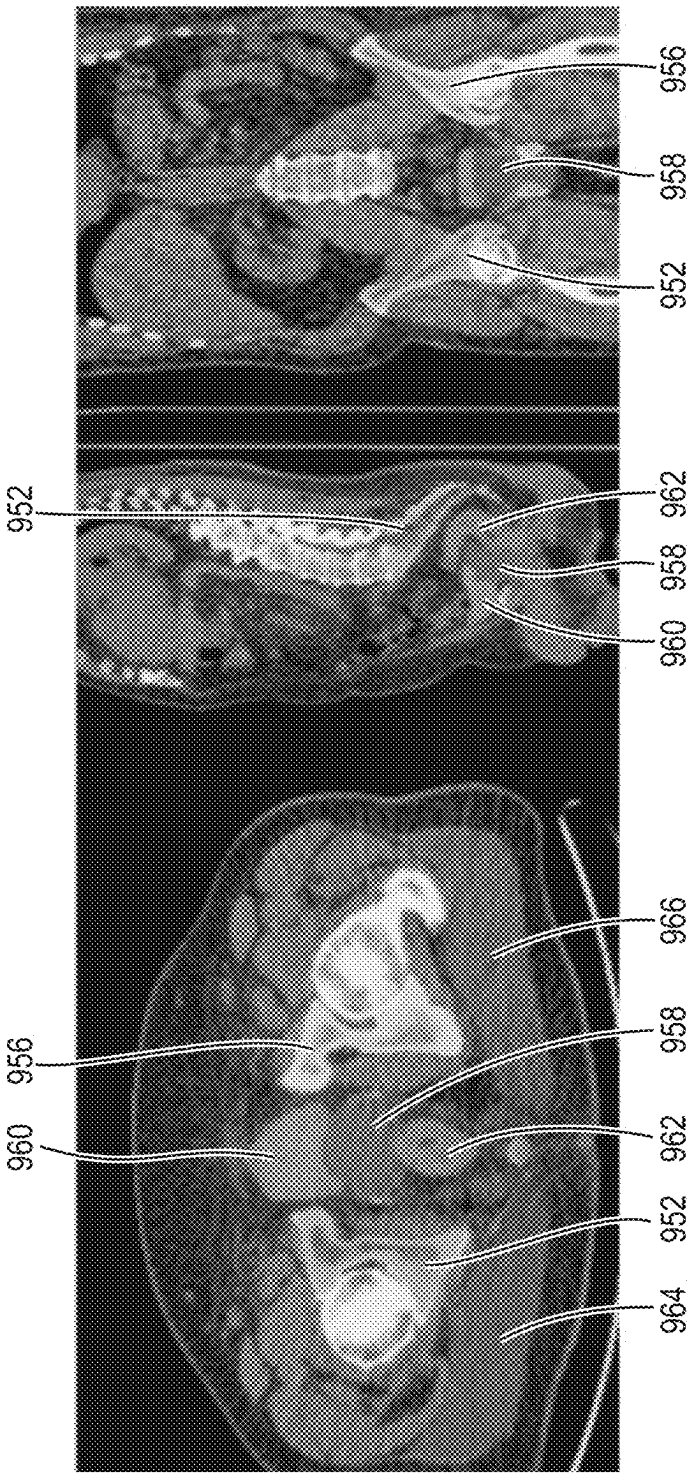

FIG. 9B

FIG. 10

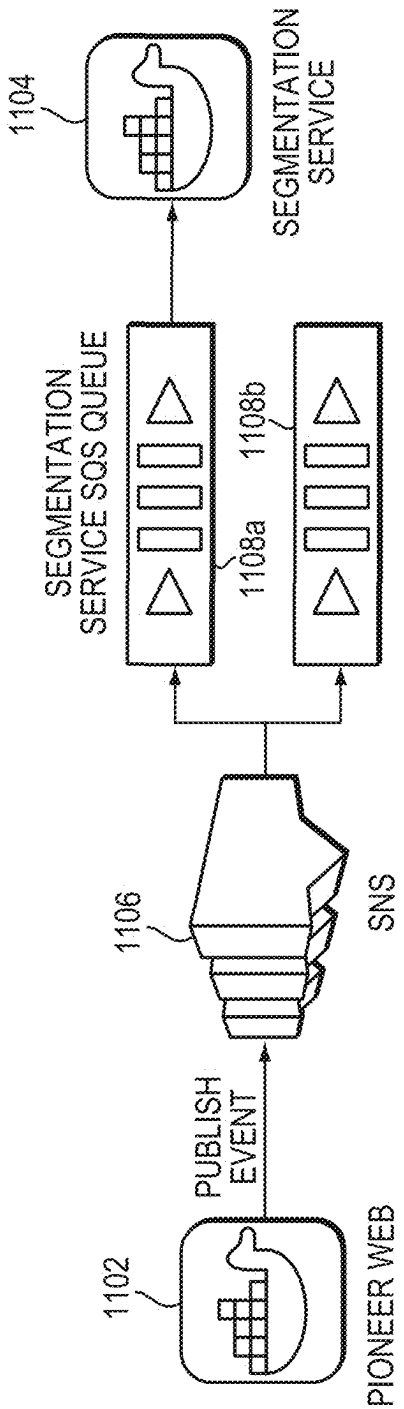
1104
SEGMENTATION SERVICE
SEGMENTATION SERVICE SQS QUEUE
1108a
1108b
1106
SNS
PUBLISH EVENT
1102
PIONEER WEB

FIG. 11

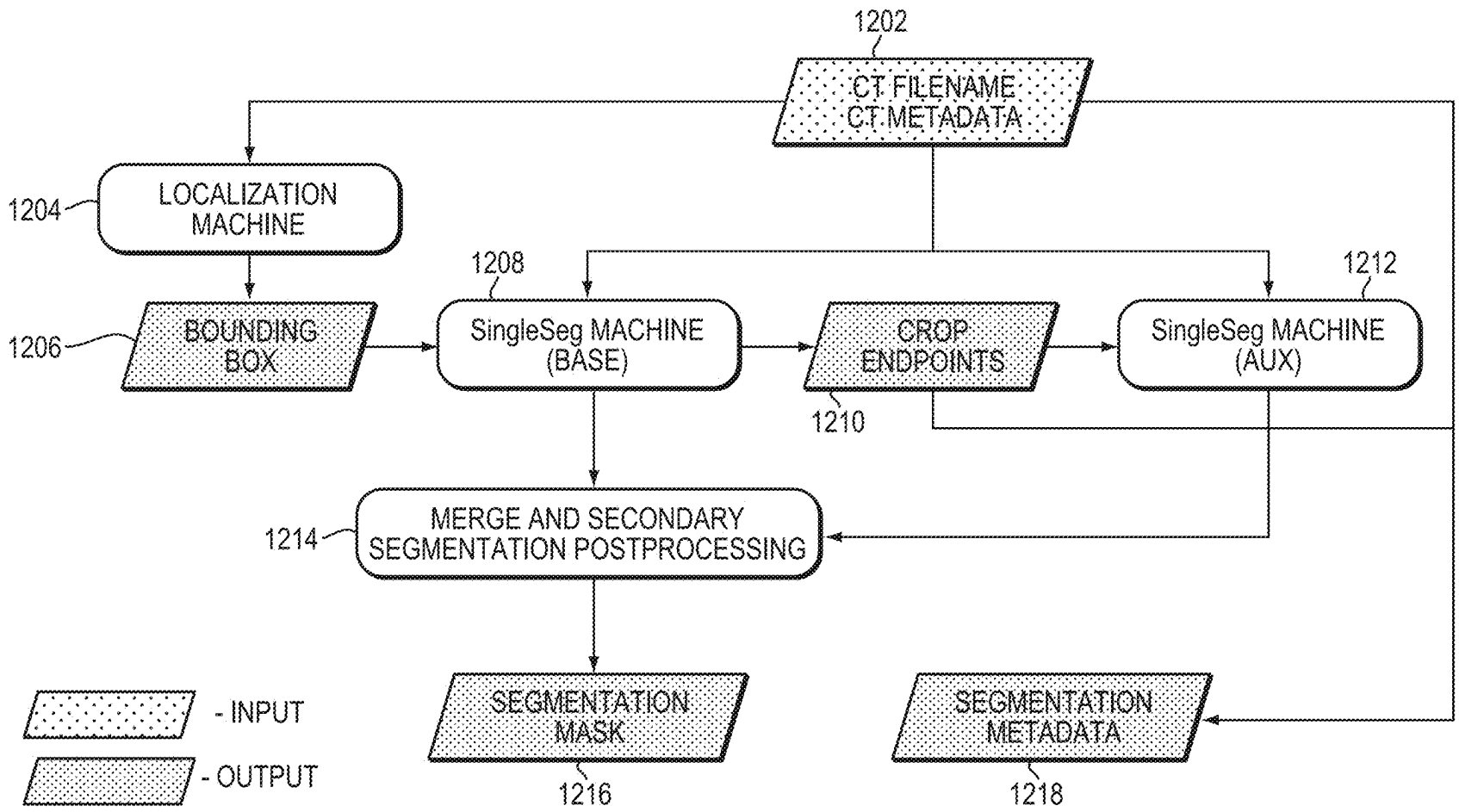
1202
CT FILENAME
CT METADATA
1204
LOCALIZATION MACHINE
1206
BOUNDING BOX
1208
SingleSeg MACHINE (BASE)
CROP ENDPOINTS
1210
1212
SingleSeg MACHINE (AUX)
1214
MERGE AND SECONDARY SEGMENTATION POSTPROCESSING
SEGMENTATION MASK
1216
SEGMENTATION METADATA
1218
- INPUT
- OUTPUT

FIG. 12

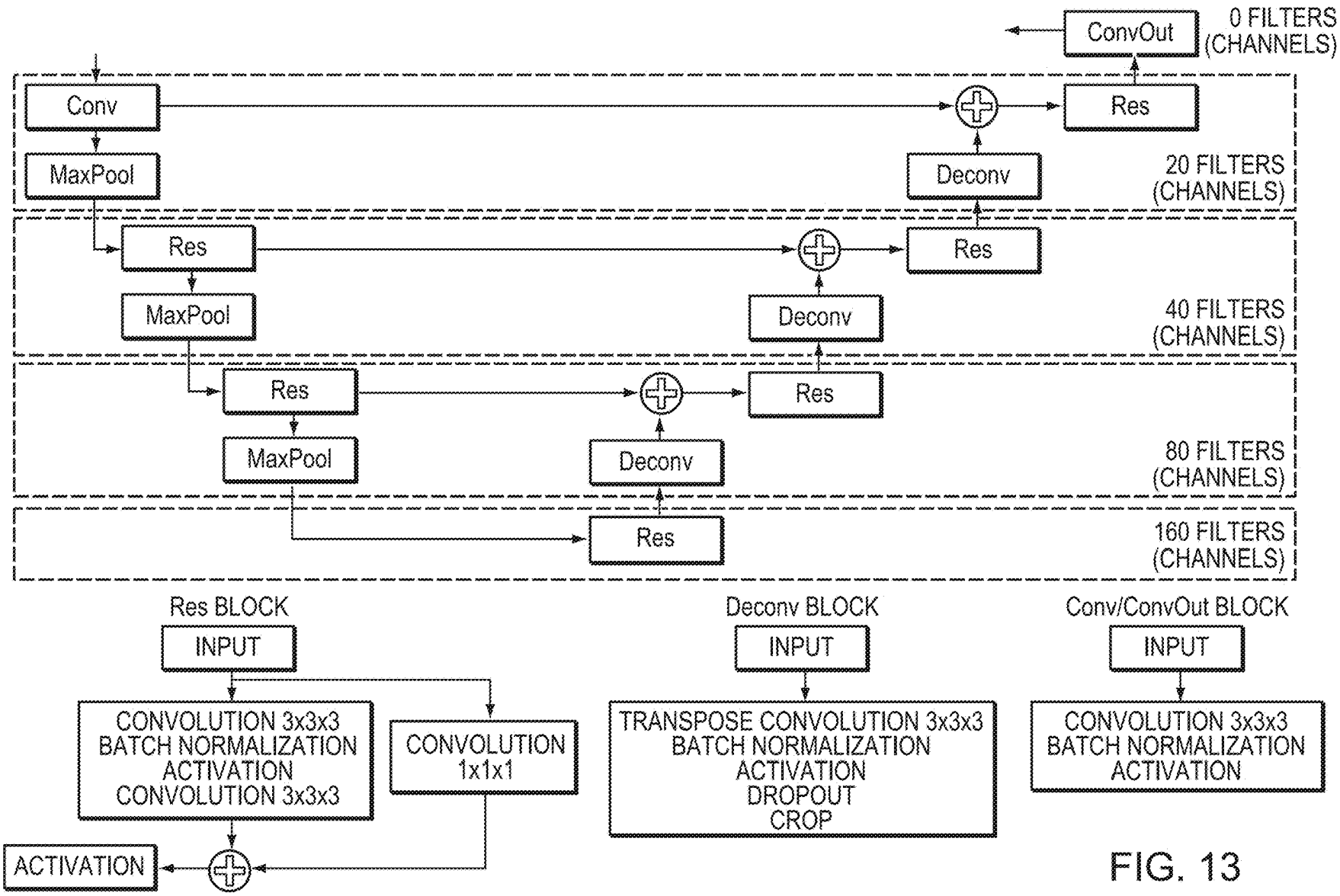
ConvOut
0 FILTERS (CHANNELS)
Conv
Res
MaxPool
Deconv
20 FILTERS (CHANNELS)
Res
Res
MaxPool
Deconv
40 FILTERS (CHANNELS)
Res
Res
MaxPool
Deconv
80 FILTERS (CHANNELS)
Res
160 FILTERS (CHANNELS)
Res BLOCK
INPUT
CONVOLUTION 3x3x3
BATCH NORMALIZATION
ACTIVATION
CONVOLUTION 3x3x3
CONVOLUTION 1x1x1
ACTIVATION
Deconv BLOCK
INPUT
TRANSPOSE CONVOLUTION 3x3x3
BATCH NORMALIZATION
ACTIVATION
DROPOUT
CROP
Conv/ConvOut BLOCK
INPUT
CONVOLUTION 3x3x3
BATCH NORMALIZATION
ACTIVATION

FIG. 13

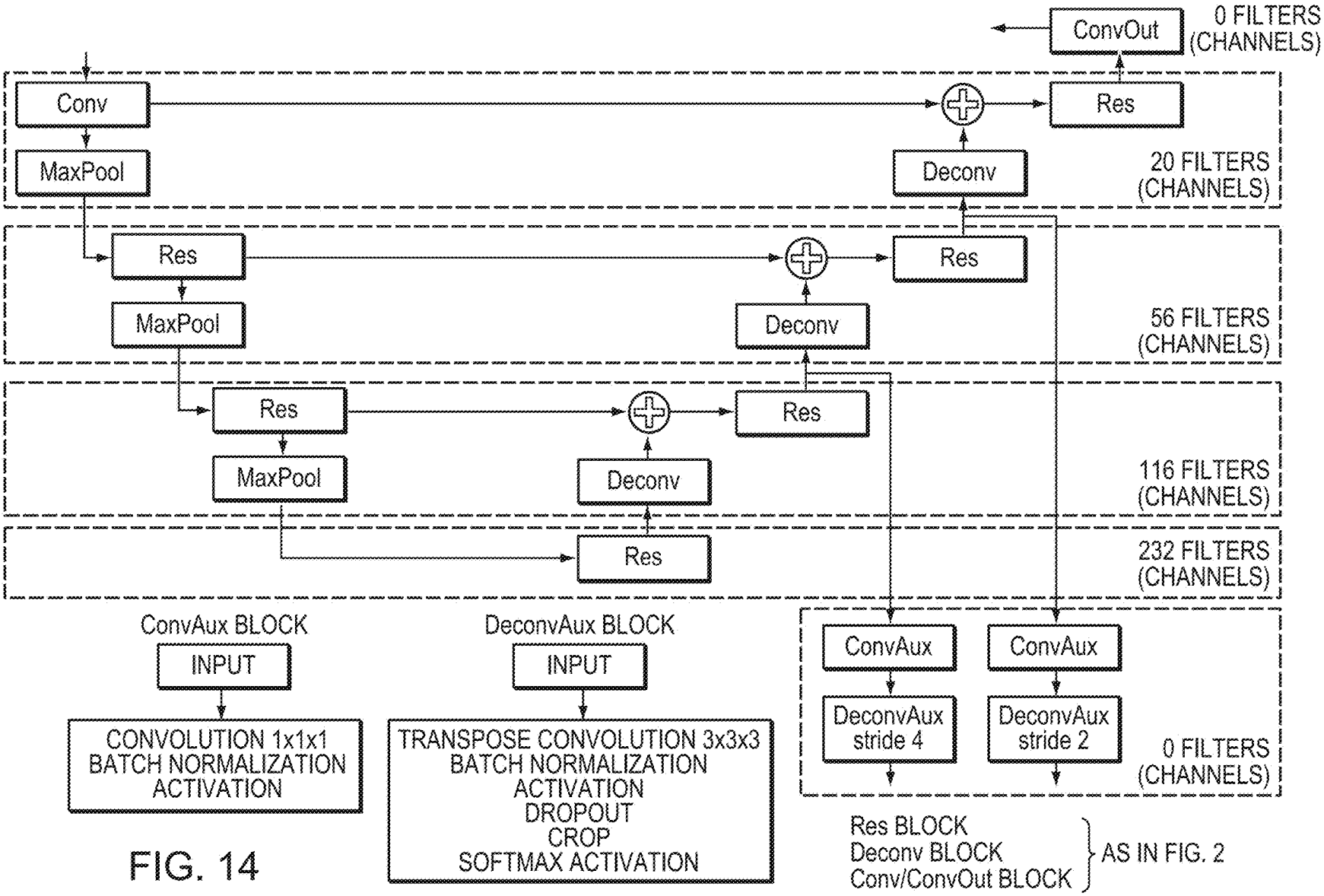
ConvOut
0 FILTERS (CHANNELS)
Conv
MaxPool
Res
Deconv
20 FILTERS (CHANNELS)
Res
MaxPool
Deconv
Res
56 FILTERS (CHANNELS)
Res
MaxPool
Deconv
Res
116 FILTERS (CHANNELS)
Res
232 FILTERS (CHANNELS)
ConvAux BLOCK
INPUT
CONVOLUTION 1x1x1
BATCH NORMALIZATION
ACTIVATION
DeconvAux BLOCK
INPUT
TRANSPOSE CONVOLUTION 3x3x3
BATCH NORMALIZATION
ACTIVATION
DROPOUT
CROP
SOFTMAX ACTIVATION
ConvAux
ConvAux
DeconvAux stride 4
DeconvAux stride 2
0 FILTERS (CHANNELS)
Res BLOCK
Deconv BLOCK
Conv/ConvOut BLOCK
AS IN FIG. 2

FIG. 14

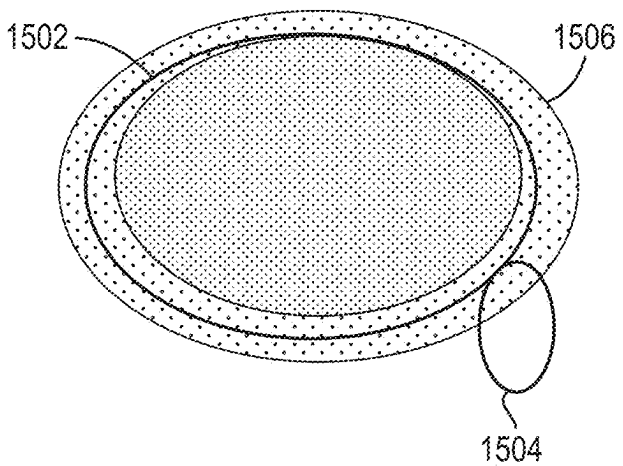

FIG. 15

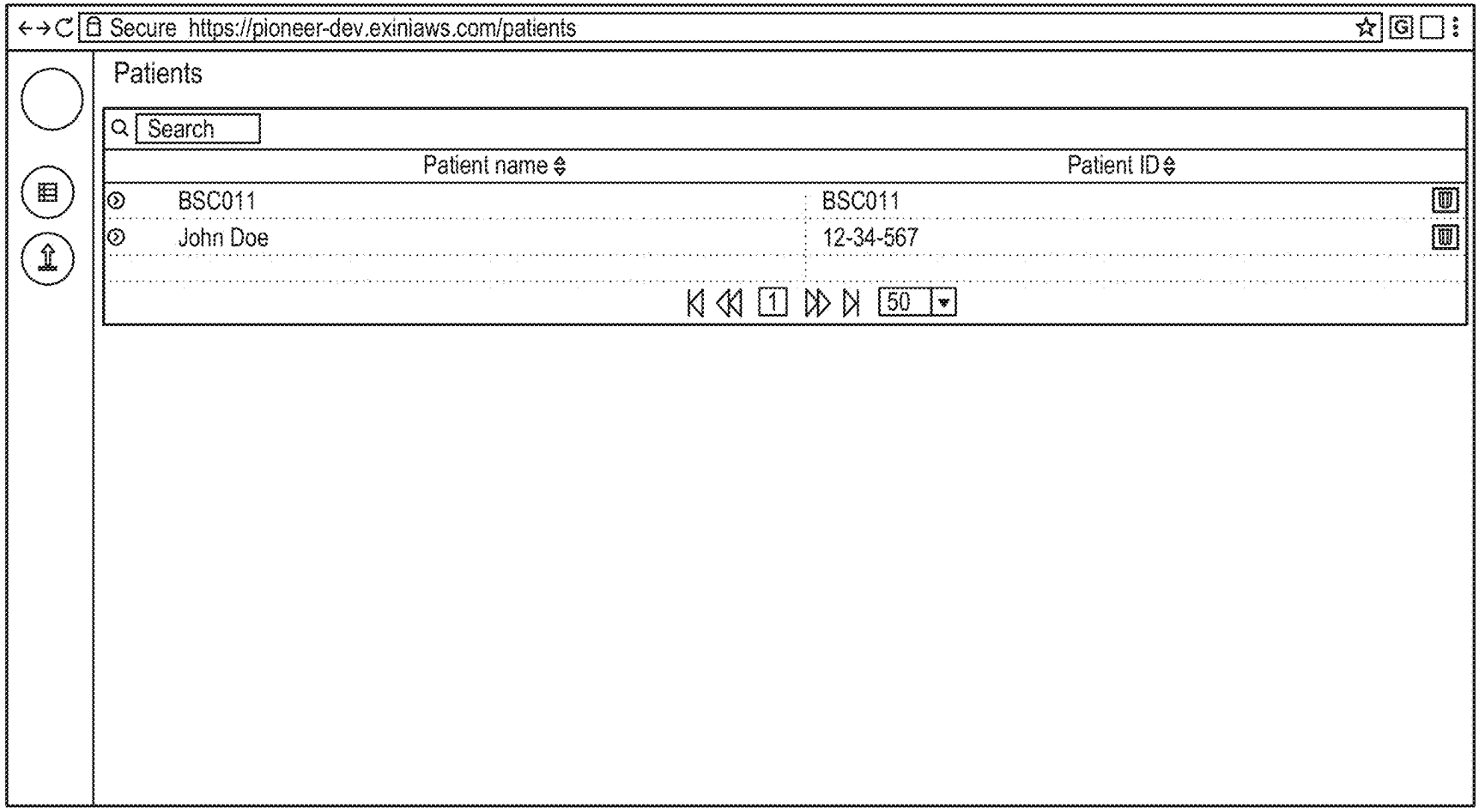
Secure https://pioneer-dev.exiniaws.com/patients
Patients
Search
Patient name
Patient ID
BSC011
BSC011
John Doe
12-34-567
1
50

FIG. 16A

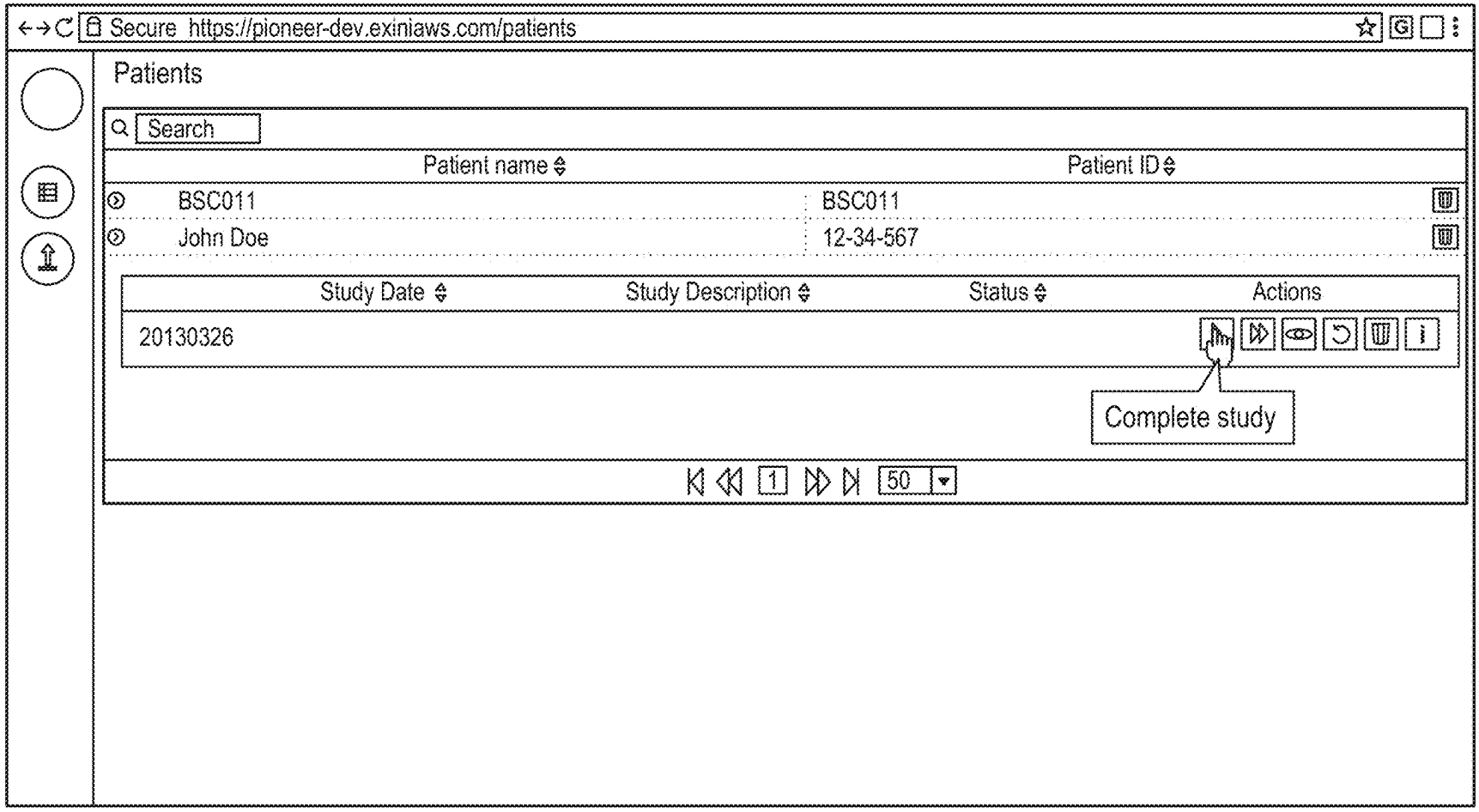
Secure https://pioneer-dev.exiniaws.com/patients
Patients
Search
Patient name
Patient ID
BSC011
BSC011
John Doe
12-34-567
Study Date
Study Description
Status
Actions
20130326
Complete study
1
50

FIG. 16B

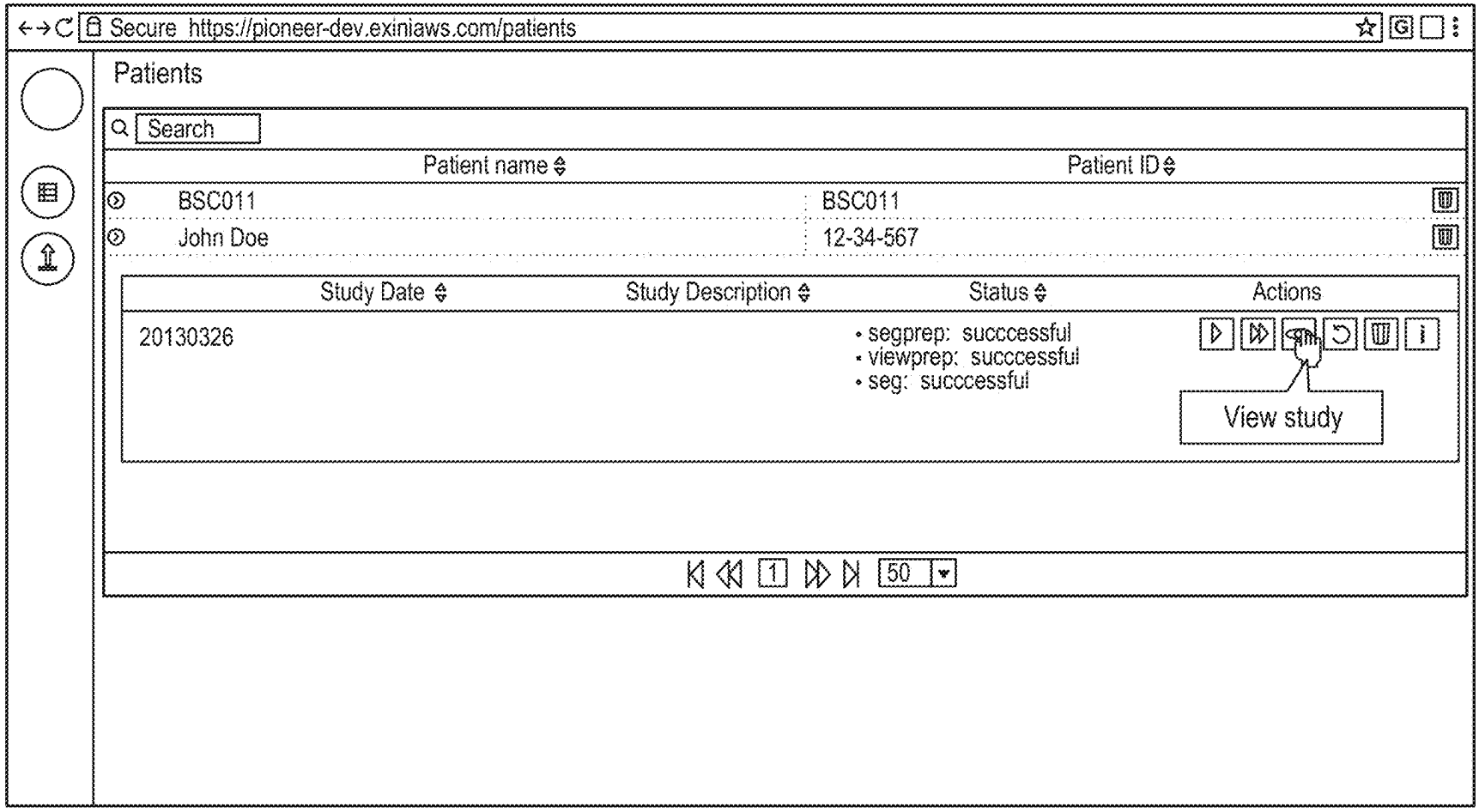
Secure https://pioneer-dev.exiniaws.com/patients
Patients
Search
Patient name
Patient ID
BSC011
BSC011
John Doe
12-34-567
Study Date
Study Description
Status
Actions
20130326
• segprep: succcessful
• viewprep: succcessful
• seg: succcessful
View study
1
50

FIG. 16C

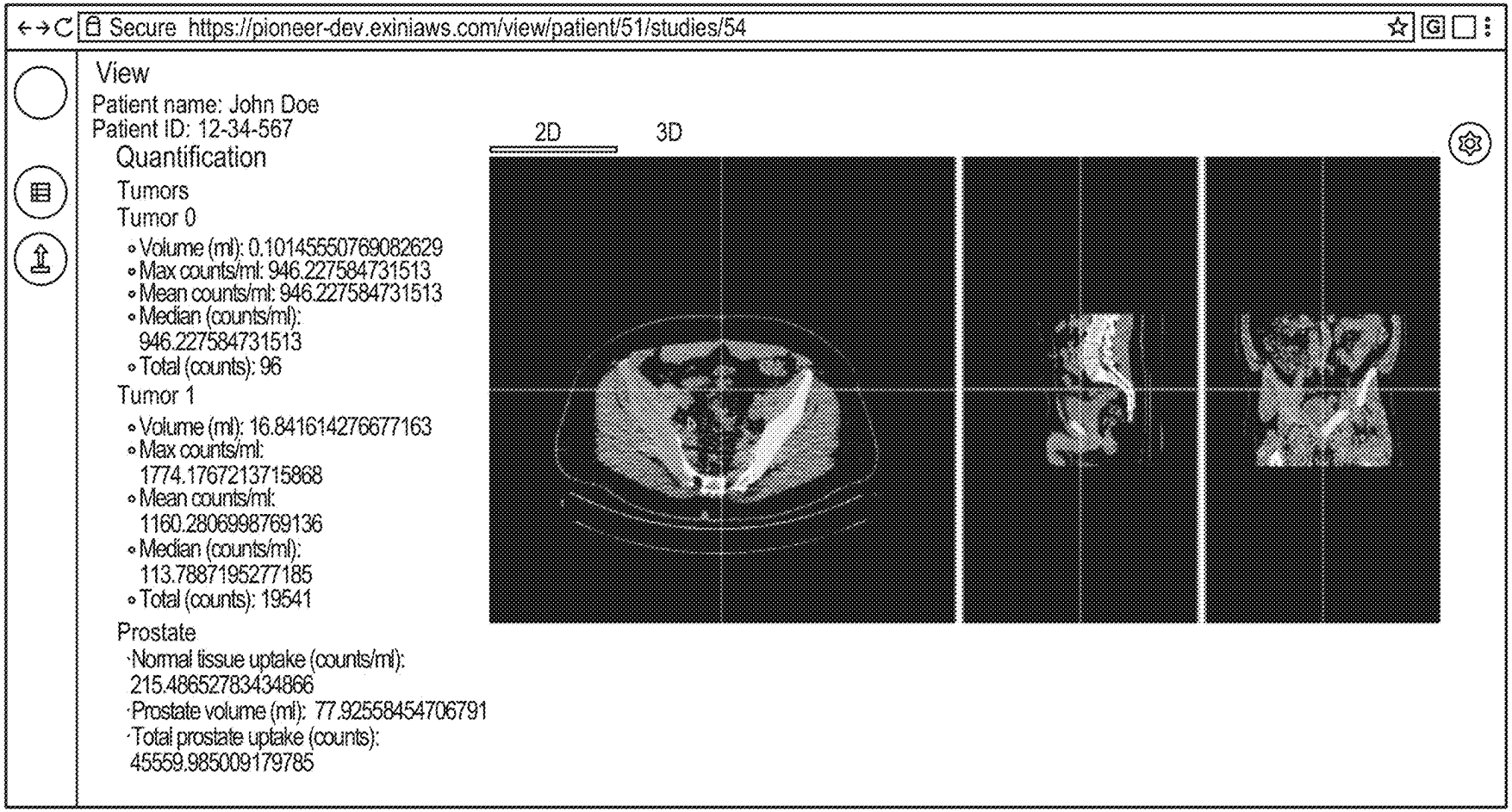
Secure https://pioneer-dev.exiniaws.com/view/patient/51/studies/54
View
Patient name: John Doe
Patient ID: 12-34-567
Quantification
Tumors
Tumor 0
Volume (ml): 0.10145550769082629
Max counts/ml: 946.227584731513
Mean counts/ml: 946.227584731513
Median (counts/ml): 946.227584731513
Total (counts): 96
Tumor 1
Volume (ml): 16.841614276677163
Max counts/ml: 1774.1767213715868
Mean counts/ml: 1160.2806998769136
Median (counts/ml): 113.7887195277185
Total (counts): 19541
Prostate
Normal tissue uptake (counts/ml): 215.48652783434866
Prostate volume (ml): 77.92558454706791
Total prostate uptake (counts): 45559.985009179785
2D
3D

FIG. 17A

Secure https://pioneer-dev.exiniaws.com/view/patient/51/studies/54

View

Patient name: John Doe
Patient ID: 12-34-567

Quantification

Tumors

Tumor 0

- Volume (ml): 0.10145550769082629
- Max counts/ml: 946.227584731513
- Mean counts/ml: 946.227584731513
- Median (counts/ml): 946.227584731513
- Total (counts): 96

Tumor 1

- Volume (ml): 16.841614276677163
- Max counts/ml: 1774.1767213715868
- Mean counts/ml: 1160.2806998769136
- Median (counts/ml): 113.7887195277185
- Total (counts): 19541

Prostate

- Normal tissue uptake (counts/ml): 215.48652783434866
- Prostate volume (ml): 77.92558454706791
- Total prostate uptake (counts): 45559.985009179785

2D 3D

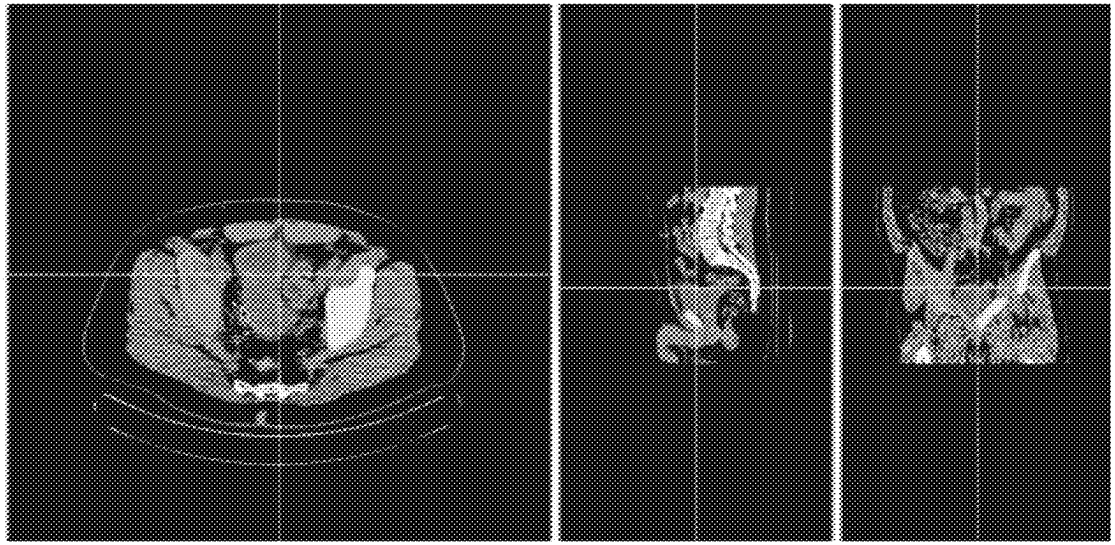

FIG. 17B

Secure https://pioneer-dev.exiniaws.com/view/patient/51/studies/54

View

Patient name: John Doe
Patient ID: 12-34-567

Quantification

Tumors

Tumor 0

- Volume (ml): 0.10145550769082629
- Max counts/ml: 946.227584731513
- Mean counts/ml: 946.227584731513
- Median (counts/ml): 946.227584731513
- Total (counts): 96

Tumor 1

- Volume (ml): 16.841614276677163
- Max counts/ml: 1774.1767213715868
- Mean counts/ml: 1160.2806998769136
- Median (counts/ml): 113.7887195277185
- Total (counts): 19541

Prostate

- Normal tissue uptake (counts/ml): 215.48652783434866
- Prostate volume (ml): 77.92558454706791
- Total prostate uptake (counts): 45559.985009179785

2D 3D

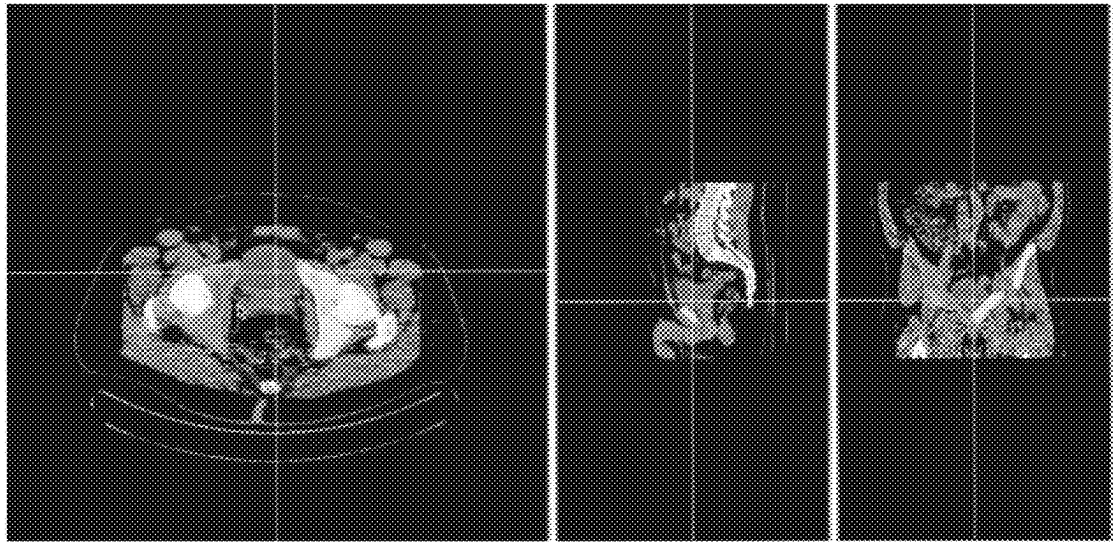

FIG. 17C

Secure https://pioneer-dev.exiniaws.com/view/patient/51/studies/54

View

Patient name: John Doe
Patient ID: 12-34-567

Quantification

Tumors

Tumor 0

- Volume (ml): 0.10145550769082629
- Max counts/ml: 946.227584731513
- Mean counts/ml: 946.227584731513
- Median (counts/ml): 946.227584731513
- Total (counts): 96

Tumor 1

- Volume (ml): 16.841614276677163
- Max counts/ml: 1774.1767213715868
- Mean counts/ml: 1160.2806998769136
- Median (counts/ml): 113.7887195277185
- Total (counts): 19541

Prostate

- Normal tissue uptake (counts/ml): 215.48652783434866
- Prostate volume (ml): 77.92558454706791
- Total prostate uptake (counts): 45559.985009179785

2D 3D

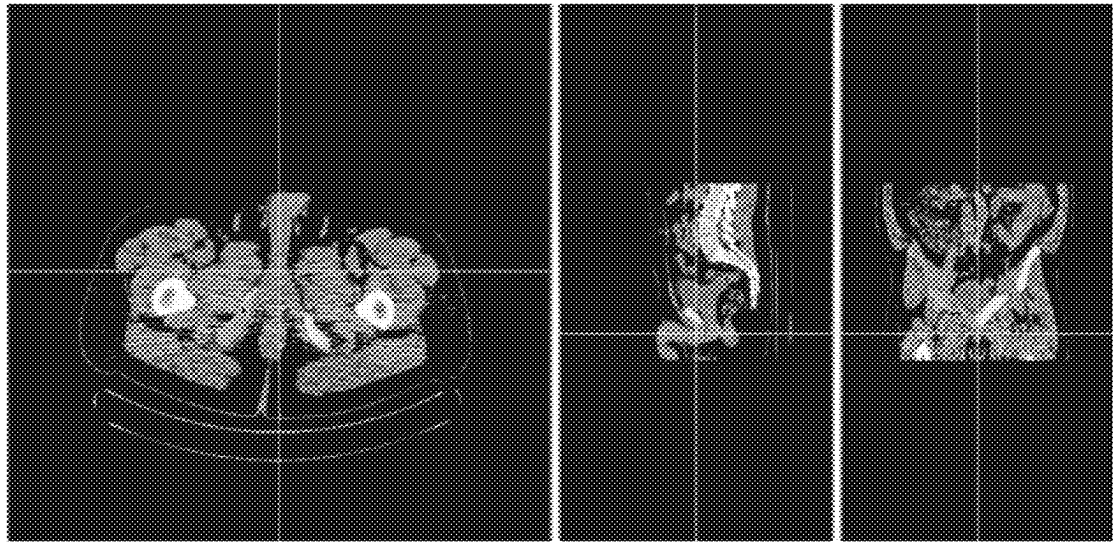

FIG. 17D

Secure https://pioneer-dev.exiniaws.com/view/patient/51/studies/54

View

Patient name: John Doe
Patient ID: 12-34-567

Quantification

Tumors

Tumor 0

- Volume (ml): 0.10145550769082629
- Max counts/ml: 946.227584731513
- Mean counts/ml: 946.227584731513
- Median (counts/ml): 946.227584731513
- Total (counts): 96

Tumor 1

- Volume (ml): 16.841614276677163
- Max counts/ml: 1774.1767213715868
- Mean counts/ml: 1160.2806998769136
- Median (counts/ml): 113.7887195277185
- Total (counts): 19541

Prostate

- Normal tissue uptake (counts/ml): 215.48652783434866
- Prostate volume (ml): 77.92558454706791
- Total prostate uptake (counts): 45559.985009179785

2D 3D

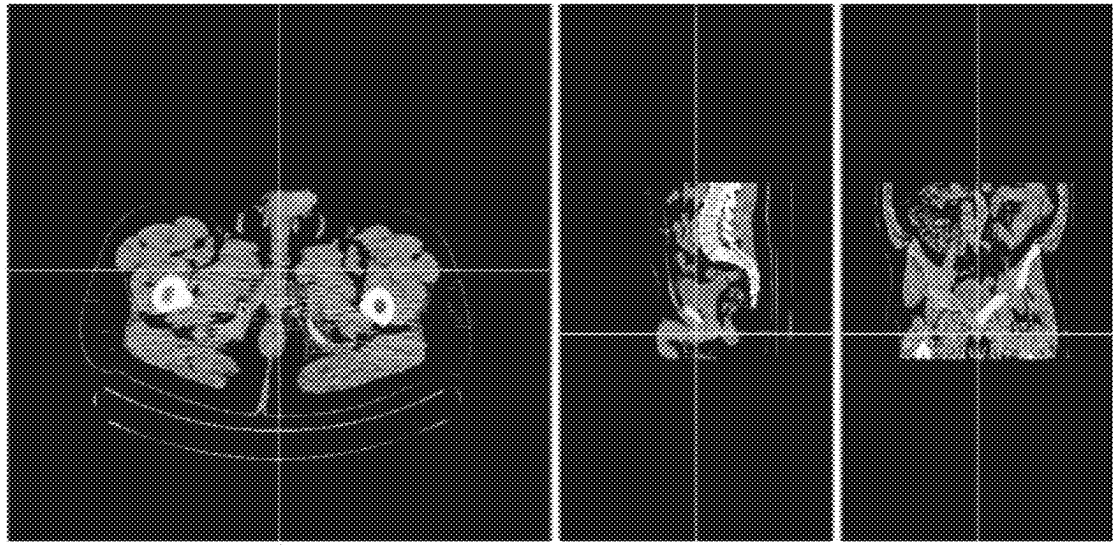

FIG. 17E

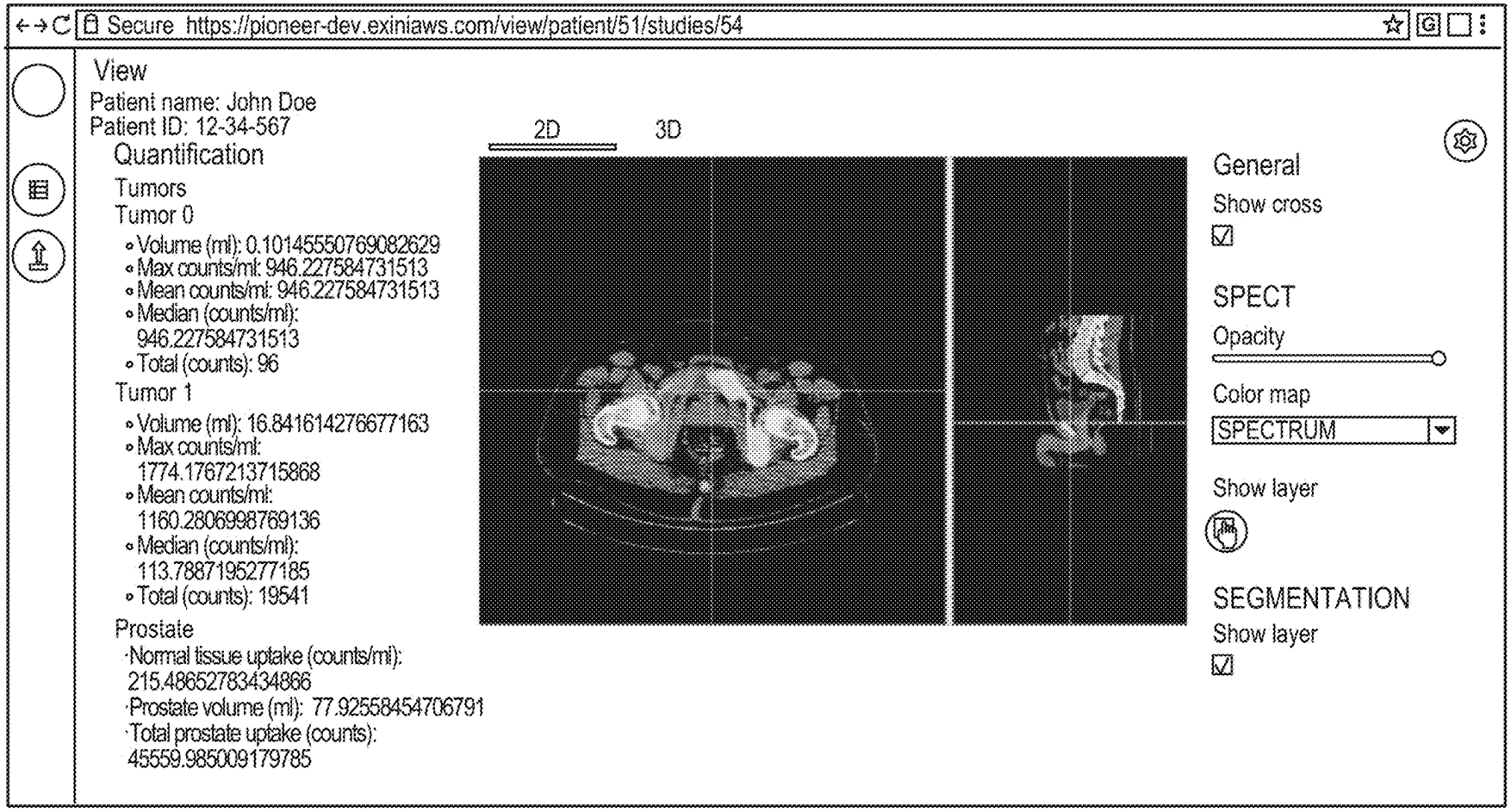
Secure https://pioneer-dev.exiniaws.com/view/patient/51/studies/54
View
Patient name: John Doe
Patient ID: 12-34-567
Quantification
Tumors
Tumor 0
Volume (ml): 0.10145550769082629
Max counts/ml: 946.227584731513
Mean counts/ml: 946.227584731513
Median (counts/ml): 946.227584731513
Total (counts): 96
Tumor 1
Volume (ml): 16.841614276677163
Max counts/ml: 1774.1767213715868
Mean counts/ml: 1160.2806998769136
Median (counts/ml): 113.7887195277185
Total (counts): 19541
Prostate
Normal tissue uptake (counts/ml): 215.48652783434866
Prostate volume (ml): 77.92558454706791
Total prostate uptake (counts): 45559.985009179785
2D
3D
General
Show cross
SPECT
Opacity
Color map
SPECTRUM
Show layer
SEGMENTATION
Show layer

FIG. 18A

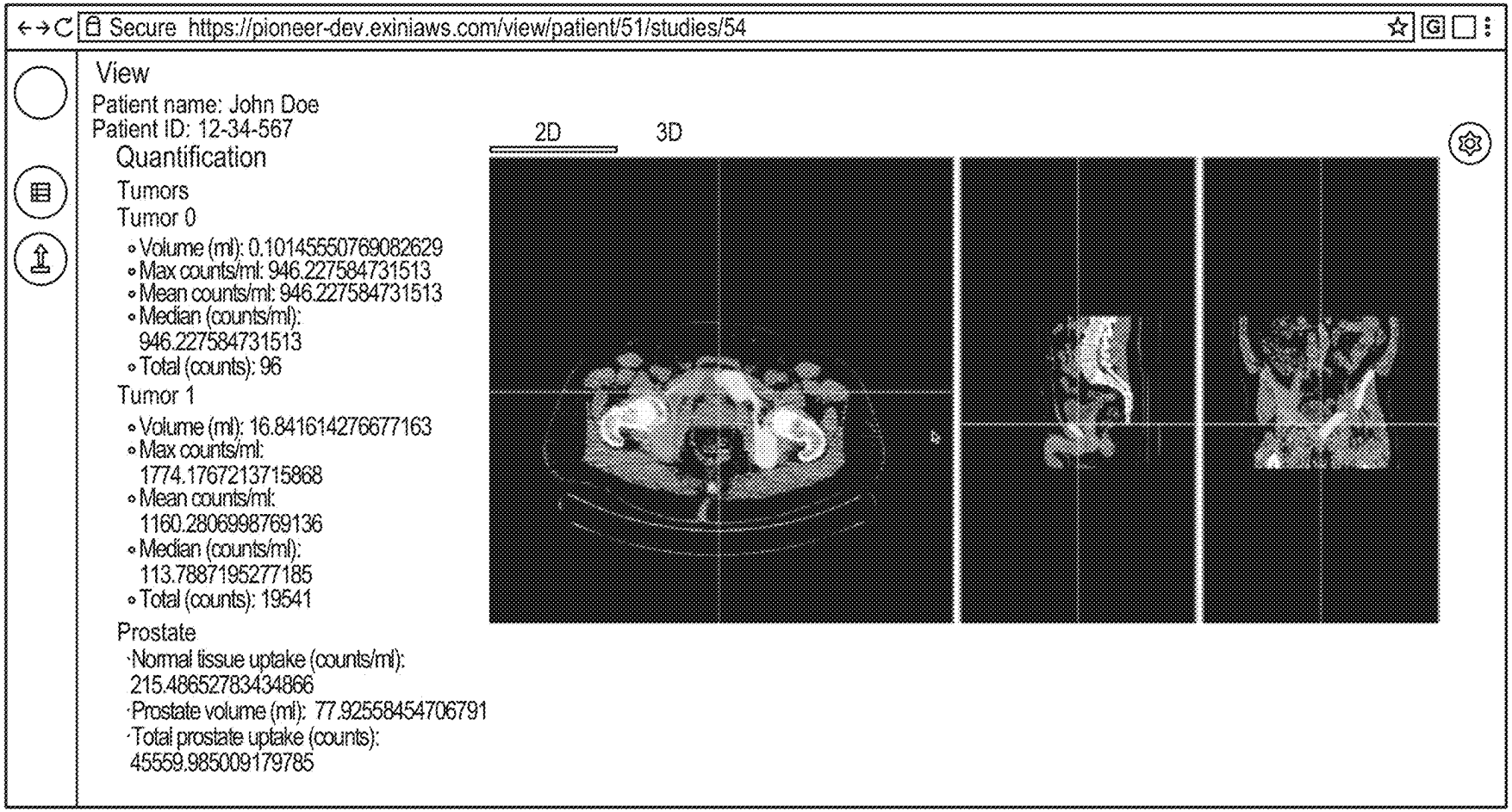
Secure https://pioneer-dev.exiniaws.com/view/patient/51/studies/54
View
Patient name: John Doe
Patient ID: 12-34-567
Quantification
Tumors
Tumor 0
Volume (ml): 0.10145550769082629
Max counts/ml: 946.227584731513
Mean counts/ml: 946.227584731513
Median (counts/ml): 946.227584731513
Total (counts): 96
Tumor 1
Volume (ml): 16.841614276677163
Max counts/ml: 1774.1767213715868
Mean counts/ml: 1160.2806998769136
Median (counts/ml): 113.7887195277185
Total (counts): 19541
Prostate
Normal tissue uptake (counts/ml): 215.48652783434866
Prostate volume (ml): 77.92558454706791
Total prostate uptake (counts): 45559.985009179785
2D
3D

FIG. 18B

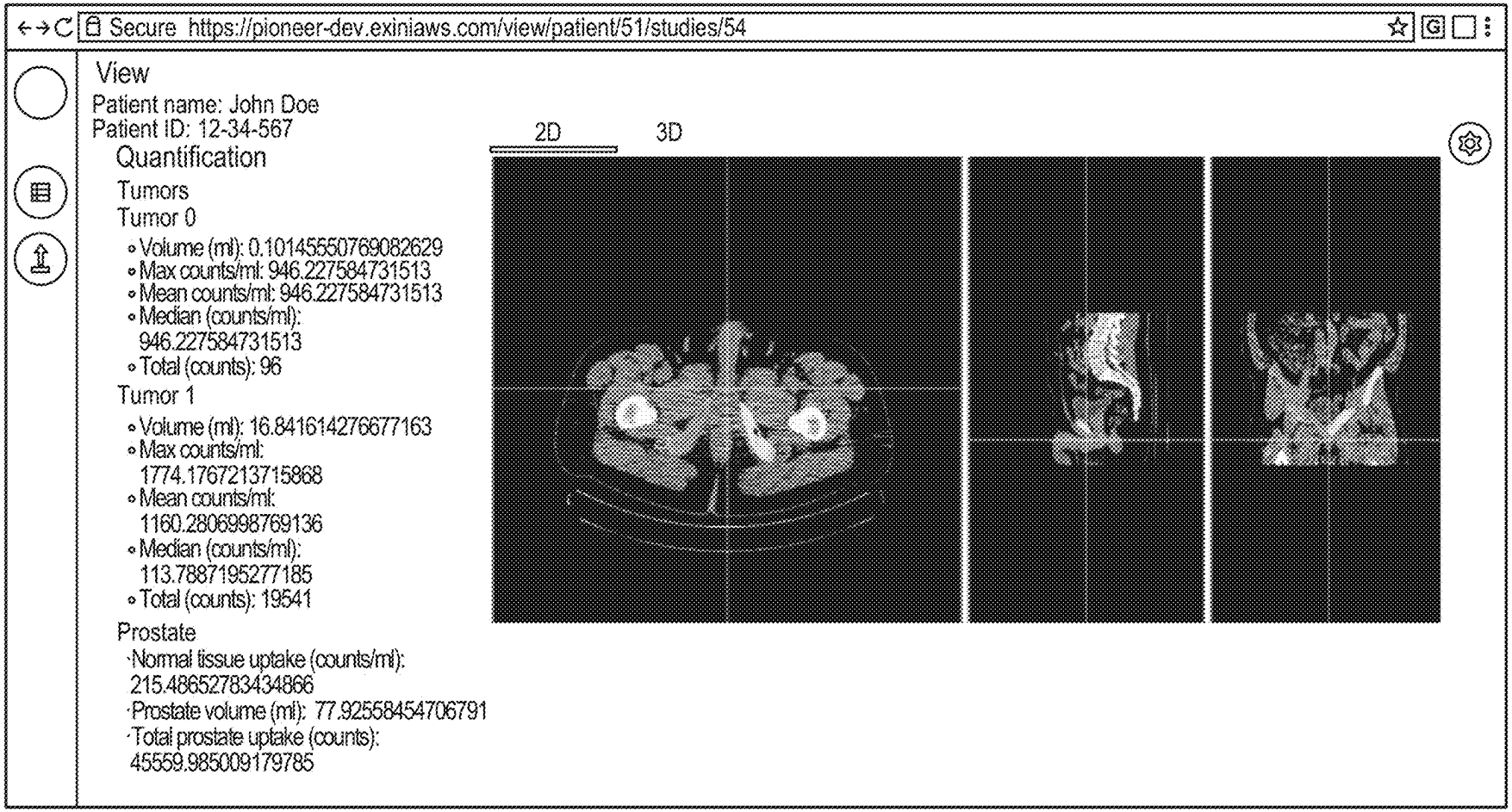
Secure https://pioneer-dev.exiniaws.com/view/patient/51/studies/54
View
Patient name: John Doe
Patient ID: 12-34-567
Quantification
Tumors
Tumor 0
Volume (ml): 0.10145550769082629
Max counts/ml: 946.227584731513
Mean counts/ml: 946.227584731513
Median (counts/ml): 946.227584731513
Total (counts): 96
Tumor 1
Volume (ml): 16.841614276677163
Max counts/ml: 1774.1767213715868
Mean counts/ml: 1160.2806998769136
Median (counts/ml): 113.7887195277185
Total (counts): 19541
Prostate
Normal tissue uptake (counts/ml): 215.48652783434866
Prostate volume (ml): 77.92558454706791
Total prostate uptake (counts): 45559.985009179785
2D
3D

FIG. 18C

Secure https://pioneer-dev.exiniaws.com/view/patient/51/studies/54

View

Patient name: John Doe
Patient ID: 12-34-567

Quantification

Tumors

Tumor 0

- Volume (ml): 0.10145550769082629
- Max counts/ml: 946.227584731513
- Mean counts/ml: 946.227584731513
- Median (counts/ml): 946.227584731513
- Total (counts): 96

Tumor 1

- Volume (ml): 16.841614276677163
- Max counts/ml: 1774.1767213715868
- Mean counts/ml: 1160.2806998769136
- Median (counts/ml): 113.7887195277185
- Total (counts): 19541

Prostate

- Normal tissue uptake (counts/ml): 215.48652783434866
- Prostate volume (ml): 77.92558454706791
- Total prostate uptake (counts): 45559.985009179785

2D 3D

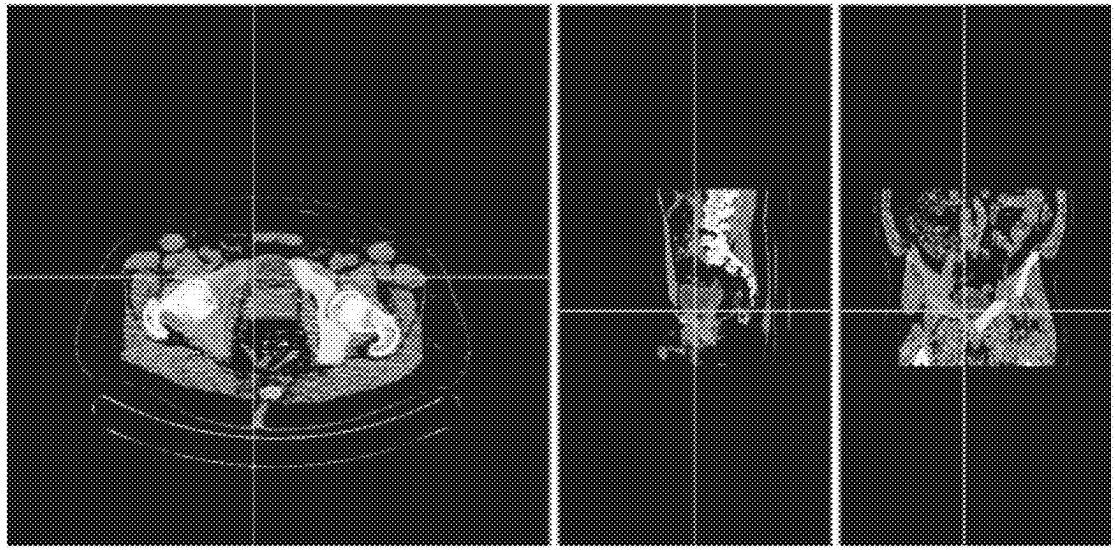

FIG. 18D

Secure https://pioneer-dev.exiniaws.com/view/patient/51/studies/54

View

Patient name: John Doe
Patient ID: 12-34-567

Quantification

Tumors

Tumor 0

- Volume (ml): 0.10145550769082629
- Max counts/ml: 946.227584731513
- Mean counts/ml: 946.227584731513
- Median (counts/ml): 946.227584731513
- Total (counts): 96

Tumor 1

- Volume (ml): 16.841614276677163
- Max counts/ml: 1774.1767213715868
- Mean counts/ml: 1160.2806998769136
- Median (counts/ml): 113.7887195277185
- Total (counts): 19541

Prostate

- Normal tissue uptake (counts/ml): 215.48652783434866
- Prostate volume (ml): 77.92558454706791
- Total prostate uptake (counts): 45559.985009179785

2D 3D

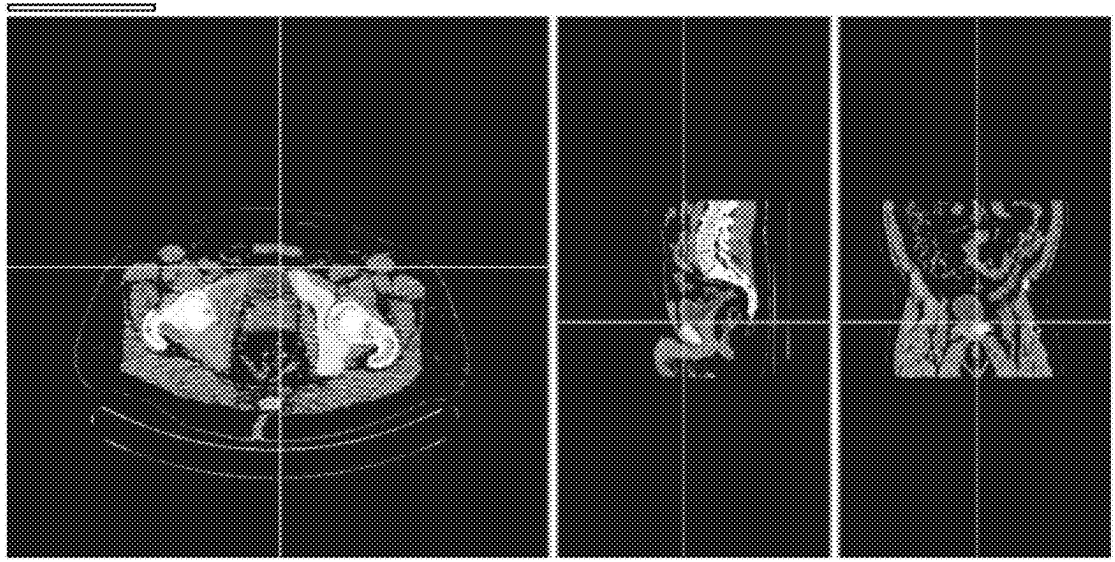

FIG. 18E

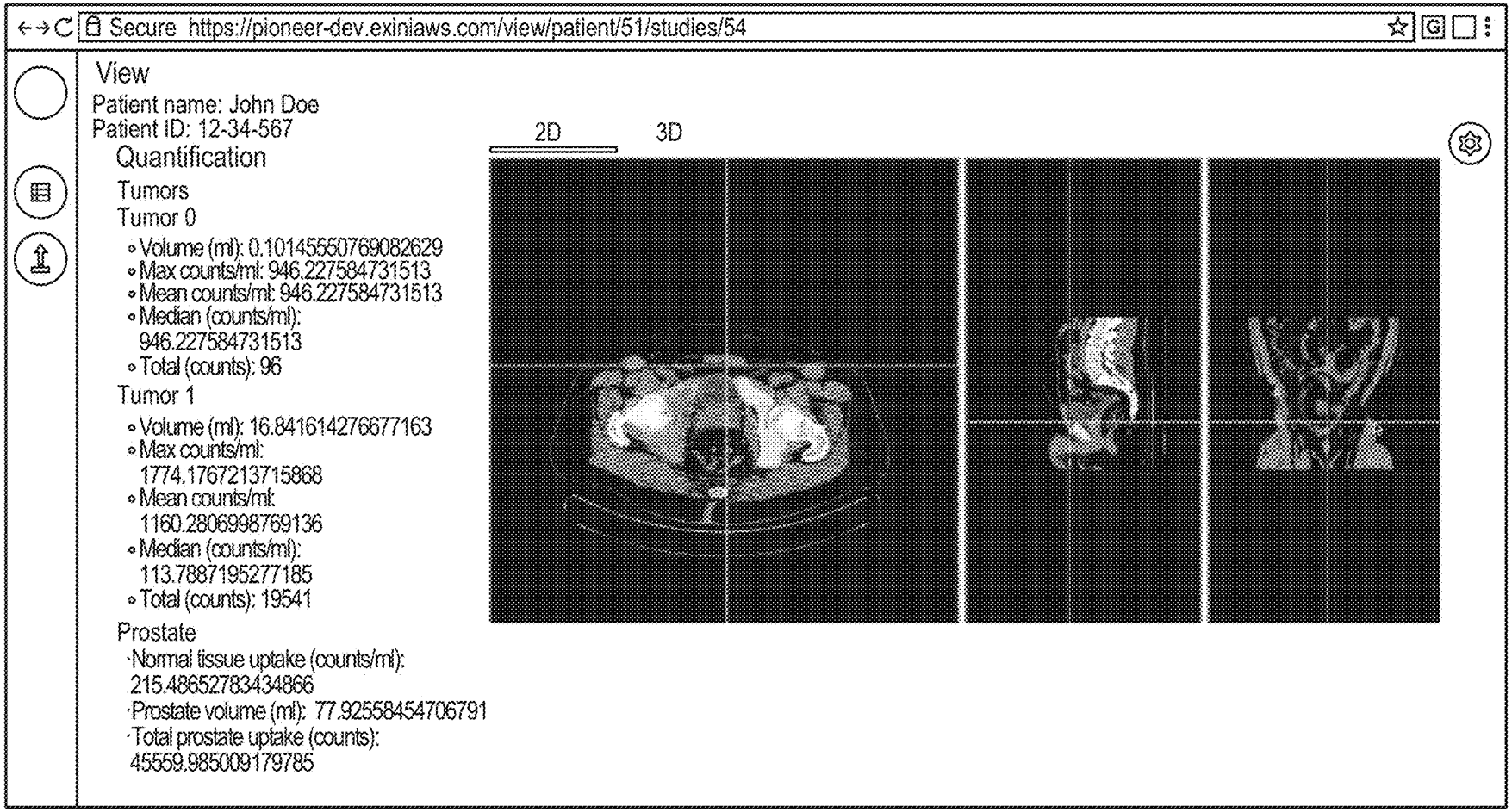
Secure https://pioneer-dev.exiniaws.com/view/patient/51/studies/54
View
Patient name: John Doe
Patient ID: 12-34-567
Quantification
Tumors
Tumor 0
Volume (ml): 0.10145550769082629
Max counts/ml: 946.227584731513
Mean counts/ml: 946.227584731513
Median (counts/ml): 946.227584731513
Total (counts): 96
Tumor 1
Volume (ml): 16.841614276677163
Max counts/ml: 1774.1767213715868
Mean counts/ml: 1160.2806998769136
Median (counts/ml): 113.7887195277185
Total (counts): 19541
Prostate
Normal tissue uptake (counts/ml): 215.48652783434866
Prostate volume (ml): 77.92558454706791
Total prostate uptake (counts): 45559.985009179785
2D
3D

FIG. 18F

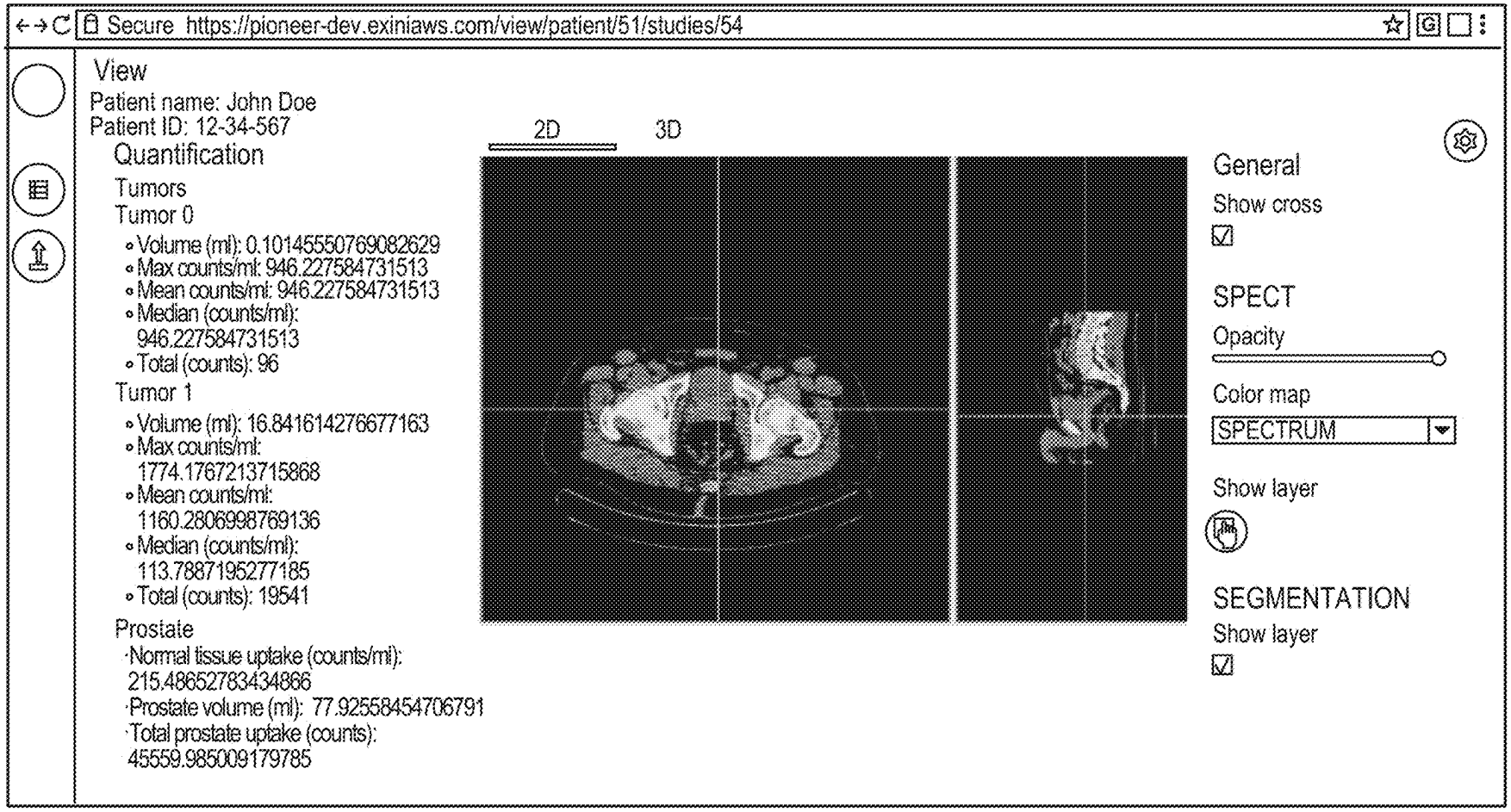
Secure https://pioneer-dev.exiniaws.com/view/patient/51/studies/54
View
Patient name: John Doe
Patient ID: 12-34-567
Quantification
Tumors
Tumor 0
Volume (ml): 0.10145550769082629
Max counts/ml: 946.227584731513
Mean counts/ml: 946.227584731513
Median (counts/ml): 946.227584731513
Total (counts): 96
Tumor 1
Volume (ml): 16.841614276677163
Max counts/ml: 1774.1767213715868
Mean counts/ml: 1160.2806998769136
Median (counts/ml): 113.7887195277185
Total (counts): 19541
Prostate
Normal tissue uptake (counts/ml): 215.48652783434866
Prostate volume (ml): 77.92558454706791
Total prostate uptake (counts): 45559.985009179785
2D
3D
General
Show cross
SPECT
Opacity
Color map
SPECTRUM
Show layer
SEGMENTATION
Show layer

FIG. 19A

Secure https://pioneer-dev.exiniaws.com/view/patient/51/studies/54

View

Patient name: John Doe
Patient ID: 12-34-567

Quantification

Tumors

Tumor 0

- Volume (ml): 0.10145550769082629
- Max counts/ml: 946.227584731513
- Mean counts/ml: 946.227584731513
- Median (counts/ml): 946.227584731513
- Total (counts): 96

Tumor 1

- Volume (ml): 16.841614276677163
- Max counts/ml: 1774.1767213715868
- Mean counts/ml: 1160.2806998769136
- Median (counts/ml): 113.7887195277185
- Total (counts): 19541

Prostate

- Normal tissue uptake (counts/ml): 215.48652783434866
- Prostate volume (ml): 77.92558454706791
- Total prostate uptake (counts): 45559.985009179785

2D 3D

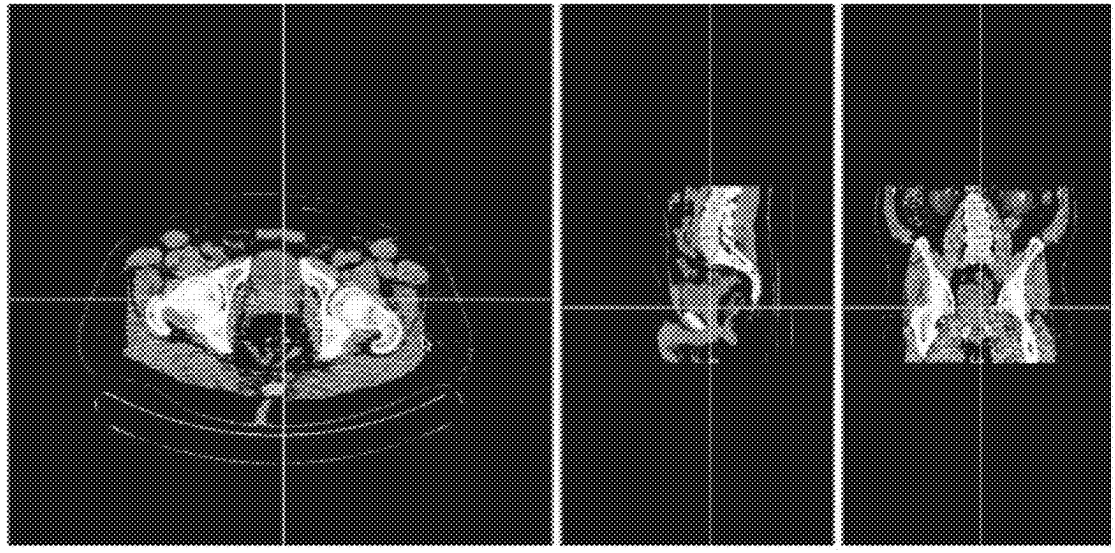

FIG. 19B

Secure https://pioneer-dev.exiniaws.com/view/patient/51/studies/54

View

Patient name: John Doe
Patient ID: 12-34-567

Quantification

Tumors

Tumor 0

- Volume (ml): 0.10145550769082629
- Max counts/ml: 946.227584731513
- Mean counts/ml: 946.227584731513
- Median (counts/ml): 946.227584731513
- Total (counts): 96

Tumor 1

- Volume (ml): 16.841614276677163
- Max counts/ml: 1774.1767213715868
- Mean counts/ml: 1160.2806998769136
- Median (counts/ml): 113.7887195277185
- Total (counts): 19541

Prostate

- Normal tissue uptake (counts/ml): 215.48652783434866
- Prostate volume (ml): 77.92558454706791
- Total prostate uptake (counts): 45559.985009179785

2D 3D

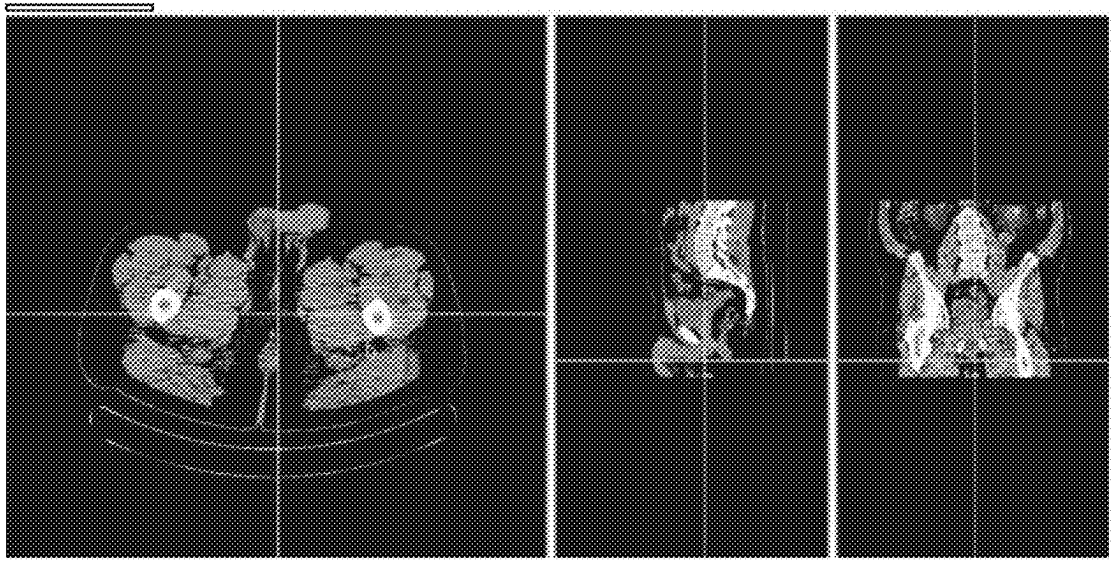

FIG. 19C

Secure https://pioneer-dev.exiniaws.com/view/patient/51/studies/54

View

Patient name: John Doe
Patient ID: 12-34-567

Quantification

Tumors

Tumor 0

- Volume (ml): 0.10145550769082629
- Max counts/ml: 946.227584731513
- Mean counts/ml: 946.227584731513
- Median (counts/ml): 946.227584731513
- Total (counts): 96

Tumor 1

- Volume (ml): 16.841614276677163
- Max counts/ml: 1774.1767213715868
- Mean counts/ml: 1160.2806998769136
- Median (counts/ml): 113.7887195277185
- Total (counts): 19541

Prostate

- Normal tissue uptake (counts/ml): 215.48652783434866
- Prostate volume (ml): 77.92558454706791
- Total prostate uptake (counts): 45559.985009179785

2D 3D

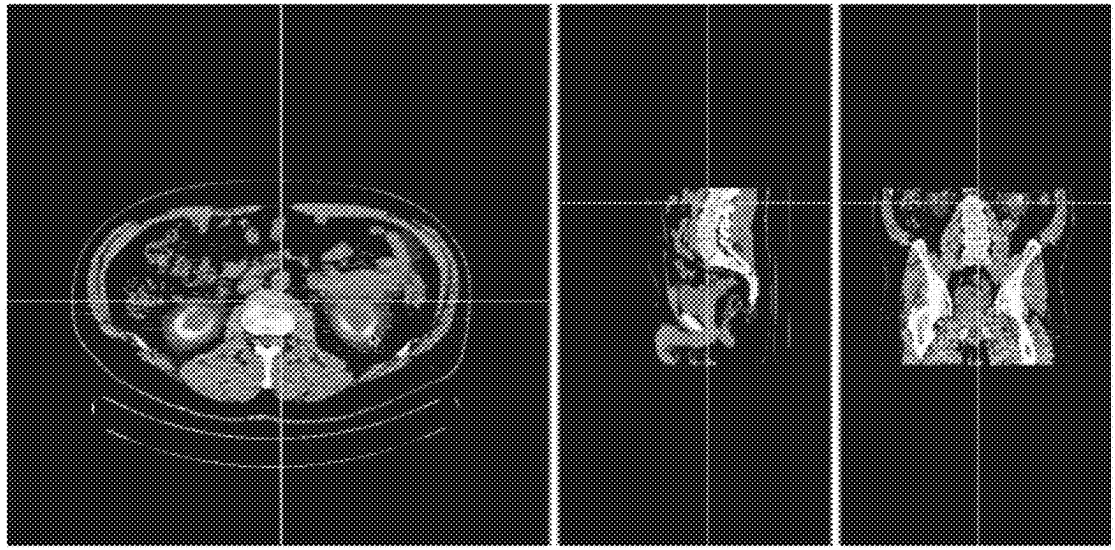

FIG. 19D

FIG. 20A

FIG. 20B

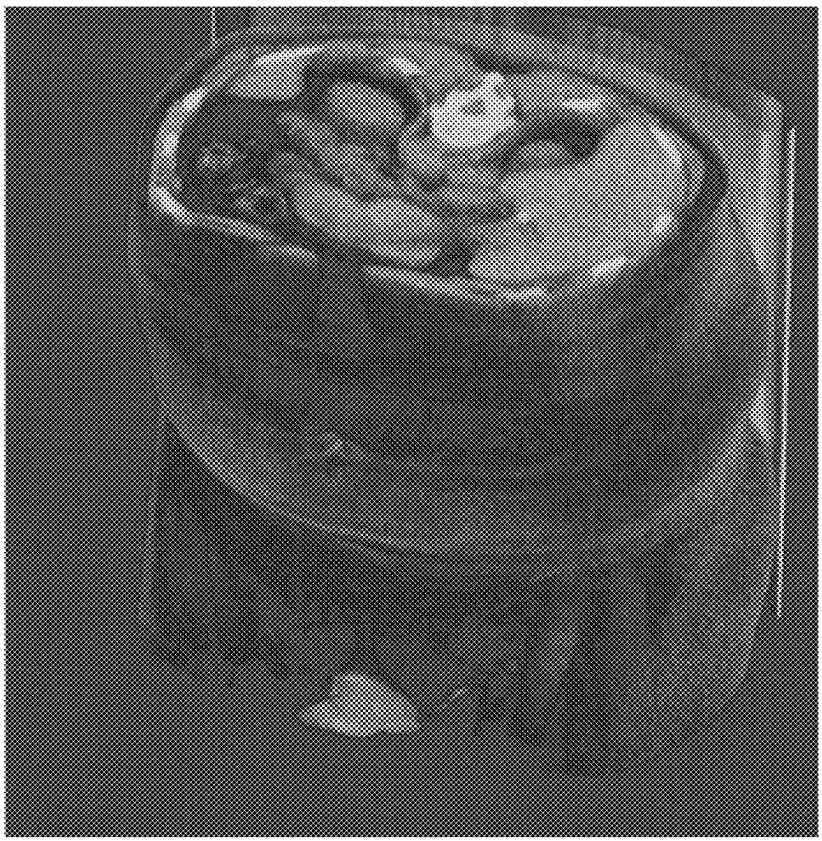

FIG. 20C

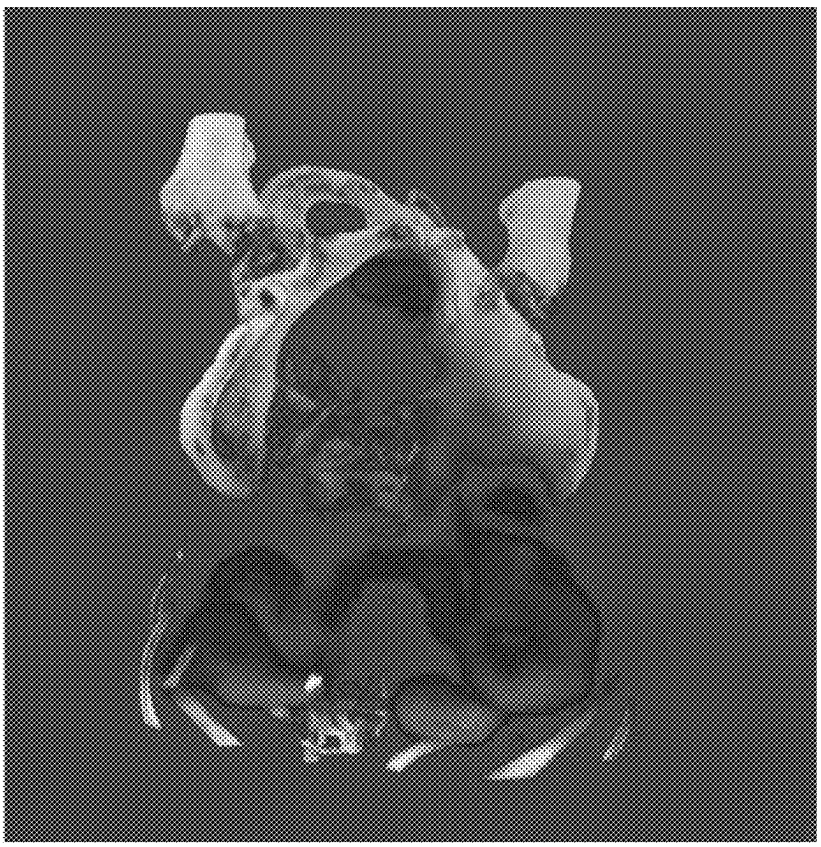

FIG. 21A

FIG. 21B

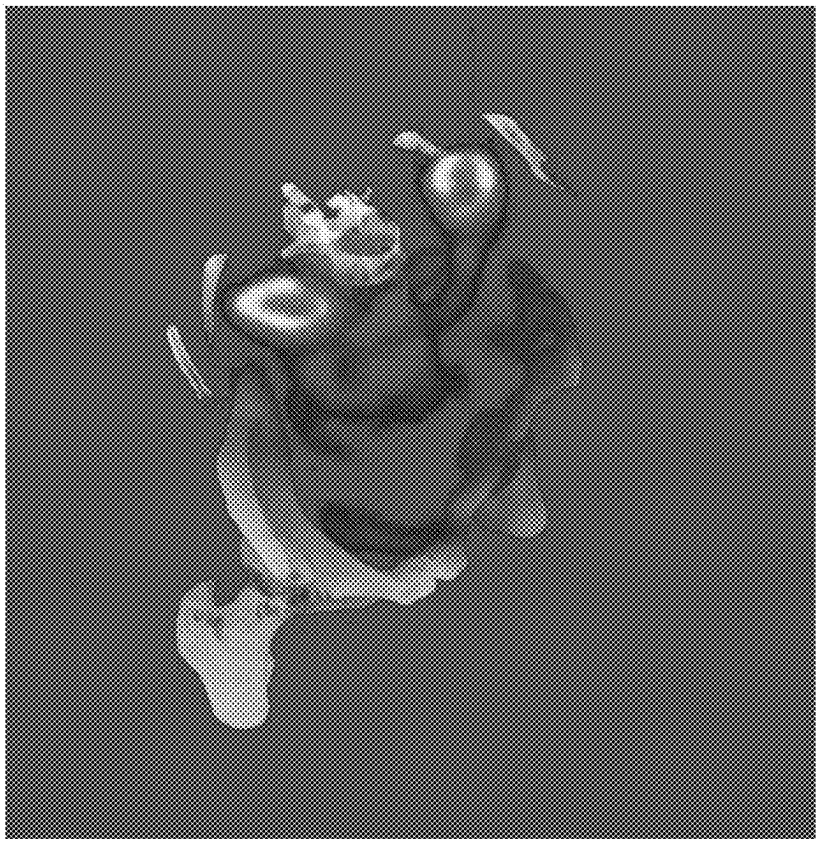

FIG. 22A

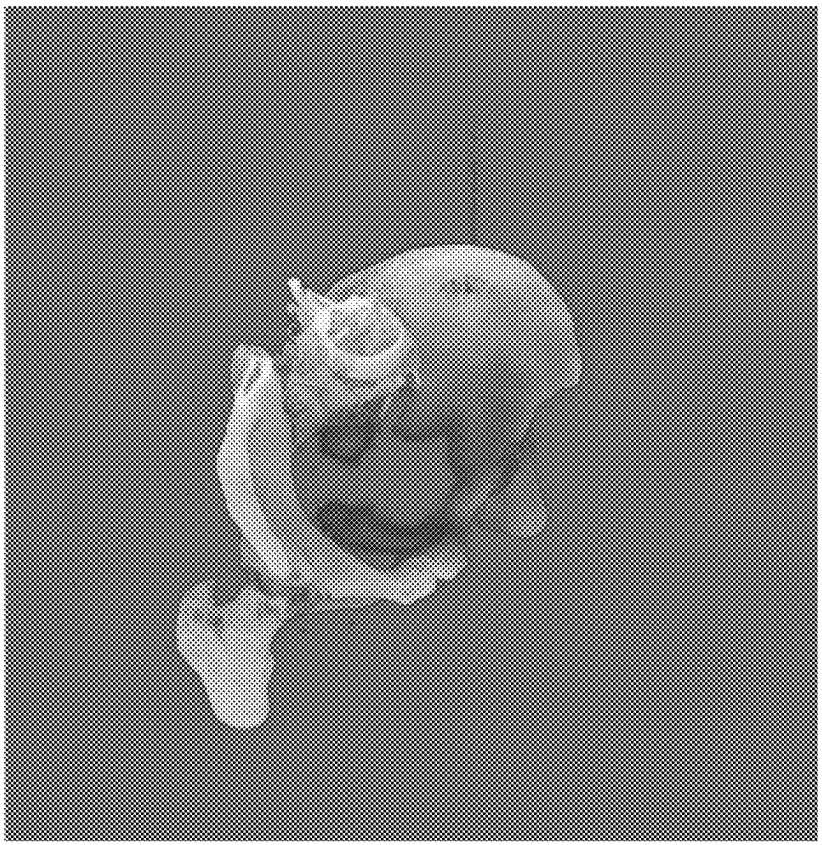

FIG. 22B

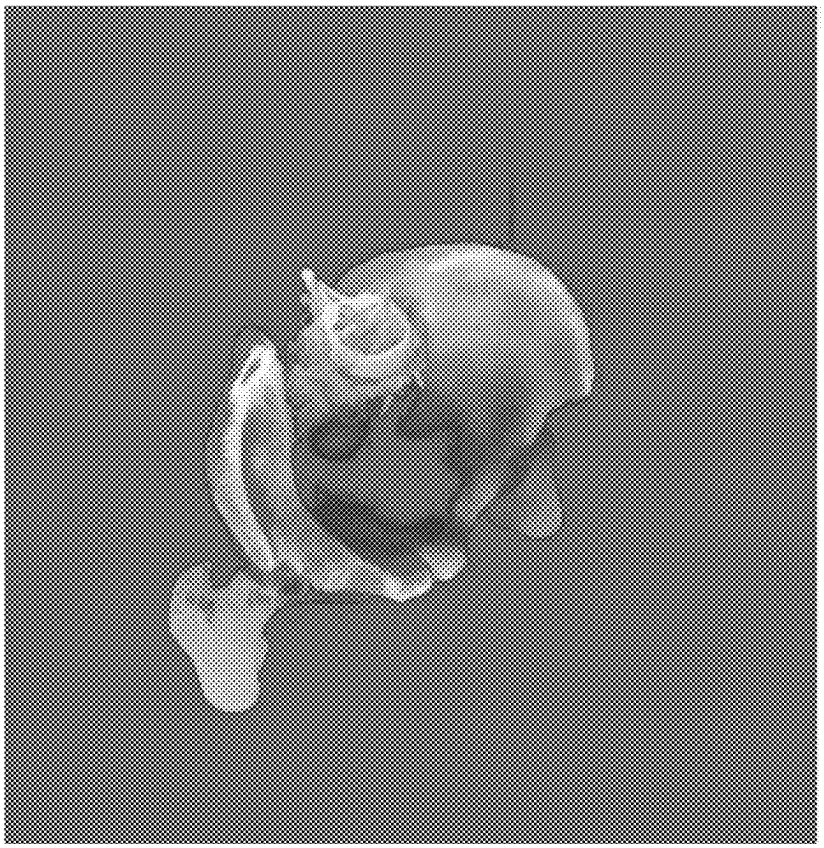

FIG. 22C

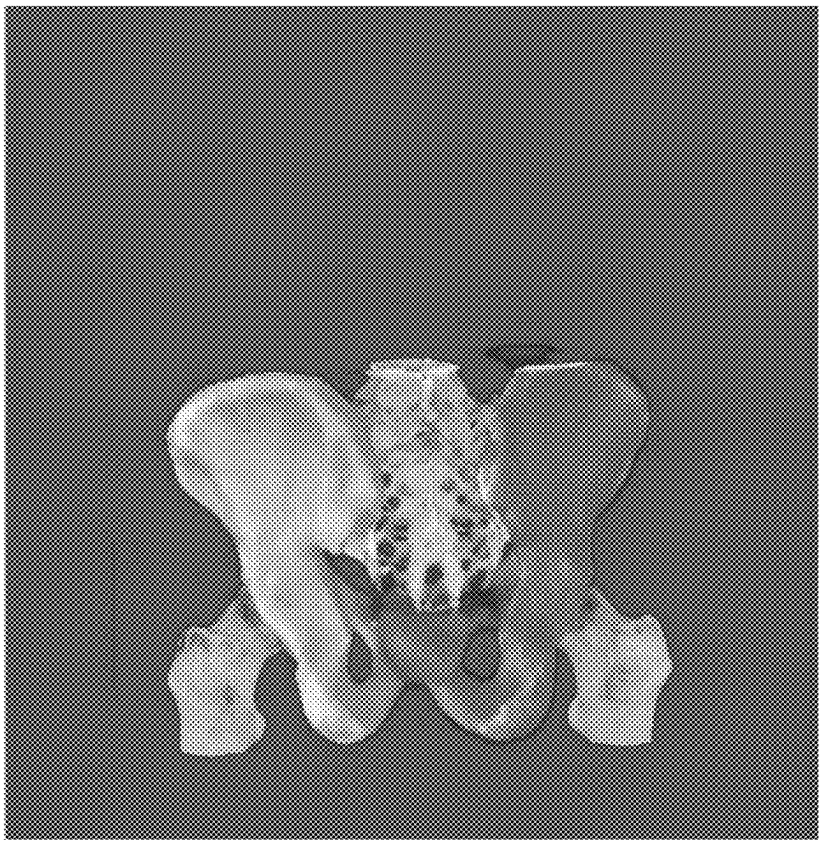

FIG. 22D

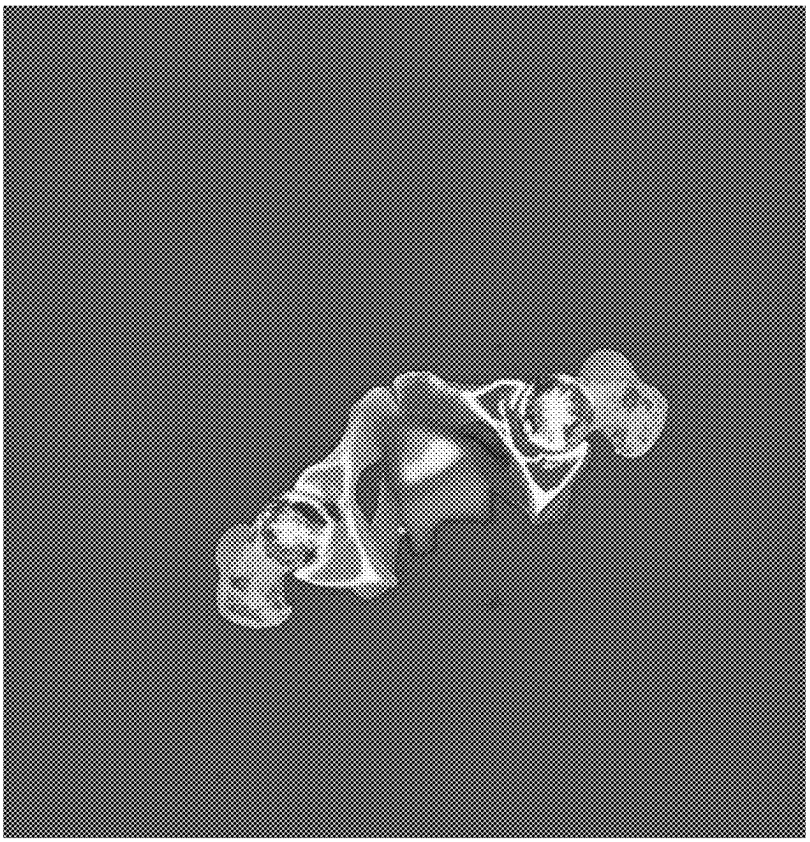

FIG. 22E

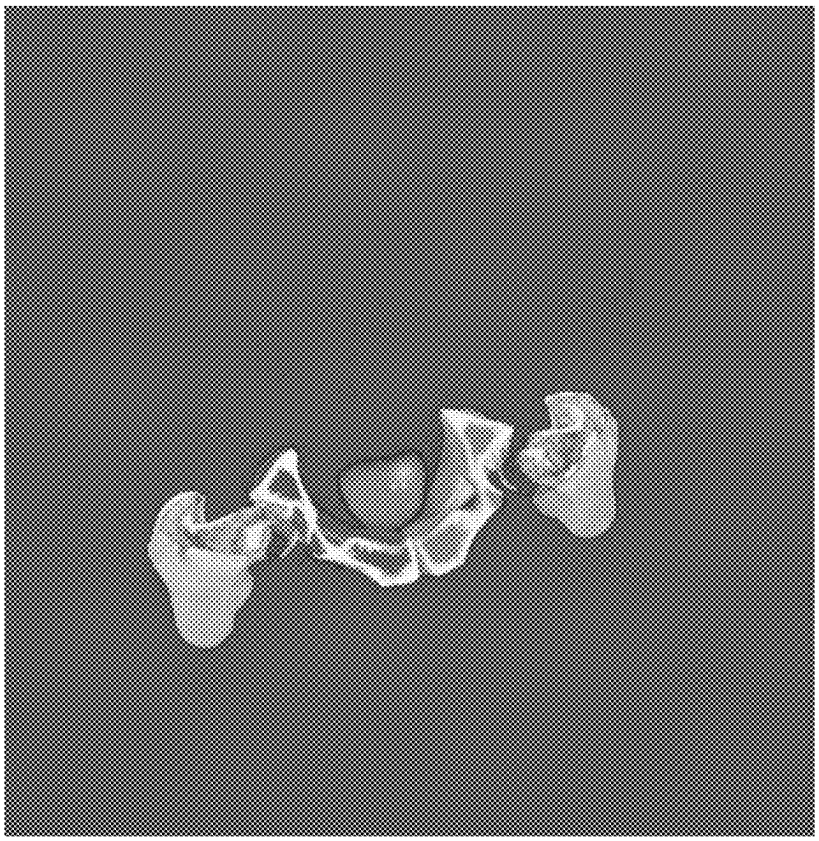

FIG. 22F

FIG. 23A

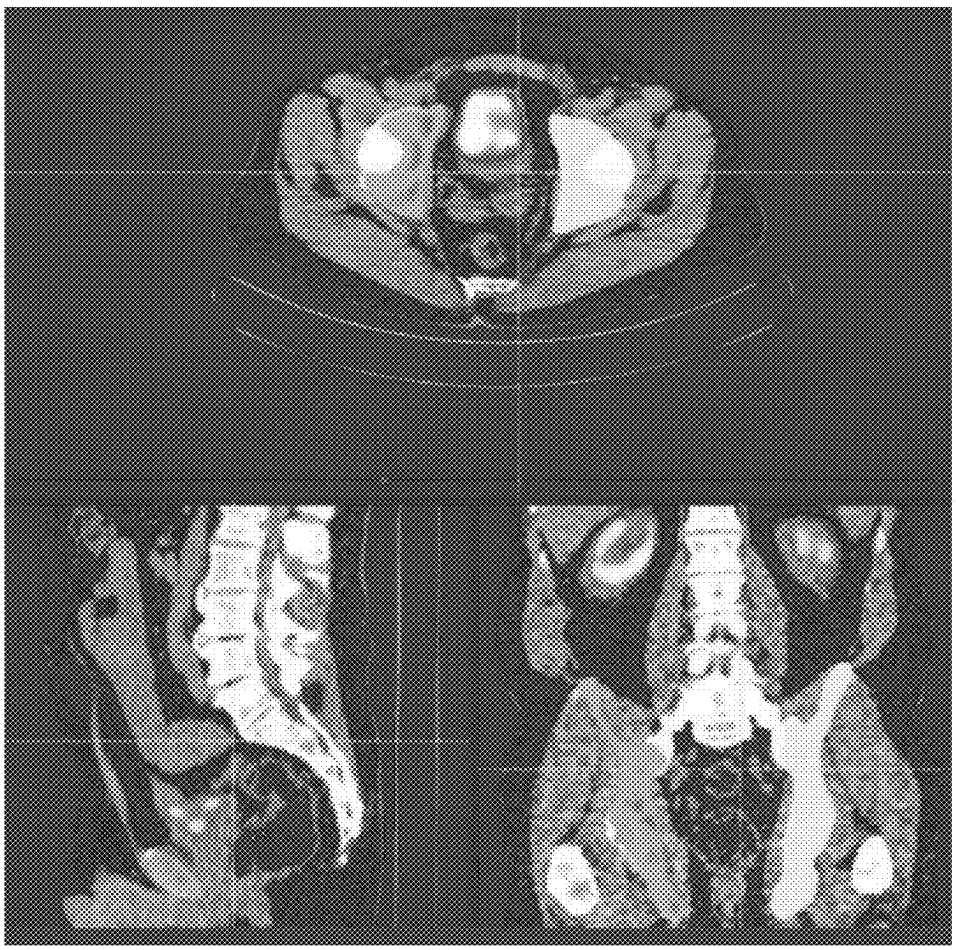

FIG. 23B

Report

REPORT DATE

DIAGNOSTIC DEVICE
Pioneer Web 1404 CADx

× esc

Patient

PATIENT NAME

PATIENT ID

AGE <BIRTH DATE>

Study data

STUDY DATE

INDEX
1.24

PREVIOUS STUDY INDEX
2.62

TECHNICIAN

PHYSICIAN

COMMENT
Lorem ipsum dolor sit amet, consectetur adipiscing elit. Morbi cursus nisi enim, ac fringilla sem accumsan quis, Cras nec arcu sed nulla elementum tinidunt faucibus a felis. Aenean a convallis arcu. Cras ac leo at leo bibendum placerat ac sit

STUDY DESCRIPTION
Lorem ipsum dolor sit amet ads

Tumor data

	TUMOR #1	TUMOR #2
Volume (ml)	7.7	7.7
Max (counts/ml)	29.312	29.312
Mean (counts/ml)	17.336	17.336
Median (counts/ml)	16.402	16.402
Max voxel intensity	3.232	3.232
Total (counts)	133.808	133.808

Prostate data

NORMAL TISSUE UPTAKE (COUNTS/ML)
731.8

PROSTATE VOLUME (ML)
80.7

TOTAL PROSTATE UPTAKE (COUNTS)
386.933

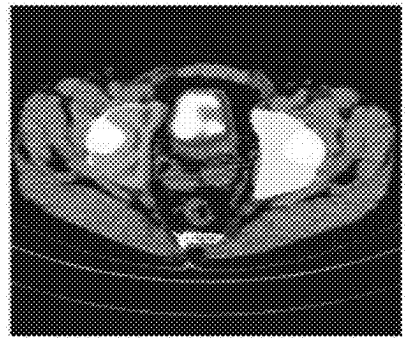

FIG. 24

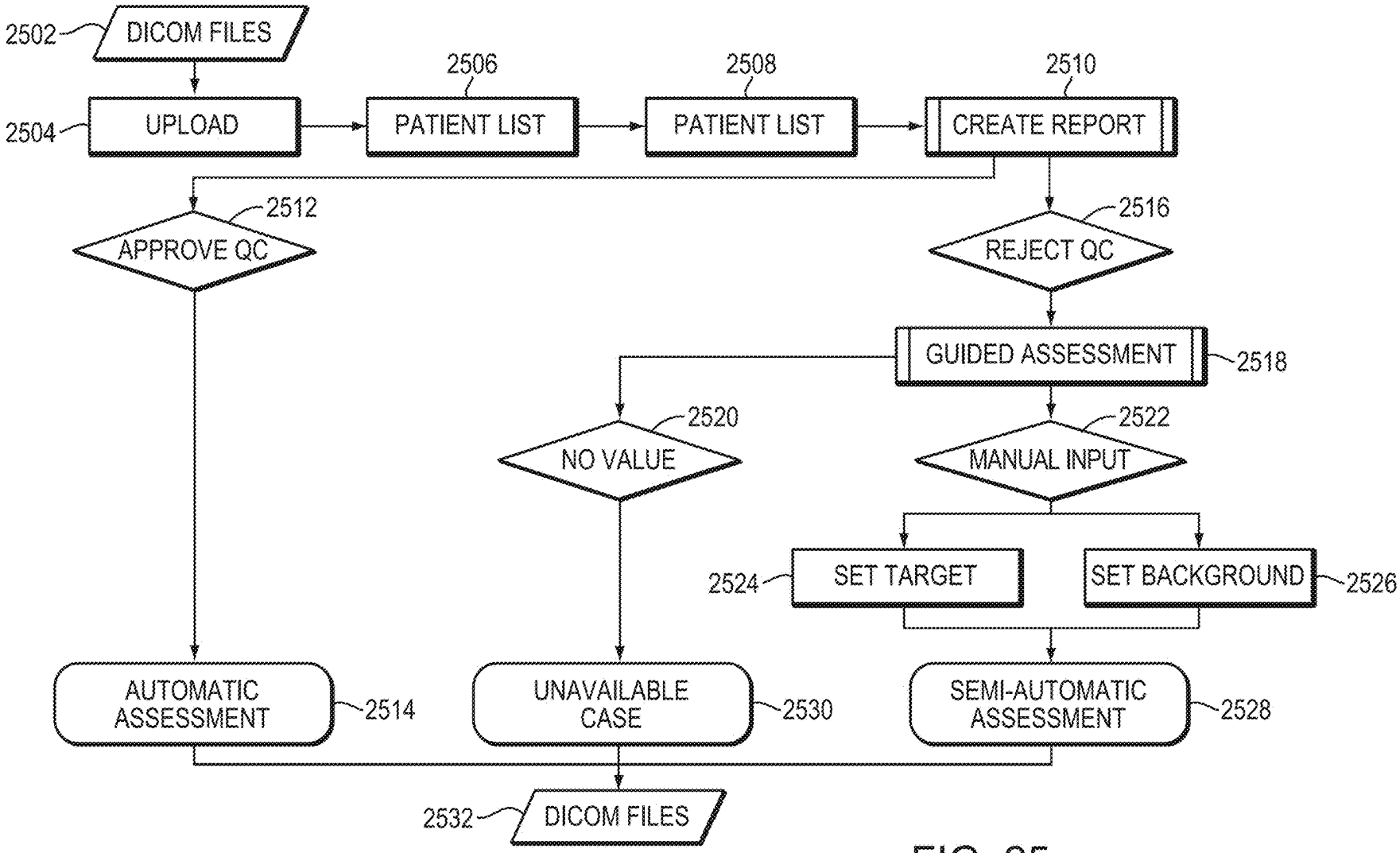
2502
DICOM FILES
2504
UPLOAD
2506
PATIENT LIST
2508
PATIENT LIST
2510
CREATE REPORT
2512
APPROVE QC
2516
REJECT QC
GUIDED ASSESSMENT
2518
2520
NO VALUE
2522
MANUAL INPUT
2524
SET TARGET
SET BACKGROUND
2526
AUTOMATIC ASSESSMENT
2514
UNAVAILABLE CASE
2530
SEMI-AUTOMATIC ASSESSMENT
2528
2532
DICOM FILES

FIG. 25

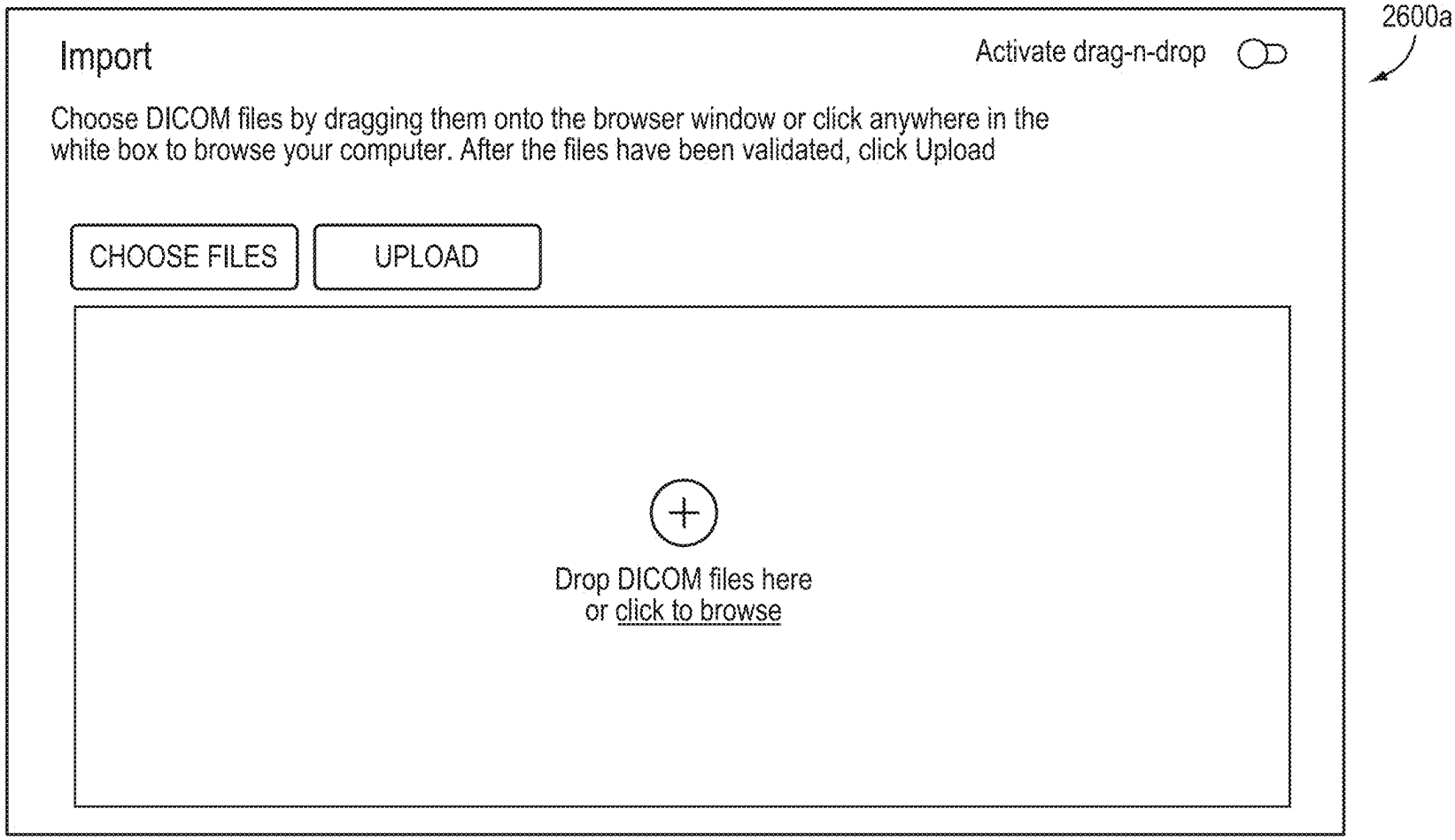
2600a
Import
Activate drag-n-drop
Choose DICOM files by dragging them onto the browser window or click anywhere in the white box to browse your computer. After the files have been validated, click Upload
CHOOSE FILES
UPLOAD
Drop DICOM files here
or click to browse

FIG. 26A

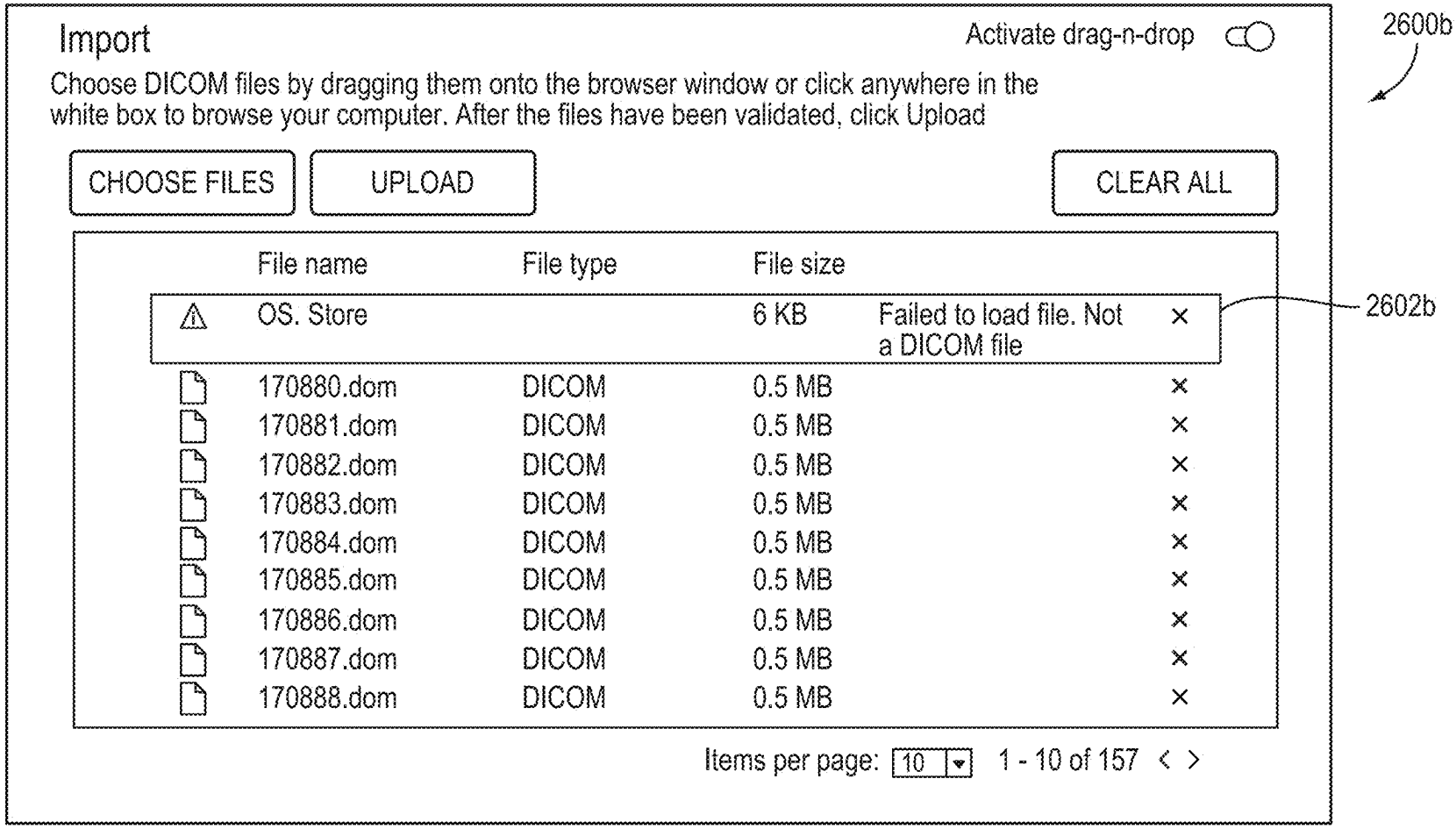
Import
Activate drag-n-drop
Choose DICOM files by dragging them onto the browser window or click anywhere in the white box to browse your computer. After the files have been validated, click Upload
CHOOSE FILES
UPLOAD
CLEAR ALL
File name
File type
File size
OS. Store
6 KB
Failed to load file. Not a DICOM file
170880.dom DICOM 0.5 MB
170881.dom DICOM 0.5 MB
170882.dom DICOM 0.5 MB
170883.dom DICOM 0.5 MB
170884.dom DICOM 0.5 MB
170885.dom DICOM 0.5 MB
170886.dom DICOM 0.5 MB
170887.dom DICOM 0.5 MB
170888.dom DICOM 0.5 MB
Items per page: 10
1 - 10 of 157
2600b
2602b

FIG. 26B

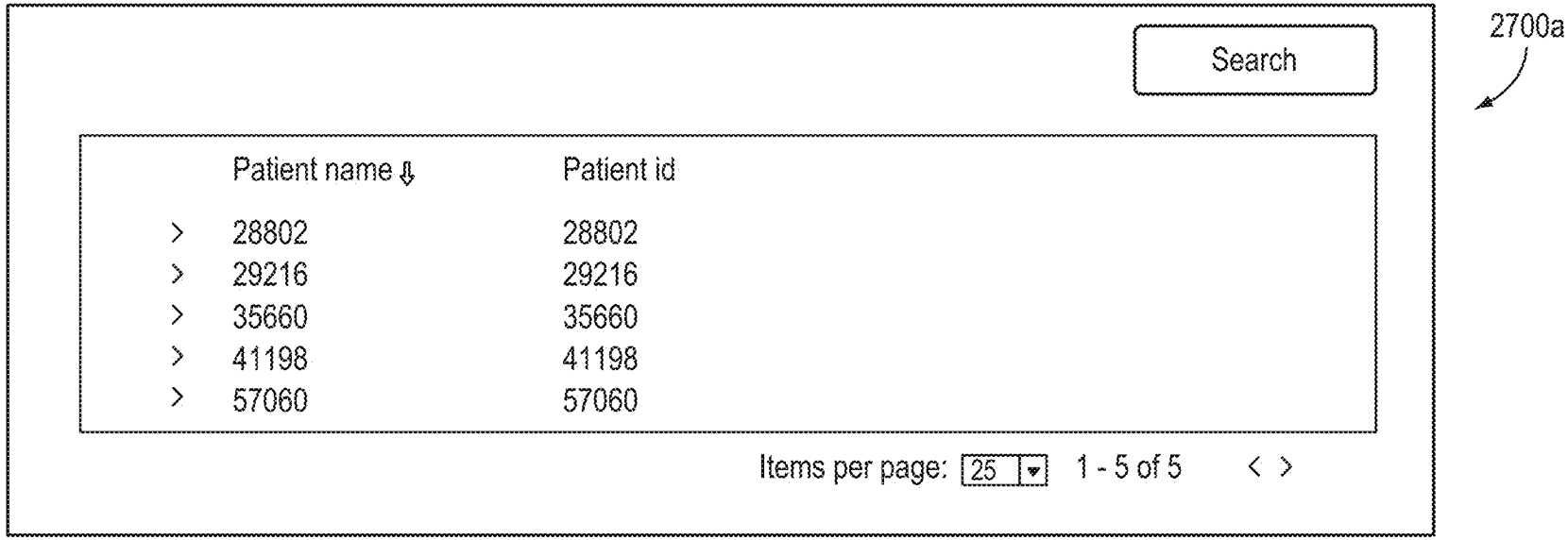

FIG. 27A

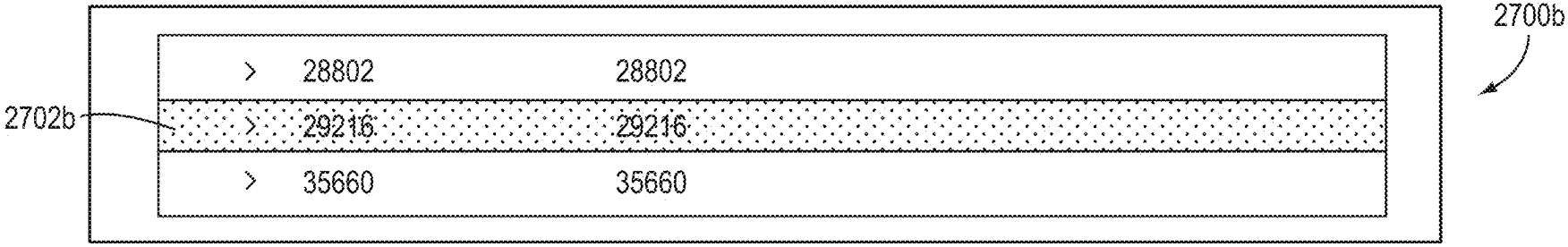

FIG. 27B

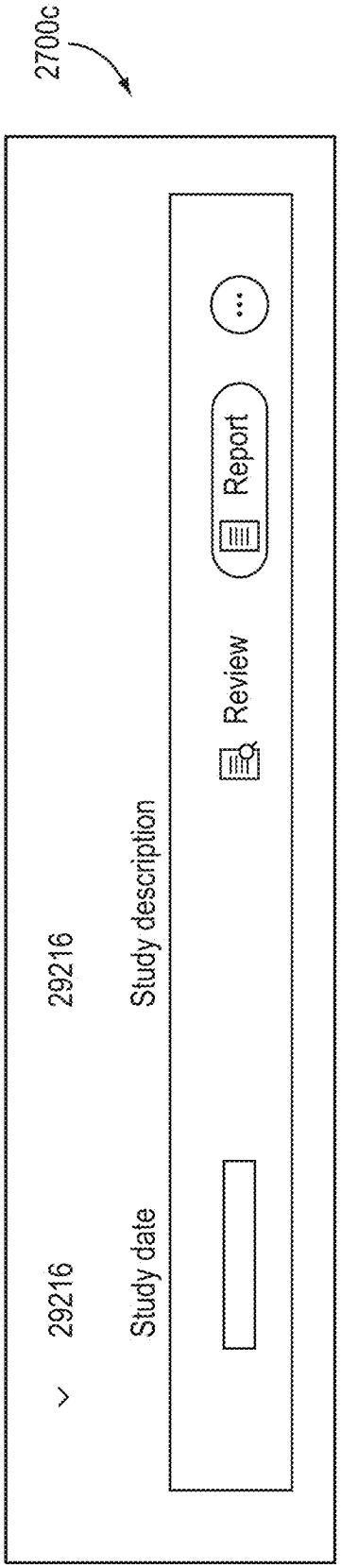
2700c
29216
Study date
29216
Study description
Review
Report

FIG. 27C

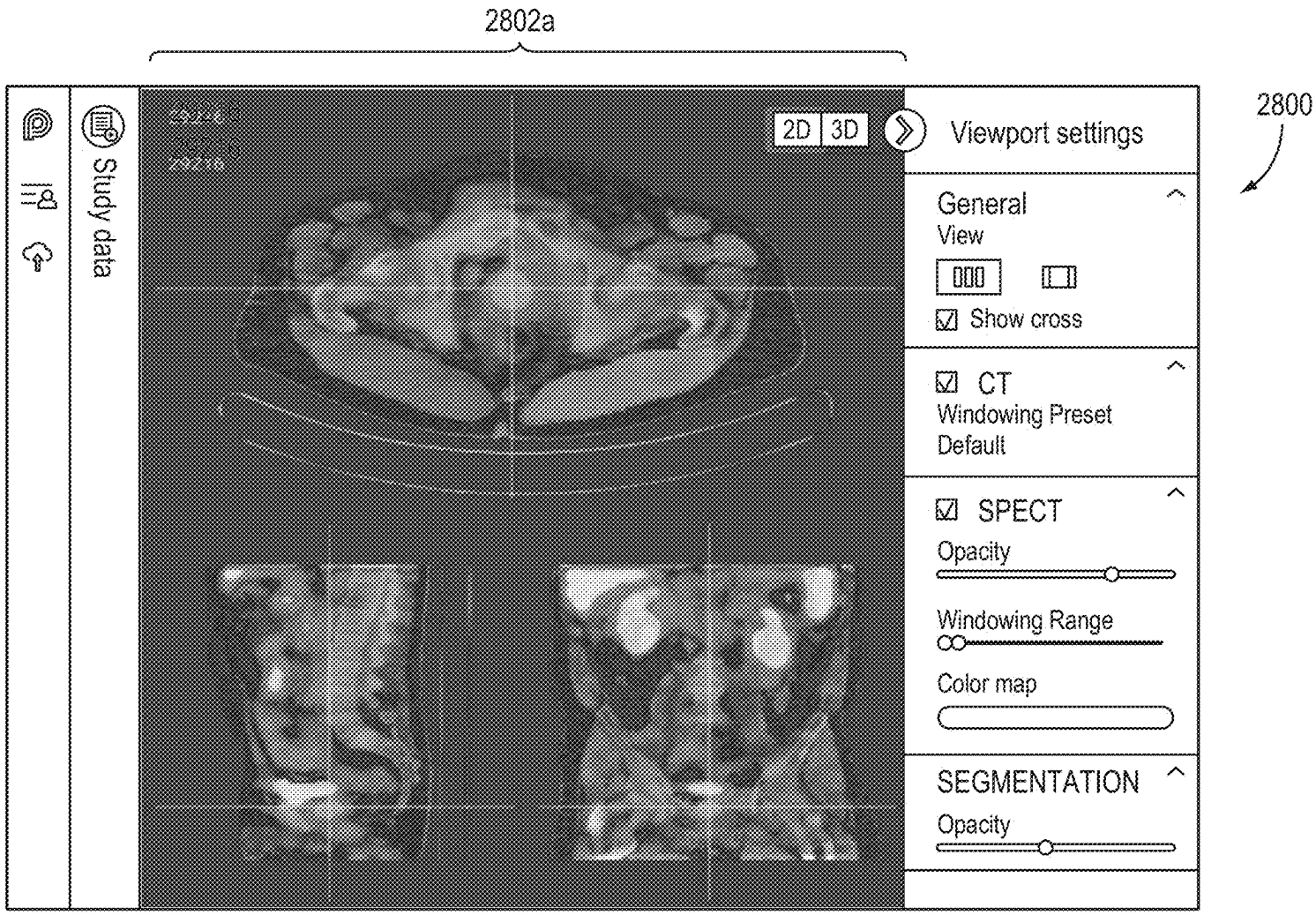
2802a
2800
Study data
2D
3D
Viewport settings
General
View
Show cross
CT
Windowing Preset
Default
SPECT
Opacity
Windowing Range
Color map
SEGMENTATION
Opacity

FIG. 28A

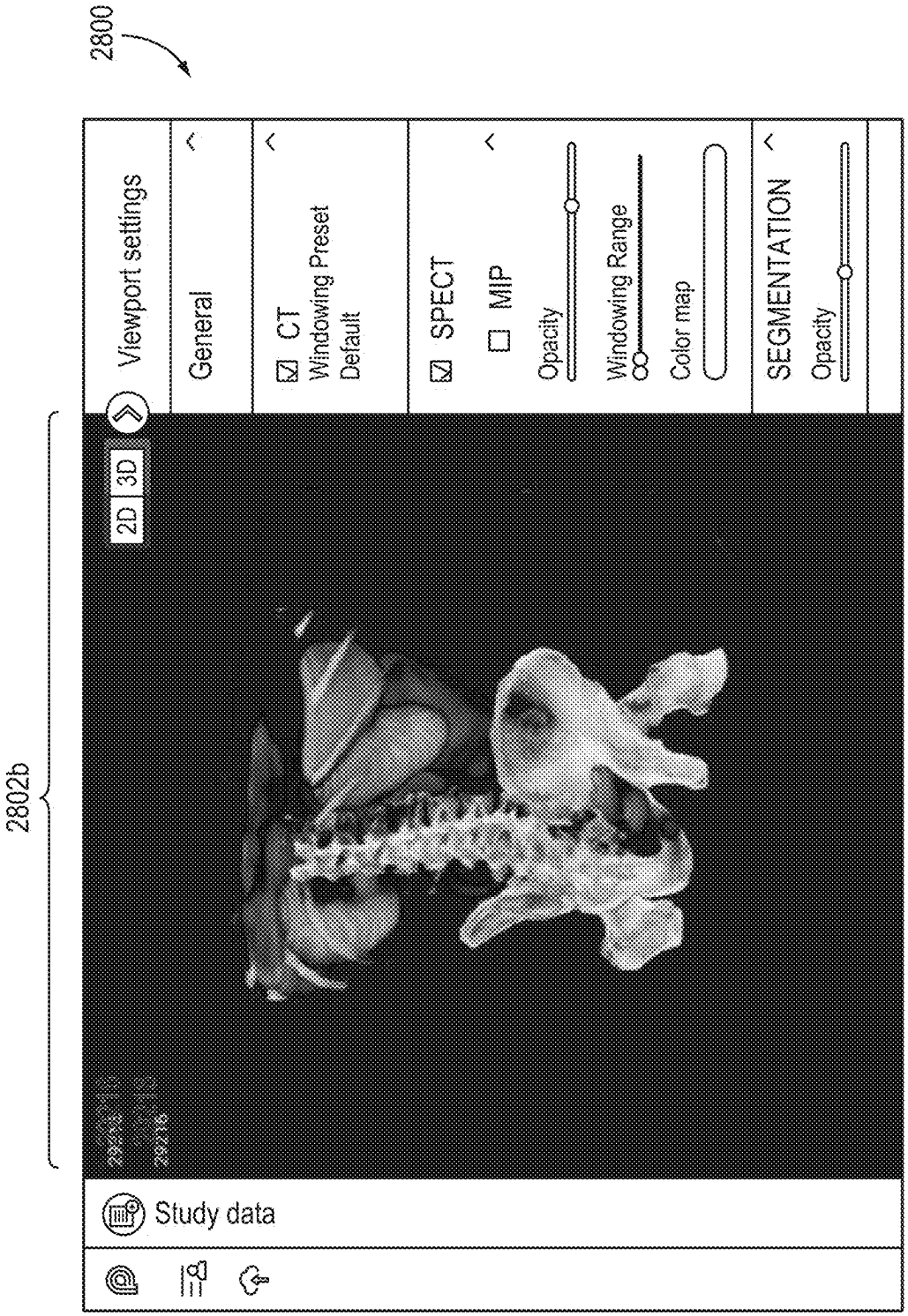
2800
2802b
Viewport settings
2D
3D
General
CT
Windowing Preset
Default
SPECT
MIP
Opacity
Windowing Range
Color map
SEGMENTATION
Opacity
Study data

FIG. 28B

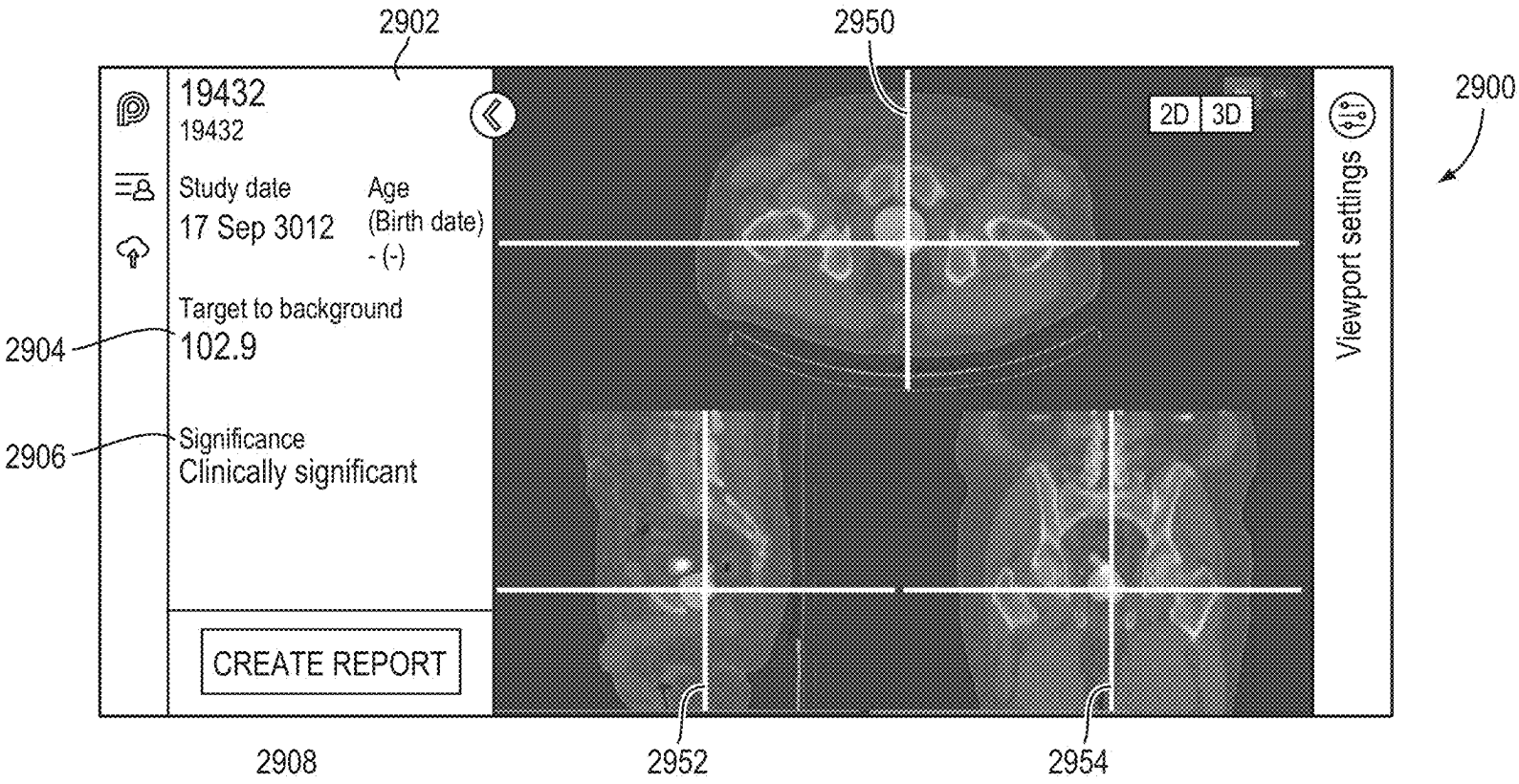
2902
2950
2900
19432
19432
Study date
17 Sep 3012
Age
(Birth date)
- (-)
Target to background
102.9
2904
Significance
Clinically significant
2906
CREATE REPORT
2D
3D
Viewport settings
2908
2952
2954

FIG. 29A

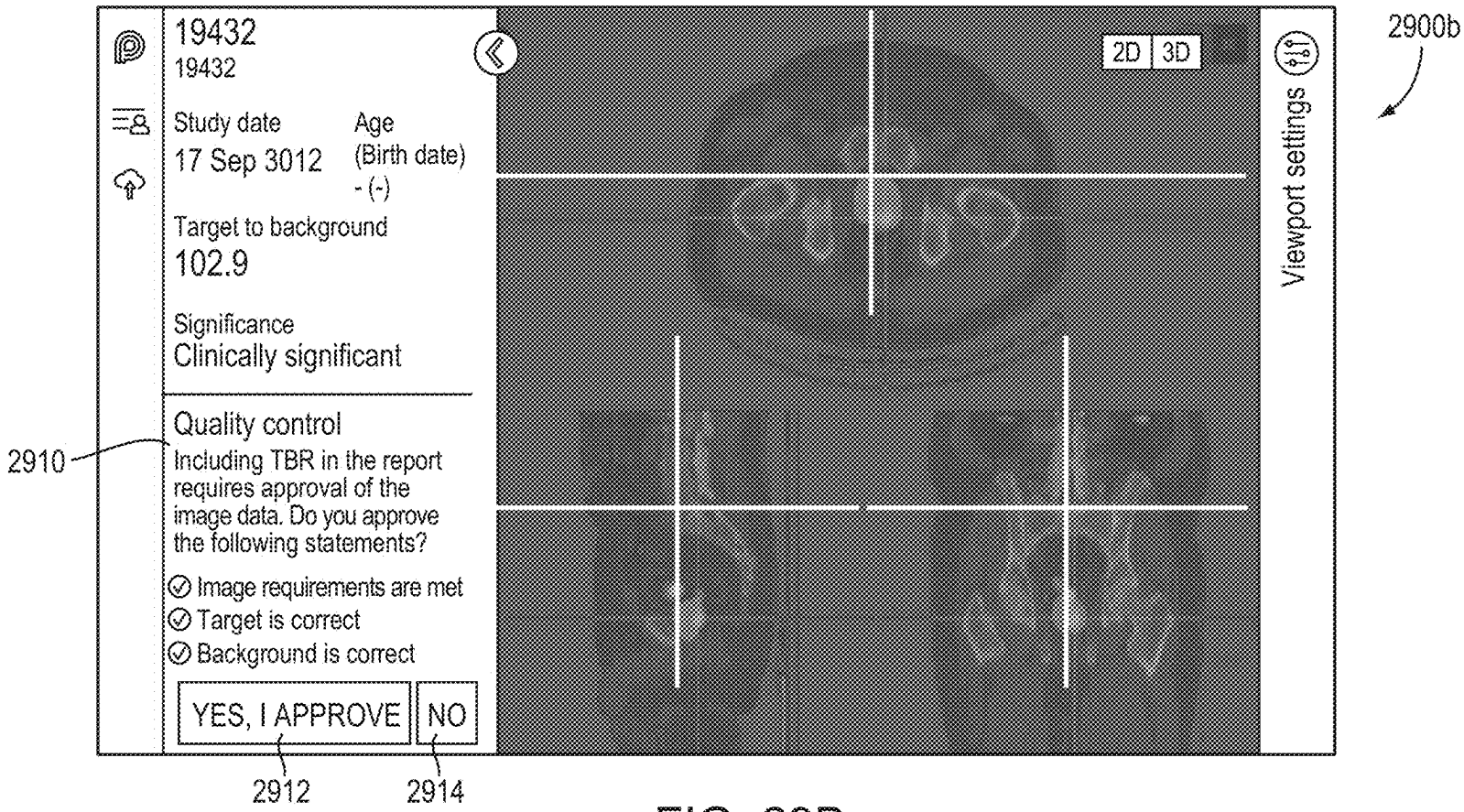
2900b
19432
19432
Study date
17 Sep 3012
Age
(Birth date)
- (-)
Target to background
102.9
Significance
Clinically significant
Quality control
Including TBR in the report requires approval of the image data. Do you approve the following statements?
Image requirements are met
Target is correct
Background is correct
YES, I APPROVE
NO
2910
2912
2914
2D
3D
Viewport settings

FIG. 29B

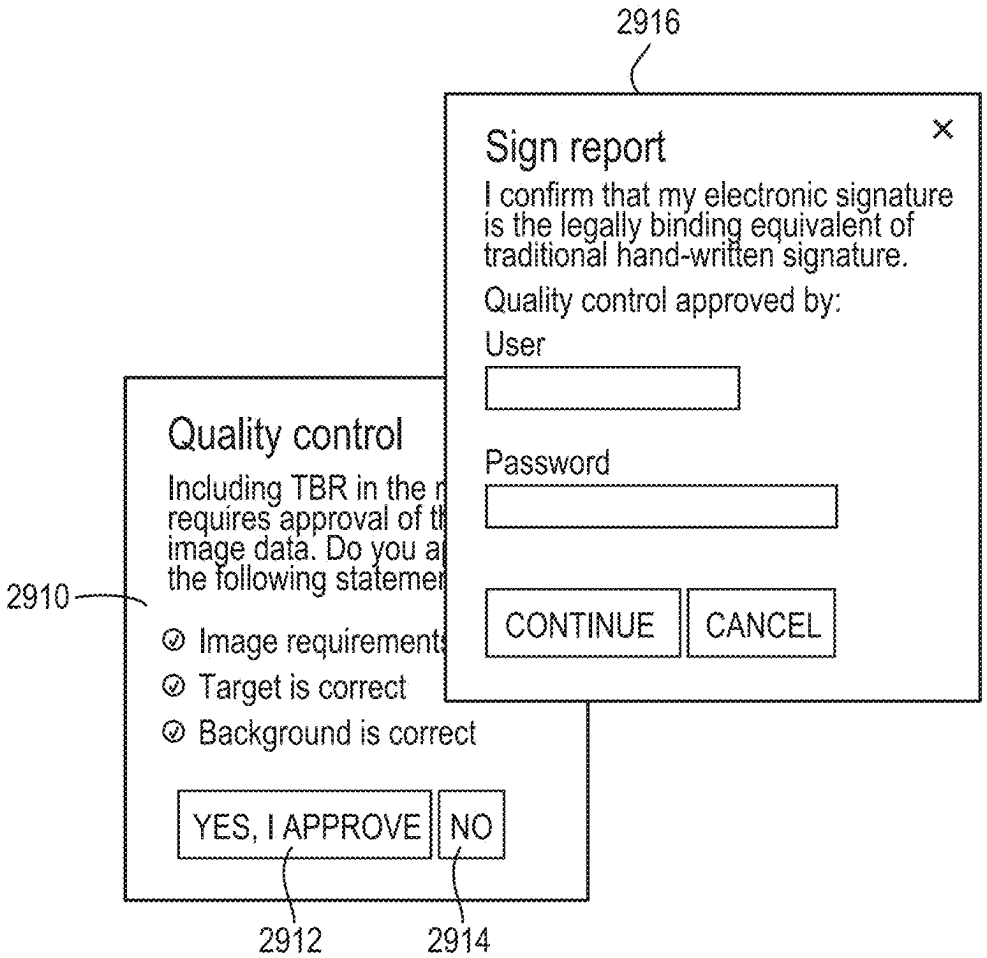
2916
Sign report
I confirm that my electronic signature is the legally binding equivalent of traditional hand-written signature.
Quality control approved by:
User
Password
CONTINUE
CANCEL
Quality control
Including TBR in the r
requires approval of th
image data. Do you ap
the following statemen
2910
Image requirements
Target is correct
Background is correct
YES, I APPROVE
NO
2912
2914

FIG. 29C

2900d

Export PNG Export DICOM ×

Report

Report ID

Diagnostic device
Pioneer 1.0.0

CAUTION - Investigation Device. Limited by Federal (or United States) law to investigational use.

Patient

Patient name
29216

Patient ID
29216

Age (Birth date)
-(-)

Study data

Study date

TBR
106.8

Significance
Clinically significant

Quality Control

Quality Control
✓ Image requirements are met
✓ Target is correct
✓ Background is correct
Quality cation
Automatic

2918

Pioneer 1.0.0 DOES NOT PROVIDE OR SUBSTITUTE FOR MEDICAL SERVICES OR ADVICE. EXINI PROVIDES Pioneer 1.0.0 FOR INFORMATIONAL PURPOSES ONLY AND Pioneer 1.0.0 DOES NOT CONTAIN OR CONSTITUTE ANY MEDICAL ADVICE OR OPINION. YOU ARE SOLELY RESPONSIBLE FOR ALL DECISIONS OR ACTIONS RESULTING FROM YOUR USE OF Pioneer 1.0.0, INCLUDING, BUT NOT LIMITED TO ANY DECISION TO PROVIDE OR SEEK, OR REFRAIN FROM PROVIDING OR SEEKING, ANY MEDICAL ADVICE OR TREATMENT. Information made available on or through Pioneer 1.0.0 should not be the sole information for making decisions and should be discussed with your healthcare provider prior to making medical decisions or to diagnose or treat a medical or health condition. Your use of Pioneer 1.0.0 does not create a doctor-patient relationship between you and EXINI

Report creation

Quality Control approved by

2920

FIG. 29D

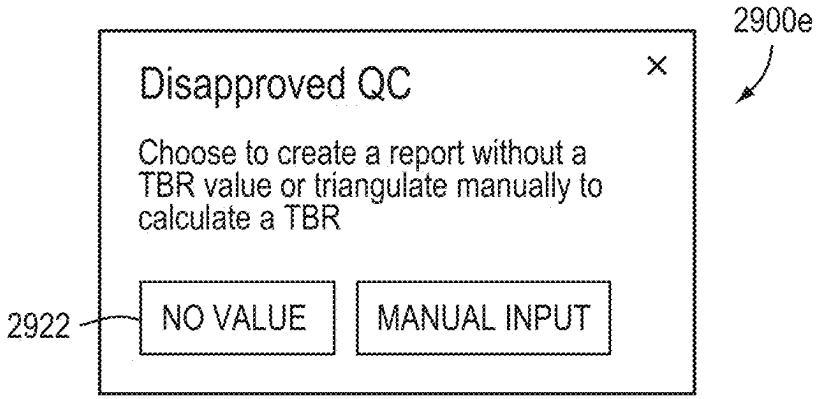

FIG. 29E

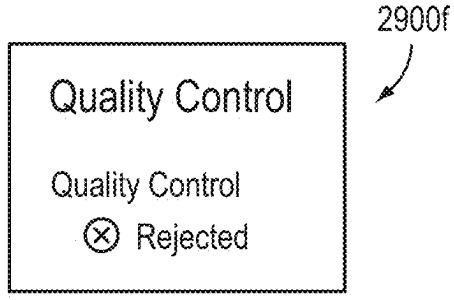

FIG. 29F

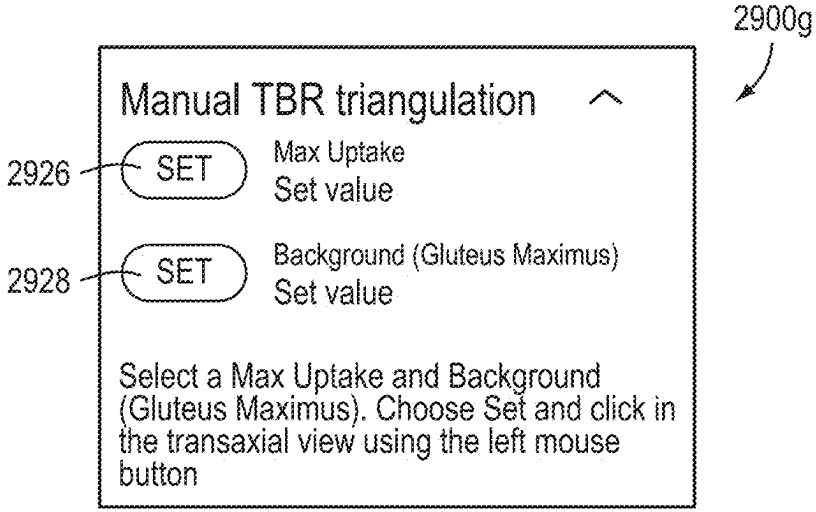

FIG. 29G

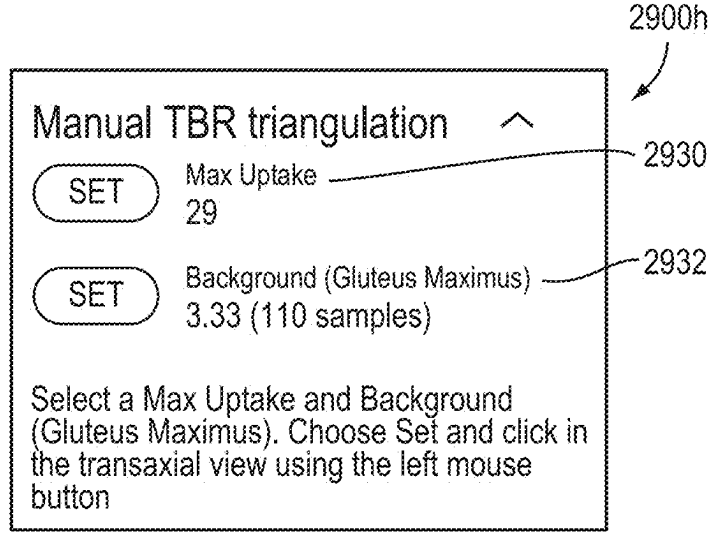

FIG. 29H

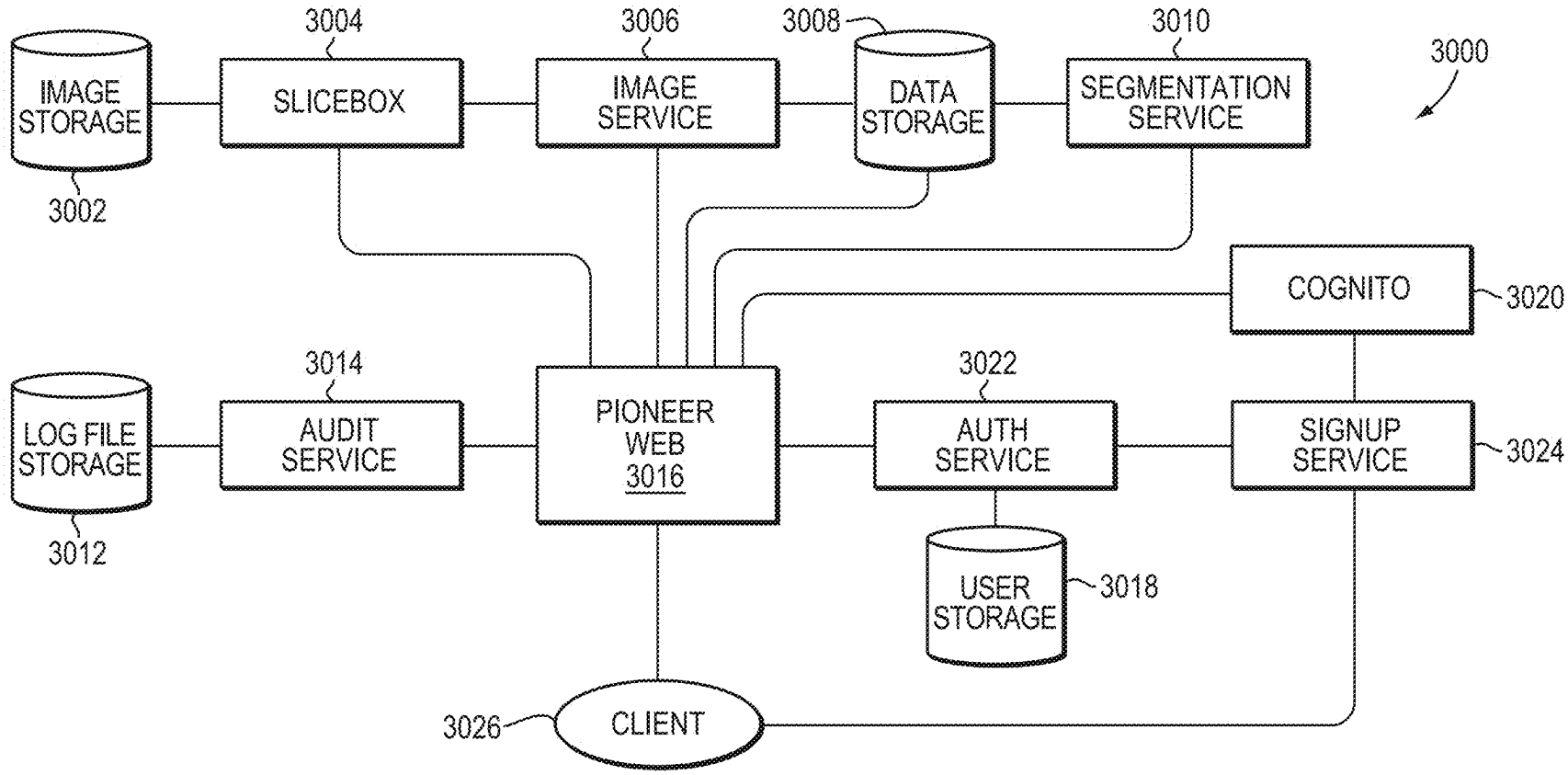
3000
IMAGE STORAGE
3002
3004
SLICEBOX
3006
IMAGE SERVICE
3008
DATA STORAGE
3010
SEGMENTATION SERVICE
COGNITO
3020
LOG FILE STORAGE
3012
3014
AUDIT SERVICE
PIONEER WEB 3016
3022
AUTH SERVICE
SIGNUP SERVICE
3024
USER STORAGE
3018
3026
CLIENT

FIG. 30

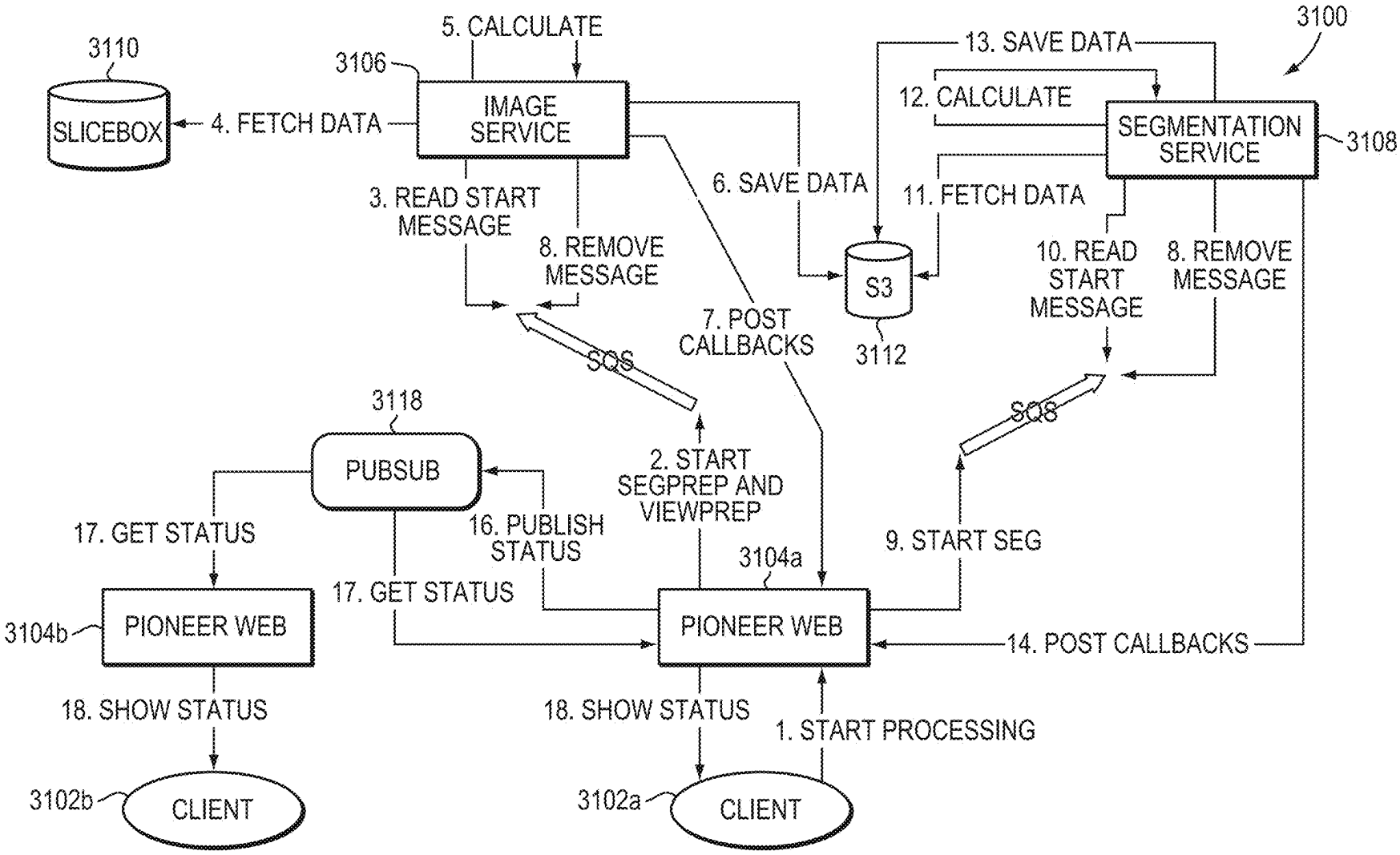
3100
3110
SLICEBOX
4. FETCH DATA
3106
IMAGE SERVICE
5. CALCULATE
3. READ START MESSAGE
8. REMOVE MESSAGE
6. SAVE DATA
7. POST CALLBACKS
SQS
S3
3112
13. SAVE DATA
12. CALCULATE
SEGMENTATION SERVICE
3108
11. FETCH DATA
10. READ START MESSAGE
8. REMOVE MESSAGE
SQS
3118
PUBSUB
2. START SEGPREP AND VIEWPREP
16. PUBLISH STATUS
17. GET STATUS
17. GET STATUS
9. START SEG
3104a
3104b
PIONEER WEB
PIONEER WEB
14. POST CALLBACKS
18. SHOW STATUS
18. SHOW STATUS
1. START PROCESSING
3102b
CLIENT
3102a
CLIENT

FIG. 31

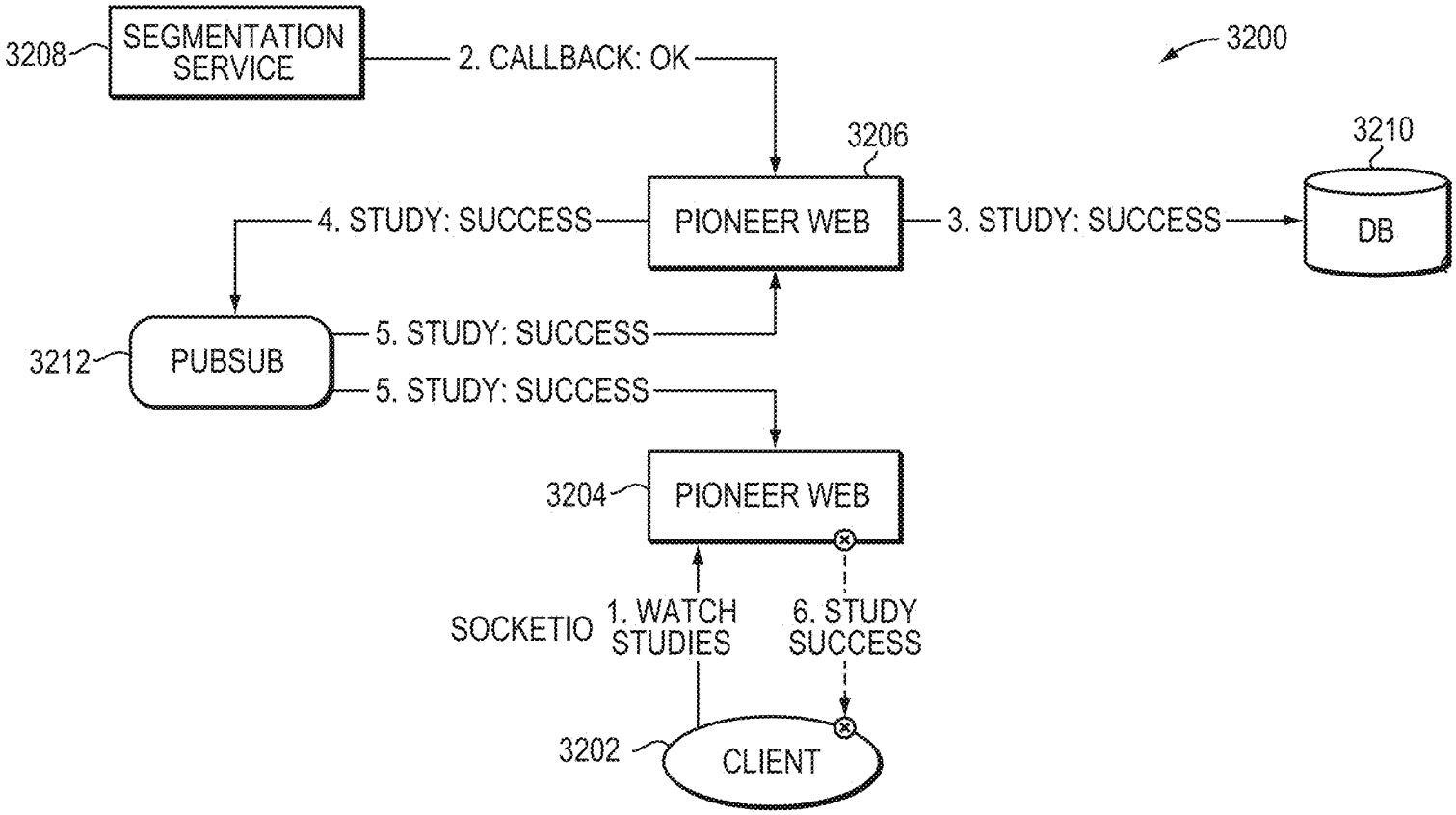
3200
3208
SEGMENTATION SERVICE
2. CALLBACK: OK
3206
3210
4. STUDY: SUCCESS
PIONEER WEB
3. STUDY: SUCCESS
DB
3212
PUBSUB
5. STUDY: SUCCESS
5. STUDY: SUCCESS
3204
PIONEER WEB
SOCKETIO
1. WATCH STUDIES
6. STUDY SUCCESS
3202
CLIENT

FIG. 32

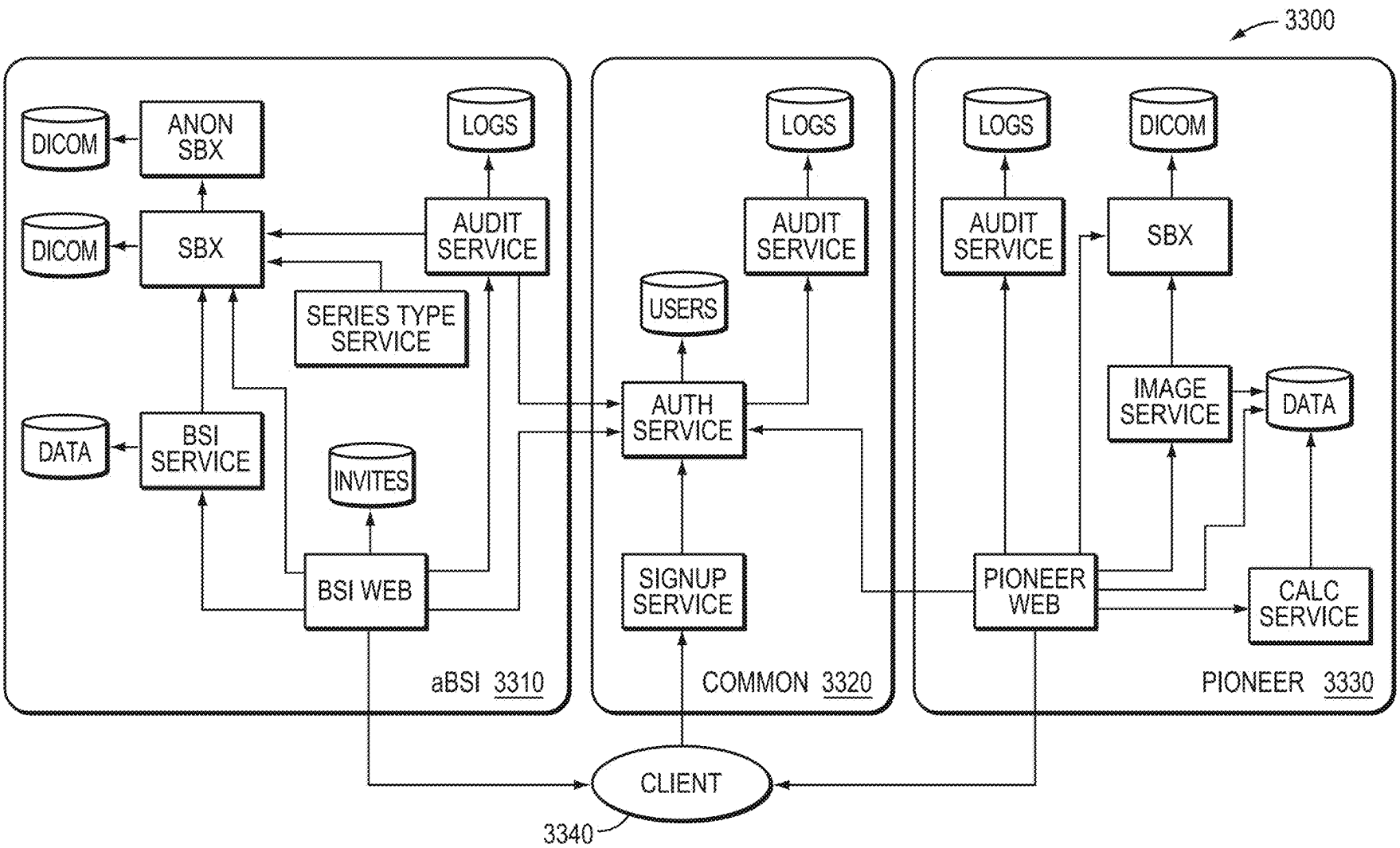
3300
DICOM
ANON SBX
LOGS
DICOM
SBX
AUDIT SERVICE
SERIES TYPE SERVICE
DATA
BSI SERVICE
INVITES
BSI WEB
aBSI 3310
LOGS
AUDIT SERVICE
USERS
AUTH SERVICE
SIGNUP SERVICE
COMMON 3320
LOGS
DICOM
AUDIT SERVICE
SBX
IMAGE SERVICE
DATA
PIONEER WEB
CALC SERVICE
PIONEER 3330
CLIENT
3340

FIG. 33

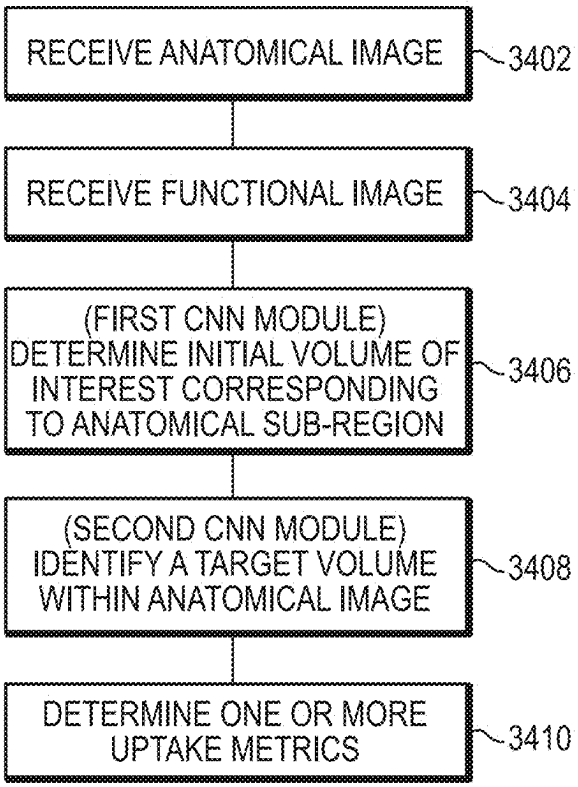
RECEIVE ANATOMICAL IMAGE
3402
RECEIVE FUNCTIONAL IMAGE
3404
(FIRST CNN MODULE) DETERMINE INITIAL VOLUME OF INTEREST CORRESPONDING TO ANATOMICAL SUB-REGION
3406
(SECOND CNN MODULE) IDENTIFY A TARGET VOLUME WITHIN ANATOMICAL IMAGE
3408
DETERMINE ONE OR MORE UPTAKE METRICS
3410

FIG. 34

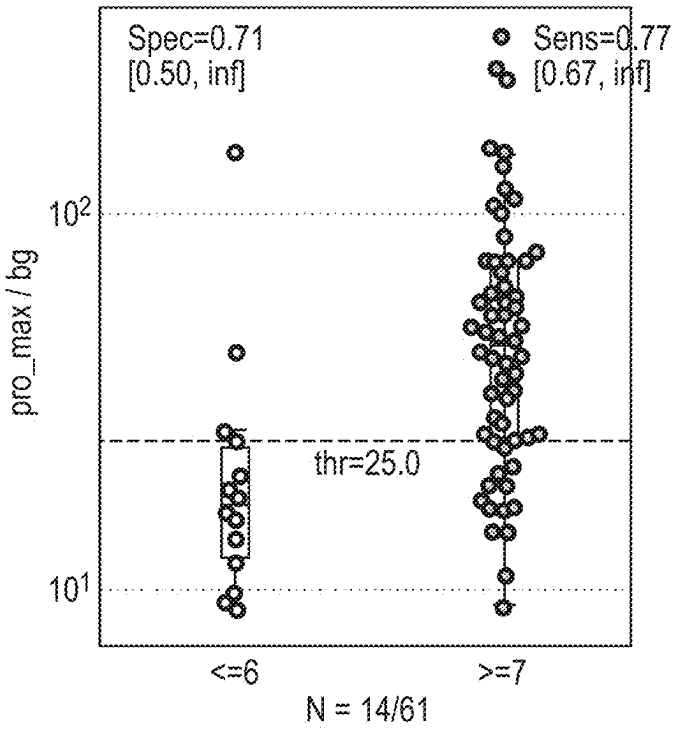

FIG. 35A

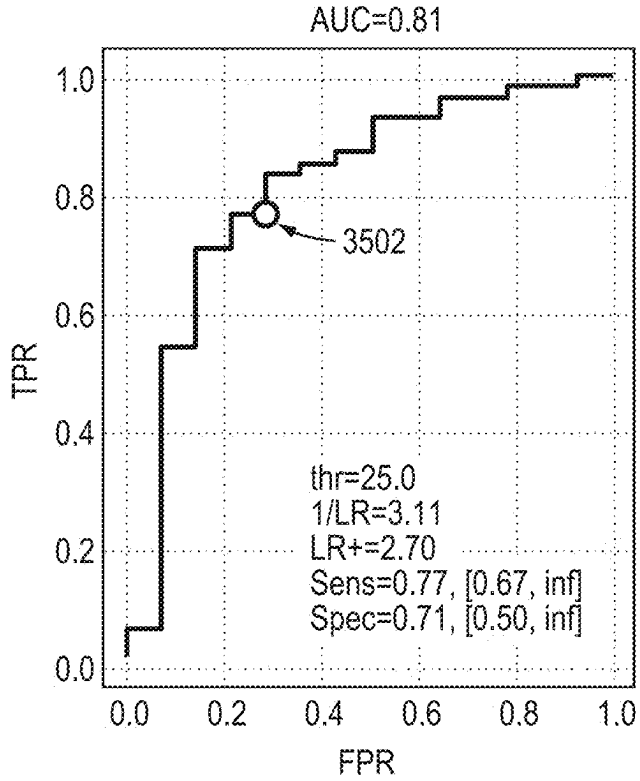

FIG. 35B

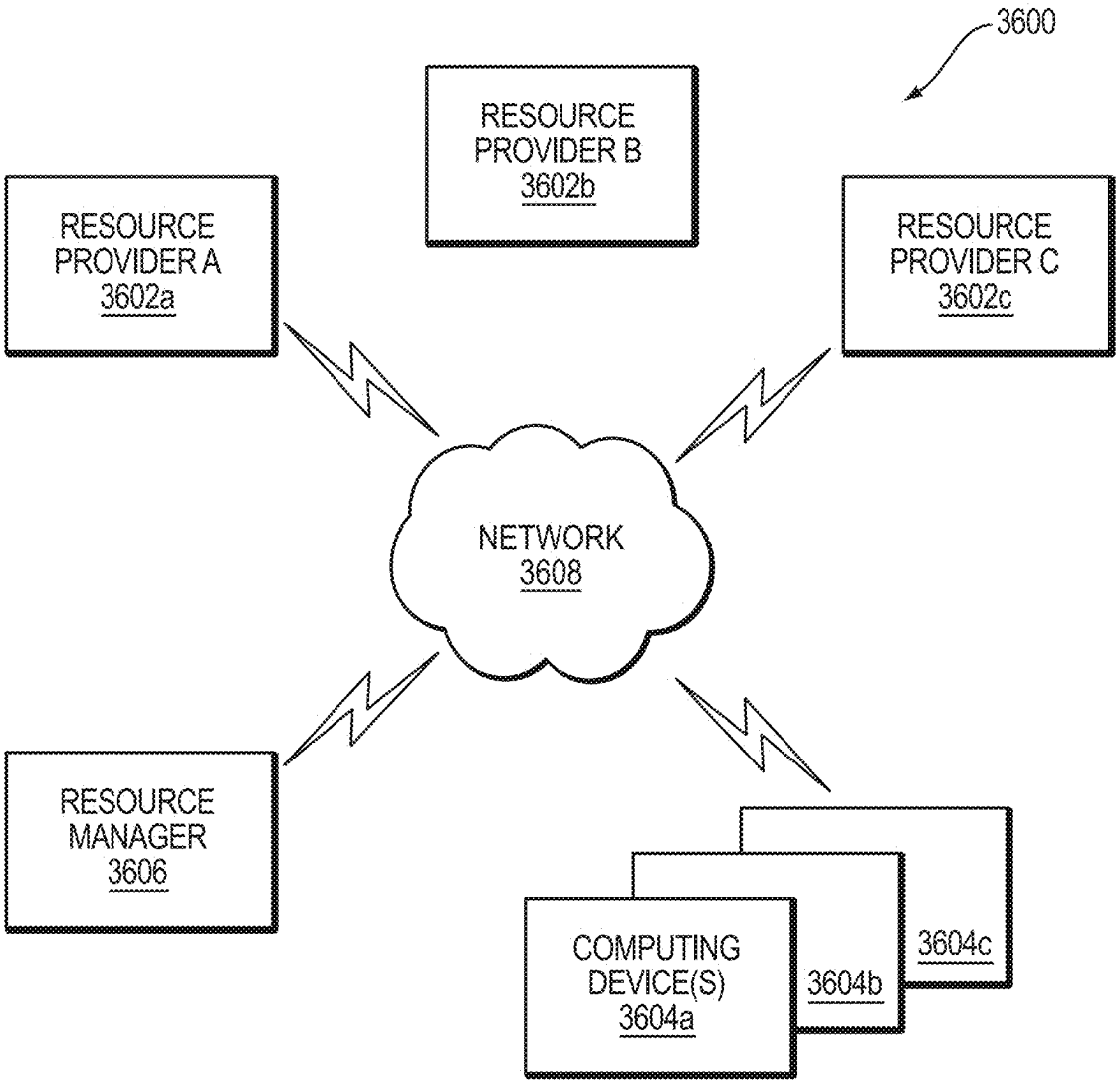
3600
RESOURCE PROVIDER B 3602b
RESOURCE PROVIDER A 3602a
RESOURCE PROVIDER C 3602c
NETWORK 3608
RESOURCE MANAGER 3606
COMPUTING DEVICE(S) 3604a
3604b
3604c

FIG. 36

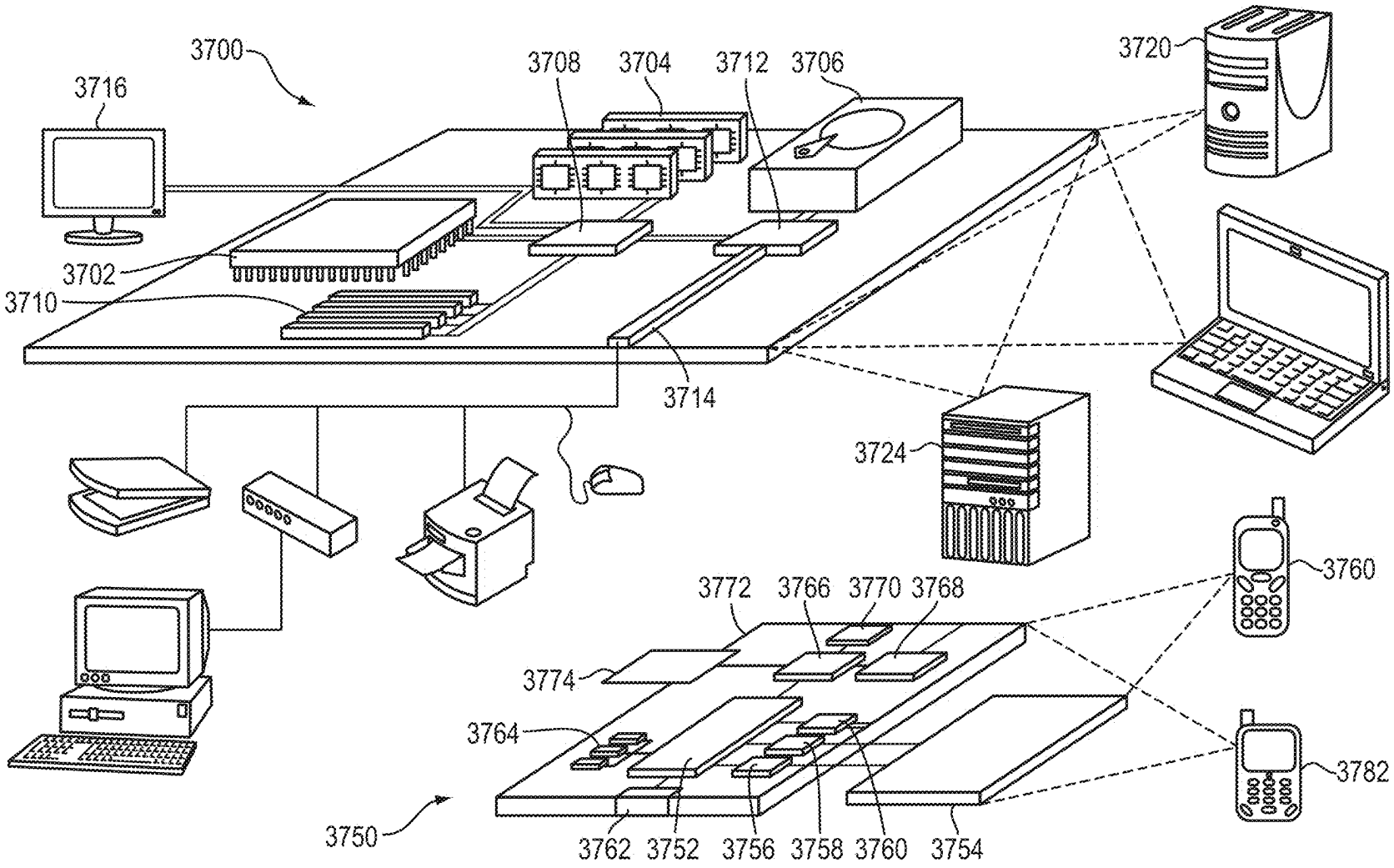
3700
3716
3708
3704
3712
3706
3720
3702
3710
3714
3724
3760
3772
3766
3770
3768
3774
3764
3782
3750
3762
3752
3756
3758
3760
3754

FIG. 37

SYSTEMS AND METHODS FOR RAPID NEURAL NETWORK-BASED IMAGE SEGMENTATION AND RADIOPHARMACEUTICAL UPTAKE DETERMINATION

CROSS REFERENCE TO RELATED APPLICATIONS

This application claims priority to and benefit of U.S. Provisional Application No. 62/614,935, filed Jan. 8, 2018, the content of which is hereby incorporated by reference in its entirety.

FIELD OF THE INVENTION

This invention relates generally to methods, systems, and architectures for automated analysis and/or presentation of medical image data. More particularly, in certain embodiments, the invention relates to automated identification of one or more particular regions of interest (e.g., corresponding to specific organs or tissue) within images of a subject and determination of radiopharmaceutical uptake within such region(s), e.g., for identification and/or staging of disease, e.g., prostate cancer.

BACKGROUND OF THE INVENTION

Targeted image analysis involves the use of radiolabeled small molecules that bind to specific receptors, enzymes and proteins in the body that are altered during the evolution of disease. After administration to a patient, these molecules circulate in the blood until they find their intended target. The bound radiopharmaceutical remains at the site of disease, while the rest of the agent clears from the body. The radioactive portion of the molecule serves as a beacon so that an image may be obtained depicting the disease location and concentration using commonly available nuclear medicine cameras, known as single-photon emission computerized tomography (SPECT) or positron emission tomography (PET) cameras, found in most hospitals throughout the world. Physicians can then use this information to determine the presence and the extent of disease in a patient. The physician can use this information to provide a recommended course of treatment to the patient and to track the progression of disease.

There are a variety of software-based analytical techniques available for analysis and enhancement of PET and SPECT images that can be used by a radiologist or physician. There are also a number of radiopharmaceuticals available for imaging particular kinds of cancer. For example, the small molecule diagnostic 1404 targets the extracellular domain of prostate specific membrane antigen (PSMA), a protein amplified on the surface of >95% of prostate cancer cells and a validated target for the detection of primary and metastatic prostate cancer. 1404 is labeled with technetium-99m, a gamma-emitter isotope that is widely available, relatively inexpensive, facilitates efficient preparation, and has spectrum characteristics attractive for nuclear medicine imaging applications.

Another example radiopharmaceutical is PyL™ (also known as [^{18}F]DCFPyL), which is a clinical-stage, fluorinated PSMA-targeted PET imaging agent for prostate cancer. A proof-of-concept study published in the April 2015 issue of the Journal of Molecular Imaging and Biology demonstrated that PET imaging with PyL™ showed high levels of PyL™ uptake in sites of putative metastatic disease and primary tumors, suggesting the potential for high sensitivity and specificity in detecting prostate cancer.

An oncologist may use images from a targeted PET or SPECT study of a patient as input in her assessment of whether the patient has a particular disease, e.g., prostate cancer, what stage of the disease is evident, what the recommended course of treatment (if any) would be, whether surgical intervention is indicated, and likely prognosis. The oncologist may use a radiologist report in this assessment. A radiologist report is a technical evaluation of the PET or SPECT images prepared by a radiologist for a physician who requested the imaging study and includes, for example, the type of study performed, the clinical history, a comparison between images, the technique used to perform the study, the radiologist's observations and findings, as well as overall impressions and recommendations the radiologist may have based on the imaging study results. A signed radiologist report is sent to the physician ordering the study for the physician's review, followed by a discussion between the physician and patient about the results and recommendations for treatment.

Thus, the process involves having a radiologist perform an imaging study on the patient, analyzing the images obtained, creating a radiologist report, forwarding the report to the requesting physician, having the physician formulate an assessment and treatment recommendation, and having the physician communicate the results, recommendations, and risks to the patient. The process may also involve repeating the imaging study due to inconclusive results, or ordering further tests based on initial results.

If an imaging study shows that the patient has a particular disease or condition (e.g., cancer), the physician discusses various treatment options, including surgery, as well as risks of doing nothing or adopting a watchful waiting or active surveillance approach, rather than having surgery.

There are limitations associated with this process, both from the perspective of the physician and from the perspective of the patient. While the radiologist's report is certainly helpful, the physician must ultimately rely on her experience in formulating an assessment and recommendation for her patient. Furthermore, the patient must place a great deal of trust in his physician. The physician may show the patient his PET/SPECT images and may tell the patient a numerical risk associated with various treatment options or likelihood of a particular prognosis, but the patient may very well struggle to make sense of this information. Moreover, the patient's family will likely have questions, particularly if cancer is diagnosed but the patient opts not to have surgery. The patient and/or his family members may search online for supplemental information and may become misinformed about risks of the diagnosed condition. A difficult ordeal may become more traumatic.

Thus, there remains a need for systems and methods for improved analysis of medical imaging studies and communication of those results, diagnoses, prognoses, treatment recommendations, and associated risks to a patient.

SUMMARY OF THE INVENTION

Presented herein are systems and methods that provide for automated analysis of three-dimensional (3D) medical images of a subject in order to automatically identify specific 3D volumes within the 3D images that correspond to specific organs and/or tissue. In certain embodiments, the accurate identification of one or more such volumes are used to automatically determine quantitative metrics that represent uptake of radiopharmaceuticals in particular organs

and/or tissue regions. These uptake metrics can be used to assess disease state in a subject, determine a prognosis for a subject, and/or determine efficacy of a treatment modality.

For example, the systems and methods described herein can be used for automated analysis of medical images in order to determine uptake metrics that provide a quantitative measure of uptake of a radiopharmaceutical such as a radionuclide labelled PSMA binding agent (e.g., ^{99m}Tc-MIP-1404, e.g., [^{18}F]DCFPyL) within a prostate of the subject. Such uptake metrics are of relevance for evaluating patient risk for prostate cancer and/or prostate cancer severity/stage within a subject. For example, it has been found that high sensitivities and specificities can be achieved for the automated classification of clinically significant prostate cancer vs. clinically non-significant prostate cancer.

In certain embodiments, the image analysis approaches described herein utilize a combination of 3D anatomical and functional images obtained for the subject. Anatomical images, such as x-ray computed tomography (CT) images, provide detailed anatomical/structural information. Functional images convey information relating to physiological activities within specific organs and/or tissue, such as metabolism, blood flow, regional chemical composition, and/or absorption. Of particular relevance are nuclear medicine images, such as single photon emission computed tomography (SPECT) and/or positron emission tomography (PET) images, which are acquired by detecting emitted radiation from the subject and which can be used to infer spatial distributions of administered radiopharmaceuticals within the subject.

For example, SPECT imaging can be used to evaluate uptake of the radiopharmaceutical ^{99m}Tc-MIP-1404 (which is 1404 labelled with ^{99m}Tc). In certain embodiments, in order to evaluate ^{99m}Tc-MIP-1404 uptake in a prostate of a subject, a CT image and a corresponding SPECT image are obtained for the subject, such that the anatomical/structural information of the CT image can be correlated with the functional information of the corresponding SPECT image. Often the CT and SPECT images are acquired via two separate scans (e.g., a first scan for the CT image and a second scan for the SPECT image) using a single multimodal imaging system, such that the subject is a substantially fixed position over the duration of the two scans. In this manner, a mapping between voxels of the CT image and those of the SPECT image is established, and volumes identified within the CT image as corresponding to specific organs and/or tissue regions can be used to identify those voxels the SPECT image that correspond to those same specific organs/and or tissue regions.

Accordingly, in certain embodiments, the image analysis approaches described herein utilize convolutional neural networks (CNNs) to accurately identify a prostate volume within the CT image that corresponds to the prostate of the subject. The identified prostate volume can be used to identify those voxels of the SPECT image that also correspond to the subject's prostate. Uptake metrics that provide a measure of uptake of the imaging agent (e.g., a labelled PSMA binding agent, e.g., ^{99m}Tc-MIP-1404 or [^{18}F]DCFPyL) in the prostate can thus be computed using the intensities of SPECT image voxels corresponding to the prostate of the subject. The uptake metrics, then, can be converted to an identification of whether or not the subject has prostate cancer and/or a quantification of risk that the subject has prostate cancer, and/or a staging of the disease (e.g., as part of disease tracking over time), which may be used by the medical practitioner in advising treatment options, and/or monitoring efficacy of administered therapy, for example.

Various advances are described herein that improve the performance of the automated measurement of uptake metrics in the prostate (or, more broadly, a particular organ or tissue region of interest) via this multi-image approach, i.e., analysis of a 3D anatomical image in combination with a 3D functional image. These advances include, for example, the automated identification of a bounding box in the 3D anatomical image (e.g., using a first convolutional neural network, CNN) to identify a pelvic region within which the prostate lies.

For example, a set of 3D anatomical images with identified physiology (e.g., identified pelvic regions) is used to train a first CNN on points representing the boundaries of the pelvic region (e.g., the vertices of a cuboid bounding box) such that the first CNN can be used to automatically identify the pelvic region in a 3D anatomical image of a subject. This provides a more standard-sized initial volumetric region of the 3D anatomical image to be subsequently processed (e.g., via a second CNN) for detailed segmentation of regions of interest within the initial volumetric region—e.g., where the bounding box bounds regions of the image corresponding to the prostate and/or the bladder and/or the rectum, and/or gluteal muscles of the subject. Imaging agent uptake metrics may then be determined from the portions of the 3D functional image that map to one or more of the identified regions of the 3D anatomical image. Note that, as used herein, the 'bounding box' isn't necessarily a cuboid, but may have other shapes. In certain embodiments, the bounding box is a cuboid.

The determination of the bounding box via the first CNN may use, as input, a significantly less dense resolution than is used for segmentation of the prostate and/or other organs within the bounding box by the second CNN. For example, a whole body 3D anatomical image having a first number of voxels (e.g., 81×68×96 voxels) may be processed via the first CNN to find the bounding box, then the second CNN may process an image corresponding to the bounding box region but having a more dense resolution, e.g., many more voxels (e.g., 94×138×253 voxels) than the first number of voxels.

The 'bounding box' approach of identifying one or more portions of a 3D anatomical image that is/are relevant to the analysis at hand, e.g., prior to applying a second CNN (for detailed segmentation), improves computational efficiency by removing a large portion of the initial 3D anatomical image prior to the more computationally intensive subsequent processing. This approach is more computationally efficient than performing the detailed segmentation on the entire initial 3D anatomical image since, for example, identification of the pelvic region (e.g., the vertices of a cuboid bounding box) is simpler than detailed segmentation of a prostate, bladder, and/or other tissues of interest. Not only is this approach more computationally efficient, it also may result in more accurate subsequent processing, e.g., the more detailed segmentation provided by the second CNN. This is because, for example, 3D anatomical images obtained at different medical institutions using different machines vary in size (e.g., where varying size means there are different numbers of voxels of the images, and/or different volumes of the patient tissue represented in the images), and training the second CNN for automated detailed segmentation of the prostate using portions of 3D anatomical training images having a more standardized image volume size, and within

which the organs and other tissue regions of interest lie, results in a more robust, accurate segmentation.

Another advance described herein that improves the performance of the automated measurement of uptake metrics in the prostate (or, more broadly, a particular organ or tissue region of interest) via this multi-image approach (i.e., analysis of a 3D anatomical image in combination with a 3D functional image) is the accurate identification of one or more tissue regions in addition to the prostate, and the accounting for imaging agent uptake in those regions in the determination of (i) uptake metrics in the prostate and/or (ii) an identification and/or staging of prostate cancer. Certain imaging agents comprising a PSMA binding agent have high uptake in certain organs, which may affect the identification of diseased tissue (e.g., prostate cancer). For example, uptake of a radionuclide labelled PSMA binding agent by the bladder may result in scattering in the 3D functional image, and may reduce accuracy of the measured imaging agent intensity in the prostate, which is located near the bladder. By training a second CNN for detailed segmentation of both the prostate and the bladder of a subject, it is possible to accurately, automatically account for a 'bleed through' or 'cross-talk' effect and/or other effects caused by uptake of the imaging agent by the bladder. Furthermore, by training the second CNN for identification of a reference region in the 3D anatomical image, e.g., the gluteal muscles, it is possible to more accurately weight/normalize imaging agent intensity measurements and improve the accuracy and diagnostic value of the uptake measurements in the prostate of the subject.

Thus, in certain embodiments, the systems and methods described herein utilize a unique combination of two CNN modules, wherein a first CNN module identifies an initial volume of interest (VOI) within the CT image and a second receives the VOI as input and identifies the prostate volume therein. As described herein, this approach allows the second CNN module to operate on a smaller input size (e.g., the VOI as opposed to the full CT image). The savings in computational resources (e.g., memory; e.g., processing time) by reducing the input size in this manner can be allocated to improving the accuracy of the second CNN module and/or used to improve the speed of the image processing approach.

In certain embodiments, the systems and methods described herein identify, along with the prostate, various additional tissue volumes within the CT image. For example, additional tissue volumes corresponding to pelvic bones, a bladder, a rectum, and gluteal muscles of the subject may be identified in addition to the prostate. As described herein, the identification of such additional tissue volumes can be used for a variety of functions and confers advantages over other approaches, such as a binary classification approach wherein voxels of the CT image are either identified as corresponding to prostate or not. In particular, identification of additional tissue volumes can, for example, (i) improve the accuracy with which the CNN module identifies the prostate volume within the CT image, (ii) provide for identification of reference regions that can be used to compute normalization values for uptake metric calculation, and (iii) allow for intensities of SPECT image voxels corresponding to prostate to be corrected for cross-talk that results, for example, from the accumulation of radiopharmaceutical within the bladder.

In certain embodiments, the image analysis approaches described herein can be used for analysis of a variety of anatomical and functional images and are not limited CT and SPECT images. For example, positron emission tomography (PET) is another functional imaging modality that provides information about the distribution of radiopharmaceutical within a subject. As with SPECT images, PET images can be used in combination with CT images to determine uptake metrics for various organs and tissue regions of interest. The approaches described herein may also be applied to a variety of organs and/or tissue regions of interest, such as bone, lymph nodes, liver, and lungs.

Accordingly, by providing for rapid and accurate identification of specific organs and tissue regions within medical images, the systems and method described herein provide for accurate and automated determination of uptake metrics that provide quantitative measures of radiopharmaceutical uptake within various organs and tissue regions within a subject. Uptake metrics determined in this automated manner provide valuable tools for assessing disease risk, state, and progression within patients, as well as treatment efficacy.

In one aspect, the invention is directed to a method for automatically processing 3D images to identify 3D volumes within the 3D images that correspond to a prostate of a subject and determining one or more uptake metrics indicative of radiopharmaceutical uptake therein (i.e., in the prostate), the method comprising: (a) receiving, by a processor of a computing device, a 3D anatomical image of the subject obtained using an anatomical imaging modality [e.g., x-ray computed tomography (CT) (e.g., a whole-body CT image; e.g., a partial body CT image); e.g., magnetic resonance imaging (MRI); e.g., 3D ultra-sound], wherein the 3D anatomical image comprises a graphical representation of tissue (e.g., soft-tissue and/or bone) within a subject, at least a portion of which corresponds to a pelvic region of the subject; (b) receiving, by the processor, a 3D functional image of the subject obtained using a functional imaging modality [e.g., single-photon emission computed tomography (SPECT); e.g., positron emission tomography (PET)], wherein the 3D functional image comprises a plurality of voxels, each representing a particular physical volume within the subject and having an intensity value that represents detected radiation emitted from the particular physical volume, wherein at least a portion of the plurality of voxels of the 3D functional image represent physical volumes within the pelvic region of the subject; (c) determining, by the processor, using a first module (e.g., a first machine learning module), an initial volume of interest (VOI) within the 3D anatomical image (e.g., a parallelepiped, e.g., a cuboid), the initial VOI corresponding to tissue within the pelvic region of the subject and excluding tissue outside the pelvic region of the subject (e.g., wherein the VOI excludes more voxels of the 3D anatomical image than it includes; e.g., wherein the VOI includes less than 25% of the voxels of the 3D anatomical image; e.g., wherein a majority of voxels within the VOI represent physical volumes within the pelvic region of the subject); (d) identifying, by the processor, using a second module (e.g., a second machine learning module), a prostate volume within the initial VOI corresponding to the prostate of the subject; and (e) determining, by the processor, (e.g., and displaying) the one or more uptake metrics using the 3D functional image and the prostate volume identified within the initial VOI of the 3D anatomical image [e.g., computing a quantity of radiopharmaceutical in the prostate of the subject based on intensity values of voxels of the 3D functional image that correspond to the prostate volume identified within the initial VOI of the 3D anatomical image; e.g., computing a sum (e.g., a weighted sum), an average, and/or a maximum of intensities of voxels of the 3D functional image representing a physical

volume occupied by the prostate of the subject] [e.g., wherein the one or more uptake metrics comprises a tumor to background ratio (TBR) value and/or wherein the method comprises determining (e.g., and displaying) a prostate cancer classification status of either (i) clinically significant or (ii) clinically non-significant based at least in part on the TBR value].

In certain embodiments, the first module receives the 3D anatomical image as input and outputs a plurality of coordinate values representing opposite corners of a rectangular volume within the 3D anatomical image (e.g., two sets of coordinate values that represent the opposite corners of the rectangular volume).

In certain embodiments, step (c) comprises determining, using the first module, a 3D pelvic bone mask that identifies a volume of the 3D anatomical image corresponding to pelvic bones (e.g., one or more (up to all) of a sacrum, a coccyx, a left hip bone, and a right hip bone) of the subject.

In certain embodiments, the first module is a Convolutional Neural Network (CNN) module (e.g., a Neural Network module that utilizes one or more convolution layers).

In certain embodiments, step (d) comprises using the second module to identify one or more additional tissue volumes within the 3D anatomical image, each volume corresponding to a specific tissue region within the subject, wherein the one or more additional tissue volumes correspond(s) to one or more specific tissue regions selected from the group consisting of: a pelvic bone (e.g., a sacrum; e.g., a coccyx; e.g., a left hip bone; e.g., a right hip bone) of the subject; a bladder of the subject; a rectum of the subject; and a gluteal muscle (e.g., a left gluteal muscle; e.g., a right gluteal muscle) of the subject.

In certain embodiments, step (d) comprises using the second module to classify each voxel within the initial VOI as corresponding a particular tissue region of a set of (predetermined) different tissue regions {e.g., the set comprising the prostate and, optionally, one or more additional tissue regions [e.g., a pelvic bone (e.g., a sacrum; e.g., a coccyx; e.g., a left hip bone; e.g., a right hip bone) of the subject; a bladder of the subject; a rectum of the subject; and a gluteal muscle (e.g., a left gluteal muscle; e.g., a right gluteal muscle]} within the subject. In certain embodiments, classifying each voxel within the initial VOI comprises: determining, via the second module, for each of a plurality of voxels within the initial VOI, a set of likelihood values, wherein the set of likelihood values comprises, for each of one or more tissue regions of the tissue region set, a corresponding likelihood value that represents a likelihood (e.g., as computed by the second module) that the voxel represents a physical volume within the tissue region; and for each of the plurality of voxels within the initial VOI, classifying the voxel as corresponding to the particular tissue region based on the set of likelihood values determined for the voxel. In certain embodiments, the second module receives as input the initial VOI (e.g., the entire initial VOI) and outputs a plurality of values comprising, for each voxel within the initial VOI, at least one of (i), (ii), and (iii) as follows: (i) a value classifying the voxel [e.g., classifying the voxel as corresponding to a specific tissue region, e.g., a region selected from a predetermined set of different tissue regions, e.g., the prostate of the subject; e.g., a pelvic bone (e.g., a sacrum; e.g., a coccyx; e.g., a left hip bone; e.g., a right hip bone) of the subject; a bladder of the subject; a rectum of the subject; and a gluteal muscle (e.g., a left gluteal muscle; e.g., a right gluteal muscle) of the subject]; (ii) a set of likelihood values for the voxel [e.g., a likelihood the voxel corresponds to a specific tissue region, e.g., a region selected from a predetermined set of different tissue regions, e.g., the prostate of the subject; e.g., a pelvic bone (e.g., a sacrum; e.g., a coccyx; e.g., a left hip bone; e.g., a right hip bone) of the subject; a bladder of the subject; a rectum of the subject; and a gluteal muscle (e.g., a left gluteal muscle; e.g., a right gluteal muscle) of the subject]; and (iii) a value identifying the voxel as not corresponding to (e.g., or as likely not corresponding to, or identifying a likelihood the voxel does not correspond to) any of a predetermined set of different tissue regions (e.g., identifying the voxel as corresponding to or as likely corresponding to, or a likelihood the voxel corresponds to, a background area, e.g., that is not of diagnostic interest) (e.g., such that the second module classifies and/or computes likelihood values for the entire VOI in one round, as opposed to operating on each voxel one at a time). In certain embodiments, the (predetermined) set of different tissue regions comprises one or more tissue regions selected from the group consisting of: the prostate of the subject; a pelvic bone (e.g., a sacrum; e.g., a coccyx; e.g., a left hip bone; e.g., a right hip bone) of the subject; a bladder of the subject; a rectum of the subject; and a gluteal muscle (e.g., a left gluteal muscle; e.g., a right gluteal muscle) of the subject.

In certain embodiments, step (d) comprises using the second module to identify a set of one or more base tissue volumes, the one or more base tissue volumes comprising the identified prostate volume and the one or more additional tissue volumes, and wherein the method further comprises: identifying, by the processor, using one or more auxiliary modules (e.g., auxiliary machine learning modules), one or more auxiliary tissue volumes within the 3D anatomical image, each auxiliary tissue volume corresponding [e.g., representing a same specific tissue region [e.g., the prostate of the subject; e.g., a pelvic bone (e.g., a sacrum; e.g., a coccyx; e.g., a left hip bone; e.g., a right hip bone) of the subject; a bladder of the subject; a rectum of the subject; and a gluteal muscle (e.g., a left gluteal muscle; e.g., a right gluteal muscle) of the subject] to a base tissue volume identified by the second module; and merging, by the processor, each auxiliary tissue volume with the corresponding base tissue volume identified by the second module (e.g., adding to the corresponding base tissue volume by incorporating portions of the corresponding auxiliary tissue volume not included in the original base tissue volume).

In certain embodiments, the method comprises: identifying, by the processor, (e.g., using the second module) a reference volume within the 3D anatomical image (e.g., within the initial VOI), the reference volume corresponding to a reference tissue region within the subject (e.g., a gluteal muscle); and at step (e), determining at least one of the one or more uptake metrics using the 3D functional image and the reference volume identified within the 3D anatomical image (e.g., computing a normalization value based on intensity values of voxels of the 3D functional image that correspond to the reference volume identified within the 3D anatomical image). In certain embodiments, the at least one of the one or more uptake metrics determined using the 3D functional image and the reference volume comprises a tumor to background ratio (TBR) value, wherein determining the TBR value comprises: determining a target intensity value using intensity values of one or more voxels of the 3D functional image that correspond to the prostate volume identified within the initial VOI of the 3D anatomical image (e.g., wherein the target intensity value is a maximum of intensities of the voxels of the 3D functional image that correspond to the prostate volume); determining a background intensity value using intensity values of one or more

voxels of the 3D functional image that correspond to the reference volume identified within the 3D anatomical image [e.g., wherein the background intensity value is an average intensity of a plurality (e.g., all) of the voxels of the 3D functional image that correspond to the identified reference volume; and determining, as the TBR value, a ratio of the target intensity value to the background intensity value. In certain embodiments, the method comprises determining a prostate cancer status for the subject based on the TBR value in comparison with one or more threshold values (e.g., predetermined threshold values). In certain embodiments, the one or more threshold values are determined using a plurality of reference TBR values [e.g., each reference TBR value having been determined from a corresponding set of reference images (e.g., a reference 3D anatomical image and a reference 3D functional image; e.g., a CT/SPECT image set)], each reference TBR value associated with a particular classification prostate cancer status (e.g., assigned by a medical practitioner)[e.g., a Gleason grade having been determined (e.g., based on histopathology from a radical prostatectomy) for a same subject for which the reference TBR value was determined]. In certain embodiments, the one or more threshold values are determined using a receiver operating characteristic (ROC) curve [e.g., using area under the curve (AUC) analysis; e.g., to provide a specific sensitivity value and/or a specific specificity value]. In certain embodiments, the method comprises determining the prostate cancer status for the subject to be (i) clinically significant if the TBR value is above a cutoff threshold or (ii) clinically non-significant if the TBR value is below the cutoff threshold.

In certain embodiments, the method comprises identifying, by the processor, (e.g., using the second module) a bladder volume within the 3D anatomical image (e.g., within the initial VOI) corresponding to a bladder of the subject; and at step (e), correcting for cross-talk from the bladder (e.g., scattering and/or partial volume effects through which radiopharmaceutical uptake in the bladder influences intensity values of voxels of the 3D functional image that represent physical volumes within the prostate) using intensities of voxels of the 3D functional image corresponding to the identified bladder volume within the 3D anatomical image [e.g., by adjusting intensities of voxels of the 3D functional image that correspond to the prostate volume based on their proximity to the identified bladder volume and/or a bladder uptake (e.g., determined based on intensities of voxels of the 3D functional image that correspond to the bladder volume); e.g., by using intensities of voxels of the 3D functional image to establish a model of radiation scattering from the bladder and adjusting intensities of voxels of the 3D functional image based on the model]. In certain embodiments, correcting for cross-talk from the bladder comprises: determining one or more bladder intensity bleed functions that model a contribution of intensity originating from radiopharmaceutical within the bladder of the subject to intensity of one or more voxels of the 3D functional image corresponding to one or more regions of the 3D anatomical image that are outside of the identified bladder volume, wherein the one or more bladder intensity bleed functions model said contribution as a function of distance from the identified bladder volume [e.g., wherein each of the one or more bladder intensity bleed functions models intensity bleed along a particular direction and is obtained by fitting a template function (e.g., an n-th degree polynomial) to intensities of voxels of the 3D functional image corresponding to the identified bladder volume within the 3D anatomical image and lying along the particular direction]; and for each of one or more voxels of the 3D functional image corresponding to the identified prostate volume within the 3D anatomical image, adjusting an intensity of the voxel for bladder cross-talk using the one or more bladder intensity bleed functions [e.g., by evaluating the one or more bladder intensity bleed functions to determine a bladder intensity bleed value for the voxel and subtracting the bladder intensity bleed value from the intensity of the voxel to obtain a corrected voxel intensity].

In certain embodiments, the method comprises: identifying, by the processor, (e.g., using the second module) a bladder volume within the 3D anatomical image (e.g., within the initial VOI) corresponding to a bladder of the subject; determining, by the processor, a dilated bladder volume by applying a morphological dilation operation to the identified bladder volume; and at step (e), determining the one or more uptake metrics using intensity values of voxels of the 3D functional image that (i) correspond to the prostate volume identified within the VOI of the 3D anatomical image, but (ii) do not correspond to regions of the 3D anatomical image within the dilated bladder volume (e.g., thereby omitting from the computation of the one or more uptake metrics those voxels of the 3D functional image that correspond to locations in the 3D anatomical image within a predefined distance from the identified bladder volume; e.g., and, accordingly, are excessively close to the identified bladder volume).

In certain embodiments, the 3D functional image is a nuclear medicine image (e.g., a single-photon emission computerized tomography (SPECT) scan; e.g., an positron emission tomography (PET) scan) of the subject following administration to the subject of the radiopharmaceutical. In certain embodiments, the radiopharmaceutical comprises a PSMA binding agent (e.g., ^{99m}Tc-MIP-1404; e.g., [^{18}F] DCFPyL). In certain embodiments, the nuclear medicine image is a single-photon emission computerized tomography (SPECT) scan of the subject obtained following administration to the subject of the radiopharmaceutical. In certain embodiments, the radiopharmaceutical comprises ^{99m}Tc-MP-1404.

In certain embodiments, the method comprises determining, based on at least a portion of the one or more uptake metrics, one or more diagnostic or prognostic values [e.g., a value that provides a measure of disease state, progression, life expectancy (e.g., overall survival), treatment efficacy, and the like for the subject (e.g., Gleason score)] for the subject. In certain embodiments, determining at least one of the one or more diagnostic or prognostic values comprises comparing an uptake metric to one or more threshold value(s). In certain embodiments, at least one of the one or more diagnostic or prognostic values estimates a risk for clinically significant prostate cancer in the subject.

In certain embodiments, the method comprises: (f) causing, by the processor, display of an interactive graphical user interface (GUI) for presentation to the user of a visual representation of the 3D anatomical image and/or the 3D functional image; and (g) causing, by the processor, graphical rendering of, within the GUI, the 3D anatomical image and/or the 3D functional image as selectable and superimposable layers, such that either can be selected for display (e.g., via a corresponding user-selectable graphical control element (e.g., a toggle element)) and rendered separately, or both selected for display and rendered together by overlaying the 3D anatomical image with the 3D functional image. In certain embodiments, step (g) comprises causing graphical rendering of a selectable and superimposable segmentation layer comprising one or more identified specific tissue

volumes within the 3D anatomical image, wherein upon selection of the segmentation layer for display, graphics representing the one or more specific tissue volumes are overlaid on the 3D anatomical image and/or the 3D functional image (e.g., as outlines; e.g., as semi-transparent color-coded volumes). In certain embodiments, the one or more specific tissue volumes comprise(s) the identified prostate volume. In certain embodiments, the method comprises, at step (g), causing rendering of a 2D cross sectional view of the 3D anatomical image and/or the 3D functional image within an interactive 2D viewer, such that a position of the 2D cross sectional view is adjustable by the user. In certain embodiments, the method comprises, at step (g), causing rendering of an interactive (e.g., rotatable; e.g., sliceable) 3D view of the 3D anatomical image and/or the 3D functional image. In certain embodiments, the method comprises causing display of, within the GUI, a graphical element (e.g., a cross-hair, a target, a colored marker, etc.) indicating a location corresponding to a voxel of the identified prostate volume (e.g., said location also corresponding to a voxel of the 3D functional image having a maximal intensity, e.g., a maximal corrected intensity, in comparison with other voxels of the 3D functional image corresponding to the identified prostate volume), thereby facilitating user review and/or quality control of the method (e.g., allowing a medical practitioner to verify the identified location corresponds to an expected physical location of the prostate of the subject). In certain embodiments, the method comprises causing display of, within the GUI, text and/or graphics representing the one or more uptake metrics determined in step (e) (e.g., and, optionally, one or more prognostic values determined therefrom) along with a quality control graphical widget for guiding the user through a quality control and reporting workflow for review and/or updating of the one or more uptake metrics (e.g., wherein the quality control graphical widget comprises a selectable graphical control element for receipt of a user input corresponding to (i) approval of the one or more uptake metrics as determined, automatically, by the processor or (ii) disapproval of the automated determination of the one or more uptake metrics). In certain embodiments, the method comprises: receiving, via the quality control graphical widget, a user input corresponding to an approval of automated determination of the one or more uptake metrics (e.g., and any prognostic values determined therefrom); and responsive to the receipt of the user input corresponding to the approval of the automated determination of the one or more uptake metrics, generating, by the processor, a report for the subject comprising a representation of the one or more automatically determined uptake metrics [e.g., the report comprising: an identification of the subject (e.g., an anonymized patient ID number); a representation (e.g., text) of the one or more determined uptake metrics (e.g., and any prognostic values determined therefrom); and a representation (e.g., graphics and/or text) of the user approval the automated determination of the one or more uptake metrics (e.g., and any prognostic values determined therefrom)].

In certain embodiments, the method comprises: receiving, via the quality control graphical widget, a user input corresponding to disapproval of automated determination of the one or more uptake metrics (e.g., and any prognostic values determined therefrom); responsive to receipt of the user input corresponding to the disapproval of the automated determination of the one or more uptake metrics, causing, by the processor, display of a voxel selection graphical element (e.g., a cursor; e.g., an adjustable cross-hair) for user selection of one or more voxels of the 3D functional image (e.g., directly or indirectly, e.g., through selection of voxels of the 3D anatomical image and subsequent determination of corresponding voxels of the 3D functional image) for use in determining updated values of the one or more uptake metrics; receiving, via the voxel selection graphical element, the user selection of one or more voxels of the 3D functional image for use in determining updated values of the one or more uptake metrics [e.g., wherein the user selection is one or more corrected background intensity measurement location(s) and/or one or more corrected prostate intensity location(s), e.g., where a user overrides automated identification of a location of the prostate and/or where the user overrides automated identification of a location of a background area, e.g., gluteal muscle]; updating, by the processor, values of the one or more uptake metrics using the user selected voxels; and generating, by the processor, a report for the subject comprising a representation (e.g., text) of the one or more updated uptake metrics [e.g., the report comprising: an identification of the subject (e.g., an anonymized patient ID number); a representation (e.g., text) of the one or more determined uptake metrics (e.g., and any prognostic values determined therefrom); and a representation (e.g., graphics and/or text) of the user approval of the determination of the one or more uptake metrics (e.g., and any prognostic values determined therefrom) using the user selected voxels (e.g., text indicating that the uptake metrics were determined via semi-automated analysis, with manual selection of voxels from the user)].

In certain embodiments, the method comprises: receiving, via the quality control graphical widget, a user input corresponding to disapproval of automated determination of the one or more uptake metrics (e.g., and any prognostic values determined therefrom); receiving, via the quality control graphical widget, a user input corresponding to a rejection of quality control (e.g., due to low image quality); and generating, by the processor, a report for the subject, wherein the report comprises an identification of the rejection of quality control.

In certain embodiments, voxels of the 3D functional image are related to voxels of the 3D anatomical image via a known relationship [e.g., each voxel of the 3D functional image is associated with one or more voxels of the 3D anatomical image; e.g., each of a plurality of sets of one or more voxels of the 3D functional image is associated with a set of one or more voxels of the 3D anatomical image; e.g., coordinates associated with voxels of the 3D functional image are related to coordinates associated with voxels of the anatomical 3D image via a known functional relationship (e.g., via a known spatial relationship between the first and second imaging modalities)].

In certain embodiments, the first module is a first CNN (convolutional neural network) module and the second module is a second CNN module, wherein the second CNN module comprises a greater number of convolutional filters than the first CNN module (e.g., at least 1.5 times as many, e.g., at least twice as many, e.g., approximately twice as many, e.g., at least three times as many, e.g., approximately three times as many).

In certain embodiments, the method comprises performing steps (a) and (c) for each of a plurality of 3D anatomical images to determine a plurality of initial VOIs, each within one of the plurality of 3D anatomical images, wherein a variability in sizes of the initial VOIs is less than (e.g., substantially less than) a variability in sizes of the 3D anatomical images (e.g., wherein variability in "sizes" means either or both of (i) and (ii) as follows: (i) variability in one or more dimensions of the anatomical volume rep-

resented in the image, e.g., as measured in mm, and (ii) variability in the number of voxels in the image along each of one or more dimensions of the image) (e.g., wherein the sizes of the 3D anatomical images (each full image from which each VOI is determined) vary by at least 200 mm, and/or by at least 300 mm, and/or by at least 400 mm, and/or by at least 500 mm, and/or by as much as 400 mm, and/or by as much as 500 mm, and/or by as much as 1000 mm, and/or by as much as 1500 mm) along each of one or more dimensions; e.g., wherein the sizes of the 3D anatomical images (each full image from which each VOI is determined) vary by at least 25 voxels, and/or by at least 50 voxels, and/or by at least 100 voxels, and/or by at least 250 voxels, and/or by at least 300 voxels, and/or by as much as 250 voxels, and/or by as much as 300 voxels, and/or by as much as 500 voxels) along each of one or more dimensions; e.g., wherein the sizes of the VOIs vary by less than or equal to 200 mm (e.g., less than or equal to 100 mm; e.g., less than or equal to 50 mm) along each of one or more dimensions; e.g. wherein the sizes of the VOIs vary by less than or equal to 250 voxels (e.g., less than or equal to 200 voxels; e.g., less than or equal to 150 voxels) along each of one or more dimensions].

In another aspect, the invention is directed to a method for automatically processing 3D images to identify 3D volumes within the 3D images that correspond to a target tissue region within a subject and determining one or more uptake metrics indicative of radiopharmaceutical uptake therein, the method comprising: (a) receiving, by a processor of a computing device, a 3D anatomical image of the subject obtained using an anatomical imaging modality [e.g., x-ray computed tomography (CT); e.g., magnetic resonance imaging (MRI); e.g., ultra-sound], wherein the 3D anatomical image comprises a graphical representation of tissue (e.g., soft-tissue and/or bone) within a pelvic region of the subject; (b) receiving, by the processor, a 3D functional image of the subject obtained using a functional imaging modality [e.g., single-photon emission computed tomography (SPECT); e.g., positron emission tomography (PET)], wherein the 3D functional image comprises a plurality of voxels, each representing a particular physical volume within the subject and having an intensity value that represents detected radiation emitted from a the particular physical volume, wherein at least a portion of the plurality of voxels of the 3D functional image represent physical volumes within the pelvic region of the subject; (c) determining, by the processor, using a first module (e.g., a first machine learning module), an initial volume of interest (VOI) within the 3D anatomical image (e.g., a rectangular prism), the initial VOI corresponding to an anatomical sub-region (e.g., a group of related tissue, such as a pelvic region, a chest region, a head and/or neck region, and the like) comprising the target region (e.g., wherein the VOI excludes more voxels of the 3D anatomical image than it includes; e.g., wherein the VOI includes less than 25% of the voxels of the 3D anatomical image; e.g., wherein a majority of voxels within the VOI represent physical volumes within the anatomical sub-region); (d) identifying, by the processor, using a second module (e.g., a second machine learning module), a target volume within the initial VOI corresponding to the target tissue region of the subject; and (e) determining, by the processor, the one or more uptake metrics using the 3D functional image and the target volume identified within the VOI of the 3D anatomical image [e.g., computing a quantity of radiopharmaceutical in the target tissue region of the subject based on intensity values of voxels of the 3D functional image that correspond to the target volume identified within the VOI of the 3D anatomical image; e.g., computing a sum (e.g., a weighted sum), an average, and/or a maximum of intensities of voxels of the 3D functional image representing a physical volume occupied by the target tissue region of the subject].

In certain embodiments, the method has one or more of the features articulated in paragraphs above.

In another aspect, the invention is directed to a method of automatically analyzing a 3D functional image [e.g., a nuclear medicine image (e.g., a SPECT image; e.g., a PET image)] to correct prostate voxel intensities for cross-talk from radiopharmaceutical uptake into a bladder, the method comprising: (a) receiving, by a processor of a computing device, a 3D anatomical image of the subject obtained using an anatomical imaging modality [e.g., x-ray computed tomography (CT); e.g., magnetic resonance imaging (MRI); e.g., 3D ultra-sound], wherein the 3D anatomical image comprises a graphical representation of tissue (e.g., soft-tissue and/or bone) within a subject, at least a portion of which corresponds to a bladder and a prostate of the subject; (b) receiving, by the processor, the 3D functional image of the subject, wherein the 3D functional image comprises a plurality of voxels, each representing a particular physical volume within the subject and having an intensity value that represents detected radiation emitted from a the particular physical volume, wherein at least a portion of the plurality of voxels of the 3D functional image represent physical volumes within the bladder and/or the prostate of the subject; (c) automatically identifying, by the processor, within the 3D anatomical image: (i) a prostate volume corresponding to a prostate of the subject and (ii) a bladder volume corresponding to a bladder of the subject; (d) automatically identifying, by the processor, within the 3D functional image, (i) a plurality of prostate voxels corresponding to the identified prostate volume and (ii) a plurality of bladder voxels corresponding to the identified bladder volume; (e) adjusting, by the processor, one or more measured intensities of the prostate voxels (e.g., one or more cumulative measurements and/or peak measurements and/or mean measurements and/or median measurements of intensity corresponding to the identified prostate volume and/or corresponding to each of, and/or cumulatively of, a plurality of regions of the identified prostate volume) based on one or more measured intensities of the bladder voxels (e.g., one or more cumulative measurements and/or peak measurements and/or mean measurements and/or median measurements of intensity corresponding to the identified bladder volume and/or corresponding to each of, and/or cumulatively of, a plurality of regions of the identified bladder volume); and (f) determining, by the processor, one or more uptake metrics indicative of radiopharmaceutical uptake within the prostate of the subject using the adjusted intensities of the prostate voxels.

In certain embodiments, the method has one or more of the features articulated in the paragraphs above.

In another aspect, the invention is directed to a method of detecting a prostate cancer status, and/or quantifying a prostate cancer risk, of a subject based on automated analysis of a 3D functional image (e.g., a SPECT image) of a portion of the subject, the method comprising: (a) acquiring, following administration to the subject of a radiopharmaceutical comprising a PSMA binding agent, the 3D functional image (e.g., a SPECT image); (b) identifying, by a processor of a computing device, a 3D target volume within the 3D functional image, the 3D target volume corresponding to a prostate of the subject; (c) determining, by the processor, using intensities of voxels of the 3D target volume, a target to background ratio (TBR) value; and (d)

causing, by the processor, graphical rendering of text and/or graphics representing the determined TBR value for display within an interactive graphical user interface (GUI) [e.g., wherein the method comprises determining (e.g., and displaying) a prostate cancer classification status of either (i) clinically significant or (ii) clinically non-significant based at least in part on the TBR value].

In certain embodiments, the method has one or more of the features articulated in the paragraphs above.

In another aspect, the invention is directed to a system for automatically processing 3D images to identify 3D volumes within the 3D images that correspond to a prostate of a subject and determining one or more uptake metrics indicative of radiopharmaceutical uptake therein (i.e., in the prostate), the system comprising: a processor; and a memory (e.g., external to or embedded in the processor) having instructions stored thereon, wherein the instructions, when executed by the processor, cause the processor to: (a) receive a 3D anatomical image of the subject obtained using an anatomical imaging modality [e.g., x-ray computed tomography (CT) (e.g., a whole-body CT image; e.g., a partial body CT image); e.g., magnetic resonance imaging (MRI); e.g., 3D ultra-sound], wherein the 3D anatomical image comprises a graphical representation of tissue (e.g., soft-tissue and/or bone) within a subject, at least a portion of which corresponds to a pelvic region of the subject; (b) receive a 3D functional image of the subject obtained using a functional imaging modality [e.g., single-photon emission computed tomography (SPECT); e.g., positron emission tomography (PET)], wherein the 3D functional image comprises a plurality of voxels, each representing a particular physical volume within the subject and having an intensity value that represents detected radiation emitted from the particular physical volume, wherein at least a portion of the plurality of voxels of the 3D functional image represent physical volumes within the pelvic region of the subject; (c) determine, using a first module (e.g., a first machine learning module), an initial volume of interest (VOI) within the 3D anatomical image (e.g., a parallelepiped, e.g., a cuboid), the initial VOI corresponding to tissue within the pelvic region of the subject and excluding tissue outside the pelvic region of the subject (e.g., wherein the VOI excludes more voxels of the 3D anatomical image than it includes; e.g., wherein the VOI includes less than 25% of the voxels of the 3D anatomical image; e.g., wherein a majority of voxels within the VOI represent physical volumes within the pelvic region of the subject); (d) identify, using a second module (e.g., a second machine learning module), a prostate volume within the initial VOI corresponding to the prostate of the subject; and (e) determine (e.g., and display) the one or more uptake metrics using the 3D functional image and the prostate volume identified within the initial VOI of the 3D anatomical image [e.g., compute a quantity of radiopharmaceutical in the prostate of the subject based on intensity values of voxels of the 3D functional image that correspond to the prostate volume identified within the initial VOI of the 3D anatomical image; e.g., compute a sum (e.g., a weighted sum) and/or an average and/or a maximum of intensities of voxels of the 3D functional image representing a physical volume occupied by the prostate of the subject] [e.g., wherein the one or more uptake metrics comprises a tumor to background ratio (TBR) value, and wherein the instructions, when executed by the processor, cause the processor to determine (e.g., and display) a prostate cancer classification status of either (i) clinically significant or (ii) clinically non-significant based at least in part on the TBR value].

In certain embodiments, the system has one or more of the features articulated in the paragraphs above.

In another aspect, the invention is directed to a system for automatically processing 3D images to identify 3D volumes within the 3D images that correspond to a target tissue region within a subject and determining one or more uptake metrics indicative of radiopharmaceutical uptake therein (i.e., in the target tissue region), the system comprising: a processor; and a memory (e.g., external to or embedded in the processor) having instructions stored thereon, wherein the instructions, when executed by the processor, cause the processor to: (a) receive a 3D anatomical image of the subject obtained using an anatomical imaging modality [e.g., x-ray computed tomography (CT); e.g., magnetic resonance imaging (MRI); e.g., ultra-sound], wherein the 3D anatomical image comprises a graphical representation of tissue (e.g., soft-tissue and/or bone) within a pelvic region of the subject; (b) receive a 3D functional image of the subject obtained using a functional imaging modality [e.g., single-photon emission computed tomography (SPECT); e.g., positron emission tomography (PET)], wherein the 3D functional image comprises a plurality of voxels, each representing a particular physical volume within the subject and having an intensity value that represents detected radiation emitted from a the particular physical volume, wherein at least a portion of the plurality of voxels of the 3D functional image represent physical volumes within the pelvic region of the subject; (c) determine, using a first module (e.g., a first machine learning module), an initial volume of interest (VOI) within the 3D anatomical image (e.g., a rectangular prism), the initial VOI corresponding to an anatomical sub-region (e.g., a group of related tissue, such as a pelvic region, a chest region, a head and/or neck region, and the like) comprising the target region (e.g., wherein the VOI excludes more voxels of the 3D anatomical image than it includes; e.g., wherein the VOI includes less than 25% of the voxels of the 3D anatomical image; e.g., wherein a majority of voxels within the VOI represent physical volumes within the anatomical sub-region); (d) identify, using a second module (e.g., a second machine learning module), a target volume within the initial VOI corresponding to the target tissue region of the subject; and (e) determine the one or more uptake metrics using the 3D functional image and the target volume identified within the VOI of the 3D anatomical image [e.g., compute a quantity of radiopharmaceutical in the target tissue region of the subject based on intensity values of voxels of the 3D functional image that correspond to the target volume identified within the VOI of the 3D anatomical image; e.g., compute a sum (e.g., a weighted sum), and/or an average, and/or a maximum of intensities of voxels of the 3D functional image representing a physical volume occupied by the target tissue region of the subject] [e.g., wherein the one or more uptake metrics comprises a tumor to background ratio (TBR) value, and wherein the instructions, when executed by the processor, cause the processor to determine (e.g., and display) a cancer classification status of either (i) clinically significant or (ii) clinically non-significant based at least in part on the TBR value].

In certain embodiments, the system has one or more of the features articulated in the paragraphs above .

In another aspect, the invention is directed to a system for detecting a prostate cancer status, and/or quantifying a prostate cancer risk, of a subject based on automated analysis of a 3D functional image (e.g., a SPECT image) of a portion of the subject, the system comprising: a processor; and a memory (e.g., external to or embedded in the proces-

sor) having instructions stored thereon, wherein the instructions, when executed by the processor, cause the processor to: (a) receive the 3D functional image (e.g., a SPECT image) of the portion (e.g., any or all) of the subject following administration to the subject of a radiopharmaceutical comprising a PSMA binding agent; (b) identify a 3D target volume within the 3D functional image, the 3D target volume corresponding to a prostate of the subject; (c) determine, using intensities of voxels of the 3D target volume, a target to background ratio (TBR) value; and (d) cause graphical rendering of text and/or graphics representing the determined TBR value for display within an interactive graphical user interface (GUI) [e.g., wherein the instructions, when executed by the processor, cause the processor to determine (e.g., and display) a prostate cancer classification status of either (i) clinically significant or (ii) clinically non-significant based at least in part on the TBR value].

In certain embodiments, the system has one or more of the features articulated in the paragraphs above.

In certain embodiments, the invention is directed to a computer-aided detection (CADe) device comprising any of the systems described herein. In certain embodiments, the instructions cause the processor to identify a classification of either clinically significant prostate cancer or clinically non-significant prostate cancer for the subject.

In certain embodiments, the invention is directed to a computer-aided diagnostic (CADx) device comprising any of the systems described herein. In certain embodiments, the instructions cause the processor to identify a classification of either clinically significant prostate cancer or clinically non-significant prostate cancer for the subject.

In certain embodiments, the invention is directed to a combination product comprising: (a) a radiolabeled PSMA binding agent (e.g., ^{99m}Tc-MIP-1404; e.g., [^{18}F]DCFPyL, e.g., other known PSMA binding agent); and (b) a computer-aided detection (CADe) device comprising any of the systems described herein. In certain embodiments, the combination product comprises a label specifying usage of the radiolabeled PSMA binding agent with the computer aided detection device.

Features of embodiments described with respect to one aspect of the invention may be applied with respect to another aspect of the invention.

BRIEF DESCRIPTION OF THE FIGURES

The patent or application file contains at least one drawing executed in color. Copies of this patent or patent application publication with color drawing(s) will be provided by the Office upon request and payment of the necessary fee.

The foregoing and other objects, aspects, features, and advantages of the present disclosure will become more apparent and better understood by referring to the following description taken in conjunction with the accompanying drawings, in which:

FIG. **1** is a block diagram showing a process for automatically identifying 3D volumes within 3D images that correspond to a prostate of a subject and determining uptake metrics indicative of radiopharmaceutical uptake therein, according to an illustrative embodiment.

FIG. **2**A is an image showing 3D view of a CT image comprising a graphical representation of soft-tissue, according to an illustrative embodiment.

FIG. **2**B is an image showing a 3D view of a CT image comprising a graphical representation of bone, according to an illustrative embodiment.

FIG. **2**C is an image showing a 3D view of a CT image comprising a graphical representation of bone overlaid with a SPECT image and graphics representing an identified tissue volume corresponding to a prostate organ within pelvic bones of a subject, according to an illustrative embodiment.

FIG. **2**D is an image showing 3D view of a CT image comprising a graphical representation of bone overlaid with a SPECT image and graphics representing an identified tissue volume corresponding to a prostate organ within pelvic bones of a subject, according to an illustrative embodiment.

FIG. **2**E is an image showing a 3D view of a CT image comprising a graphical representation of bone overlaid with a SPECT image, according to an illustrative embodiment.

FIG. **3**A is a set of images, each image showing a 2D cross-sectional view of a 3D CT image overlaid with graphics representing an identified initial volume of interest (VOI) within the 3D CT image, according to an illustrative embodiment.

FIG. **3**B is a set images, each image showing a 2D cross-sectional view of a 3D CT image overlaid with graphics representing an identified initial volume of interest (VOI) within the 3D CT image, according to an illustrative embodiment.

FIG. **4**A is a set of images showing 2D cross sectional views of a CT image of a subject and a cuboidal region identified as an initial volume of interest within the CT image, according to an illustrative embodiment.

FIG. **4**B is a set of images showing 2D cross sectional views of a CT image of a subject along with identified tissue volumes corresponding to pelvic bones and a prostate of the subject.

FIG. **5**A is a set of images showing 2D cross sectional views of a CT image of a subject and a cuboidal region identified as an initial volume of interest within the CT image, according to an illustrative embodiment.

FIG. **5**B is a set of images showing 2D cross sectional views of a CT image of a subject along with identified tissue volumes corresponding to pelvic bones and a prostate of the subject.

FIG. **6**A is a set of images showing 2D cross sectional views of a CT image of a subject and a cuboidal region identified as an initial volume of interest within the CT image, according to an illustrative embodiment.

FIG. **6**B is a set of images, each image showing a 2D cross-sectional view of a 3D CT image overlaid with graphics representing an identified initial volume of interest (VOI) within the 3D CT image, according to an illustrative embodiment.

FIG. **6**C is a set of images, each image showing a 2D cross-sectional view of a 3D CT image overlaid with graphics representing an identified initial volume of interest (VOI) within the 3D CT image, according to an illustrative embodiment.

FIGS. **7**A-**7**E present a block diagram of a CNN module architecture (localization network) for identifying a volume of interest (e.g., VOI) corresponding to a pelvic region within a CT image of a subject (wherein the VOI is subsequently processed by a second CNN module for more detailed segmentation/identification of the prostate and/or other tissues within the pelvic region), according to an illustrative embodiment.

FIGS. **7**F-**7**J present a block diagram of a CNN module architecture (segmentation network) for processing the previously-identified VOI for precise segmentation of the pros-

tate and/or other tissues within the pelvic region, according to an illustrative embodiment.

FIG. **8**A is a set images, each showing a 2D cross-sectional view of a 3D CT image overlaid with graphics representing identified tissue volumes corresponding to three different pelvic bones (left and right hip bones and the sacrum), according to an illustrative embodiment.

FIG. **8**B is an image showing a 3D view of a 3D CT image overlaid with graphics representing identified tissue volumes corresponding to three different pelvic bones (left and right hip bones and the sacrum), according to an illustrative embodiment.

FIG. **9**A is an image showing a 2D cross-sectional view of a 3D CT image overlaid with graphics representing identified tissue volumes corresponding to pelvic bones (left and right hip bones) and a prostate of a subject, according to an illustrative embodiment.

FIG. **9**B is a set of images showing different 2D cross sectional views of a 3D CT image overlaid with graphics representing identified tissue volumes corresponding to pelvic bones, gluteal muscles, a rectum, a prostate, and a bladder of a subject, according to an illustrative embodiment.

FIG. **10** is an image showing a 2D cross sectional view of a low quality 3D CT image overlaid with graphics representing identified tissue volumes corresponding to pelvic bones and a prostate of a subject, according to an illustrative embodiment.

FIG. **11** is a schematic showing an example architecture wherein image segmentation for identification of a prostate volume as described herein is performed by a dedicated module, according to an illustrative embodiment.

FIG. **12** is a block flow diagram showing an example architecture of modules for performing CNN-based image segmentation, according to an illustrative embodiment.

FIG. **13** is a block flow diagram showing a structure of a CNN, according to an illustrative embodiment.

FIG. **14** is a block flow diagram showing a structure of a CNN that performs auxiliary predictions, according to an illustrative embodiment.

FIG. **15** is a schematic illustrating cross-talk between a bladder and a prostate of a subject, according to an illustrative embodiment.

FIG. **16**A is a screenshot of a graphical user interface (GUI) for reviewing patient image data showing a window for selecting subjects for whom to analyze and/or review data, according to an illustrative embodiment.

FIG. **16**B is a screenshot of a graphical user interface (GUI) for reviewing patient image data showing a window for selecting subjects for whom to analyze and/or review data, along with a graphical control element for initiating processing of and reviewing patient image data, according to an illustrative embodiment.

FIG. **16**C is a screenshot of a graphical user interface (GUI) for reviewing patient image data showing a window for selecting subjects for whom to analyze and/or review data, along with a graphical control element for initiating processing of and reviewing patient image data, according to an illustrative embodiment.

FIG. **17**A is a screenshot of a GUI for reviewing patient image data showing a window comprising a set of images each showing a different 2D cross sectional view of a CT image of a subject overlaid with a SPECT image of the subject and graphics representing identified tissue volumes, according to an illustrative embodiment.

FIG. **17**B is a screenshot of a GUI for reviewing patient image data showing a window comprising a set of images each showing a different 2D cross sectional view of a CT image of a subject overlaid with a SPECT image of the subject and graphics representing identified tissue volumes, according to an illustrative embodiment.

FIG. **17**C is a screenshot of a GUI for reviewing patient image data showing a window comprising a set of images each showing a different 2D cross sectional view of a CT image of a subject overlaid with a SPECT image of the subject and graphics representing identified tissue volumes, according to an illustrative embodiment.

FIG. **17**D is a screenshot of a GUI for reviewing patient image data showing a window comprising a set of images each showing a different 2D cross sectional view of a CT image of a subject overlaid with a SPECT image of the subject and graphics representing identified tissue volumes, according to an illustrative embodiment.

FIG. **17**E is a screenshot of a GUI for reviewing patient image data showing a window comprising a set of images each showing a different 2D cross sectional view of a CT image of a subject overlaid with a SPECT image of the subject and graphics representing identified tissue volumes, according to an illustrative embodiment.

FIG. **18**A is a screenshot of a GUI for reviewing patient image data showing a window comprising a graphical control element for toggling display of selectable layers illustrating a user toggling of a SPECT image layer off, according to an illustrative embodiment.

FIG. **18**B is a screenshot of a GUI for reviewing patient image data showing a window comprising a set of images each showing a different 2D cross sectional view of a CT image of a subject overlaid with graphics representing identified tissue volumes, according to an illustrative embodiment.

FIG. **18**C is a screenshot of a GUI for reviewing patient image data showing a window comprising a set of images each showing a different 2D cross sectional view of a CT image of a subject overlaid with graphics representing identified tissue volumes, according to an illustrative embodiment.

FIG. **18**D is a screenshot of a GUI for reviewing patient image data showing a window comprising a set of images each showing a different 2D cross sectional view of a CT image of a subject overlaid with graphics representing identified tissue volumes, according to an illustrative embodiment.

FIG. **18**E is a screenshot of a GUI for reviewing patient image data showing a window comprising a set of images each showing a different 2D cross sectional view of a CT image of a subject overlaid with graphics representing identified tissue volumes, according to an illustrative embodiment.

FIG. **18**F is a screenshot of a GUI for reviewing patient image data showing a window comprising a set of images each showing a different 2D cross sectional view of a CT image of a subject overlaid with graphics representing identified tissue volumes, according to an illustrative embodiment.

FIG. **19**A is a screenshot of a GUI for reviewing patient image data showing a window comprising a graphical control element for toggling display of selectable layers illustrating a user toggling of a SPECT image layer and a segmentation layer on and off, respectively, according to an illustrative embodiment.

FIG. **19**B is a screenshot of a GUI for reviewing patient image data showing a window comprising a set of images each showing a different 2D cross sectional view of a CT

image of a subject overlaid with a SPECT image of the subject, according to an illustrative embodiment.

FIG. **19**C is a screenshot of a GUI for reviewing patient image data showing a window comprising a set of images each showing a different 2D cross sectional view of a CT image of a subject overlaid with a SPECT image of the subject, according to an illustrative embodiment.

FIG. **19**D is a screenshot of a GUI for reviewing patient image data showing a window comprising a set of images each showing a different 2D cross sectional view of a CT image of a subject overlaid with a SPECT image of the subject, according to an illustrative embodiment.

FIG. **20**A is a screenshot of a GUI for reviewing patient image data showing a window comprising an image showing a 3D view of a CT image of a subject comprising a graphical representation of soft tissue overlaid with a SPECT image of the subject, according to an illustrative embodiment.

FIG. **20**B is a screenshot of a GUI for reviewing patient image data showing a window comprising an image showing a 3D view of a CT image of a subject comprising a graphical representation of soft tissue overlaid with a SPECT image of the subject, according to an illustrative embodiment.

FIG. **20**C is a screenshot of a GUI for reviewing patient image data showing a window comprising an image showing a 3D view of a CT image of a subject comprising a graphical representation of soft tissue overlaid with a SPECT image of the subject, according to an illustrative embodiment.

FIG. **21**A is a screenshot of a GUI for reviewing patient image data showing a window comprising an image showing a 3D view of a CT image of a subject comprising a graphical representation of bone overlaid with a SPECT image of the subject, according to an illustrative embodiment.

FIG. **21**B is a screenshot of a GUI for reviewing patient image data showing a window comprising an image showing a 3D view of a CT image of a subject comprising a graphical representation of bone overlaid with a SPECT image of the subject, according to an illustrative embodiment.

FIG. **22**A is a screenshot of a GUI for reviewing patient image data showing a window comprising an image showing a 3D view of a CT image of a subject comprising a graphical representation of bone overlaid with a SPECT image of the subject, according to an illustrative embodiment.

FIG. **22**B is a screenshot of a GUI for reviewing patient image data showing a window comprising an image showing a 3D view of a CT image of a subject comprising a graphical representation of bone overlaid with a SPECT image of the subject, according to an illustrative embodiment.

FIG. **22**C is a screenshot of a GUI for reviewing patient image data showing a window comprising an image showing a 3D view of a CT image of a subject comprising a graphical representation of bone overlaid with a SPECT image of the subject and graphics representing identified tissue volumes, according to an illustrative embodiment.

FIG. **22**D is a screenshot of a GUI for reviewing patient image data showing a window comprising an image showing a 3D view of a CT image of a subject comprising a graphical representation of bone overlaid with a SPECT image of the subject and graphics representing identified tissue volumes, according to an illustrative embodiment.

FIG. **22**E is a screenshot of a GUI for reviewing patient image data showing a window comprising an image showing a 3D view of a CT image of a subject comprising a graphical representation of bone overlaid with a SPECT image of the subject and graphics representing identified tissue volumes, according to an illustrative embodiment.

FIG. **22**F is a screenshot of a GUI for reviewing patient image data showing a window comprising an image showing a 3D view of a CT image of a subject comprising a graphical representation of bone overlaid with a SPECT image of the subject and graphics representing identified tissue volumes, according to an illustrative embodiment.

FIG. **23**A is a screenshot of a GUI for reviewing patient image data showing a window comprising an image showing a 3D view of a CT image of a subject comprising a graphical representation of bone overlaid with a SPECT image of the subject, according to an illustrative embodiment.

FIG. **23**B is a screenshot of a GUI for reviewing patient image data showing a window comprising an image showing a 3D view of a CT image of a subject comprising a graphical representation of bone overlaid with a SPECT image of the subject, according to an illustrative embodiment.

FIG. **24** is a screenshot of a GUI for reviewing patient image data showing a window comprising a generated report for a subject, according to an illustrative embodiment.

FIG. **25** is a block flow diagram showing a workflow for user interaction with a GUI in which the user reviews images, segmentation results, and uptake metrics, and generates reports, according to an illustrative embodiment.

FIG. **26**A is a screenshot of a view of a GUI window that allows a user to upload images, according to an illustrative embodiment.

FIG. **26**B is a screenshot of a view of a GUI window showing a listing of images uploaded by a user, according to an illustrative embodiment.

FIG. **27**A is a screenshot of a view of a GUI window showing a listing of patients, according to an illustrative embodiment.

FIG. **27**B is screenshot of a view of a GUI window showing a listing of patients, according to an illustrative embodiment.

FIG. **27**C is a screenshot of a view of a GUI window showing a selected patient and menu providing a user with options for reviewing study data and generating a report, according to an illustrative embodiment.

FIG. **28**A is a screenshot of a GUI for reviewing patient image data showing a window comprising an image showing a 3D view of a CT image of a subject comprising a graphical representation of bone overlaid with a SPECT image of the subject and graphics representing identified tissue volumes, according to an illustrative embodiment.

FIG. **28**B is a screenshot of a GUI for reviewing patient image data showing a window comprising an image showing a 3D view of a CT image of a subject comprising a graphical representation of bone overlaid with a SPECT image of the subject, according to an illustrative embodiment.

FIG. **29**A is a screenshot of a GUI for reviewing patient image data showing a window for reviewing a determined uptake metric, according to an illustrative embodiment.

FIG. **29**B is a screenshot of a GUI for reviewing patient image data showing a quality control graphical widget, according to an illustrative embodiment.

FIG. **29**C is a screenshot of a view of a quality control graphical widget allowing a user to sign a generated report, according to an illustrative embodiment.

FIG. **29**D is a screenshot showing a generated report (e.g., an auto-generated report), according to an illustrative embodiment.

FIG. **29**E is a screenshot of a view of a quality control graphical widget displayed in respond to a user input of disapproval of automated determination of an uptake metric, according to an illustrative embodiment.

FIG. **29**F is a screenshot of a portion of a generate report showing a graphical indication of rejection of quality control, according to an illustrative embodiment.

FIG. **29**G is a screenshot of a quality control graphical widget allowing a user to manually update one or more values used in determination of an uptake metric, according to an illustrative embodiment.

FIG. **29**H is a screenshot of a quality control graphical widget allowing a user to manually update one or more values used in determination of an uptake metric, according to an illustrative embodiment.

FIG. **30** is a block diagram showing a microservice network architecture for performing image segmentation to identify prostate volumes within images, determine uptake metrics, and provide results to a client, according to an illustrative embodiment.

FIG. **31** is a block flow diagram showing dataflow between microservices of a cloud-based application in order to process a study by performing image segmentation and determining uptake metrics, according to an illustrative embodiment.

FIG. **32** is a block flow diagram showing communication between microservices of a cloud-based application and a client, according to an illustrative embodiment.

FIG. **33** is a block diagram of an example architecture for implementing a cloud-based platform comprising a cloud-based application for performing image segmentation and computing uptake metrics in accordance with the systems and methods described herein, according to an illustrative embodiment.

FIG. **34** is a block diagram showing a process for automatically identifying 3D target volumes within 3D images and determining uptake metrics indicative of radiopharmaceutical uptake therein, according to an illustrative embodiment.

FIG. **35**A is a swarm plot of clinically non-significant and clinically significant images.

FIG. **35**B is an ROC curve determined based on varying a TBR threshold computed in accordance with the systems and methods described herein.

FIG. **36** is a block diagram of an exemplary cloud computing environment, used in certain embodiments.

FIG. **37** is a block diagram of an example computing device and an example mobile computing device used in certain embodiments.

The features and advantages of the present disclosure will become more apparent from the detailed description set forth below when taken in conjunction with the drawings, in which like reference characters identify corresponding elements throughout. In the drawings, like reference numbers generally indicate identical, functionally similar, and/or structurally similar elements.

DETAILED DESCRIPTION

It is contemplated that systems, architectures, devices, methods, and processes of the claimed invention encompass variations and adaptations developed using information from the embodiments described herein. Adaptation and/or modification of the systems, architectures, devices, methods, and processes described herein may be performed, as contemplated by this description.

Throughout the description, where articles, devices, systems, and architectures are described as having, including, or comprising specific components, or where processes and methods are described as having, including, or comprising specific steps, it is contemplated that, additionally, there are articles, devices, systems, and architectures of the present invention that consist essentially of, or consist of, the recited components, and that there are processes and methods according to the present invention that consist essentially of, or consist of, the recited processing steps.

It should be understood that the order of steps or order for performing certain action is immaterial so long as the invention remains operable. Moreover, two or more steps or actions may be conducted simultaneously.

The mention herein of any publication, for example, in the Background section, is not an admission that the publication serves as prior art with respect to any of the claims presented herein. The Background section is presented for purposes of clarity and is not meant as a description of prior art with respect to any claim.

Documents are incorporated herein by reference as noted. Where there is any discrepancy in the meaning of a particular term, the meaning provided in the Definition section above is controlling.

Headers are provided for the convenience of the reader—the presence and/or placement of a header is not intended to limit the scope of the subject matter described herein.

As used herein, "radionuclide" refers to a moiety comprising a radioactive isotope of at least one element. Exemplary suitable radionuclides include but are not limited to those described herein. In some embodiments, a radionuclide is one used in positron emission tomography (PET). In some embodiments, a radionuclide is one used in single-photon emission computed tomography (SPECT). In some embodiments, a non-limiting list of radionuclides includes ^{99m}Tc, ^{111}In, ^{64}Cu, ^{67}Ga, ^{68}Ga, ^{186}Re, ^{188}Re, ^{153}Sm, ^{177}Lu, ^{67}Cu, ^{123}I, ^{124}I, ^{125}I, ^{126}I, ^{131}I, ^{11}C, ^{13}N, ^{15}O, ^{18}F, ^{153}Sm, ^{166}Ho, ^{177}Lu, ^{149}Pm, ^{90}Y, ^{213}Bi, ^{103}Pd, ^{109}Pd, ^{159}Gd, ^{140}La, ^{198}Au, ^{199}Au, ^{169}Yb, ^{175}Yb, ^{165}Dy, ^{166}Dy, ^{105}Ru, ^{111}Ag, ^{89}Zr, ^{225}Ac, ^{82}Rb, ^{75}Br, ^{76}Br, ^{77}Br, ^{80}Br, ^{80m}Br, ^{82}Br, ^{83}Br, ^{211}At and ^{192}Ir.

As used herein, the term "radiopharmaceutical" refers to a compound comprising a radionuclide. In certain embodiments, radiopharmaceuticals are used for diagnostic and/or therapeutic purposes. In certain embodiments, radiopharmaceuticals include small molecules that are labeled with one or more radionuclide(s), antibodies that are labeled with one or more radionuclide(s), and antigen-binding portions of antibodies that are labeled with one or more radionuclide(s).

As used herein, "3D" or "three dimensional" with reference to an "image" means conveying information about three dimensions. A 3D image may be rendered as a dataset in three dimensions and/or may be displayed as a set of two-dimensional representations, or as a three-dimensional representation.

As used herein, an "image"—for example, a 3-D image of a subject—includes any visual representation, such as a photo, a video frame, streaming video, as well as any electronic, digital or mathematical analogue of a photo, video frame, or streaming video. Any apparatus described herein, in certain embodiments, includes a display for displaying an image or any other result produced by the

processor. Any method described herein, in certain embodiments, includes a step of displaying an image or any other result produced via the method.

As used herein, a "subject" means a human or other mammal (e.g., rodent (mouse, rat, hamster), pig, cat, dog, horse, primate, rabbit, and the like).

As used herein, "administering" an agent means introducing a substance (e.g., an imaging agent) into a subject. In general, any route of administration may be utilized including, for example, parenteral (e.g., intravenous), oral, topical, subcutaneous, peritoneal, intraarterial, inhalation, vaginal, rectal, nasal, introduction into the cerebrospinal fluid, or instillation into body compartments.

As used herein, the terms "filter", and "filtering", as in a "filtering function" or a "filter", refer to a function that operates on localized portions of an input array (e.g., a multi-dimensional array) of data (e.g., image data, e.g., values computed by a layer of a CNN), referred to herein as "subpatches", computing, for a given subpatch, a response value. In general, a filter is applied in a sliding window fashion across the array to compute a plurality of response values for the array. In particular, for a given multidimensional array, a subpatch of the array can be a rectangular region of the array having a specific size (e.g., having the same number of dimensions as the array). For example, for a 6×3×3 array, a given 3×3×3 subpatch refers to a given 3×3×3 set of adjacent values (e.g., a neighborhood) of the array, such that there are five distinct 3×3×3 subpatches in the 6×3×3 array (each patch shifted one position over along the first dimension).

For example, a filtering function can compute, for a given subpatch of an array, a response value using the values of the subpatch. A filtering function can be applied in a sliding window fashion across an array, computing, for each of a plurality of subpatches of the array, a response value. The computed response values can be stored in an output array such that the positional correspondence between response values and the subpatches of the input array is maintained.

For example, at a first step, beginning with a subpatch in a corner of an input array, a filter can compute a first response value, and store the first response value in a corresponding corner of an output array. In certain embodiments, at a second step, the filter then computes a second response value for a second subpatch, shifted one position over along a specific dimension of the input array. The second response value can be stored in a corresponding position of the output array—that is, shifted one position over along a same dimension of the output array. The step of shifting position of the subpatch, computing a response value, and storing the response value in a corresponding position of the output array can be repeated for the full input array, along each dimension of the input array. In certain embodiments (e.g., a strided filtering approach), the subpatch for which the filter computes a response value is shifted more than one position at a time along a given dimension, such that response values are not computed for every possible subpatch of the input array.

As used herein, the term "convolutional neural network (CNN)" refers to a type of artificial neural network where at least one layer performs one or more filtering functions. As used herein, the term "convolution layer" refers to a layer of a CNN that receives as input an input array and computes an output array, wherein values of the output array are computed by applying one or more filters to the input array. In particular, in certain embodiments, a convolution layer receives as input an input array having n+1 dimensions and produces an output array also having n+1 dimensions. The first n dimensions of input and output arrays operated on by filtering layers of a CNN are referred to herein as "spatial dimensions". The $(n+1)^{th}$ dimension of the input is referred to herein as the "input channel" dimension. The size of the input channel dimension is referred to herein as the "number of input channels". The $(n+1)^{th}$ dimension of the output is referred to herein as the "output channel" dimension. The size of the input channel dimension is referred to herein as the "number of output channels".

In certain embodiments, a convolution layer computes response values by applying a filter that operates on subpatches that are smaller than the input array along the spatial dimensions, but extend across the full output channel dimension. For example, an $N \times M \times L \times K_0$ size input array, has three spatial dimensions and K_0 output channels. Filters of a convolution layer may operate on subpatches having sizes of $N_f \times M_f \times L_f \times K_0$, where $N_f \leq N$, $M_f \leq M$ and $L_f \leq L$. Often, a filter of a convolutional layer operates on subpatches having sizes where $N_f < N$, $M_f < M$ and/or $L_f < L$. For example, in certain embodiments, $N_f << N$, $M_f << M$ and/or $L_f << L$.

Accordingly, for each of one or more filters applied by a convolution layer, response values computed by a given filter are stored in a corresponding output channel. Accordingly, a convolution layer that receives an input array having n+1 dimensions computes an output array also having n+1 dimensions, wherein the $(n+1)^{th}$ dimension represents the output channels corresponding to the one or more filters applied by the convolution layer. In this manner, an output array computed by a given convolution layer can be received as input by a subsequent convolution layer.

As used herein, the term "size" in reference to a filter of a convolution layer refers to a size along spatial dimensions of subpatches on which the filter operates (e.g., the subpatch size along the output channel dimension is taken as the full number of output channels). As used herein, the term "size", in reference to a convolution layer, as in "size of a convolution layer" refers to a size of filters of the convolution layer (e.g., each filter of the convolution layer having a same size). In certain embodiments, a filter of a convolution layer has a number of variable parameters that are determined via a machine learning training process. In certain embodiments, the number of parameters of a given filter equals the number of values in a subpatch that the given filter operates on. For example, a size $N_f \times M_f \times L_f$ filter that operates on an input array with K_0 output channels has $N_f \times M_f \times L_f \times K_0$ parameters. In certain embodiments, a filter is implemented as an array, and the response value determined by the filter for a given subpatch is computed as a dot product between the filter and the given subpatch.

As used herein, the term "fully convolutional neural network (FCNN)" refers to a CNN wherein each layer of the CNN is a convolution layer.

As used herein, the term "volume", as used in reference to an input or output of a layer of a CNN refers to an input array received or an output array computed by a CNN layer.

As used herein, the term "CNN module" refers to a computer implemented process that implements a specific CNN in order to determine, for a given input, such as an image (e.g., a 2D image; e.g., a 3D image) one or more output values. For example, a CNN module may receive as input a 3D image of a subject (e.g., a CT image; e.g., an MRI), and for each voxel of the image, determine a value that represents a likelihood that the voxel lies within a region of the 3D image that corresponds to a representation of a particular organ or tissue of the subject. A CNN module may be software and/or hardware. For example, a CNN module may be implemented entirely as software, or certain func-

tions of a CNN module may be carried out via specialized hardware (e.g., via an application specific integrated circuit (ASIC)).

As used herein, the term "tissue" refers to bone (osseous tissue) as well as soft-tissue.

The systems and methods described herein provide for automated analysis of medical images of a subject in order to automatically identify regions of interest that correspond to particular organs and/or tissue that are represented in the images. In certain embodiments, convolutional neural network (CNN) modules are employed in order to accurately segment images. In certain embodiments, the accurate automated identification of particular organs and/or tissue in images of a subject allows for quantitative metrics that measure uptake of radiopharmaceuticals (e.g., radiolabeled small molecules; e.g., radiolabeled antibodies; e.g., radiolabeled antigen-binding portions of antibodies) in particular organs to be determined.

In certain embodiments, the systems and methods described herein facilitate automated identification of regions of interest that correspond to particular organs or tissue in which tumors and/or tumor metastases may be present. Radionuclide labelled molecules that selectively bind to specific tumor cell surface proteins may be utilized in combination with the approaches described herein for imaging tumors. For example, the molecule 1404 binds specifically to Prostate Specific Membrane Antigen (PSMA), which is over expressed on many cancer cells. The molecule 1404 may be labelled with a radionuclide, such as ^{99m}Tc, for use in single-photon emission computed tomography (SPECT) imaging.

In certain embodiments, uptake metrics of radiopharmaceuticals are relevant to assessing disease state and prognosis in a subject.

A. Identifying Prostate Volumes and Determining Uptake Metrics

FIG. **1** shows a process **100** for automatically processing 3D images to identify 3D volumes that correspond to a prostate of a subject and determining one or more uptake metrics indicative of radiopharmaceutical uptake therein.

Referring to Steps **102** and **104** of Process **100** in FIG. **1**:

The various panels of FIG. **2** illustrate CT images (FIG. **2**A and FIG. **2**B) showing bone and soft-tissue, and highlight the pelvic bones (green **202** and blue **206** in FIGS. **2**C and **2**D) and prostate (purple **204** in FIGS. **2**C and **2**D). The highlighted regions are automatically generated by the systems and methods described herein, and identify the pelvic bones and prostate. FIG. **2**E shows a SPECT image (the bright pink and purple regions **252**, **254**, and **256**) overlaid on a CT image. As can be seen, the CT image provides detailed anatomical information, while the anatomical/structural information in the SPECT image is more limited. Accordingly, it is possible to segment the CT image, and use a mapping between voxels of the CT image and those of the SPECT image to identify particular voxels of the SPECT image that correspond to tissue volumes of interest, such as the prostate, bladder, rectum, and gluteal muscle, for example.

Referring to Steps **106** and **108** of Process **100** in FIG. **1**:

The approach of identifying the prostate volume within the CT image first uses a first machine learning module (e.g., a CNN module) to identify an initial volume of interest within the CT image. This produces a standardized input to a second machine learning module (e.g., a second CNN module) that is responsible for identifying the prostate volume. The second CNN module may also identify other tissue volumes, such as pelvic bones, gluteal muscles, rectum, and bladder. The first and second machine learning modules may be combined and implemented as a single module and/or a single software application. The first and second machine learning modules may also be implemented separately, e.g., as separate software applications.

i. Bounding Box Generation (Localization Machine)

FIGS. **3**-**5** present examples of the processing of various CT images showing, first, the identification of the initial volume of interest (VOI) (panels A) and, second, the segmentation of the prostate and pelvic bones (the prostate volume is represented by the blue-green volume in the middle). As shown in these examples, the initial CT image size can substantially depending on the imaging system used, the imaging protocol followed by the radiologist, and other factors, but the initial VOI size is fairly standard.

For example, initial 3D anatomical images may range in size from as large as 700 mm×700 mm×1870 mm (depth×width×height) (i.e. a full body scan), or even larger, to as small as 180 mm×240 mm×290 mm (covering the pelvic bone), or even smaller. In the examples described herein, the smallest tested matrix size of an initial 3D anatomical image is 256×256×76 pixels. The bounding boxes (e.g., identified by the first CNN) for the examples described herein have approximate size ranges of 180-220 mm×240-320 mm×290-380 mm. Matrix sizes of the bounding boxes for the example described herein are in the range of 80-220×150-390×50-300 pixels.

In the example, 3D anatomical images for training the first CNN to detect pelvic region bounding boxes had the following image dimensions:

Training Images (3D Anatomical Images):
#rows: 247-512 (sp 1.37), size (mm): 340-700
#columns: 319-512 (sp 1.37), size (mm): 430-700
#slices: 274-624 (sp 3.0), size (mm): 820-1870

In the example, 3D anatomical images for validating the first CNN for detection of bounding boxes had the following image dimensions, with the resulting range in dimensions of bounding boxes identified by the first CNN:

Validation Images (3D Anatomical Images):
#rows: 256-512, size (mm): 500-600
#columns: 256-512, size (mm): 500-600
#slices: 76-427, size (mm): 380-1070
Bounding Boxes:
#rows: 82-222, size (mm): 180-220
#columns: 148-386, size (mm): 240-320
#slices: 50-295, size (mm): 290-380

The following are three example approaches for automatically generating a bounding box (cuboid) for the pelvic region from an initial 3D anatomical image, for use in subsequent processing for detailed identification of the prostate.

In a first approach, the first CNN receives as input the grayscale CT image (a single input channel) and outputs coordinates of the opposite corners of the bounding box.

In a second approach, the grayscale CT image is processed via thresholding to produce a thresholded image with a rough identification of the pelvic region. In this second approach, the first CNN receives two input channels—one being the grayscale CT image and the other being the thresholded image. The second CNN outputs coordinates of opposite corners of the bounding box.

In a third approach, the first CNN is essentially a rough version of the second CNN—that is, the first CNN identifies a prostate, pelvic bones, and a sacrum (and background). The bounding box is generated using the identified pelvic

bones (e.g., by drawing the smallest box that fits the pelvic bones, or maybe adding some buffer distance). A distinction here is that the output of the first CNN is not merely coordinates of cuboid vertices. In this approach, likelihood values are automatically determined for each voxel of the image that give the likelihood as to how the voxel is classified—e.g., whether the voxel is prostate, left/right pelvic bone, sacrum, or background, for example.

In one illustrative embodiment of this third approach, the localization and segmentation networks are very similar. The localization network segments left and right pelvic bones, sacrum and the background (4 classes in all) in very downsampled images. Based on this rough segmentation of the pelvic bones, a bounding box is created. The segmentation network then segments the pelvic bones, the prostate, and the background within this bounding box and at higher resolution. The localization CNN and the segmentation CNN have identical architectures. The differences are in what input shape they require, where the localization network resize images to size (81, 68, 96) and the segmentation CNN resize pelvic images (as output from the localization network) to size (94, 138, 253). Also, the number of convolutional filters differs. The segmentation network has 20 convolutional filters in the first layer whereas the localization network only has 8. The size and number of filters of subsequent layers are scaled, as is shown in the flow charts herein. To create the bounding box after the localization network, the method finds the corners of the first segmentation and draws a square around it with a margin. The input images to the localization network are small because they have been downsampled to a lower resolution, whereas the segmentation process a cropped version of the CT image in the original resolution.

The FIG. **6**A shows an example of approach 1. FIG. **6**B and FIG. **6**C show a comparison between approach 1 and approach 3.

FIGS. **7**A-E show an example architecture **700** of the first CNN network described herein. The CNN module architecture (localization network) is used for identifying a volume of interest (e.g., VOI) corresponding to a pelvic region within a CT image of a subject (wherein the VOI is subsequently processed by a second machine learning module (e.g., a second CNN module) for more detailed segmentation/identification of the prostate and/or other tissues within the pelvic region).

ii. Prostate Volume and Additional Tissue Volume Determination (Single Segmentation Machine)

FIGS. **7**F-J show an example architecture **750** of the second CNN network described herein. As noted above, the second CNN operates on the VOI to identify a prostate volume, as well as various additional tissue volumes. Additional tissue volumes can include left/right pelvic bones, a sacrum, a bladder, gluteal muscles, and a rectum. Identifying multiple tissue volumes, as opposed to performing a binary classification (e.g., where voxels are simply identified as prostate or background) improves the accuracy of the classification approach.

FIG. **8**A shows left and right pelvic bones (blue, **806** and yellow, **802**) and the sacrum (red, **804**) in 2D, and FIG. **8**B shows the same in 3D.

FIG. **9**A shows left and right pelvic bones (red, **902** and yellow, **906**) and a prostate (blue, **904**).

FIG. **9**B shows segmentation of left and right pelvic bones (two lighter green regions, **952** and **956**), prostate (dark green, **958**), bladder (greenish beige, **960**), a rectum (brown, **962**), and gluteal muscles (blue, **964** and red, **966**).

FIG. **10** shows a low quality CT image, where segmentation still worked.

iii. Segmentation Module Architecture

Data Input and Output

FIG. **11** shows an example architecture **1100** in which image segmentation as described herein is performed by a Segmentation Service module **1104** that receives requests to process images (e.g., perform segmentation as described herein) from a client facing module, Pioneer Web **1102**.

The particular example architecture **1100** shown in FIG. **11** is used in an embodiment of the image segmentation and analysis systems and methods described herein, in particular a cloud-based software application, referred to as Pioneer. Pioneer is a software device to assist in the assessment and characterization of prostate cancer in the prostate gland using MIP-1404 SPECT/CT image data. The software uses artificial intelligence to automatically segment the image data into distinct anatomical regions and then analyzes the volumetric regions of interest (ROI). Pioneer extracts quantitative data from ROIs to assist in determining the presence or absence of clinically significant prostate cancer.

The architecture and module organization shown in FIG. **11**, as well as other architectures and module organizations described herein with respect to Pioneer, may be adapted for use with other imaging modalities and/or other radiopharmaceuticals. For example, a variety of radiopharmaceuticals suitable for use with SPECT imaging are described herein, in section M "Imaging Agents" below. Various 3D functional imaging modalities may also be used for imaging radiopharmaceutical uptake in a subject, and combined with a 3D anatomical imaging modality, such as, but not limited to CT imaging, and analyzed via adapted versions of the approached described herein with respect to Pioneer. For example, various nuclear medicine imaging modalities, such as PET imaging may be used to image radiopharmaceutical uptake. Like SPECT imaging, PET imaging may be performed in combination with CT imaging to obtain an image set comprising a PET image and a CT image—a CT/PET image. Accordingly, the approaches described herein with respect to Pioneer, and CT/SPECT images may also be adapted for use with CT/PET images. Various radiopharmaceuticals suitable for use with PET imaging are also described in section M "Imaging Agents", below.

Turning again to FIG. **11**, as shown in FIG. **11**, Pioneer is implemented as a cloud based service using Amazon Web Services, in which Simple Notification Service (SNS) and Simple Queue Service (SQS) messaging is used to handle requests. The Segmentation Service **1104** listens for requests on a dedicated SQS queue. Events that occur in Pioneer Web **1102** are published to a dedicated SNS topic "Pioneer Events" **1106**. To allow for parallel asynchronous processing, a fanout pattern may be used, such that SNS messages are sent to a topic and then replicated and pushed to multiple Amazon SQS queues **1108***a*, **1108***b*, of which the Segmentation Service is a consumer.

The Segmentation Service **1104** may download input data (e.g., image data) from source Uniform Resource Locators (URLs) provided by the requester (e.g., Pioneer Web **1102**) and that link to datasets in a local filesystem. In certain embodiments, the input data comprises a pre-processed 3D anatomical image, such as a CT image and a 3D functional image, such as a SPECT scan. Image metadata may also be included, along with the 3D anatomical and functional images.

In certain embodiments, CT and SPECT images have resolutions meeting particular requirements, established for the system. For example, CT images with resolutions rang-

ing from 1.0 to 2.2 mm in x and y directions and between 1.0 and 5.0 mm in a z (slice) direction may be used. In certain embodiments, SPECT images with resolutions ranging from 2.9 to 4.8 mm in all directions are used.

Once Segmentation Service **1104** has performed image segmentation to identify a prostate volume and any additional tissue volumes in a particular CT image, as described herein, Segmentation Service **1104** provides segmentation output data that identifies the prostate volume within the particular CT image for storage and/or further processing (e.g., display in a GUI; e.g., computation of uptake metrics). In certain embodiments, a request issued to the Segmentation Service **1104** includes a target URL that specifies a storage location for the segmentation output data. Accordingly, the Segmentation Service **1104** may upload segmentation output data to the target URL included in the request.

The segmentation output data may include data such as a segmentation mask set, that identifies each voxel of the 3D anatomical image (e.g., CT image) as corresponding to a particular tissue region or as background, as determined by the second machine learning module described herein. The segmentation mask set may include, or be used to determine, for each particular tissue region, a corresponding segmentation mask that identifies voxels of the CT image classified as belonging to that particular tissue region. For example, a segmentation mask set may be stored in a .tiled.png format, with voxels labelled with different numerical labels identifying different particular tissue regions or background. An example set of labels for various tissue regions is shown below, with voxels identified as background labeled with 0:

```
{'prostate': 1,
'gluteus_maximus_left': 2,
'gluteus_maximus_right': 3,
'rectum': 4,
'urinary_bladder': 5,
'sacrum_and_coccyx': 6,
'hip_bone_left': 7,
'hip_bone_right': 8
}
```

In certain embodiments, the segmentation mask set identifies a prostate volume and a reference volume (e.g., a left gluteal muscle) and labels all other voxels as background.

In certain embodiments, segmentation mask metadata is also included in the segmentation output data. Segmentation mask metadata may be used to store information about the particular image(s) processed, such as a number of voxels in each direction (e.g., a number of rows, columns, and slices) and their spacing.

In certain embodiments, the Segmentation Service **1104** also performs quantification using results of the segmentation, such as identified prostate and reference volumes, and intensities of voxels of the 3D functional image (e.g., SPECT image). This quantification is discussed in more detail herein, for example, in the subsection below entitled, "Uptake metrics". For example, for use in computing a target to background ratio (TBR) value for the subject, as described herein, the Segmentation Service **1104** may identify a prostate maximum intensity voxel, along with a background value. The prostate maximum intensity voxel is a voxel identified as having a maximum intensity within a set of voxels of the 3D functional image corresponding to the identified prostate volume. In certain embodiments, as described herein, voxels of the 3D functional image corresponding to the identified prostate volume are corrected for cross-talk (also referred to as bleed) from a bladder of the subject, and the prostate maximum intensity voxel is identified following correction for bladder cross-talk. The background value used for determination of the TBR value is an average over intensities of a plurality of voxels of the 3D functional image that correspond to a reference volume, such as a volume corresponding to a left gluteal muscle of the subject, within the 3D anatomical image. As described herein, typically all voxels corresponding to the identified reference volume are used to compute the background value.

Data corresponding to the quantification performed by the Segmentation Service **1104** may be included in the segmentation output data. For example, quantification results may be included in a quantification result dictionary, as shown in the .json format example below:

```
{
"prostate_max": 988.0,
"prostate_max_pos": {
"z": 92,
"y": 74,
"x": 67
},
"background": 9.056859205776174,
}
```

Keys of the quantification result dictionary in the above example are as follows: "prostate_max" stores an intensity of the prostate maximum intensity voxel; "prostate_max_pos" stores a location of the prostate maximum intensity voxel in the SPECT image; and "background" stores the background value.

Example Segmentation Service Architecture Including CNN Module Organization and Interaction

FIG. **12** shows an example architecture **1200** of modules for performing the CNN-based image segmentation as described herein. The example architecture **1200** includes a first machine learning module (referred in FIG. **12** as "Localization Machine") **1204** for identifying an initial VOI, and a second machine learning module (referred to as "SingleSegMachine (base)" in FIG. **12**, short for "base Single Segmentation Machine") **1208** for identifying a prostate volume, additional tissue volumes, and a reference volume as described herein. Inputs and outputs of the first and second machine learning modules are also shown, along with several additional modules, including auxiliary machine learning modules (referred to as SingleSegMachine (aux) in FIG. **12**, short for "auxiliary Single Segmentation Machine") **1212** and a module **1214** for merging outputs of the second machine learning module (base Single Segmentation Machine) and any auxiliary machine learning modules (auxiliary Single Segmentation Machines) and performing postprocessing. Outputs generated by the module organization shown in FIG. **12** include a segmentation mask set **1216** that identifies various tissue volumes in a 3D anatomical image (e.g., a CT image) and segmentation metadata **1218**.

As described herein, the first machine learning module **1204** receives as input a CT image **1202** and produces a bounding box that identifies an initial VOI corresponding to a pelvic region of the subject. The second machine learning module **1208** receives, as input, the initial VOI along with the CT image **1202**. The second machine learning module **1208** may add a crop margin to the initial VOI (e.g., add a margin about the initial bounding box to expand the bounding box) and provide the crop endpoints to auxiliary machine learning modules. As described herein, the second machine learning module **1208** identifies a prostate volume within the initial VOI. The second machine learning module

1208 may also identify additional tissue volumes corresponding to additional tissue regions within the subject, such as a left gluteal muscle, a bladder, and left and right hip bones. A tissue volume corresponding to a left gluteal muscle of the subject may be used as a reference volume, for example to compute a background value in determining a TBR value for the subject, as described herein. A tissue volume corresponding to a bladder of the subject may be used for correcting intensity values of voxels of a SPECT image for bladder cross-talk, for example as described herein, in section B "Correcting for Bladder Intensity Bleed Through". Identified tissue volumes corresponding to a left and right hip bone of the subject may be used for postprocessing.

In certain embodiments, as described herein, performance may be improved by using, in addition to the second machine learning module **1208**, one or more auxiliary machine learning modules **1212** that perform image segmentation in a similar fashion to the second machine learning module, identifying a prostate volume and additional tissue volumes (e.g., as shown in FIGS. **12**, **1208** and **1212**). These auxiliary tissue volumes, identified by the auxiliary machine learning modules, may be merged, via module **1214**, with the base tissue volumes (the prostate volume and any additional tissue volumes) identified using the second machine learning module **1208**.

In certain embodiments, the first and second machine learning modules, and any auxiliary machine learning modules, are implemented as trained CNN modules. Each trained CNN module may be represented (e.g., via computer code) as a directory that comprises an associated trained neural network with model structure and weights. Neural network libraries, such as Keras, can be used to represent trained CNN modules in this manner. The dictionary representing a particular CNN module may also include metadata that describes any preprocessing to be performed on an image before it is fed as input to the particular CNN module. Metadata describing how the neural network model was built and trained may also be included.

Accordingly, a particular CNN module may perform steps such as (1) loading and preprocessing an image, given an image file name and image metadata; (2) feeding the preprocessed image through the associated trained neural network (e.g., as included in the directory representing the particular CNN module) to obtain a raw prediction output (e.g., a map that includes, for each of one or more voxels of the CT image, a likelihood (e.g., probability) that that voxel belongs to a particular category as determined by a trained neural network); and (3) postprocess the raw prediction output. As described herein, the first machine learning module **1204** may postprocess the raw prediction output produced by its associated trained neural network to determine crop endpoints of a bounding box corresponding to an initial VOL The second machine learning module **1208** may postprocess the raw prediction output produced by its associated trained neural network to determine a segmentation mask set that labels voxels of the CT image with values (e.g., numerical values) that indicate a particular tissue volume to which they correspond or identify the voxels as background, as determined by the second machine learning module.

An example model structure of a CNN module implementation of the first machine learning module (Localization Machine in FIG. **12**) **1204** is shown in FIG. **13**. An example model structure of a CNN module implementation of the second machine learning module (Single Segmentation Machine in FIG. **12**) **1208** is shown in FIG. **14**.

Example first machine learning module (Localization Machine) Implementation

As described herein, the first machine learning module identifies an initial VOI—e.g., a "bounding box" that identifies a region of the CT image that corresponds to a pelvic region of the subject, which includes pelvic bones of the subject, along with tissue regions such as a prostate, a bladder, a rectum, and left and right gluteal muscles. An identification of the bounding box (e.g., crop endpoints) is provided to the second machine learning module, as well as any auxiliary machine learning modules, allowing them to limit their processing to a small, specific, target region of the CT image as opposed to having to operate on and process the entire CT image. This reduces the amount of data processed by these machine learning modules, which perform computationally intensive fine segmentation, thereby improving their performance and efficiency.

In an example implementation of the first machine learning module in accordance with approach 3 as described herein, Localization Machine **1204** in FIG. **12** extracts a bounding box (to identify the initial VOI) from a coarse segmentation of a CT image performed by its associated trained neural network (a CNN), referred to as a Localization CNN.

In certain embodiments, the CT image is preprocessed to prepare it for segmentation by the Localization CNN. A configuration file may be used to specify the preprocessing steps and parameters. The preprocessing may include steps such as cropping the CT image to remove one or more regions that correspond to surrounding air, normalizing intensities of voxels in the CT image, and resizing the CT image (e.g., to produce a resized CT image that conforms to a fixed input size expected by the Localization CNN). The intensity normalization preprocessing step adjusts intensities of voxels of the CT image to produce a particular mean and standard deviation of intensities over all voxels of the CT image. For example, voxel intensities of the CT image may be normalized by subtracting a first fixed value and then dividing by a second fixed value, to produce a CT image in which a mean intensity over all voxels is specific mean value (e.g., 0) and a standard deviation of intensities over all voxels is a specific standard deviation value (e.g., 1). The resizing step may be performed by sampling the CT image.

The Localization CNN receives the preprocessed CT image as input and passes it through a series of layers as shown in FIG. **13**. The output of the Localization CNN is a coarse segmentation, e.g., represented via a first segmentation mask set, that classifies voxels of the preprocessed CT image as belonging to one of four categories, three representing particular tissue regions: (i) a sacrum and coccyx, (ii) a left hip bone, (iii) a right hip bone, and a fourth category, (iv) background (e.g., everything else). This coarse segmentation is obtained from a raw prediction map generated by the Localization CNN. The raw prediction map has a same shape—that is a same set of voxels as the preprocessed CT image received as input, but with four channels. Each channel corresponds to a particular classification category—(i) sacrum and coccyx, (ii) left hip bone, (iii) right hip bone, and (iv) background. Each channel represents a probability map for the classification category to which it corresponds. That is, each particular channel corresponding to a particular classification category includes, for each voxel of the preprocessed CT image, a likelihood value representing probability that the voxel belongs to that particular category (e.g., represents a physical volume inside the tissue region that the category represents, or represents

background). Accordingly, for each voxel, a sum over the likelihood values for that voxel in each channel is 1.

To determine the first segmentation mask set that classifies each voxel as belonging to a particular category, each voxel of the preprocessed CT image is assigned to the category (e.g., tissue region or background) having a largest likelihood value (e.g., probability) for that voxel. The determined first segmentation mask set has a same shape as the preprocessed CT image, and labels each voxel with a value identifying the category that it is classified as belonging to. For example, a particular voxel may be labeled with a numerical value, such as 1, 2, or 3 corresponding to categories (i), (ii), and (iii) as described above, or a value 0 zero if it is classified as a background voxel.

A bounding box that identifies an initial VOI may be determined from the first segmentation mask set as a smallest box (e.g., rectangular volume) that comprises all voxels labeled as belonging to categories (i)-(iii). Coordinates identifying the bounding box (e.g., coordinates of opposite corners of a rectangular volume corresponding to the bounding box) are determined and output as crop endpoints. In certain embodiments, wherein the preprocessed CT image input to the Localization CNN is a resized version of the original CT image, the coordinates identifying the bounding box are transformed to a coordinate system of the original CT image and output as crop endpoints.

Example Second Machine Learning Module (Segmentation Machine) Implementation

In the example architecture of FIG. **12**, a second machine learning module, also referred to as a base Single Segmentation Machine **1208** (SingleSegMachine (base) in FIG. **12**) performs a high-resolution segmentation of a CT image to identify a prostate volume corresponding to a prostate of the subject, along with additional tissue volumes corresponding to specific tissue regions, such as left and right gluteal muscles, a rectum, a bladder, a sacrum and coccyx, and left and right hip bones.

In certain embodiments, the CT image is preprocessed to prepare it for segmentation by the second machine learning module. As with Localization Machine **1204**, a configuration file may be used to specify preprocessing steps and parameters. Preprocessing steps may include normalizing intensities of the CT image, similar to the approach described above with respect to Localization Machine **1204**. The CT image may also be cropped using the crop endpoints that identify the initial VOI (bounding box) and are output by the Localization Machine **1204**, to produce a reduced, fixed size preprocessed CT image input for providing as input to a trained neural network (a trained CNN) associated with and implemented in Single Segmentation Machine **1208**. Preprocessing may also include a resizing step.

Similar to the Localization CNN of the Localization Machine, the Single Segmentation Machine implements a trained CNN, referred to as a Segmentation CNN, that receives as input the preprocessed CT image. The Segmentation CNN passes the preprocessed CT image through a series of layers, and outputs a second raw prediction map. Similar to the raw prediction map produced by the Localization CNN, the second raw prediction map includes multiple channels, each corresponding to a different particular category into which each voxel of the input CT image is to be classified. Each channel represents a probability map for the classification category to which it corresponds and includes, for each voxel of the preprocessed CT image, a likelihood value corresponding to a probability (as determined by the Segmentation CNN) that the voxel belongs to that category.

As described above, the second raw prediction map output by the Segmentation CNN comprises a channel corresponding to a prostate of the subject. The second raw prediction map may include other channels, corresponding to various additional tissue regions, such as a left gluteal muscle, a right gluteal muscle, a rectum, a urinary bladder, a sacrum and coccyx, a left hip bone, and a right hip bone. The second raw prediction map may also include a background channel.

Certain variants of high-resolution segmentation CNN's give predictions from multiple levels of the network, resulting in multiple probability maps per category. These multiple probability maps are referred to as auxiliary predictions. The CNN model structure shown in FIG. **13** corresponds to a model structure that does not produce auxiliary predictions, and the CNN model structure shown in FIG. **14** is for a model that produces auxiliary predictions. In certain embodiments, while a number of filters in a top layer (e.g., **20** filters in FIGS. **13** and **28** filters in FIG. **14**) may vary, a number of filters in subsequent, lower layers doubles each layer down. In certain embodiments, the Segmentation CNN produces a single probability map, and does not produce any auxiliary predictions. In certain embodiments, the Segmentation CNN produces auxiliary predictions.

In certain embodiments, when the Segmentation CNN produces auxiliary prediction map, likelihood values for each category as included in the second raw prediction map and each auxiliary probability map are averaged together, such that for a particular voxel, a single likelihood value for each category is determined.

In certain embodiments, to determine a second, fine segmentation mask set that classifies each voxel as belonging to a particular category, each voxel of the preprocessed CT image is assigned to the highest probability value. In certain embodiments, a number of labels in the fine segmentation mask set is reduced, such that only certain tissue volumes, such as a prostate volume and a reference volume (e.g., a left gluteal muscle volume) are included in the fine segmentation mask set.

Auxiliary Single Segmentation Machines

In certain embodiments, one or more auxiliary machine learning modules are used to produce auxiliary fine segmentation mask sets, similar to the fine segmentation mask set generated by the second machine learning module. These auxiliary fine segmentation mask sets identify a same set of tissue volumes as the fine segmentation mask set generated by the second machine learning module. In this manner, the second machine learning module generates a base fine segmentation mask set, and the one or more auxiliary machine learning modules each generate an auxiliary fine segmentation mask set, thereby providing a parallel set of classifications for voxels of the CT image.

In certain embodiments, for each category representing a particular tissue region, a corresponding base fine segmentation mask (e.g., that identifies a volume in the CT image determined via the base Single Segmentation Machine as corresponding to the particular tissue region) of or determined using the base fine segmentation mask set and one or more corresponding auxiliary fine segmentation masks (e.g., each identifying a volume of the CT image determined via an auxiliary Single Segmentation Machine as corresponding to the same particular tissue region) are merged, to produce a merged fine segmentation mask. For example, for a particular category, certain voxels in the one or more auxiliary fine segmentation masks may be identified (e.g., labeled) as belonging to the particular category, but not

belong to a set of voxels in the base fine segmentation mask that are identified as belonging to the particular category. These voxels may be added (e.g., by labeling them as such) to the set of voxels identified as belonging to the particular category in the base fine segmentation mask to produce the final merged fine segmentation mask. For example, in the architecture shown in FIG. **12**, base Single Segmentation Machine **1208** produces a base fine segmentation mask and one or more auxiliary Single Segmentation Machine(s) **1212** each produces an auxiliary segmentation mask. The base fine segmentation mask produced by base Single Segmentation Machine **1208** is merged with the one or more auxiliary fine segmentation masks produced by the auxiliary Single Segmentation Machine(s) **1212** by module **1214** to produce a final fine segmentation mask set **1216** comprising a final fine segmentation mask for each category.

In certain embodiments, one or more of the final fine segmentation masks are filtered such that only a largest connected part is retained. In certain embodiments, when filtering to retain only a largest connected component of a prostate segmentation mask (e.g., a final fine segmentation mask that identifies a volume of the CT image corresponding to a prostate of the subject) is performed, a subset of connected components of the prostate segmentation mask is considered. The subset comprises only components that (i) have a center of mass lying in between the hip bones' centers of mass in a left-right direction of an axial plane (x direction) and (ii) lie within a bounding box defined so that the left and right hip bones are just contained.

iv. Uptake Metrics

Referring to step **110** of process **100** in FIG. **1**, one or more uptake metrics are determined, from which diagnosis or staging of a condition (e.g., prostate cancer) may be informed or automatically rendered. The one or more uptake metrics are determined using the 3D functional image and the prostate volume identified within the VOI of the 3D anatomical image. For example, a quantity of radiopharmaceutical in the prostate of the subject may be computed based on intensity values of voxels of the 3D functional image that correspond to the prostate volume identified within the VOI of the 3D anatomical image. This may involve computing a sum (e.g., a weighted sum), an average, and/or a maximum of intensities of voxels of the 3D functional image representing a physical volume occupied by the prostate of the subject. In certain embodiments, this involves computing a normalization value based on intensity values of voxels of the 3D functional image that correspond to a reference volume identified within the 3D anatomical image. For example, the normalization value for intensities identified in the prostate may be normalized using intensity values of one or more voxels that correspond to the gluteal muscles, or another reference volume within the VOI (or, in certain embodiments, elsewhere within the 3D anatomical image). The uptake metrics, then, can be converted to an identification of whether or not the subject has prostate cancer and/or a quantification of risk that the subject has prostate cancer, and/or a staging of the disease (e.g., as part of disease tracking over time), which may be used by the medical practitioner in advising treatment options, and/or monitoring efficacy of administered therapy, for example.

Target to Background Ratio

In certain embodiments, one or more uptake metrics determined include(s) a target to background ratio (TBR) value for the subject. Determining the TBR value comprises determining (i) a target intensity value using intensity values of one or more voxels of the 3D functional image (e.g., PET or SPECT image) that correspond to the prostate volume identified within the initial VOI of the 3D anatomical image (e.g., CT image), and (ii) determining a background intensity value using intensity values of one or more voxels of the 3D functional image that correspond to an identified reference volume. The TBR value is computed as a ratio of the target intensity value to the background intensity value.

In particular, in certain embodiments, the target intensity value is a maximum of intensities of the voxels of the 3D functional image (e.g., PET or SPECT image) that correspond to the identified prostate volume. As described above, a prostate maximum intensity voxel corresponding to a voxel identified as having a maximum intensity within a set of voxels of the 3D functional image corresponding to the identified prostate volume. The target value may then be taken as the intensity of the prostate maximum intensity voxel. The background intensity value may be computed as an average over intensities of a plurality of voxels of the 3D functional image that correspond to the identified reference volume. As described herein, a gluteal muscle, such as a left gluteal muscle, or a portion thereof, may be used as the identified reference volume.

For example, TBR values may be computed from a SPECT/CT image for a subject recorded following administration of a radiopharmaceutical such as 1404 to the subject. The SPECT image corresponds to the 3D functional image and the CT image corresponds to the anatomical image. The image segmentation approaches described herein may be used to identify, within the CT image, a prostate volume along with a reference volume corresponding to a left gluteal muscle of the subject. A prostate segmentation mask and a left gluteal muscle segmentation mask may be used to identify the prostate volume and the left gluteal reference volume, respectively.

The prostate volume segmentation mask identifies voxels of the CT image that are classified as belonging to a prostate of the subject via the machine learning segmentation approaches described herein. In certain embodiments, in order to identify voxels of the SPECT image that correspond to the identified prostate volume within the CT image, voxels of the prostate segmentation mask are mapped to corresponding voxels of the SPECT image. Since the prostate segmentation mask identifies voxels in the CT image, it may have a different resolution from the SPECT image (e.g., since the SPECT and CT images may have different resolutions). Interpolation (e.g., bilinear interpolation) and/or sampling may be used to match a resolution of the prostate segmentation mask to the resolution of the SPECT image, such that each voxel of the prostate segmentation mask maps to a particular corresponding voxel of the SPECT image. In this manner, a SPECT prostate mask that identifies voxels in the SPECT image that correspond to the prostate volume identified within the CT image is obtained. A SPECT left gluteal muscle mask that identifies those voxels in the SPECT image that correspond to the identified left gluteal muscle reference volume in the CT image may be obtained in a similar fashion.

The SPECT left gluteal muscle mask may be used to determine the background intensity value. In particular, intensities of voxels in the SPECT image identified by the SPECT left gluteal muscle mask are extracted and partitioned into quartiles. The background value is computed as a mean over the extracted left gluteal muscle voxel intensities that fall within a first and third quartile. Other approaches for computing a background value, such as computing an overall mean or a median over all extracted left gluteal muscle voxel intensities, may also be used. The above described approach of partitioning the extracted left

gluteal muscle voxel intensities into quartiles, was found to be more stable against outliers than computing an overall mean and more precise than a median (e.g., since the intensities are discretized and many of them have a same value). The determined background intensity value may be output and stored in a result dictionary, e.g., under a key 'background'.

The target intensity value may be computed using the SPECT prostate mask. A prostate maximum intensity voxel may be identified as a voxel of the SPECT prostate mask and having a maximal SPECT image intensity. The target intensity value is determined as the intensity of the prostate maximum intensity voxel. Both the target value intensity value and a location of the prostate maximum intensity voxel may be stored. For example, a result dictionary may store the target intensity value and the prostate maximum intensity voxel location under keys such as "prostate_max" and "prostate_max_position", respectively. In certain embodiments, intensities of voxels of the SPECT image corresponding to the identified prostate volume are corrected for bladder "cross-talk" or "bleed" as described in section B below, prior to determining the target intensity value, such that, for example, the maximum intensity stored is a maximum corrected intensity and the prostate maximum intensity voxel is a voxel of the SPECT prostate mask having a maximum corrected intensity.

In certain embodiments, a prostate cancer status for a subject may be determined by comparing a determined TBR value for the subject with one or more threshold values. In particular, a determined TBR value may be compared with a particular threshold value (e.g., a cutoff threshold) to distinguish between patients who have clinically significant prostate cancer (e.g., assigned a status of clinically significant) from those who do not (e.g., assigned a status of clinically non-significant). Example 4 below shows an example approach for determining a TBR threshold value based on TBR values computed from reference images, in order to obtain a desired sensitivity and specificity.

B. Correcting for Bladder Intensity Bleed Through

FIG. **15**. is a schematic illustrating cross-talk of imaging agent intensity from a bladder to a prostate of a subject. In the figure, reference **1502** is a bladder, **1506** is the cross-talk/intensity that bleeds from the bladder, and **1504** is the prostate. Certain imaging agents comprising a PSMA binding agent have high uptake in the bladder, which may affect the identification of diseased tissue (e.g., prostate cancer). For example, uptake of a radionuclide labelled PSMA binding agent by the bladder may result in scattering in the 3D functional image, and may reduce accuracy of the measured imaging agent intensity in the prostate, which is located near the bladder. By training a second CNN for detailed segmentation of both the prostate and the bladder of a subject, it is possible to accurately, automatically account for a 'bleed through' or 'cross-talk' effect and/or other effects caused by uptake of the imaging agent by the bladder. Furthermore, by training the second CNN for identification of a reference region in the 3D anatomical image, e.g., the gluteal muscles, it is possible to more accurately weight/normalize imaging agent intensity measurements and improve the accuracy and diagnostic value of the uptake measurements in the prostate of the subject.

i. Bladder Dilation

In certain embodiments, bladder cross-talk correction includes a step wherein an identified bladder volume is dilated (e.g., via morphological dilation) with two iterations. This dilation may be used to prohibit high intensities very close to the segmented urinary bladder to be used for determination of a target intensity value in computing a TBR value (e.g., selected as a maximal intensity), and also to stabilize a bladder suppression approach described below.

ii. Bladder Suppression Computation

In certain embodiments, a bladder suppression method is used to remove intensity bleed from the bladder to other regions of the functional image. An amount of suppression, that is, intensity bleed to remove from a particular voxel of the functional image is dependent on a distance from that voxel to a core bladder region, corresponding to a region of the bladder having high intensity voxels.

In certain embodiments, bladder suppression is made if a maximum functional image intensity within a volume of the functional image identified as corresponding to a bladder (e.g., corresponding to a bladder volume identified within a 3D anatomical image; e.g. as identified via a urinary bladder mask) is more than a specific multiplier value times a determined background intensity value. As described herein, a background intensity value may be determined based on intensities of voxels of the 3D functional image corresponding to a reference volume identified within the 3D anatomical image, for example a gluteal muscle volume. For example, bladder suppression may be performed if a maximum functional image intensity within a region corresponding to the identified bladder volume is 15 times a determined background value (e.g., the bladder-to-background ratio should be at least 15).

In certain embodiments, bladder suppression is computed from and applied to a portion of the 3D functional image that lies within a bladder suppression bounding box of a specific size about the identified bladder volume. For example, a bladder suppression bounding box that contains the urinary bladder with a margin of a predetermined size in a particular direction (e.g., 40 mm in the vertical direction) and is a same number of voxels in the other directions may be determined.

For example, after masking out a region of the 3D functional image corresponding the prostate, the core bladder region may be determined as a region of the 3D functional image within the bladder suppression bounding box comprising voxels having intensities within a specific fraction of a maximum intensity within the bounding box (e.g., not including voxels of the masked out prostate region). For example, the core bladder region may be determined as the region comprising voxels having intensities greater than or equal to 50% of the maximum intensity within the bladder suppression bounding box. The core bladder region may include high-intensity regions that were not included in the original bladder mask.

In certain embodiments, one or more bladder intensity bleed functions are determined to perform bladder suppression and thereby correct intensities of voxels of the 3D functional image for bladder cross-talk. For example, the 3D functional image may be cropped using the bladder suppression bounding box and a determined background intensity value subtracted from intensities of voxels within the cropped image region. Sample intensities are then collected to determine how bladder intensity (e.g., intensity originating from radiopharmaceutical uptake within a bladder of the subject) decreases as one moves away from the bladder. The samples are collected starting at an extreme top, an extreme front, an extreme right and an extreme left of the core bladder region and then moving straight up, forward, right or left respectively, one voxel at a time. If an edge of the cropped image region is encountered, extrapolated intensi-

ties may be used as samples, for example linear extrapolation from a previous two or more samples.

The intensity samples provide four curves of intensity (e.g., sets of sampled intensity data points) decrease from the bladder core, to each of which a template function may be fit to establish four bladder intensity bleed functions that model bladder intensity variation as a function of distance from the core bladder region. Before further analysis, such as fitting, outlier removal may be performed, for example to remove the curve farthest away from the others. A template function such as an n-th degree polynomial (e.g., a 5th degree polynomial) is fitted to the data points in the remaining three curves, resulting in a function modelling the bladder intensity bleed as a function of the distance to the core bladder. This bladder intensity bleed function describes how much should be subtracted from the original intensities to obtain corrected intensities, depending on the distance to the core bladder region.

In certain embodiments, to decrease a risk that the bladder intensity bleed function underestimates bleed in the direction of the bladder (the bleed might vary to some extent between different directions), before fitting to the sampled intensity data points, the distances are multiplied with an expansion factor (e.g., ranging from 1 to 2; e.g., 1.2), so that the fit bladder intensity bleed function is stretched out. Risk of underestimating bladder intensity bleed may also be reduced by multiplying the sampled intensity data points by a scaling factor. The scaling factor may be variable scaling factor having a value that depends on the bladder-to-background intensity ratio. For example, a scaling factor that has a particular value when the bladder to background ratio is sufficiently high and increases (e.g., linearly) with lower bladder-to-background ratios may be used. For example, the sample intensities may be multiplied with a factor that is 1.2 when the bladder-to background ratio is sufficiently high and for lower bladder-to-background ratios increases linearly from 0 for a bladder-to-background ratio of 15. This approach of multiplying the sampled intensity data points with a scaling factor also improves robustness of the bladder suppression approach.

In certain embodiments, a reach of bladder suppression, that is, a farthest distance from the bladder where it is applied, is based on where the decay rate of the function is sufficiently small. If the decay rate never gets sufficiently small then the distance is chosen as a length of the intensity sample vectors. In certain embodiments, it is ensured that bladder suppression at all distances is non-negative.

Once determined, the bladder intensity bleed function may be evaluated at locations of various voxels of the 3D functional image, for example at voxel locations corresponding to locations within the prostate of the subject, to determine a bladder intensity bleed value for each particular voxel location. Accordingly, an intensity of a particular voxel may be corrected for bladder cross-talk by subtracting, from the intensity of the particular voxel, a determined bladder intensity bleed value at a location of the particular voxel. Intensities of voxels at various locations within the 3D functional image, for example at locations corresponding to an identified prostate volume (e.g., identified within a 3D anatomical image), may be corrected for bladder cross-talk in this manner.

iii. Corrected Prostate Maximal Intensity and Location

In certain embodiments, the bladder suppression approach described herein is used to correct intensity values of voxels of the 3D functional image that correspond a prostate volume identified within the 3D anatomical image, and uptake metrics, such as a TBR value, are determined using the corrected intensity values.

C. Visualizing Image Data and Computed Uptake Metrics

FIG. **16**A shows a window of the GUI interface with two subjects (patients) listed. The user can select a desired subject to process and view their image data.

FIG. **16**B shows an exemplary GUI with graphical control elements for processing and navigating subject data, which appears after the user selected the subject "John Doe". The user clicks a selectable button element to complete processing of image data for the selected subject.

In FIG. **16**C, after processing of the selected subject's image data is complete, the user clicks another selectable button to view the processed image data and computed uptake metrics.

In FIGS. **17**A-**17**E a 2D viewer is displayed. FIGS. **17**A-**17**E show a set of 2D cross-sectional views of CT image data overlaid with the SPECT image as well as graphics representing identified tissue volumes—specifically, a prostate and pelvic bones. The user can scan through the cross sectional slices as shown in the figures.

The CT image and SPECT image are rendered as selectable layers which can be toggled on and off. The graphics representing identified tissue volumes are also rendered as a selectable segmentation layer. In FIG. **18**A the user toggles display of the SPECT image layer off, such that only the CT image and segmentation layers are displayed. In FIGS. **18**B-**18**F the user scans through the cross sections.

In FIG. **19**A the user toggles display of the SPECT image layer on, and the segmentation layer off. FIGS. **19**B-**19**D show the user scanning through the cross-sectional views again, this time with only the CT image and the SPECT image layers displayed.

FIGS. **20**A-**20**C show a rotatable and sliceable 3D viewer for viewing the CT image along with overlaid with SPECT image data, wherein the CT image comprises a graphical representation of soft-tissue.

FIGS. **21**A-**21**B also show the rotatable and sliceable 3D viewer, this time with only a graphical representation of bone in the CT image displayed.

FIGS. **22**A-**22**F show how a user can use the 3D viewer to inspect the image data and automated identification of the prostate and other additional tissue regions. The user slices down to focus on the pelvic region in FIG. **22**B and turns on the segmentation layer to display graphics representing the identified prostate volume and pelvic bone volumes overlaid on the CT image as colorized regions. The user can slice and rotate the image to view the bright spots of the SPECT image intensity in the prostate region (purple volume).

FIGS. **23**A and **23**B show the viewer, but with a black background to improve contrast and mimic a radiologist scan.

FIG. **24** shows a report (e.g., an auto-generated report) with various uptake metrics.

D. User Interface, Quality Control, and Reporting

In certain embodiments, the systems and methods described herein are implemented as part of a GUI-based workflow that allows a user, such as a medical practitioner (e.g., a radiologist, a technician) to upload images of patients (subjects), initiate an automated analysis in accordance with the approaches described herein, in which a prostate volume is identified in a 3D anatomical image and used to determine

uptake metrics using corresponding voxels of a 3D functional image. The user may then view results of the automated analysis, including the determined uptake metrics and any prognostic values determined therefrom. The user may be guided through a quality control workflow, in which they choose to approve or disapprove the results of the automated analysis, and, if the results are approved, generate a report for the patient. The quality control workflow may also allow the user to manually adjust and update the results of the automated analysis, for example via an interaction with the GUI, and generate a report based on the manually updated results.

FIG. **25** shows an example workflow **2500**, used in certain embodiments for analysis of SPECT/CT images. As shown in FIG. **25**, the user may upload 2504 SPECT/CT images that conform to a specific accepted standard format **2502**, specifically the DICOM standard in the example of FIG. **25**. FIG. **26**A shows an example GUI window **2600***a* of a web-based portal that allows a user to upload 2504 images. FIG. **26**B shows an updated view **2600***b* of the GUI window shown in FIG. **26**A, in which several images have been selected for upload, and checked for conformance with the DICOM standard. One image is identified as not conforming to the DICOM standard, and indicated as failed to upload **2602***b*.

Returning to FIG. **25**, in another step **2506**, the user may view a list of patients for which images have been uploaded. FIG. **27**A shows a view **2700***a* of a GUI window listing patients via anonymized numerical identifiers. FIG. **27**B shows another view **2700***b* of the GUI window shown in FIG. **27**A, in which a row of the patient list corresponding to a specific patient is highlighted for selection. FIG. **27**C shows another view **2700***c* of the GUI, wherein upon selection of the row corresponding to the specific patient, a menu listing studies performed for the specific patient is displayed, including selectable buttons that allow the user to review image data for the study and generate a report.

In certain embodiments, the user review of the image data, along with any automated analysis results performed using the image data, is a prerequisite for generating a report. The user review of image data and automated analysis may be required to validate accuracy of image segmentation. For example, as shown in FIG. **25**, following viewing of the patient list **2506** and selection of a patient, in a next step **2508**, the user reviews the image data for the patient and results of automated processing as described herein.

In particular, in the review step **2508** of the workflow **2500** shown in FIG. **25**, a user examines SPECT/CT image data for the selected patient using a GUI based viewer. The user may select to view and examine the SPECT/CT image data as a set of 2D slices or as a 3D rendering. FIG. **28**A shows a view of the GUI viewer **2800** in which the SPECT/CT image data is displayed as a set of 2D slices **2802***a*. FIG. **28**B shows a view of the GUI based viewer **2800** in which the SPECT/CT image data is displayed as a 3D rendering **2802***b*.

As shown in FIG. **28**A and FIG. **28**B, GUI viewer **2800** displays the SPECT image and the CT image as selectable layers, overlaid on each other. The user may select one layer at a time, to view the SPECT and/or CT image alone, or may select both a CT layer and a SPECT layer to view the SPECT image overlaid on the CT image. The user may adjust an opacity of the SPECT image, e.g., to emphasize or deemphasize the SPECT image features overlaid on the CT image. The user may also view a segmentation layer that shows locations of various tissue regions identified via the second machine learning module within the CT image, as described herein. In this manner, the user may, for example, validate the image segmentation performed by the second machine learning module via visual inspection of the CT image layer and the segmentation layer.

The user may also view and validate the one or more uptake metrics determined via the automated image analysis approaches described herein. For example, FIG. **29**A shows a GUI view **2900** in which a panel **2902** of the GUI displays an automatically determined TBR value **2904** for the patient. The panel also displays a determined TBR based classification **2906**, indicating that the TBR value is associated with clinically significant prostate cancer.

In certain embodiments, in order to aid in the user validation of the determined uptake metrics, a graphical element is displayed within the GUI to indicate a location of a voxel of the identified prostate volume. For example, as described herein, when a TBR value is computed as a ratio of a target intensity value to a background intensity value, a maximal intensity of voxels in the SPECT image corresponding to the identified prostate volume is identified. Accordingly, the GUI may display a graphical element that indicates a location of a voxel of the SPECT image corresponding to the identified prostate volume and having a maximal intensity in comparison with other voxels of the SPECT image that correspond to the identified prostate volume. In this manner, a position of a maximum SPECT intensity voxel corresponding to a location within the prostate volume is displayed to the user. The user may then visually verify, for example by inspection of the relation of the graphical element in comparison with the CT image, that this maximum SPECT intensity voxel indeed lies within the prostate of the subject. For example, as shown in FIG. **29**A, a set of cross-hair graphical elements **2950**, **2952**, and **2954** identifying a location of the maximum SPECT intensity voxel are overlaid on the 2D slices shown in the image viewer.

Returning to FIG. **25**, in another step **2510**, the user may choose to generate a report summarizing analysis performed for the patient using the uploaded SPECT/CT images, and be guided through a quality control workflow. For example, as shown in FIG. **29**A, the user may select (e.g., click) a create report button **2908** of the GUI. Upon the user selection of the create report button **2908**, a quality control graphical widget **2910** is displayed as shown in FIG. **29**B. The quality control graphical widget **2910** may guide a user to check if various acceptance criteria are met. For example, the quality control graphical widget **2910** guides a user to check that image requirements are met, and that a target value and background value, as used in determining a TBR value, are correct. The user may approve the automated analysis results, via selection of button **2912**, or may disapprove the automated analysis results, via selection of button **2914**.

As shown in FIG. **25**, following user approval of the quality control check **2512**, the automated assessment results **2514** are used to generate a report **2532** for the patient. As shown in FIG. **29**C, prior to generation a report, the user may be presented with a widget **2916** requesting their confirmation of approval of the quality control. FIG. **29**D shows an example report **2900***d*. The report may include an identification of the quality control criteria **2918**, along with an identification of the user that approved the quality control and signed the report **2920**.

As shown in FIG. **25**, if the user disapproves **2516** the automated determination of the uptake metric (e.g., TBR), the quality control widget may begin a guided assessment **2518** workflow. In the guided assessment workflow, the user may manually update values used in determining the one or

more uptake metrics via a manual interaction with the GUI. The user may also provide an input that indicates that the images for the patient cannot be used for accurately determining uptake metrics may also be received via the quality control widget. For example, following a user input corresponding to disapproval of the quality control, a GUI element such as that shown in FIG. **29**E may be presented to the user. The GUI element **2900***e* shown in FIG. **29**E allows the user to select whether no TBR value can be determined for the patient, via selection of button **2922**, or whether they would like to manually update the target and background intensity values used for the TBR value calculation, via selection of button **2924**.

For example, if the user determines (e.g., via visual inspection of the images) that the images are of too poor quality to use for accurate determination of a TBR value, the user may select button **2922** in GUI element **2900***e* to identify the case as unevaluable. As shown in FIG. **25**, follow receipt of the user identification of the case as unevaluable **2520**, the case is marked as unevaluable **2530**, and a report **2532** is produced that identifies quality control as rejected. FIG. **29**F shows an example of graphics and text **2900***f* that may be included in such a report to identify the quality control as rejected.

In certain embodiments, the user may elect to update the target and/or background intensity values used for determining the TBR value via a manual interaction with the GUI. Once a user input indicating that they wish to update the target and/or background intensity values is received **2522**, they are guided to manually set a target value **2524** and/or a background value **2526**. FIG. **29**G shows a view **2900***g* of a manual input graphical widget displayed to the user to allow them to set a target and/or background value. The user may click on button **2926** to manually set the target intensity value via interaction with the GUI. Upon selection of button **2926**, the user is presented with a voxel selection graphical element that allows them to select a voxel of the SPECT image to use as the maximum intensity voxel in computing the TBR value. For example, the user may be provided with a movable cross-hair that allows them to locate positions in the SPECT and CT images, such as the cross-hairs shown in FIG. **29**A. The user may move the cross-hairs and/or click on locations within the viewer to select a particular voxel to use as the maximum intensity voxel. As shown in FIG. **29**H, an updated view **2900***h* of the manual input graphical widget may show an intensity value **2930** of the selected maximum intensity voxel that will be used as an updated target intensity value for computing an updated TBR value.

The user may also select button **2928** to set a background value to use in computing the TBR value. Upon selection of button **2928**, the user may be presented with a voxel selection element and guided to select multiple voxels that they identify (e.g., based on visual inspection of the CT image layer and/or segmentation layer displayed in the GUI viewer) as belonging to the left gluteal muscle. Since the background intensity value for computing TBR is an average over intensities of multiple voxels of the SPECT image corresponding to physical locations within the left gluteal muscle, the user may be guided to select a sufficient number of voxels to ensure an accurate background intensity value is determined. For example, as shown in the view **2900***h* of the manual input graphical widget shown in FIG. **29**H, when the user is selecting voxels to use in determining an update background intensity value, a number of samples may be displayed along with the updated value of the background intensity **2932**. In certain embodiments, the user is required to select at least a predefined number of samples (e.g., 100), and the displayed background intensity value and number of samples **2932** includes a visual indication (e.g., color change) to let the user know once a sufficient number of samples has been selected.

Returning to FIG. **25**, once the user has completed manual input of an updated target value and/or an updated background intensity value, an updated TBR value is computed using the updated values and stored as a semi-automatic assessment **2528**. A report **2532** may then be generate using the semi-automatic assessment results.

E. Example Cloud-Based Architecture and Service Organization

In certain embodiments, the systems and methods described herein are implemented as a cloud-based application. The cloud-based application may use multiple modules to implement various functionalities, such as a client facing module that provides an interface for receiving input from a user and presenting them with image data and results. The client facing module may, in turn, interface with other modules, such as a segmentation service module that performs automated image segmentation to identify a prostate volume and compute uptake metrics as described herein.

FIG. **30** shows an example microservice network architecture **3000** for implementing the systems and methods described herein as a cloud-based application. The particular example microservice network is used in the example cloud-based application referred to as Pioneer, as described herein. In the example microservice network architecture **3000** of FIG. **30**, microservice Pioneer web **3016** is a client facing module that serves a client **3026** to provide them with an interface (e.g., by serving code instruction such as javascript and HTML) for interacting with stored images and analysis results. Pioneer web **3016** also communicates with other microservices, as shown in FIG. **30**. Audit service **3014** logs events and saves event logs in a log file storage database **3012**. Cognito **3020** stores and authenticates users. Auth service **3022** tracks user groups and customer product registrations. Signup service **3024** is a front-end service that allows users to sign up, e.g., for use of the cloud-based system. Slicebox **3004** stores image files in a standardized DICOM format, including 3D anatomical images such as CT images, and 3D functional images such as SPECT and PET images. Images are stored in image storage database **3002**. Image service **3006** reads images (e.g, DICOM files) and stores images and image metadata in a specific (e.g., convenient; e.g., standardized) format. Segmentation service **3010** performs automated image segmentation and uptake metric determination as described herein. Segmentation service **3010** fetches image data prepared by image service **3006** from data storage database **3008**, performs image segmentation and uptake metric determination, and stores results in the data storage database **3008**.

The architecture shown in FIG. **30** can be used to implement applications and platforms described herein on a variety of datacenters, including publicly available datacenters. The datacenter provides infrastructure in the form of servers and networks and provides services for e.g. networking, messaging, authentication, logging and storage. The architecture **3000** for the application uses a series of functional units with limited scope referred to as microservices. Each microservice handles an isolated set of tasks such as image storage, calculation of a risk index, identification of medical image type, and other tasks. Services (e.g., microservices) can communicate with each other using standard protocols such as Hypertext Transfer Protocol (HTTP).

Organizing the application into a network of microservices, as shown in the architecture **3000** of FIG. **30**, allows for parts of the platform to be scaled individually to meet high demand and to ensure minimal downtime. In certain embodiments, such an architecture allows for components to be improved or replaced without affecting other parts of the application, or platforms that include the application along with others.

FIG. **31** is a block flow diagram showing an example dataflow **3100** for performing automated segmentation and analysis of CT/SPECT images using a microservice network such as the one shown in FIG. **30**. Images uploaded by a user are stored in slicebox **3110**. A user may initiate processing of a study (e.g., images for a patient) to initiate automated image segmentation and analysis, for example via an interaction with Pioneer web **3104***a* via a client **3102***a*. Processing of a study may also begin automatically (e.g., following uploading of images; e.g., at regular time intervals). As shown in FIG. **31**, once processing of a study is initiated, Pioneer web **3104***a* interacts with Image service **3106** to initiate preparation (e.g., preprocessing; e.g., formatting) of image data for automated segmentation and analysis. Image service **3106** saves preprocessed images in database S3 **3112**. Pioneer web **3104***a* initiates image segmentation and analysis by Segmentation service (e.g., by sending a SQS message). Segmentation service **3108** fetches image data comprising a 3D anatomical image and a 3D functional image, such as a CT/SPECT image, from S3 **3112**. Segmentation service **3108** performs image segmentation to identify tissue volumes, including a prostate volume, within the 3D anatomical image, and uses the identified tissue volumes and the 3D functional image to compute one or more uptake metrics as described herein. Results of the automated image segmentation and uptake metric determination are saved in S3 **3112**. Segmentation service posts a callback to Pioneer web **3104***a* indicating whether results were successfully obtained or if an error/exception occurred. Upon receipt of the callback, Pioneer web **3104***a* publishes an updated status for the study on channel Pubsub **3118**. Multiple Pioneer web services **3104***a* and **3104***b* may receive the status update for the study and notify clients **3102***a* and **3102***b* with which they interact of the status update.

FIG. **32** shows a data flow **3200** between microservices showing how a client may request statuses of studies and be notified of study status updates in a manner similar to that described above with reference to FIG. **31**. As shown in FIG. **32**, a client **3202** may send study ids to a Pioneer web service instance **3204** that receives status updates via Pub/Sub channel **3212**. Callbacks for completed calculations (e.g., completed image segmentation and uptake metric analysis as described herein) may enter Pioneer web from any Segmentation service **3208**. A status for a completed calculation for a study may be saved in a database **3210** and an updated status for the study is sent to the Pub/Sub channel **3212**. All Pioneer web instances (e.g., **3204** and **3206**) subscribe to the status updates and may provide a status update (e.g., a notification of a completed calculation for the study) to a client **3202** with which they interact.

In certain embodiments, for example as described above with respect to FIG. **30** and FIG. **31**, implementations of the systems and methods described herein may include an Image service module that performs image data preprocessing and formatting, for example to provide appropriately formatted image data to a Segmentation service that performs automated image segmentation and uptake metric determination.

The image service module may preprocess different images from various modalities, including 3D functional and 3D anatomical images, to standardize and format the images. For example, preprocessing of a 3D functional image (e.g., a nuclear medicine image, such as a SPECT image), may include performing basic compliance checks and interpreting voxel intensity values as specified in a standard format (e.g., DICOM PS3 NM Image IOD). Frames of the 3D functional image may be arranged in a particular order corresponding to a direction along the subject, such as a head-to-feet order. A position may be adjusted to represent an outer corner of a first voxel. Attributes from the 3D functional image that may be needed in further processing may also be extracted.

Preprocessing of a 3D anatomical image, such as a CT image, may also include performing basic compliance checks and interpreting voxel intensity values as specified in a standard format (e.g., DICOM PS3 NM Image IOD). Slices of the 3D anatomical image may be arranged in a particular order corresponding to a direction along the subject, such as a head-to-feet order. Cropping bounds to remove one or more regions of the 3D anatomical image that correspond to air around an imaged patient may also be determined. A position may be adjusted to represent an outer corner of a first voxel. Attributes from the 3D anatomical image that may be needed in further processing may also be extracted.

FIG. **33** shows an architecture **3300** illustrating how a cloud-based application implementing the image segmentation and analysis approaches described herein, may be combined with other systems for performing other types of image analysis, to provide a cloud-based platform that a client/user may use to multiple image analysis applications. The architecture **3300** shown in FIG. **33** includes a set **3320** of microservices that are common between two or more applications. The left **3310** and right **3330** panels show microservices in two applications. Microservice network **3330** implements a version of the Pioneer cloud-based application, as described herein, and provides for automated analysis of CT/SPECT images, calculation of uptake metrics, such as TBR, and generation of reports. The microservice network **3310** shown in the left panel implements web-based application, referred to as aBSI, that analyzes whole-body scans obtained with a gamma camera, and computes an automated bone scan index (BSI). Further details regarding aBSI and automated BSI determination are provided in U.S. patent application Ser. No. 15/794,220, filed Oct. 10, 2017, the content of which is hereby incorporated by reference in its entirety.

F. Identifying Other Target Volumes of Interest and Computing Uptake Metrics

With regard to FIG. **34**, the approaches described herein can be used to identify other target volumes, e.g., lungs, lymph nodes, bone, liver. Other image types can be used. Various radiopharmaceuticals can be used to generate 3D functional images. For example, in certain embodiments, 1404 is the imaging agent used for SPECT images, and, in certain embodiments, PyL is the imaging agent used for PET images. In one embodiment, imaging is performed over the whole body of the subject for detection of disease (e.g., tumors) in tissue, e.g., in lymph nodes. The total number of tumors and/or the size and/or another metric associated with the spreading and/or quantity of diseased tissue (e.g., cancer) is/are determined automatically using methods described herein. For example, in process **3400** a 3D anatomical image

and a corresponding 3D functional image are received at steps **3402** and **3404**, respectively. A first CNN may be used to efficiently identify **3406** one or more sub-regions of an initial 3D anatomical image for more detailed segmentation by a second CNN **3408**, and the corresponding 3D functional image is analyzed within the identified one or more sub-regions to quantify overall imaging agent uptake and/or to provide a computed metric indicative of the level and/or extent of disease in the subject **3410**.

G. Example 1: Automated Detection and Quantification of Prostatic PSMA Uptake from SPECT/CT Imaging

In this example, 99mTc MIP-1404, a small-molecule inhibitor of prostate-specific membrane antigen (PSMA) was used to detect clinically significant disease in prostate cancer. An objective of this example was to develop a deep learning model for the automatic detection and quantification of prostatic MIP-1404 uptake in SPECT/CT images.

A deep-learning algorithm was developed based on convolutional neural networks for automatically segmenting the prostate and pelvic bones from CT images. The algorithm as designed to process both high- and low-dose CT images as well as whole and part body field of views, with no manual interaction necessary. The training material consisted of 100 diagnostic CT images (all male) with complete and distinct segmentations, performed manually, for relevant anatomical regions. The algorithm was validated on the MIP-1404 phase II study including 102 high-risk prostate cancer patients who all underwent PSMA imaging prior to radical prostatectomy. All validation scans were quantified manually using the OsiriX medical image viewer (Pixmeo SARL), by measuring the maximum uptake in a circular ROI placed inside the prostate in the slice and region with highest uptake values determined visually. The automatic algorithm uses its volumetric segmentations to measure uptake at every voxel in the prostate, and registers the maximum uptake. The Pearson correlation coefficient was used to assess the concordance between manual and automated quantification of prostatic uptake.

The algorithm based on the lining material had 2.7 million parameters and was optimized using Adam, a variant of gradient descent. In the test set, 1404 images of 34 patients (33%; 34/102) were excluded due to excessive CT artifacts, incomplete data and/or data format problems. Computation time on the evaluable patients (N=68) was 13 seconds (per case) on commodity hardware. The automated maximum uptake value was significantly correlated to the manually obtained in the prostate ($r=0.95$, 95% CI=[0.91,0.97]; slope=0.89, 95% CI=[0.80,0.98]; $p<0.0001$). The algorithm was fully automated and deterministic, resulting in 100% repeatability.

This example demonstrates the feasibility of an objective and automated measure of MIP-1404 uptake in the prostate.

H. Example 2: Technical and Clinical Performance of Automated Segmentation and Uptake Metric Determination

Example 2 shows evaluation of technical and clinical performance of an embodiment automated image segmentation and uptake metric determination approaches described herein implement via an example cloud-based application referred to as Pioneer. To establish the hypothesis generating algorithm for Pioneer, MIP-1404 SPECT/CT image data from two clinical studies were used, including healthy volunteers (a phase 1 study: MIP-1404-1301) and patients with prostate cancer who had histopathology data available following radical prostatectomy (a phase 2 study: MIP-1404-201). Data comparing the receiver operating characteristic plot (ROC), sensitivity, specificity, positive and negative predictive values produced by Pioneer with those obtained by traditional manual reads, showed that Pioneer could be a useful tool to assist radiologists in MIP-1404 image interpretation; thereby facilitating the evaluation of patients with prostate cancer.

i. Technical Performance

The analytical verification of the algorithm's segmentation and quantification performance criteria and the motivation was prospectively defined as detailed in OTHA-2262 and OTHA-2263, respectively. Total of sixty-one 1404 SPECT/CT images and standard for care read from nuclear medicine physician was used as benchmark to evaluate the analytical performance. All manual reads were done independently and blindly to the technical performance acceptance criteria.

The prostate segmentation performance test demonstrated mean dice of 0.77 and a standard deviation of 0.012. The lower endpoint of the one sided 95% confidence interval was 0.75, higher than the pre-defined threshold in OTHA-2262 (0.70). The background (gluteus maximus left) segmentation performance test demonstrated mean dice of 0.94 and a standard deviation of 0.002. The lower endpoint of the one sided 95% confidence interval was 0.94, higher than the pre-defined threshold in OTHA-2262 (0.80).

Only in four of the total 61 (6.6%) of the target locations predicted by the automated Pioneer software were classified by the human expert (nuclear medicine reader) as faulty. The outcome was better than that specified in OTHA-2263.

ii. Clinical Performance

In a retrospective ad hoc analysis of clinical performance, fourteen healthy volunteers (phase 1 study MIP-1404-1301) and 105 subjects with prostate cancer patients (phase 2 study MIP-1404-201) were combined in a single cohort for analysis with Pioneer. Subjects in MIP-1404-201 who received prior therapy for prostate cancer were excluded.

Images that had CT artifacts or could not be reconstructed for automated analysis were also excluded. A total of 75 images were evaluated from 61 subjects with prostate cancer and 14 normal volunteers.

Pioneer's automated assessment was evaluated against the histopathological truth standard for those who had been diagnosed with prostate cancer and had undergone radical prostatectomy following MIP-1404 SPECT/CT imaging. For healthy volunteers the assumption was made that they had no prostate cancer based on their normal PSA and pelvic MRI at the time of study. Spearman's rho was used to assess the correlation with Gleason score. Area under the receiver operating characteristic (ROC) curve was employed to determine the performance of the algorithm in detecting prostate cancer in the prostate gland. Sensitivity and specificity was determined from the optimal threshold/cutoff value from the ROC curve.

The automated quantitative assessment of the 1404 images correlated with Gleason score (rho: 0.54; $p<0.0001$). The ROC curve demonstrated an AUC of 0.80 (95% CI: 67-94). The optimal threshold for the binary TBR-based result in distinguishing clinically significant prostate cancer from clinically non-significant cancer or normal prostate was determined to be 25. Using this threshold, Pioneer distinguished clinically significant from clinically non-significant prostate cancer or normal prostates with a sensitivity

of 75% and specificity of 80% using 1404 SPECT/CT images from the MIP-1404-1301 and MIP-1404-201 studies.

Accordingly, Pioneer improves on manual reads by providing (i) more objective and reproducible read performance across all diagnostic endpoints, and (ii) point estimates for key diagnostic performance parameters, e.g. sensitivity, specificity, that have been shown to be consistently >70% using histopathology as the truth standard.

I. Example 3: Example Cloud Based Software for Automated and Semi-Automated Analysis of 1404 CT/SPECT Images

Example 3 is an example of a cloud-based software platform, referred to as Pioneer that implements an embodiment of the automated image analysis approaches described herein. Pioneer is a cloud-based software platform, implemented according to regulatory and data safety standards, where users can upload 1404 SPECT/CT image data, view it using 2-dimensional and 3-dimensional medical image viewers accessed through the user's ordinary internet browser, and review and export TBR values. The software also provides a quality control workflow where users can assess the quality of the analysis with options to reject and/or adjust the automated analysis.

Thus, under the supervision of the user, the software employs an artificial intelligence algorithm to automatically identify and analyze the regions of interest (ROIs). Pioneer extracts image data from the ROIs to provide an objective analysis—Target to background (TBR)—based on uptake in the prostate and background. Since signals in the prostate are often obscured by signals from the urinary bladder (MIP-1404 being excreted in urine), capability was also built in the software to segment the bladder and suppress bladder associated signals, thus enabling prostatic signals to be measured more accurately.

The non-clinical performance data of Pioneer include verification and validation (V&V) assessments, including definition of test methods. Pre-determined acceptance criteria were designed to ensure, at a minimum, equivalent performance with state of the art (manual assessment). The verification included software unit testing, integration testing and software system testing with functional testing of all software requirements. The validation process was performed to ensure that the system meets the user requirements specification. The V&V test results showed that Pioneer meets its intended use, user and software requirements.

J. Example 4: Selection of TBR Threshold for Clinically Significant Findings

Example 4 is an example showing how a TBR threshold value for partitioning patient prostate cancer pathology into clinically significant and clinically non-significant classifications can be determined.

Two datasets of SPECT/CT images were combined to select an appropriate threshold value. A first dataset comprised images of healthy individuals, taken from a phase I study of the 1404 drug. This dataset contained originally 14 images. Segmentation of a prostate within the images was performed in accordance with the approaches described herein and two images where segmentation of the prostate clearly failed were excluded, resulting in 12 remaining images. A second data set comprised images of individuals with prostate cancer, originating from a phase II study of the 1404 drug. The images were partitioned based on the subject's Gleason grades on histopathology from radical prostatectomy. A total Gleason Score of 7 or above was considered clinically significant and total Gleason Score 6 or below was considered clinically non-significant. This dataset contained originally 65 images (63 clinically significant, 2 clinically non-significant), after excluding one image where the image did not cover the entire pelvic region and one image where the segmentation of prostate had clearly failed, 63 remained (61 clinically significant, 2 clinically non-significant).

In summary, 14 images without clinically significant pathology and 61 images with clinically significant pathology were used.

A software package implementing an embodiment of the automated image segmentation and uptake metric determination approaches described herein, ctseg package version 1.0.0rcIII, was used to compute TBR values for the images.

FIG. **35**A shows a swarm plot of clinically non-significant (<=6 on the x-axis) and clinically significant images (>=7 on the x-axis). A threshold of 25 gives a sensitivity of 0.77 (lower endpoint of Jeffreys one-sided 95% confidence interval is 0.67) and a specificity of 0.71 (lower endpoint of Jeffreys one-sided 95% confidence interval is 0.50) on the test data. FIG. **35**B shows a ROC curve based on varying the TBR threshold. The point for TBR threshold 25 is marked **3502** (red circular marker).

As shown in FIGS. **35** A and **35**B, a threshold value of 25 provided a value for distinguishing between patients who do have clinically significant prostate cancer and those who do not. However, since there are few data points very close to the threshold, the estimates of sensitivity and specificity are not robust to small random variations in data. To get more robust estimates, the R package 'scdensity' was used to estimate smooth unimodal densities for the distribution of log TBR values for clinically non-significant and significant images respectively. From this, estimates for sensitivity and specificity were computed for different TBR thresholds, see Table 1.

TABLE 1

Robust estimates of sensitivity and specificity for different TBR thresholds.

TBR threshold	Specificity	Sensitivity
22	0.68	0.79
23	0.70	0.78
24	0.73	0.76
25	0.75	0.75
26	0.76	0.73
27	0.78	0.72
28	0.79	0.70

Accordingly, based on the analysis described in this example, a TBR threshold of 25 was selected based on a desired specificity and sensitivity. These preliminary studies based on Phase 1 and Phase 2 data have shown improved diagnostic accuracy of MIP-1404 SPECT/CT using the automated method in comparison to manual reads.

K. Example 5: Application of AI to Phase 3 Study MIP-1404-3301 ("proSPECT-AS")

MIP1404-3301 is a pivotal phase 3 multicenter trial of ^{99m}Tc-MIP1404 Injection for the detection of prostate cancer. MIP-1404-3301 is titled "A Phase 3 Study to Evaluate the Safety and Efficacy of 1404 SPECT/CT Imaging to

MIM Ex1039
MIM Software Inc. v. Progenics Pharmaceuticals, Inc.
Trial IPR2025-00630

Detect Clinically Significant Prostate Cancer in Men with Biopsy Proven Low-Grade Prostate Cancer who are Candidates for Active Surveillance". Cohort A patients were men with biopsy-proven low to intermediate grade prostate cancer (Gleason score 3+3 or 3+4) who were candidates for active surveillance but elected to have radical prostatectomy. Cohort B patients were biopsy-proven very low risk prostate cancer patients who scheduled to undergo routine re-biopsy as part or routine active surveillance. The phase 3 study was initiated in December 2015, and enrollment is now complete. The computer-assisted diagnosis (CADx) software device is to be used as the primary reading methodology to analyze the primary end-points in Study MIP-1404-3301.

There are two co-primary endpoints:

Specificity of ^{99m}Tc-MIP1404 to detect clinically significant prostate cancer when compared to histopathology following radical prostatectomy (cohort A) or prostate biopsy (cohort B) using automated reading technology;

Sensitivity of ^{99m}Tc-MIP1404 to detect clinically significant prostate cancer when compared to histopathology following radical prostatectomy (cohort A) or prostate biopsy (cohort B) using automated reading technology.

The 1404 image data from the Phase 3 trial were collected by a central imaging core laboratory. The image analysis is conducted by a radiologist using the automated software device. The medical software device is used in the assessment and characterization of prostate cancer, using a radioactive PSMA targeting imaging agent, for example as a Computer Aided Detection (CADe) device. The analysis is useful in estimating the risk for clinically significant prostate cancer in a patients. The device is also useful as a combination product comprising 1404 radioactive diagnostic agent indicated for the imaging of patients with prostate cancer in combination with the automated software device, for the automated assessment, characterization and diagnosis of prostate cancer, for example as a Computer-aided Diagnostic (CADx) device. The 1404 imaging results help estimate the risk for clinically significant prostate cancer in these patients. The software uses artificial intelligence to automatically segment the image data into distinct anatomical regions and then analyzes the volumetric regions of interest (ROI). The software extracts quantitative data from ROIs to assist in determining the presence or absence of clinically significant prostate cancer. The software device is used to assist radiologist and physicians in the assessment, characterization and quantification of prostate cancer in SPECT/CT and PET/CT images. The device is indicated for evaluation of patients presenting high-risk or low-risk screening, diagnostic imaging workup, or evaluation of extent of disease. The results from the image analysis are useful in guiding treatment decisions for the patients by the physicians.

L. Example 6: Training and Validation of Convolutional Neural Networks Implemented by the First Machine Learning Module (Localization Machine) and Second Machine Learning Module (Segmentation Machine)

Example 5 is an example showing training and validation of CNN modules used to segment CT images to identify various tissue volumes, including a prostate volume, in accordance with the aspects and embodiments described herein. In this example, the neural networks were defined and trained using the Keras framework with the Tensorflow backend.

i. Training and Validation Data

The training and validation data comprised CT images coupled with semi-automated segmentations corrected by a radiologist delineating all or some of the following body parts: (i) a prostate; (ii) a urinary bladder; (iii) a rectum; (iv) a left gluteus maximus; (v) a right gluteus maximus; (vi) a left hip bone; (vii) a right hip bone; and (viii) a sacrum and coccyx

To train a localization CNN, 90 high quality CT images were used with segmentations of all the body parts above. For training a segmentation CNN for high resolution segmentation of left gluteus maximus, these and 10 images of the same type were used. For training a segmentation CNN for high resolution segmentation of the prostate, an additional data set of 73 lower-quality images with more anatomical variation in prostate and urinary bladder (due to disease) was used. These additional images were matched with segmentations of the prostate and the urinary bladder only. Pseudo labels for rectum, left and right hip bone, and sacrum and coccyx were generated for these 73 images. The pseudo labels are predicted labels generated using a previously trained network (a network trained on the 100 high quality CT images). The pseudo labels were merged with the manual labels before training.

ii. Training Configuration

Each training run was defined by a configuration file named config.json. The configuration file included parameters for: (i) which data set is used; (ii) data preprocessing; (iii) partitioning data into training and validation sets; (iv) model structure; and (v) training hyperparameters.

This configuration file is used when the trained model is used for inference, to ensure that the same image preprocessing is done during inference as during training.

iii. Preprocessing

The configuration file defines which preprocessing steps are applied during training. Several preprocessing steps were included. Cropping preprocessing steps were performed to remove surrounding air for localization training and to crop out a bounding box defined by pelvic bones, urinary bladder, rectum and prostate for segmentation. A fixed intensity normalization step was performed by subtraction of a fixed value and then division by another fixed value, where the values are chosen so that on average the intensities of voxels in the images have a mean intensity 0 and a standard deviation 1. Images were also reshaped to a fixed size by resampling. For localization, the resolution in each direction decreased by a factor of 4 for an image with median sizes in each direction. For high-resolution segmentation the resolution does not change for an image with median sizes in each dimension. Other preprocessing steps included one-hot-encoding of segmentation labels, segmentation label reweighting as defined in section iv. "Optimization", below, and data augmentation, as defined in section iv. "Optimization", below.

Some preprocessing steps are performed offline in order to speed up the training, resulting in preprocessed data sets. The config.json that belongs to the training only defines those preprocessing steps that are done online.

For localization training, the preprocessing steps for the offline preprocessing is stored in a separate file meta_data/prep_config.json in the trained CNN directory.

iv. Optimization

The loss function used for training is voxel-wise categorical cross entropy, weighted such that all voxel belonging to one class (in the true labeling) together have the same weight as all voxels belonging to any other class (when the label frequencies equal the median frequencies across the data

set). This approach balances the classes and is important for prostate segmentation since the prostate is very small in comparison to, e.g., the background.

The loss is optimized using mini-batch descent with the Adam optimizer for around 2000-3000 epochs. The batch size equals 1. A batch size of 1 means that batch normalization turns into instance normalization (since the batch is only one sample). For improved performance, instance normalization is enforced also during inference.

The learning rate is determined by a learning rate schedule with a very low learning rate (e.g., 1×10^{-5}) for the first few epochs, then decreasing in steps from a high learning rate (e.g. 1×10^{-2}). After 250 epochs the learning rate is halved, then halved again after 500 more epochs, then halved again after 1000 more epochs. To decrease overfitting, dropout is used. Dropout rates vary between 0.2 and 0.5 for different networks (but the rate same in all places where it is applied for a given network, as shown, for example, in FIG. **13** and FIG. **14**). Appropriate rates of dropout are based on experience from multiple trainings and how it affects the difference in performance on training and validation sets.

A training approach where the training image data is augmented by adding random distortions was used prevent the neural networks from focusing on fine details in the images. Training the neural networks (e.g., the localization CNN and segmentation CNN) in this manner allows them to handle (e.g., perform effective localization and/or segmentation of) images with image artifacts that are not present or not common in the training data.

The random distortions added to augment the training data include additive or multiplicative noise and added smoothed salt noise. These random distortions are applied independently with certain probabilities. These random distortions are scheduled to be not used for the first few hundred epochs so that the network first learns to handle images without artifacts, then the noise level is gradually increased. The intensity distortions are only applied to the 100 high-quality CT images, not the 73 low-quality images since they already have artifacts.

The localization CNN is trained to handle (e.g., receive as input) whole-body images as well as different partial-body images. To this end, augmentation with random crops of the image (always keeping the entire pelvic bounding box) is used.

v. Computational Resources

The localization trainings were done on a Nvidia GeForce GTX 1050, where a training took a few hours.

The high resolution segmentation trainings were done on a Nvidia GeForce GTX 1080 Ti, where training took 2-3 days.

vi. Model Selection

To optimize neural network structures and select hyper parameters for the training it is necessary to have metrics measuring performance. The main metric for evaluating the progress of training is Sorensen-Dice score (referred to hereafter as "Dice score"): the weighted score (weighting described above in section iv. "Optimization") or the score for individual body parts (prostate or left gluteus maximus).

When aggregating results over multiple images, most often averages of evaluated Dice scores are used (e.g., as metrics). In certain cases, a frequency of images with Dice scores below a certain level is used.

For each localization training run, the model that had best average weighted Dice score for the training images was selected. For segmentation trainings used to train the segmentation neural network to segment the prostate, the Dice score for prostate was used as a basis for selection. For segmentation trainings used to train the segmentation neural network to segment the left gluteus maximus the Dice score for left gluteus maximus was a basis for selection. For segmentation trainings with auxiliary predictions, the Dice scores were based on the prediction from the main output—that is, the output which is present also when there are no auxiliary predictions.

When training the localization CNN, 30% of the 90 CT images were reserved for validation, such that performance of the localization CNN could be evaluated using images that it was not trained on. To train the segmentation CNN for high-resolution prostate segmentation, 23 of the low-quality CT images were set aside for validation, such that only 50 of the low quality images were used in training (resulting in 150 CT images for training in total).

Metrics corresponding to a precision in cropping was used when selecting between different localization trainings. Cropping precision was evaluated based on several metrics/aspects. In particular, one metric was that as few images as possible of the 90 training and validation images should need a crop margin above 0.1 to encompass the entire pelvic bones. Another metric was that an error in distance to the bounding box walls should be as small as possible (evaluated by looking at box plots of errors). Another metric was that on 102 low-quality CT images (without ground truth segmentations available), 2D projections of them with the coarse segmentation and final bounding box overlaid should show good agreement between segmentation and anatomy, especially that the appropriate region was covered.

When selecting between different high-resolution segmentation trainings, the following metrics/aspects were considered: (i) Dice scores for training and validation data; (ii) precision and recall for prostate for training and validation data; (iii) overlap between ground-truth bladder and predicted prostate; and (iv) examples of segmentations overlaid on CT-images in a CT image viewer where one can scroll through the slices in the sagittal, axial and coronal planes.

Accordingly, this example provides an example of an approach that can be used to train neural network models used in the localization machine learning module (first machine learning module) and segmentation machine learning modules (second machine learning module and any auxiliary segmentation machine learning modules) described herein.

M. Imaging Agents

In certain embodiments, 3D functional images are nuclear medicine images that use imaging agents comprising radiopharmaceuticals. Nuclear medicine images are obtained following administration of a radiopharmaceutical to a patient, and provide information regarding the distribution of the radiopharmaceutical within the patient. Radiopharmaceuticals are compounds that comprise a radionuclide.

Nuclear medicine images (e.g., PET scans; e.g., SPECT scans; e.g., whole-body scans; e.g. composite PET-CT images; e.g., composite SPECT-CT images) detect radiation emitted from the radionuclides of radiopharmaceuticals to form an image. The distribution of a particular radiopharmaceutical within a patient may be determined by biological mechanisms such as blood flow or perfusion, as well as by specific enzymatic or receptor binding interactions. Different radiopharmaceuticals may be designed to take advantage of different biological mechanisms and/or particular specific enzymatic or receptor binding interactions and thus, when administered to a patient, selectively concentrate within particular types of tissue and/or regions within the patient.

Greater amounts of radiation are emitted from regions within the patient that have higher concentrations of radiopharmaceutical than other regions, such that these regions appear brighter in nuclear medicine images. Accordingly, intensity variations within a nuclear medicine image can be used to map the distribution of radiopharmaceutical within the patient. This mapped distribution of radiopharmaceutical within the patient can be used to, for example, infer the presence of cancerous tissue within various regions of the patient's body.

For example, upon administration to a patient, technetium 99m methylenediphosphonate (^{99m}Tc MDP) selectively accumulates within the skeletal region of the patient, in particular at sites with abnormal osteogenesis associated with malignant bone lesions. The selective concentration of radiopharmaceutical at these sites produces identifiable hotspots—localized regions of high intensity in nuclear medicine images. Accordingly, presence of malignant bone lesions associated with metastatic prostate cancer can be inferred by identifying such hotspots within a whole-body scan of the patient. Risk indices that correlate with patient overall survival and other prognostic metrics indicative of disease state, progression, treatment efficacy, and the like, can be computed based on automated analysis of intensity variations in whole-body scans obtained following administration of ^{99m}Tc MDP to a patient. In certain embodiments, other radiopharmaceuticals can also be used in a similar fashion to ^{99m}Tc MDP.

In certain embodiments, the particular radiopharmaceutical used depends on the particular nuclear medicine imaging modality used. For example ^{18}F sodium fluoride (NaF) also accumulates in bone lesions, similar to ^{99m}Tc MDP, but can be used with PET imaging. In certain embodiments, PET imaging may also utilize a radioactive form of the vitamin choline, which is readily absorbed by prostate cancer cells.

In certain embodiments, radiopharmaceuticals that selectively bind to particular proteins or receptors of interest—particularly those whose expression is increased in cancerous tissue may be used. Such proteins or receptors of interest include, but are not limited to tumor antigens, such as CEA, which is expressed in colorectal carcinomas, Her2/neu, which is expressed in multiple cancers, BRCA 1 and BRCA 2, expressed in breast and ovarian cancers; and TRP-1 and -2, expressed in melanoma.

For example, human prostate-specific membrane antigen (PSMA) is upregulated in prostate cancer, including metastatic disease. PSMA is expressed by virtually all prostate cancers and its expression is further increased in poorly differentiated, metastatic and hormone refractory carcinomas. Accordingly, radiopharmaceuticals corresponding to PSMA binding agents (e.g., compounds that a high affinity to PSMA) labelled with one or more radionuclide(s) can be used to obtain nuclear medicine images of a patient from which the presence and/or state of prostate cancer within a variety of regions (e.g., including, but not limited to skeletal regions) of the patient can be assessed. In certain embodiments, nuclear medicine images obtained using PSMA binding agents are used to identify the presence of cancerous tissue within the prostate, when the disease is in a localized state. In certain embodiments, nuclear medicine images obtained using radiopharmaceuticals comprising PSMA binding agents are used to identify the presence of cancerous tissue within a variety of regions that include not only the prostate, but also other organs and tissue regions such as lungs, lymph nodes, and bones, as is relevant when the disease is metastatic.

In particular, upon administration to a patient, radionuclide labelled PSMA binding agents selectively accumulate within cancerous tissue, based on their affinity to PSMA. In a similar manner to that described above with regard to ^{99m}Tc MDP, the selective concentration of radionuclide labelled PSMA binding agents at particular sites within the patient produces detectable hotspots in nuclear medicine images. As PSMA binding agents concentrate within a variety of cancerous tissues and regions of the body expressing PSMA, localized cancer within a prostate of the patient and/or metastatic cancer in various regions of the patient's body can be detected, and evaluated. As described in the following, risk indices that correlate with patient overall survival and other prognostic metrics indicative of disease state, progression, treatment efficacy, and the like, can be computed based on automated analysis of intensity variations in nuclear medicine images obtained following administration of a PSMA binding agent radiopharmaceutical to a patient.

A variety of radionuclide labelled PSMA binding agents may be used as radiopharmaceutical imaging agents for nuclear medicine imaging to detect and evaluate prostate cancer. In certain embodiments, the particular radionuclide labelled PSMA binding agent that is used depends on factors such as the particular imaging modality (e.g., PET; e.g., SPECT) and the particular regions (e.g., organs) of the patient to be imaged. For example, certain radionuclide labelled PSMA binding agents are suited for PET imaging, while others are suited for SPECT imaging. For example, certain radionuclide labelled PSMA binding agents facilitate imaging a prostate of the patient, and are used primarily when the disease is localized, while others facilitate imaging organs and regions throughout the patient's body, and are useful for evaluating metastatic prostate cancer.

A variety of PSMA binding agents and radionuclide labelled versions thereof are described in U.S. Pat. Nos. 8,778,305, 8,211,401, and 8,962,799, each of which are incorporated herein by reference in their entireties.

i. PET Imaging Radionuclide Labelled PSMA Binding Agents

In certain embodiments, the radionuclide labelled PSMA binding agent is a radionuclide labelled PSMA binding agent appropriate for PET imaging.

In certain embodiments, the radionuclide labelled PSMA binding agent comprises [18F]DCFPyL (also referred to as PyL™; also referred to as DCFPyL-18F):

[18F]DCFPyL

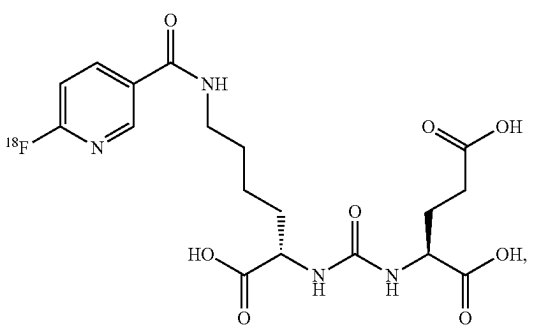

or a pharmaceutically acceptable salt thereof.

In certain embodiments, the radionuclide labelled PSMA binding agent comprises [18F]DCFBC:

[18F]DCFBC

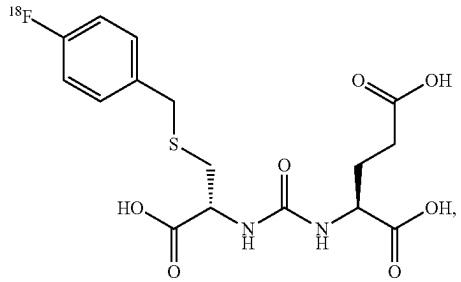

or a pharmaceutically acceptable salt thereof.

In certain embodiments, the radionuclide labelled PSMA binding agent comprises ^{68}Ga-PSMA-HBED-CC (also referred to as ^{68}Ga-PSMA-11):

^{68}Ga-PSMA-HBED-CC

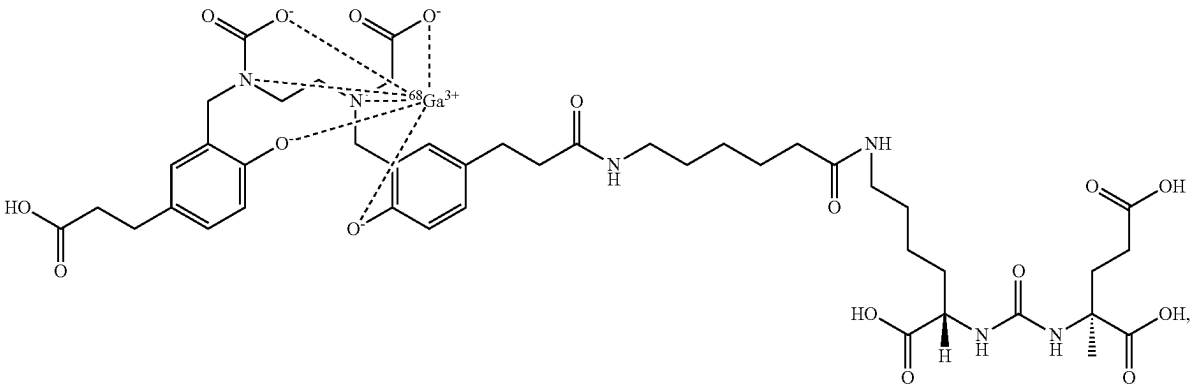

or a pharmaceutically acceptable salt thereof.

In certain embodiments, the radionuclide labelled PSMA binding agent comprises PSMA-617:

PSMA-617

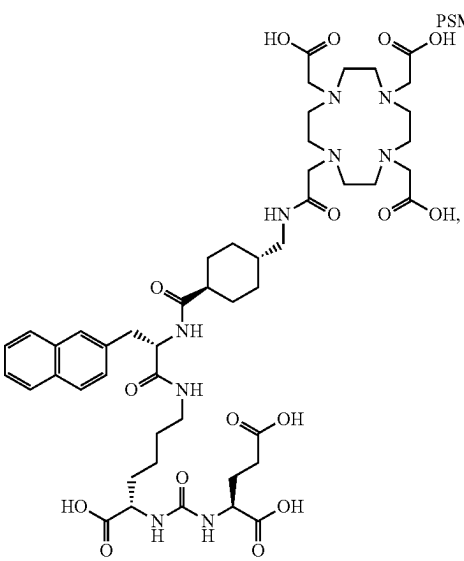

or a pharmaceutically acceptable salt thereof. In certain embodiments, the radionuclide labelled PSMA binding agent comprises ^{68}Ga-PSMA-617, which is PSMA-617 labelled with ^{68}Ga, or a pharmaceutically acceptable salt thereof. In certain embodiments, the radionuclide labelled PSMA binding agent comprises ^{177}Lu-PSMA-617, which is PSMA-617 labelled with ^{177}Lu, or a pharmaceutically acceptable salt thereof.

In certain embodiments, the radionuclide labelled PSMA binding agent comprises PSMA-I&T:

PSMA-I&T

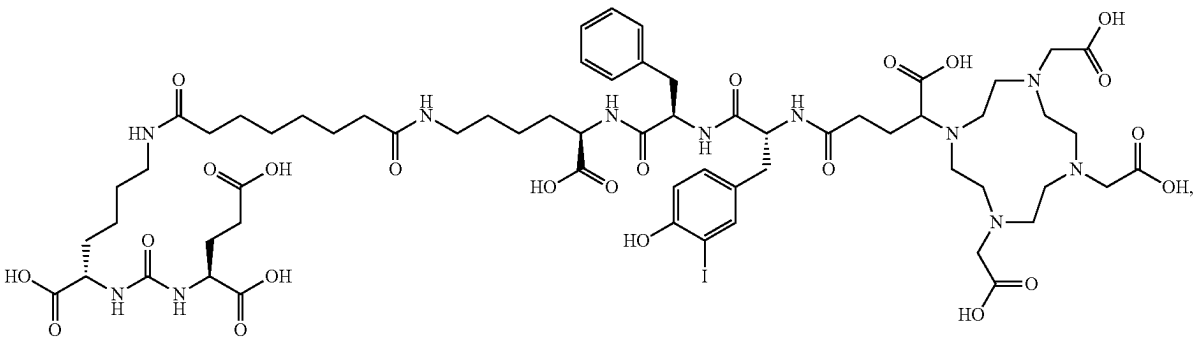

PSMA-I&T

or a pharmaceutically acceptable salt thereof. In certain embodiments, the radionuclide labelled PSMA binding agent comprises ^{68}Ga-PSMA-I&T, which is PSMA-I&T labelled with ^{68}Ga, or a pharmaceutically acceptable salt thereof.

In certain embodiments, the radionuclide labelled PSMA binding agent comprises PSMA-1007:

PSMA-1007

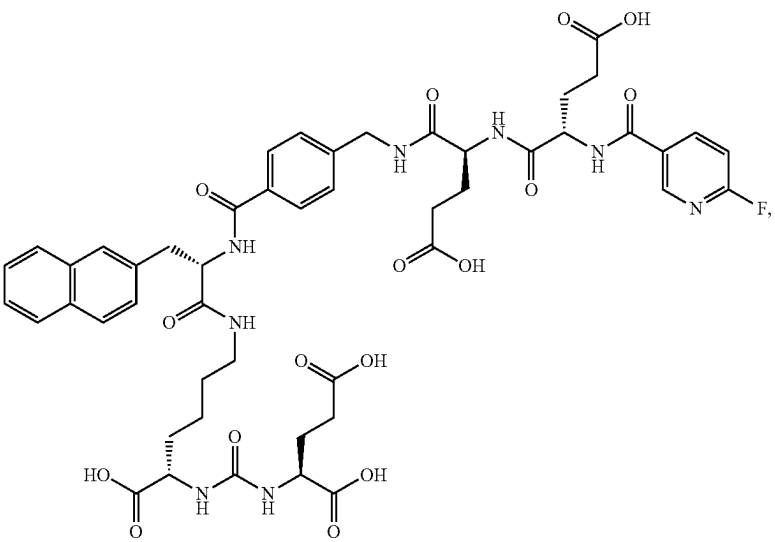

or a pharmaceutically acceptable salt thereof. In certain embodiments, the radionuclide labelled PSMA binding agent comprises ^{18}F-PSMA-1007, which is PSMA-1007 labelled with ^{18}F, or a pharmaceutically acceptable salt thereof.

MIM Ex1039
MIM Software Inc. v. Progenics Pharmaceuticals, Inc.
Trial IPR2025-00630

ii. SPECT Imaging Radionuclide Labelled PSMA Binding Agents

In certain embodiments, the radionuclide labelled PSMA binding agent is a radionuclide labelled PSMA binding agent appropriate for SPECT imaging.

In certain embodiments, the radionuclide labelled PSMA binding agent comprises 1404 (also referred to as MIP-1404):

1404

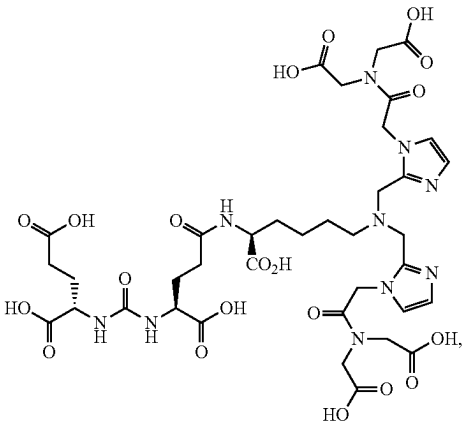

or a pharmaceutically acceptable salt thereof.

In certain embodiments, the radionuclide labelled PSMA binding agent comprises 1405 (also referred to as MIP-1405):

1405

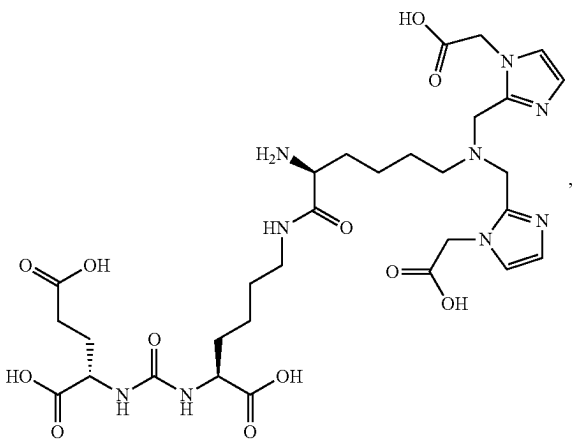

or a pharmaceutically acceptable salt thereof.

In certain embodiments, the radionuclide labelled PSMA binding agent comprises 1427 (also referred to as MIP-1427):

1427

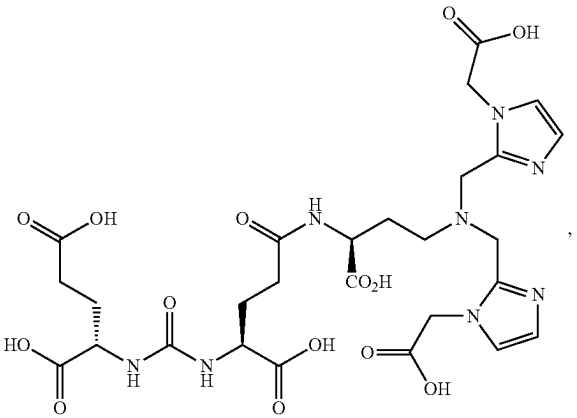

or a pharmaceutically acceptable salt thereof.

In certain embodiments, the radionuclide labelled PSMA binding agent comprises 1428 (also referred to as MIP-1428):

1428

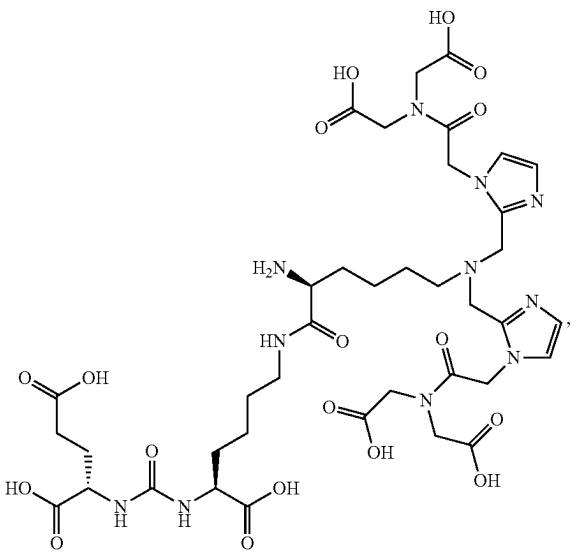

or a pharmaceutically acceptable salt thereof.

In certain embodiments, the PSMA binding agent is labelled with a radionuclide by chelating it to a radioisotope of a metal [e.g., a radioisotope of technetium (Tc) (e.g., technetium-99m (^{99m}Tc)); e.g., a radioisotope of rhenium (Re) (e.g., rhenium-188 (^{188}Re); e.g., rhenium-186 (^{186}Re)); e.g., a radioisotope of yttrium (Y) (e.g., ^{90}Y); e.g., a radioisotope of lutetium (Lu) (e.g., ^{177}Lu); e.g., a radioisotope of gallium (Ga) (e.g., ^{68}Ga; e.g., ^{67}Ga); e.g., a radioisotope of indium (e.g., ^{111}In); e.g., a radioisotope of copper (Cu) (e.g., ^{67}Cu)].

In certain embodiments, 1404 is labelled with a radionuclide (e.g., chelated to a radioisotope of a metal). In certain embodiments, the radionuclide labelled PSMA binding agent comprises ^{99m}Tc-MIP-1404, which is 1404 labelled with (e.g., chelated to)^{99m}Tc:

^{99m}Tc-MIP-1404

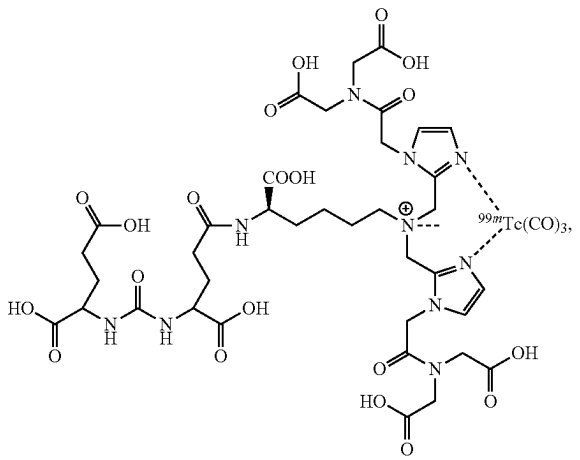

or a pharmaceutically acceptable salt thereof. In certain embodiments, 1404 may be chelated to other metal radioisotopes [e.g., a radioisotope of rhenium (Re) (e.g., rhenium-188 (^{188}Re); e.g., rhenium-186 (^{186}Re)); e.g., a radioisotope of yttrium (Y) (e.g., ^{90}Y); e.g., a radioisotope of lutetium (Lu)(e.g., ^{177}Lu); e.g., a radioisotope of gallium (Ga) (e.g., ^{68}Ga; e.g., ^{67}Ga); e.g., a radioisotope of indium (e.g., ^{111}In); e.g., a radioisotope of copper (Cu) (e.g., ^{67}Cu)] to form a compound having a structure similar to the structure shown above for ^{99m}Tc-MIP-1404, with the other metal radioisotope substituted for ^{99m}Tc.

In certain embodiments, 1405 is labelled with a radionuclide (e.g., chelated to a radioisotope of a metal). In certain embodiments, the radionuclide labelled PSMA binding agent comprises ^{99m}Tc-MIP-1405, which is 1405 labelled with (e.g., chelated to)^{99m}Tc:

^{99m}Tc-MIP-1405

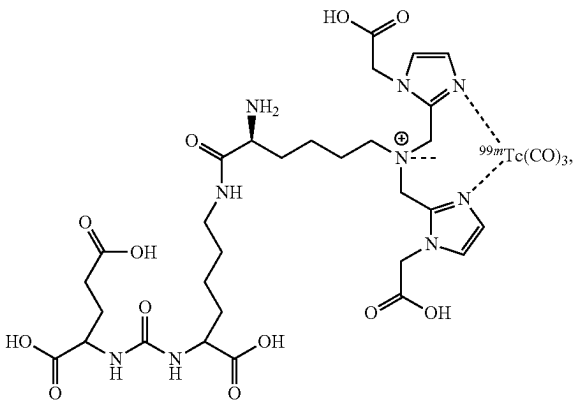

or a pharmaceutically acceptable salt thereof. In certain embodiments, 1405 may be chelated to other metal radioisotopes [e.g., a radioisotope of rhenium (Re) (e.g., rhenium-188 (^{188}Re); e.g., rhenium-186 (^{186}Re)); e.g., a radioisotope of yttrium (Y) (e.g., ^{90}Y); e.g., a radioisotope of lutetium (Lu)(e.g., ^{177}Lu); e.g., a radioisotope of gallium (Ga) (e.g., ^{68}Ga; e.g., ^{67}Ga); e.g., a radioisotope of indium (e.g., ^{111}In); e.g., a radioisotope of copper (Cu) (e.g., ^{67}Cu)] to form a compound having a structure similar to the structure shown above for ^{99m}Tc-MIP-1405, with the other metal radioisotope substituted for ^{99m}Tc.

In certain embodiments, 1427 is labelled with (e.g., chelated to) a radioisotope of a metal, to form a compound according to the formula below:

1427

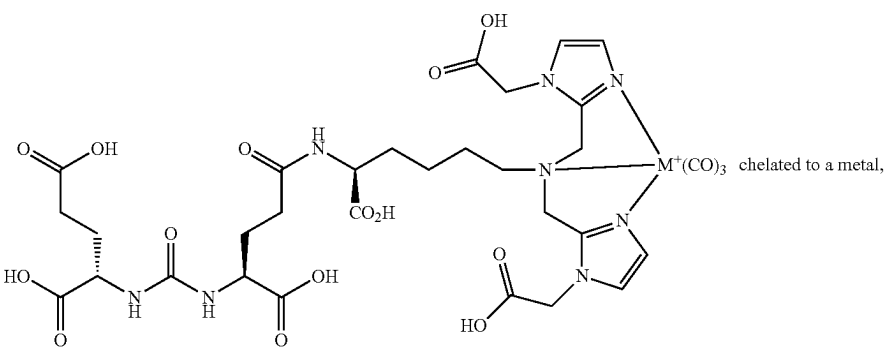

or a pharmaceutically acceptable salt thereof, wherein M is a metal radioisotope [e.g., a radioisotope of technetium (Tc) (e.g., technetium-99m (^{99m}Tc)); e.g., a radioisotope of rhenium (Re) (e.g., rhenium-188 ^{188}Re); (e.g., rhenium-186 (^{186}Re)); e.g., a radioisotope of yttrium (Y) (e.g., ^{90}Y); e.g., a radioisotope of lutetium (Lu)(e.g., ^{177}Lu); e.g., a radioisotope of gallium (Ga) (e.g., ^{68}Ga; e.g., ^{67}Ga); e.g., a radioisotope of indium (e.g., ^{111}In); e.g., a radioisotope of copper (Cu) (e.g., ^{67}Cu)] with which 1427 is labelled.

In certain embodiments, 1428 is labelled with (e.g., chelated to) a radioisotope of a metal, to form a compound according to the formula below:

1428

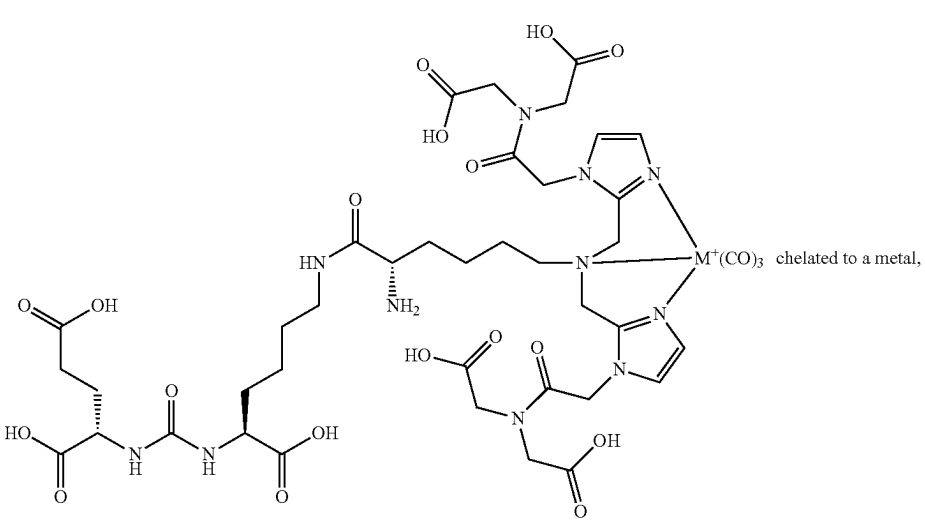

or a pharmaceutically acceptable salt thereof, wherein M is a metal radioisotope [e.g., a radioisotope of technetium (Tc) (e.g., technetium-99m (^{99m}Tc)); e.g., a radioisotope of rhenium (Re) (e.g., rhenium-188 (^{188}Re); e.g., rhenium-186 (^{186}Re)); e.g., a radioisotope of yttrium (Y) (e.g., ^{90}Y); e.g., a radioisotope of lutetium (Lu)(e.g., ^{177}Lu); e.g., a radioisotope of gallium (Ga) (e.g., ^{68}Ga; e.g., ^{67}Ga); e.g., a radioisotope of indium (e.g., ^{111}In); e.g., a radioisotope of copper (Cu) (e.g., ^{67}Cu)] with which 1428 is labelled.

In certain embodiments, the radionuclide labelled PSMA binding agent comprises PSMA I&S:

or a pharmaceutically acceptable salt thereof. In certain embodiments, the radionuclide labelled PSMA binding agent comprises ^{99m}Tc-PSMA I&S, which is PSMA I&S labelled with ^{99m}Tc, or a pharmaceutically acceptable salt thereof.

N. Computer System and Network Architecture

As shown in FIG. **36**, an implementation of a network environment **3600** for use in providing systems, methods, and architectures described herein is shown and described. In brief overview, referring now to FIG. **36**, a block diagram of an exemplary cloud computing environment **3600** is shown and described. The cloud computing environment **3600** may include one or more resource providers **3602***a*, **3602***b*, **3602***c* (collectively, **3602**). Each resource provider **3602** may include computing resources. In some implementations, computing resources may include any hardware and/or software used to process data. For example, computing resources may include hardware and/or software capable of executing algorithms, computer programs, and/or computer applications. In some implementations, exemplary computing resources may include application servers and/or databases with storage and retrieval capabilities. Each

PSMA I&S

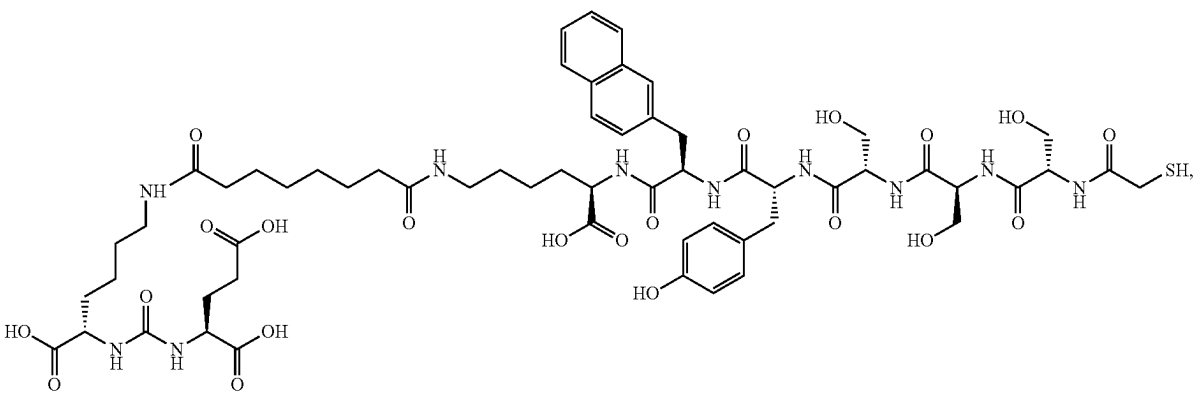

resource provider **3602** may be connected to any other resource provider **3602** in the cloud computing environment **3600**. In some implementations, the resource providers **3602** may be connected over a computer network **3608**. Each resource provider **3602** may be connected to one or more computing device **3604***a*, **3604***b*, **3604***c* (collectively, **3604**), over the computer network **3608**.

The cloud computing environment **3600** may include a resource manager **3606**. The resource manager **3606** may be connected to the resource providers **3602** and the computing devices **3604** over the computer network **3608**. In some implementations, the resource manager **3606** may facilitate the provision of computing resources by one or more resource providers **3602** to one or more computing devices **3604**. The resource manager **3606** may receive a request for a computing resource from a particular computing device **3604**. The resource manager **3606** may identify one or more resource providers **3602** capable of providing the computing resource requested by the computing device **3604**. The resource manager **3606** may select a resource provider **3602** to provide the computing resource. The resource manager **3606** may facilitate a connection between the resource provider **3602** and a particular computing device **3604**. In some implementations, the resource manager **3606** may establish a connection between a particular resource provider **3602** and a particular computing device **3604**. In some implementations, the resource manager **3606** may redirect a particular computing device **3604** to a particular resource provider **3602** with the requested computing resource.

FIG. **37** shows an example of a computing device **3700** and a mobile computing device **3750** that can be used to implement the techniques described in this disclosure. The computing device **3700** is intended to represent various forms of digital computers, such as laptops, desktops, workstations, personal digital assistants, servers, blade servers, mainframes, and other appropriate computers. The mobile computing device **3750** is intended to represent various forms of mobile devices, such as personal digital assistants, cellular telephones, smart-phones, and other similar computing devices. The components shown here, their connections and relationships, and their functions, are meant to be examples only, and are not meant to be limiting.

The computing device **3700** includes a processor **3702**, a memory **3704**, a storage device **3706**, a high-speed interface **3708** connecting to the memory **3704** and multiple high-speed expansion ports **3710**, and a low-speed interface **3712** connecting to a low-speed expansion port **3714** and the storage device **3706**. Each of the processor **3702**, the memory **3704**, the storage device **3706**, the high-speed interface **3708**, the high-speed expansion ports **3710**, and the low-speed interface **3712**, are interconnected using various busses, and may be mounted on a common motherboard or in other manners as appropriate. The processor **3702** can process instructions for execution within the computing device **3700**, including instructions stored in the memory **3704** or on the storage device **3706** to display graphical information for a GUI on an external input/output device, such as a display **3716** coupled to the high-speed interface **3708**. In other implementations, multiple processors and/or multiple buses may be used, as appropriate, along with multiple memories and types of memory. Also, multiple computing devices may be connected, with each device providing portions of the necessary operations (e.g., as a server bank, a group of blade servers, or a multi-processor system). Thus, as the term is used herein, where a plurality of functions are described as being performed by "a processor", this encompasses embodiments wherein the plurality of functions are performed by any number of processors (one or more) of any number of computing devices (one or more). Furthermore, where a function is described as being performed by "a processor", this encompasses embodiments wherein the function is performed by any number of processors (one or more) of any number of computing devices (one or more) (e.g., in a distributed computing system).

The memory **3704** stores information within the computing device **3700**. In some implementations, the memory **3704** is a volatile memory unit or units. In some implementations, the memory **3704** is a non-volatile memory unit or units. The memory **3704** may also be another form of computer-readable medium, such as a magnetic or optical disk.

The storage device **3706** is capable of providing mass storage for the computing device **3700**. In some implementations, the storage device **3706** may be or contain a computer-readable medium, such as a floppy disk device, a hard disk device, an optical disk device, or a tape device, a flash memory or other similar solid state memory device, or an array of devices, including devices in a storage area network or other configurations. Instructions can be stored in an information carrier. The instructions, when executed by one or more processing devices (for example, processor **3702**), perform one or more methods, such as those described above. The instructions can also be stored by one or more storage devices such as computer- or machine-readable mediums (for example, the memory **3704**, the storage device **3706**, or memory on the processor **3702**).

The high-speed interface **3708** manages bandwidth-intensive operations for the computing device **3700**, while the low-speed interface **3712** manages lower bandwidth-intensive operations. Such allocation of functions is an example only. In some implementations, the high-speed interface **3708** is coupled to the memory **3704**, the display **3716** (e.g., through a graphics processor or accelerator), and to the high-speed expansion ports **3710**, which may accept various expansion cards (not shown). In the implementation, the low-speed interface **3712** is coupled to the storage device **3706** and the low-speed expansion port **3714**. The low-speed expansion port **3714**, which may include various communication ports (e.g., USB, Bluetooth®, Ethernet, wireless Ethernet) may be coupled to one or more input/output devices, such as a keyboard, a pointing device, a scanner, or a networking device such as a switch or router, e.g., through a network adapter.

The computing device **3700** may be implemented in a number of different forms, as shown in the figure. For example, it may be implemented as a standard server **3720**, or multiple times in a group of such servers. In addition, it may be implemented in a personal computer such as a laptop computer **3722**. It may also be implemented as part of a rack server system **3724**. Alternatively, components from the computing device **3700** may be combined with other components in a mobile device (not shown), such as a mobile computing device **3750**. Each of such devices may contain one or more of the computing device **3700** and the mobile computing device **3750**, and an entire system may be made up of multiple computing devices communicating with each other.

The mobile computing device **3750** includes a processor **3752**, a memory **3764**, an input/output device such as a display **3754**, a communication interface **3766**, and a transceiver **3768**, among other components. The mobile computing device **3750** may also be provided with a storage device, such as a micro-drive or other device, to provide additional storage. Each of the processor **3752**, the memory **3764**, the

display **3754**, the communication interface **3766**, and the transceiver **3768**, are interconnected using various buses, and several of the components may be mounted on a common motherboard or in other manners as appropriate.

The processor **3752** can execute instructions within the mobile computing device **3750**, including instructions stored in the memory **3764**. The processor **3752** may be implemented as a chipset of chips that include separate and multiple analog and digital processors. The processor **3752** may provide, for example, for coordination of the other components of the mobile computing device **3750**, such as control of user interfaces, applications run by the mobile computing device **3750**, and wireless communication by the mobile computing device **3750**.

The processor **3752** may communicate with a user through a control interface **3758** and a display interface **3756** coupled to the display **3754**. The display **3754** may be, for example, a TFT (Thin-Film-Transistor Liquid Crystal Display) display or an OLED (Organic Light Emitting Diode) display, or other appropriate display technology. The display interface **3756** may comprise appropriate circuitry for driving the display **3754** to present graphical and other information to a user. The control interface **3758** may receive commands from a user and convert them for submission to the processor **3752**. In addition, an external interface **3762** may provide communication with the processor **3752**, so as to enable near area communication of the mobile computing device **3750** with other devices. The external interface **3762** may provide, for example, for wired communication in some implementations, or for wireless communication in other implementations, and multiple interfaces may also be used.

The memory **3764** stores information within the mobile computing device **3750**. The memory **3764** can be implemented as one or more of a computer-readable medium or media, a volatile memory unit or units, or a non-volatile memory unit or units. An expansion memory **3774** may also be provided and connected to the mobile computing device **3750** through an expansion interface **3772**, which may include, for example, a SIMM (Single In Line Memory Module) card interface. The expansion memory **3774** may provide extra storage space for the mobile computing device **3750**, or may also store applications or other information for the mobile computing device **3750**. Specifically, the expansion memory **3774** may include instructions to carry out or supplement the processes described above, and may include secure information also. Thus, for example, the expansion memory **3774** may be provide as a security module for the mobile computing device **3750**, and may be programmed with instructions that permit secure use of the mobile computing device **3750**. In addition, secure applications may be provided via the SIMM cards, along with additional information, such as placing identifying information on the SIMM card in a non-hackable manner.

The memory may include, for example, flash memory and/or NVRAM memory (non-volatile random access memory), as discussed below. In some implementations, instructions are stored in an information carrier. that the instructions, when executed by one or more processing devices (for example, processor **3752**), perform one or more methods, such as those described above. The instructions can also be stored by one or more storage devices, such as one or more computer- or machine-readable mediums (for example, the memory **3764**, the expansion memory **3774**, or memory on the processor **3752**). In some implementations, the instructions can be received in a propagated signal, for example, over the transceiver **3768** or the external interface **3762**.

The mobile computing device **3750** may communicate wirelessly through the communication interface **3766**, which may include digital signal processing circuitry where necessary. The communication interface **3766** may provide for communications under various modes or protocols, such as GSM voice calls (Global System for Mobile communications), SMS (Short Message Service), EMS (Enhanced Messaging Service), or MMS messaging (Multimedia Messaging Service), CDMA (code division multiple access), TDMA (time division multiple access), PDC (Personal Digital Cellular), WCDMA (Wideband Code Division Multiple Access), CDMA2000, or GPRS (General Packet Radio Service), among others. Such communication may occur, for example, through the transceiver **3768** using a radio-frequency. In addition, short-range communication may occur, such as using a Bluetooth®, Wi-Fi™, or other such transceiver (not shown). In addition, a GPS (Global Positioning System) receiver module **3770** may provide additional navigation- and location-related wireless data to the mobile computing device **3750**, which may be used as appropriate by applications running on the mobile computing device **3750**.

The mobile computing device **3750** may also communicate audibly using an audio codec **3760**, which may receive spoken information from a user and convert it to usable digital information. The audio codec **3760** may likewise generate audible sound for a user, such as through a speaker, e.g., in a handset of the mobile computing device **3750**. Such sound may include sound from voice telephone calls, may include recorded sound (e.g., voice messages, music files, etc.) and may also include sound generated by applications operating on the mobile computing device **3750**.

The mobile computing device **3750** may be implemented in a number of different forms, as shown in the figure. For example, it may be implemented as a cellular telephone **3780**. It may also be implemented as part of a smart-phone **3782**, personal digital assistant, or other similar mobile device.

Various implementations of the systems and techniques described here can be realized in digital electronic circuitry, integrated circuitry, specially designed ASICs (application specific integrated circuits), computer hardware, firmware, software, and/or combinations thereof. These various implementations can include implementation in one or more computer programs that are executable and/or interpretable on a programmable system including at least one programmable processor, which may be special or general purpose, coupled to receive data and instructions from, and to transmit data and instructions to, a storage system, at least one input device, and at least one output device.

These computer programs (also known as programs, software, software applications or code) include machine instructions for a programmable processor, and can be implemented in a high-level procedural and/or object-oriented programming language, and/or in assembly/machine language. As used herein, the terms machine-readable medium and computer-readable medium refer to any computer program product, apparatus and/or device (e.g., magnetic discs, optical disks, memory, Programmable Logic Devices (PLDs)) used to provide machine instructions and/or data to a programmable processor, including a machine-readable medium that receives machine instructions as a machine-readable signal. The term machine-readable signal refers to any signal used to provide machine instructions and/or data to a programmable processor.

To provide for interaction with a user, the systems and techniques described here can be implemented on a com-

puter having a display device (e.g., a CRT (cathode ray tube) or LCD (liquid crystal display) monitor) for displaying information to the user and a keyboard and a pointing device (e.g., a mouse or a trackball) by which the user can provide input to the computer. Other kinds of devices can be used to provide for interaction with a user as well; for example, feedback provided to the user can be any form of sensory feedback (e.g., visual feedback, auditory feedback, or tactile feedback); and input from the user can be received in any form, including acoustic, speech, or tactile input.

The systems and techniques described here can be implemented in a computing system that includes a back end component (e.g., as a data server), or that includes a middleware component (e.g., an application server), or that includes a front end component (e.g., a client computer having a graphical user interface or a Web browser through which a user can interact with an implementation of the systems and techniques described here), or any combination of such back end, middleware, or front end components. The components of the system can be interconnected by any form or medium of digital data communication (e.g., a communication network). Examples of communication networks include a local area network (LAN), a wide area network (WAN), and the Internet.

The computing system can include clients and servers. A client and server are generally remote from each other and typically interact through a communication network. The relationship of client and server arises by virtue of computer programs running on the respective computers and having a client-server relationship to each other.

In some implementations, the various modules described herein can be separated, combined or incorporated into single or combined modules. The modules depicted in the figures are not intended to limit the systems described herein to the software architectures shown therein.

Elements of different implementations described herein may be combined to form other implementations not specifically set forth above. Elements may be left out of the processes, computer programs, databases, etc. described herein without adversely affecting their operation. In addition, the logic flows depicted in the figures do not require the particular order shown, or sequential order, to achieve desirable results. Various separate elements may be combined into one or more individual elements to perform the functions described herein.

Throughout the description, where apparatus and systems are described as having, including, or comprising specific components, or where processes and methods are described as having, including, or comprising specific steps, it is contemplated that, additionally, there are apparatus, and systems of the present invention that consist essentially of, or consist of, the recited components, and that there are processes and methods according to the present invention that consist essentially of, or consist of, the recited processing steps.

It should be understood that the order of steps or order for performing certain action is immaterial so long as the invention remains operable. Moreover, two or more steps or actions may be conducted simultaneously.

While the invention has been particularly shown and described with reference to specific preferred embodiments, it should be understood by those skilled in the art that various changes in form and detail may be made therein without departing from the spirit and scope of the invention as defined by the appended claims.

What is claimed is:

1. A method for automatically processing 3D images to identify 3D volumes within the 3D images that correspond to a prostate of a subject and determining one or more uptake metrics indicative of radiopharmaceutical uptake therein, the method comprising:

(a) receiving, by a processor of a computing device, a 3D anatomical image of the subject obtained using an anatomical imaging modality, wherein the 3D anatomical image comprises a graphical representation of tissue within a subject, at least a portion of which corresponds to a pelvic region of the subject;

(b) receiving, by the processor, a 3D functional image of the subject obtained using a functional imaging modality, wherein the 3D functional image comprises a plurality of voxels, each representing a particular physical volume within the subject and having an intensity value that represents detected radiation emitted from the particular physical volume, wherein at least a portion of the plurality of voxels of the 3D functional image represent physical volumes within the pelvic region of the subject;

(c) determining, by the processor, using a first module, an initial volume of interest (VOI) within the 3D anatomical image, the initial VOI corresponding to tissue within the pelvic region of the subject and excluding tissue outside the pelvic region of the subject;

(d) identifying, by the processor, using a second module, a prostate volume within the initial VOI corresponding to the prostate of the subject; and

(e) determining, by the processor, the one or more uptake metrics using the 3D functional image and the prostate volume identified within the initial VOI of the 3D anatomical image, and

wherein the method comprises:

identifying, by the processor, a reference volume within the 3D anatomical image, the reference volume corresponding to a reference tissue region within the subject; and

at step (e), determining at least one of the one or more uptake metrics using the 3D functional image and the reference volume identified within the 3D anatomical image.

2. The method of claim **1**, wherein the at least one of the one or more uptake metrics determined using the 3D functional image and the reference volume comprises a tumor to background ratio (TBR) value, and wherein determining the TBR value comprises:

determining a target intensity value using intensity values of one or more voxels of the 3D functional image that correspond to the prostate volume identified within the initial VOI of the 3D anatomical image;

determining a background intensity value using intensity values of one or more voxels of the 3D functional image that correspond to the reference volume identified within the 3D anatomical image; and

determining, as the TBR value, a ratio of the target intensity value to the background intensity value.

3. The method of claim **2**, comprising determining a prostate cancer status for the subject based on the TBR value in comparison with one or more threshold values.

4. The method of claim **3**, wherein the one or more threshold values are determined using a plurality of reference TBR values, each reference TBR value associated with a particular classification prostate cancer status.

5. The method of claim **3**, wherein the one or more threshold values are determined using a receiver operating characteristic (ROC) curve.

6. The method of claim **3**, comprising determining the prostate cancer status for the subject to be (i) clinically significant if the TBR value is above a cutoff threshold or (ii) clinically non-significant if the TBR value is below the cutoff threshold.

7. The method of claim **1**, the method comprising:

identifying, by the processor, a bladder volume within the 3D anatomical image corresponding to a bladder of the subject; and

at step (e), correcting for cross-talk from the bladder using intensities of voxels of the 3D functional image corresponding to the identified bladder volume within the 3D anatomical image.

8. The method of claim **7**, wherein correcting for cross-talk from the bladder comprises:

determining one or more bladder intensity bleed functions that model a contribution of intensity originating from radiopharmaceutical within the bladder of the subject to intensity of one or more voxels of the 3D functional image corresponding to one or more regions of the 3D anatomical image that are outside of the identified bladder volume, wherein the one or more bladder intensity bleed functions model said contribution as a function of distance from the identified bladder volume; and

for each of one or more voxels of the 3D functional image corresponding to the identified prostate volume within the 3D anatomical image, adjusting an intensity of the voxel for bladder cross-talk using the one or more bladder intensity bleed functions.

9. The method of claim **1**, comprising:

identifying, by the processor, a bladder volume within the 3D anatomical image corresponding to a bladder of the subject;

determining, by the processor, a dilated bladder volume by applying a morphological dilation operation to the identified bladder volume; and

at step (e), determining the one or more uptake metrics using intensity values of voxels of the 3D functional image that (i) correspond to the prostate volume identified within the VOI of the 3D anatomical image, but (ii) do not correspond to regions of the 3D anatomical image within the dilated bladder volume.

10. The method of claim **1**, wherein the 3D functional image is a nuclear medicine image of the subject following administration to the subject of the radiopharmaceutical.

11. The method of claim **10**, wherein the radiopharmaceutical comprises a PSMA binding agent.

12. The method of claim **10**, wherein the nuclear medicine image is a single-photon emission computerized tomography (SPECT) scan of the subject obtained following administration to the subject of the radiopharmaceutical.

13. The method of claim **10**, wherein the radiopharmaceutical comprises ^{99m}Tc-MIP-1404.

14. The method of claim **1**, the method comprising:

causing, by the processor, display of an interactive graphical user interface (GUI) for presentation to the user of a visual representation of the 3D anatomical image and/or the 3D functional image; and

(g) causing, by the processor, graphical rendering of, within the GUI, the 3D anatomical image and/or the 3D functional image as selectable and superimposable layers, such that either can be selected for display and rendered separately, or both selected for display and rendered together by overlaying the 3D anatomical image with the 3D functional image.

15. The method of claim **14**, comprising causing display of, within the GUI, text and/or graphics representing the one or more uptake metrics determined in step (e) along with a quality control graphical widget for guiding the user through a quality control and reporting workflow for review and/or updating of the one or more uptake metrics.

16. The method of claim **15**, comprising:

receiving, via the quality control graphical widget, a user input corresponding to an approval of automated determination of the one or more uptake metrics; and

responsive to the receipt of the user input corresponding to the approval of the automated determination of the one or more uptake metrics, generating, by the processor, a report for the subject comprising a representation of the one or more automatically determined uptake metrics.

17. The method of claim **15**, comprising:

receiving, via the quality control graphical widget, a user input corresponding to disapproval of automated determination of the one or more uptake metrics;

responsive to receipt of the user input corresponding to the disapproval of the automated determination of the one or more uptake metrics, causing, by the processor, display of a voxel selection graphical element for user selection of one or more voxels of the 3D functional image for use in determining updated values of the one or more uptake metrics;

receiving, via the voxel selection graphical element, the user selection of one or more voxels of the 3D functional image for use in determining updated values of the one or more uptake metrics;

updating, by the processor, values of the one or more uptake metrics using the user selected voxels; and

generating, by the processor, a report for the subject comprising a representation of the one or more updated uptake metrics.

18. The method of claim **15**, comprising:

receiving, via the quality control graphical widget, a user input corresponding to disapproval of automated determination of the one or more uptake metrics;

receiving, via the quality control graphical widget, a user input corresponding to a rejection of quality control; and

generating, by the processor, a report for the subject, wherein the report comprises an identification of the rejection of quality control.

19. The method of claim **14**, wherein step (g) comprises causing graphical rendering of a selectable and superimposable segmentation layer comprising one or more identified specific tissue volumes within the 3D anatomical image, wherein upon selection of the segmentation layer for display, graphics representing the one or more specific tissue volumes are overlaid on the 3D anatomical image and/or the 3D functional image.

20. The method of claim **19**, wherein the one or more specific tissue volumes comprise(s) the identified prostate volume.

21. The method of claim **14**, the method comprising, at step (g), causing rendering of a 2D cross sectional view of the 3D anatomical image and/or the 3D functional image within an interactive 2D viewer, such that a position of the 2D cross sectional view is adjustable by the user.

22. The method of claim **14** the method comprising, at step (g), causing rendering of an interactive 3D view of the 3D anatomical image and/or the 3D functional image.

23. The method of claim **14**, comprising causing display of, within the GUI, a graphical element indicating a location corresponding to a voxel of the identified prostate volume, thereby facilitating user review and/or quality control of the method.

24. The method of claim **1**, wherein the first module receives the 3D anatomical image as input and outputs a plurality of coordinate values representing opposite corners of a rectangular volume within the 3D anatomical image.

25. The method of claim **1**, wherein step (c) comprises determining, using the first module, a 3D pelvic bone mask that identifies a volume of the 3D anatomical image corresponding to pelvic bones of the subject.

26. The method of claim **1**, wherein the first module is a Convolutional Neural Network (CNN) module.

27. The method of claim **1**, wherein step (d) comprises using the second module to identify one or more additional tissue volumes within the 3D anatomical image, each volume corresponding to a specific tissue region within the subject, wherein the one or more additional tissue volumes correspond(s) to one or more specific tissue regions selected from the group consisting of:

a pelvic bone of the subject;
a bladder of the subject;
a rectum of the subject; and
a gluteal muscle of the subject.

28. The method of claim **27**, wherein step (d) comprises using the second module to identify a set of one or more base tissue volumes, the one or more base tissue volumes comprising the identified prostate volume and the one or more additional tissue volumes, and wherein the method further comprises:

identifying, by the processor, using one or more auxiliary modules, one or more auxiliary tissue volumes within the 3D anatomical image, each auxiliary tissue volume corresponding to a base tissue volume identified by the second module; and

merging, by the processor, each auxiliary tissue volume with the corresponding base tissue volume identified by the second module.

29. The method of claim **1**, wherein step (d) comprises using the second module to classify each voxel within the initial VOI as corresponding a particular tissue region of a set of different tissue regions within the subject.

30. The method of claim **29**, wherein classifying each voxel within the initial VOI comprises:

determining, via the second module, for each of a plurality of voxels within the initial VOI, a set of likelihood values, wherein the set of likelihood values comprises, for each of one or more tissue regions of the tissue region set, a corresponding likelihood value that represents a likelihood that the voxel represents a physical volume within the tissue region; and

for each of the plurality of voxels within the initial VOI, classifying the voxel as corresponding to the particular tissue region based on the set of likelihood values determined for the voxel.

31. The method of claim **29**, wherein the second module receives as input the initial VOI and outputs a plurality of values comprising, for each voxel within the initial VOI, at least one of (i), (ii), and (iii) as follows:

a value classifying the voxel;
(ii) a set of likelihood values for the voxel; and
(iii) a value identifying the voxel as not corresponding to any of a predetermined set of different tissue regions.

32. The method of claim **29**, wherein the set of different tissue regions comprises one or more tissue regions selected from the group consisting of:

the prostate of the subject;
a pelvic bone of the subject;
a bladder of the subject;
a rectum of the subject; and
a gluteal muscle f the subject.

33. The method of claim **1**, the method comprising determining, based on at least a portion of the one or more uptake metrics, one or more diagnostic or prognostic values for the subject.

34. The method of claim **33**, wherein determining at least one of the one or more diagnostic or prognostic values comprises comparing an uptake metric to one or more threshold value(s).

35. The method of claim **33**, wherein at least one of the one or more diagnostic or prognostic values estimates a risk for clinically significant prostate cancer in the subject.

36. The method of claim **1**, wherein voxels of the 3D functional image are related to voxels of the 3D anatomical image via a known relationship.

37. The method of claim **1**, wherein the first module is a first CNN (convolutional neural network) module and the second module is a second CNN module, wherein the second CNN module comprises a greater number of convolutional filters than the first CNN module.

38. The method of claim **1**, comprising performing steps (a) and (c) for each of a plurality of 3D anatomical images to determine a plurality of initial VOIs, each within one of the plurality of 3D anatomical images, wherein a variability in sizes of the initial VOIs is less than a variability in sizes of the 3D anatomical images.

39. A system for automatically processing 3D images to identify 3D volumes within the 3D images that correspond to a prostate of a subject and determining one or more uptake metrics indicative of radiopharmaceutical uptake therein, the system comprising:

a processor; and

a memory having instructions stored thereon, wherein the instructions, when executed by the processor, cause the processor to:

(a) receive a 3D anatomical image of the subject obtained using an anatomical imaging modality, wherein the 3D anatomical image comprises a graphical representation of tissue within a subject, at least a portion of which corresponds to a pelvic region of the subject;

(b) receive a 3D functional image of the subject obtained using a functional imaging modality, wherein the 3D functional image comprises a plurality of voxels, each representing a particular physical volume within the subject and having an intensity value that represents detected radiation emitted from the particular physical volume, wherein at least a portion of the plurality of voxels of the 3D functional image represent physical volumes within the pelvic region of the subject;

(c) determine, using a first module, an initial volume of interest (VOI) within the 3D anatomical image, the initial VOI corresponding to tissue within the pelvic region of the subject and excluding tissue outside the pelvic region of the subject;

(d) identify, using a second module, a prostate volume within the initial VOI corresponding to the prostate of the subject; and

(e) determine the one or more uptake metrics using the 3D functional image and the prostate volume identified within the initial VOI of the 3D anatomical image, and wherein the instructions, when executed by the processor, cause the processor to:

identify a reference volume within the 3D anatomical image, the reference volume corresponding to a reference tissue region within the subject; and

at step (e), determine at least one of the one or more uptake metrics using the 3D functional image and the reference volume identified within the 3D anatomical image.

40. A method for automatically processing 3D images to identify 3D volumes within the 3D images that correspond to a prostate of a subject and determining one or more uptake metrics indicative of radiopharmaceutical uptake therein, the method comprising:

(a) receiving, by a processor of a computing device, a 3D anatomical image of the subject obtained using an anatomical imaging modality, wherein the 3D anatomical image comprises a graphical representation of tissue within a subject, at least a portion of which corresponds to a pelvic region of the subject;

(b) receiving, by the processor, a 3D functional image of the subject obtained using a functional imaging modality, wherein the 3D functional image comprises a plurality of voxels, each representing a particular physical volume within the subject and having an intensity value that represents detected radiation emitted from the particular physical volume, wherein at least a portion of the plurality of voxels of the 3D functional image represent physical volumes within the pelvic region of the subject;

(c) determining, by the processor, using a first module, an initial volume of interest (VOI) within the 3D anatomical image, the initial VOI corresponding to tissue within the pelvic region of the subject and excluding tissue outside the pelvic region of the subject;

(d) identifying, by the processor, using a second module, a prostate volume within the initial VOI corresponding to the prostate of the subject; and

(e) determining, by the processor, the one or more uptake metrics using the 3D functional image and the prostate volume identified within the initial VOI of the 3D anatomical image, and

wherein the method further comprises:

identifying, by the processor, a bladder volume within the 3D anatomical image corresponding to a bladder of the subject; and

at step (e), correcting for cross-talk from the bladder using intensities of voxels of the 3D functional image corresponding to the identified bladder volume within the 3D anatomical image.

41. A method for automatically processing 3D images to identify 3D volumes within the 3D images that correspond to a prostate of a subject and determining one or more uptake metrics indicative of radiopharmaceutical uptake therein, the method comprising:

(a) receiving, by a processor of a computing device, a 3D anatomical image of the subject obtained using an anatomical imaging modality, wherein the 3D anatomical image comprises a graphical representation of tissue within a subject, at least a portion of which corresponds to a pelvic region of the subject;

(b) receiving, by the processor, a 3D functional image of the subject obtained using a functional imaging modality, wherein the 3D functional image comprises a plurality of voxels, each representing a particular physical volume within the subject and having an intensity value that represents detected radiation emitted from the particular physical volume, wherein at least a portion of the plurality of voxels of the 3D functional image represent physical volumes within the pelvic region of the subject;

(c) determining, by the processor, using a first module, an initial volume of interest (VOI) within the 3D anatomical image, the initial VOI corresponding to tissue within the pelvic region of the subject and excluding tissue outside the pelvic region of the subject;

(d) identifying, by the processor, using a second module, a prostate volume within the initial VOI corresponding to the prostate of the subject; and

(e) determining, by the processor, the one or more uptake metrics using the 3D functional image and the prostate volume identified within the initial VOI of the 3D anatomical image, and

wherein the method further comprises:

identifying, by the processor, a bladder volume within the 3D anatomical image corresponding to a bladder of the subject;

determining, by the processor, a dilated bladder volume by applying a morphological dilation operation to the identified bladder volume; and

at step (e), determining the one or more uptake metrics using intensity values of voxels of the 3D functional image that (i) correspond to the prostate volume identified within the VOI of the 3D anatomical image, but (ii) do not correspond to regions of the 3D anatomical image within the dilated bladder volume.

42. A method for automatically processing 3D images to identify 3D volumes within the 3D images that correspond to a prostate of a subject and determining one or more uptake metrics indicative of radiopharmaceutical uptake therein, the method comprising:

(a) receiving, by a processor of a computing device, a 3D anatomical image of the subject obtained using an anatomical imaging modality, wherein the 3D anatomical image comprises a graphical representation of tissue within a subject, at least a portion of which corresponds to a pelvic region of the subject;

(b) receiving, by the processor, a 3D functional image of the subject obtained using a functional imaging modality, wherein the 3D functional image comprises a plurality of voxels, each representing a particular physical volume within the subject and having an intensity value that represents detected radiation emitted from the particular physical volume, wherein at least a portion of the plurality of voxels of the 3D functional image represent physical volumes within the pelvic region of the subject;

(c) determining, by the processor, using a first module, an initial volume of interest (VOI) within the 3D anatomical image, the initial VOI corresponding to tissue within the pelvic region of the subject and excluding tissue outside the pelvic region of the subject;

(d) identifying, by the processor, using a second module, a prostate volume within the initial VOI corresponding to the prostate of the subject;

(e) determining, by the processor, the one or more uptake metrics using the 3D functional image and the prostate volume identified within the initial VOI of the 3D anatomical image;

causing, by the processor, display of an interactive graphical user interface (GUI) for presentation to the user of

a visual representation of the 3D anatomical image and/or the 3D functional image; and

(g) causing, by the processor, graphical rendering of, within the GUI, the 3D anatomical image and/or the 3D functional image as selectable and superimposable layers, such that either can be selected for display and rendered separately, or both selected for display and rendered together by overlaying the 3D anatomical image with the 3D functional image.

43. A method for automatically processing 3D images to identify 3D volumes within the 3D images that correspond to a prostate of a subject and determining one or more uptake metrics indicative of radiopharmaceutical uptake therein, the method comprising:

(a) receiving, by a processor of a computing device, a 3D anatomical image of the subject obtained using an anatomical imaging modality, wherein the 3D anatomical image comprises a graphical representation of tissue within a subject, at least a portion of which corresponds to a pelvic region of the subject;

(b) receiving, by the processor, a 3D functional image of the subject obtained using a functional imaging modality, wherein the 3D functional image comprises a plurality of voxels, each representing a particular physical volume within the subject and having an intensity value that represents detected radiation emitted from the particular physical volume, wherein at least a portion of the plurality of voxels of the 3D functional image represent physical volumes within the pelvic region of the subject;

(c) determining, by the processor, using a first module, an initial volume of interest (VOI) within the 3D anatomical image, the initial VOI corresponding to tissue within the pelvic region of the subject and excluding tissue outside the pelvic region of the subject;

(d) identifying, by the processor, using a second module, a prostate volume within the initial VOI corresponding to the prostate of the subject; and

(e) determining, by the processor, the one or more uptake metrics using the 3D functional image and the prostate volume identified within the initial VOI of the 3D anatomical image;

wherein step (d) comprises using the second module to identify one or more additional tissue volumes within the 3D anatomical image, each volume corresponding to a specific tissue region within the subject, wherein the one or more additional tissue volumes correspond(s) to one or more specific tissue regions selected from the group consisting of:

a pelvic bone of the subject;

a bladder of the subject;

a rectum of the subject; and

a gluteal muscle of the subject; and

wherein the method further comprises:

identifying, by the processor, using one or more auxiliary modules, one or more auxiliary tissue volumes within the 3D anatomical image, each auxiliary tissue volume corresponding to a base tissue volume identified by the second module; and

merging, by the processor, each auxiliary tissue volume with the corresponding base tissue volume identified by the second module.

44. A method for automatically processing 3D images to identify 3D volumes within the 3D images that correspond to a prostate of a subject and determining one or more uptake metrics indicative of radiopharmaceutical uptake therein, the method comprising:

(a) receiving, by a processor of a computing device, a 3D anatomical image of the subject obtained using an anatomical imaging modality, wherein the 3D anatomical image comprises a graphical representation of tissue within a subject, at least a portion of which corresponds to a pelvic region of the subject;

(b) receiving, by the processor, a 3D functional image of the subject obtained using a functional imaging modality, wherein the 3D functional image comprises a plurality of voxels, each representing a particular physical volume within the subject and having an intensity value that represents detected radiation emitted from the particular physical volume, wherein at least a portion of the plurality of voxels of the 3D functional image represent physical volumes within the pelvic region of the subject;

(c) determining, by the processor, using a first module, an initial volume of interest (VOI) within the 3D anatomical image, the initial VOI corresponding to tissue within the pelvic region of the subject and excluding tissue outside the pelvic region of the subject;

(d) identifying, by the processor, using a second module, a prostate volume within the initial VOI corresponding to the prostate of the subject;

(e) determining, by the processor, the one or more uptake metrics using the 3D functional image and the prostate volume identified within the initial VOI of the 3D anatomical image; and

determining, by the processor, based on at least a portion of the one or more uptake metrics, one or more diagnostic or prognostic values for the subject, wherein for at least one of the one or more diagnostic or prognostic values said determining comprises comparing an uptake metric to one or more threshold value(s).

45. A method for automatically processing 3D images to identify 3D volumes within the 3D images that correspond to a prostate of a subject and determining one or more uptake metrics indicative of radiopharmaceutical uptake therein, the method comprising:

(a) receiving, by a processor of a computing device, a 3D anatomical image of the subject obtained using an anatomical imaging modality, wherein the 3D anatomical image comprises a graphical representation of tissue within a subject, at least a portion of which corresponds to a pelvic region of the subject;

(b) receiving, by the processor, a 3D functional image of the subject obtained using a functional imaging modality, wherein the 3D functional image comprises a plurality of voxels, each representing a particular physical volume within the subject and having an intensity value that represents detected radiation emitted from the particular physical volume, wherein at least a portion of the plurality of voxels of the 3D functional image represent physical volumes within the pelvic region of the subject;

(c) determining, by the processor, using a first module, an initial volume of interest (VOI) within the 3D anatomical image, the initial VOI corresponding to tissue within the pelvic region of the subject and excluding tissue outside the pelvic region of the subject;

(d) identifying, by the processor, using a second module, a prostate volume within the initial VOI corresponding to the prostate of the subject;

(e) determining, by the processor, the one or more uptake metrics using the 3D functional image and the prostate volume identified within the initial VOI of the 3D anatomical image; and

determining, by the processor, based on at least a portion of the one or more uptake metrics, one or more diagnostic or prognostic values for the subject, wherein at least one of the one or more diagnostic or prognostic values estimates a risk for clinically significant prostate cancer in the subject.

46. A method for automatically processing 3D images to identify 3D volumes within the 3D images that correspond to a prostate of a subject and determining one or more uptake metrics indicative of radiopharmaceutical uptake therein, the method comprising:

(a) receiving, by a processor of a computing device, a 3D anatomical image of the subject obtained using an anatomical imaging modality, wherein the 3D anatomical image comprises a graphical representation of tissue within a subject, at least a portion of which corresponds to a pelvic region of the subject;

(b) receiving, by the processor, a 3D functional image of the subject obtained using a functional imaging modality, wherein the 3D functional image comprises a plurality of voxels, each representing a particular physical volume within the subject and having an intensity value that represents detected radiation emitted from the particular physical volume, wherein at least a portion of the plurality of voxels of the 3D functional image represent physical volumes within the pelvic region of the subject;

(c) determining, by the processor, using a first module, an initial volume of interest (VOI) within the 3D anatomical image, the initial VOI corresponding to tissue within the pelvic region of the subject and excluding tissue outside the pelvic region of the subject;

(d) identifying, by the processor, using a second module, a prostate volume within the initial VOI corresponding to the prostate of the subject; and

(e) determining, by the processor, the one or more uptake metrics using the 3D functional image and the prostate volume identified within the initial VOI of the 3D anatomical image,

wherein the first module is a first CNN (convolutional neural network) module and the second module is a second CNN module, wherein the second CNN module comprises a greater number of convolutional filters than the first CNN module.

47. A method for automatically processing 3D images to identify 3D volumes within the 3D images that correspond to a prostate of a subject and determining one or more uptake metrics indicative of radiopharmaceutical uptake therein, the method comprising:

(a) receiving, by a processor of a computing device, a 3D anatomical image of the subject obtained using an anatomical imaging modality, wherein the 3D anatomical image comprises a graphical representation of tissue within a subject, at least a portion of which corresponds to a pelvic region of the subject;

(b) receiving, by the processor, a 3D functional image of the subject obtained using a functional imaging modality, wherein the 3D functional image comprises a plurality of voxels, each representing a particular physical volume within the subject and having an intensity value that represents detected radiation emitted from the particular physical volume, wherein at least a portion of the plurality of voxels of the 3D functional image represent physical volumes within the pelvic region of the subject;

(c) determining, by the processor, using a first module, an initial volume of interest (VOI) within the 3D anatomical image, the initial VOI corresponding to tissue within the pelvic region of the subject and excluding tissue outside the pelvic region of the subject;

(d) identifying, by the processor, using a second module, a prostate volume within the initial VOI corresponding to the prostate of the subject; and

(e) determining, by the processor, the one or more uptake metrics using the 3D functional image and the prostate volume identified within the initial VOI of the 3D anatomical image,

wherein the method comprises performing steps (a) and (c) for each of a plurality of 3D anatomical images to determine a plurality of initial VOIs, each within one of the plurality of 3D anatomical images, wherein a variability in sizes of the initial VOIs is less than a variability in sizes of the 3D anatomical images.

48. A system for automatically processing 3D images to identify 3D volumes within the 3D images that correspond to a prostate of a subject and determining one or more uptake metrics indicative of radiopharmaceutical uptake therein, the system comprising:

a processor; and

a memory having instructions stored thereon, wherein the instructions, when executed by the processor, cause the processor to:

(a) receive a 3D anatomical image of the subject obtained using an anatomical imaging modality, wherein the 3D anatomical image comprises a graphical representation of tissue within a subject, at least a portion of which corresponds to a pelvic region of the subject;

(b) receive a 3D functional image of the subject obtained using a functional imaging modality, wherein the 3D functional image comprises a plurality of voxels, each representing a particular physical volume within the subject and having an intensity value that represents detected radiation emitted from the particular physical volume, wherein at least a portion of the plurality of voxels of the 3D functional image represent physical volumes within the pelvic region of the subject;

(c) determine, using a first module, an initial volume of interest (VOI) within the 3D anatomical image, the initial VOI corresponding to tissue within the pelvic region of the subject and excluding tissue outside the pelvic region of the subject;

(d) identify, using a second module, a prostate volume within the initial VOI corresponding to the prostate of the subject; and

(e) determine the one or more uptake metrics using the 3D functional image and the prostate volume identified within the initial VOI of the 3D anatomical image, and

wherein the instructions further cause the processor to:

identify a bladder volume within the 3D anatomical image corresponding to a bladder of the subject; and

at step (e), correct for cross-talk from the bladder using intensities of voxels of the 3D functional image corresponding to the identified bladder volume within the 3D anatomical image.

49. A system for automatically processing 3D images to identify 3D volumes within the 3D images that correspond

to a prostate of a subject and determining one or more uptake metrics indicative of radiopharmaceutical uptake therein, the system comprising:

a processor; and

a memory having instructions stored thereon, wherein the instructions, when executed by the processor, cause the processor to:

(a) receive a 3D anatomical image of the subject obtained using an anatomical imaging modality, wherein the 3D anatomical image comprises a graphical representation of tissue within a subject, at least a portion of which corresponds to a pelvic region of the subject;

(b) receive a 3D functional image of the subject obtained using a functional imaging modality, wherein the 3D functional image comprises a plurality of voxels, each representing a particular physical volume within the subject and having an intensity value that represents detected radiation emitted from the particular physical volume, wherein at least a portion of the plurality of voxels of the 3D functional image represent physical volumes within the pelvic region of the subject;

(c) determine, using a first module, an initial volume of interest (VOI) within the 3D anatomical image, the initial VOI corresponding to tissue within the pelvic region of the subject and excluding tissue outside the pelvic region of the subject;

(d) identify, using a second module, a prostate volume within the initial VOI corresponding to the prostate of the subject; and

(e) determine the one or more uptake metrics using the 3D functional image and the prostate volume identified within the initial VOI of the 3D anatomical image, and

wherein the instructions further cause the processor to:

identify a bladder volume within the 3D anatomical image corresponding to a bladder of the subject;

determine a dilated bladder volume by applying a morphological dilation operation to the identified bladder volume; and

at step (e), determine the one or more uptake metrics using intensity values of voxels of the 3D functional image that (i) correspond to the prostate volume identified within the VOI of the 3D anatomical image, but (ii) do not correspond to regions of the 3D anatomical image within the dilated bladder volume.

50. A system for automatically processing 3D images to identify 3D volumes within the 3D images that correspond to a prostate of a subject and determining one or more uptake metrics indicative of radiopharmaceutical uptake therein, the system comprising:

a processor; and

a memory having instructions stored thereon, wherein the instructions, when executed by the processor, cause the processor to:

(a) receive a 3D anatomical image of the subject obtained using an anatomical imaging modality, wherein the 3D anatomical image comprises a graphical representation of tissue within a subject, at least a portion of which corresponds to a pelvic region of the subject;

(b) receive a 3D functional image of the subject obtained using a functional imaging modality, wherein the 3D functional image comprises a plurality of voxels, each representing a particular physical volume within the subject and having an intensity value that represents detected radiation emitted from the particular physical volume, wherein at least a portion of the plurality of voxels of the 3D functional image represent physical volumes within the pelvic region of the subject;

(c) determine, using a first module, an initial volume of interest (VOI) within the 3D anatomical image, the initial VOI corresponding to tissue within the pelvic region of the subject and excluding tissue outside the pelvic region of the subject;

(d) identify, using a second module, a prostate volume within the initial VOI corresponding to the prostate of the subject;

(e) determine the one or more uptake metrics using the 3D functional image and the prostate volume identified within the initial VOI of the 3D anatomical image;

cause display of an interactive graphical user interface (GUI) for presentation to the user of a visual representation of the 3D anatomical image and/or the 3D functional image; and

(g) cause graphical rendering of, within the GUI, the 3D anatomical image and/or the 3D functional image as selectable and superimposable layers, such that either can be selected for display and rendered separately, or both selected for display and rendered together by overlaying the 3D anatomical image with the 3D functional image.

51. A system for automatically processing 3D images to identify 3D volumes within the 3D images that correspond to a prostate of a subject and determining one or more uptake metrics indicative of radiopharmaceutical uptake therein, the system comprising:

a processor; and

a memory having instructions stored thereon, wherein the instructions, when executed by the processor, cause the processor to:

(a) receive a 3D anatomical image of the subject obtained using an anatomical imaging modality, wherein the 3D anatomical image comprises a graphical representation of tissue within a subject, at least a portion of which corresponds to a pelvic region of the subject;

(b) receive a 3D functional image of the subject obtained using a functional imaging modality, wherein the 3D functional image comprises a plurality of voxels, each representing a particular physical volume within the subject and having an intensity value that represents detected radiation emitted from the particular physical volume, wherein at least a portion of the plurality of voxels of the 3D functional image represent physical volumes within the pelvic region of the subject;

(c) determine, using a first module, an initial volume of interest (VOI) within the 3D anatomical image, the initial VOI corresponding to tissue within the pelvic region of the subject and excluding tissue outside the pelvic region of the subject;

(d) identify, using a second module, a prostate volume within the initial VOI corresponding to the prostate of the subject; and

(e) determine the one or more uptake metrics using the 3D functional image and the prostate volume identified within the initial VOI of the 3D anatomical image;

wherein step (d) comprises using the second module to identify one or more additional tissue volumes

within the 3D anatomical image, each volume corresponding to a specific tissue region within the subject, wherein the one or more additional tissue volumes correspond(s) to one or more specific tissue regions selected from the group consisting of:

a pelvic bone of the subject;

a bladder of the subject;

a rectum of the subject; and

a gluteal muscle of the subject; and

wherein the instructions further cause the processor to:

identify, using one or more auxiliary modules, one or more auxiliary tissue volumes within the 3D anatomical image, each auxiliary tissue volume corresponding to a base tissue volume identified by the second module; and

merge each auxiliary tissue volume with the corresponding base tissue volume identified by the second module.

52. A system for automatically processing 3D images to identify 3D volumes within the 3D images that correspond to a prostate of a subject and determining one or more uptake metrics indicative of radiopharmaceutical uptake therein, the system comprising:

a processor; and

a memory having instructions stored thereon, wherein the instructions, when executed by the processor, cause the processor to:

(a) receive a 3D anatomical image of the subject obtained using an anatomical imaging modality, wherein the 3D anatomical image comprises a graphical representation of tissue within a subject, at least a portion of which corresponds to a pelvic region of the subject;

(b) receive a 3D functional image of the subject obtained using a functional imaging modality, wherein the 3D functional image comprises a plurality of voxels, each representing a particular physical volume within the subject and having an intensity value that represents detected radiation emitted from the particular physical volume, wherein at least a portion of the plurality of voxels of the 3D functional image represent physical volumes within the pelvic region of the subject;

(c) determine, using a first module, an initial volume of interest (VOI) within the 3D anatomical image, the initial VOI corresponding to tissue within the pelvic region of the subject and excluding tissue outside the pelvic region of the subject;

(d) identify, using a second module, a prostate volume within the initial VOI corresponding to the prostate of the subject;

(e) determine the one or more uptake metrics using the 3D functional image and the prostate volume identified within the initial VOI of the 3D anatomical image; and

(f) determine, based on at least a portion of the one or more uptake metrics, one or more diagnostic or prognostic values for the subject, wherein for at least one of the one or more diagnostic or prognostic values said determining comprises comparing an uptake metric to one or more threshold value(s).

53. A system for automatically processing 3D images to identify 3D volumes within the 3D images that correspond to a prostate of a subject and determining one or more uptake metrics indicative of radiopharmaceutical uptake therein, the system comprising:

a processor; and

a memory having instructions stored thereon, wherein the instructions, when executed by the processor, cause the processor to:

(a) receive a 3D anatomical image of the subject obtained using an anatomical imaging modality, wherein the 3D anatomical image comprises a graphical representation of tissue within a subject, at least a portion of which corresponds to a pelvic region of the subject;

(b) receive a 3D functional image of the subject obtained using a functional imaging modality, wherein the 3D functional image comprises a plurality of voxels, each representing a particular physical volume within the subject and having an intensity value that represents detected radiation emitted from the particular physical volume, wherein at least a portion of the plurality of voxels of the 3D functional image represent physical volumes within the pelvic region of the subject;

(c) determine, using a first module, an initial volume of interest (VOI) within the 3D anatomical image, the initial VOI corresponding to tissue within the pelvic region of the subject and excluding tissue outside the pelvic region of the subject;

(d) identify, using a second module, a prostate volume within the initial VOI corresponding to the prostate of the subject;

(e) determine the one or more uptake metrics using the 3D functional image and the prostate volume identified within the initial VOI of the 3D anatomical image; and

(f) determine, based on at least a portion of the one or more uptake metrics, one or more diagnostic or prognostic values for the subject, wherein at least one of the one or more diagnostic or prognostic values estimates a risk for clinically significant prostate cancer in the subject.

54. A system for automatically processing 3D images to identify 3D volumes within the 3D images that correspond to a prostate of a subject and determining one or more uptake metrics indicative of radiopharmaceutical uptake therein, the system comprising:

a processor; and

a memory having instructions stored thereon, wherein the instructions, when executed by the processor, cause the processor to:

(a) receive a 3D anatomical image of the subject obtained using an anatomical imaging modality, wherein the 3D anatomical image comprises a graphical representation of tissue within a subject, at least a portion of which corresponds to a pelvic region of the subject;

(b) receive a 3D functional image of the subject obtained using a functional imaging modality, wherein the 3D functional image comprises a plurality of voxels, each representing a particular physical volume within the subject and having an intensity value that represents detected radiation emitted from the particular physical volume, wherein at least a portion of the plurality of voxels of the 3D functional image represent physical volumes within the pelvic region of the subject;

(c) determine, using a first module, an initial volume of interest (VOI) within the 3D anatomical image, the initial VOI corresponding to tissue within the pelvic region of the subject and excluding tissue outside the pelvic region of the subject;

(d) identify, using a second module, a prostate volume within the initial VOI corresponding to the prostate of the subject; and

(e) determine the one or more uptake metrics using the 3D functional image and the prostate volume identified within the initial VOI of the 3D anatomical image, wherein the first module is a first CNN (convolutional neural network) module and the second module is a second CNN module, wherein the second CNN module comprises a greater number of convolutional filters than the first CNN module.

55. A system for automatically processing 3D images to identify 3D volumes within the 3D images that correspond to a prostate of a subject and determining one or more uptake metrics indicative of radiopharmaceutical uptake therein, the system comprising:

a processor; and

a memory having instructions stored thereon, wherein the instructions, when executed by the processor, cause the processor to:

(a) receive a 3D anatomical image of the subject obtained using an anatomical imaging modality, wherein the 3D anatomical image comprises a graphical representation of tissue within a subject, at least a portion of which corresponds to a pelvic region of the subject;

(b) receive a 3D functional image of the subject obtained using a functional imaging modality, wherein the 3D functional image comprises a plurality of voxels, each representing a particular physical volume within the subject and having an intensity value that represents detected radiation emitted from the particular physical volume, wherein at least a portion of the plurality of voxels of the 3D functional image represent physical volumes within the pelvic region of the subject;

(c) determine, using a first module, an initial volume of interest (VOI) within the 3D anatomical image, the initial VOI corresponding to tissue within the pelvic region of the subject and excluding tissue outside the pelvic region of the subject;

(d) identify, using a second module, a prostate volume within the initial VOI corresponding to the prostate of the subject; and

(e) determine the one or more uptake metrics using the 3D functional image and the prostate volume identified within the initial VOI of the 3D anatomical image, wherein the instructions cause the processor to perform steps (a) and (c) for each of a plurality of 3D anatomical images to determine a plurality of initial VOIs, each within one of the plurality of 3D anatomical images, wherein a variability in sizes of the initial VOIs is less than a variability in sizes of the 3D anatomical images.

* * * * *

JS 44 (Rev. 10/20)

CIVIL COVER SHEET

The JS 44 civil cover sheet and the information contained herein neither replace nor supplement the filing and service of pleadings or other papers as required by law, except as provided by local rules of court. This form, approved by the Judicial Conference of the United States in September 1974, is required for the use of the Clerk of Court for the purpose of initiating the civil docket sheet. *(SEE INSTRUCTIONS ON NEXT PAGE OF THIS FORM.)*

I. (a) PLAINTIFFS

Progenics Pharmaceuticals, Inc. and EXINI Diagnostics AB

(b) County of Residence of First Listed Plaintiff Middlesex, MA
(EXCEPT IN U.S. PLAINTIFF CASES)

(c) Attorneys *(Firm Name, Address, and Telephone Number)*

Choate Hall & Stewart LLP, 2 Int'l Pl, Boston MA 02110, 617-248-5000

DEFENDANTS

MIM Software Inc.

County of Residence of First Listed Defendant Cuyahoga, OH
(IN U.S. PLAINTIFF CASES ONLY)

NOTE: IN LAND CONDEMNATION CASES, USE THE LOCATION OF THE TRACT OF LAND INVOLVED.

Attorneys *(If Known)*

II. BASIS OF JURISDICTION *(Place an "X" in One Box Only)*

- [ ] 1 U.S. Government Plaintiff
- [x] 3 Federal Question *(U.S. Government Not a Party)*
- [ ] 2 U.S. Government Defendant
- [ ] 4 Diversity *(Indicate Citizenship of Parties in Item III)*

III. CITIZENSHIP OF PRINCIPAL PARTIES *(Place an "X" in One Box for Plaintiff and One Box for Defendant) (For Diversity Cases Only)*

	PTF	DEF		PTF	DEF
Citizen of This State	[ ] 1	[ ] 1	Incorporated *or* Principal Place of Business In This State	[ ] 4	[ ] 4
Citizen of Another State	[ ] 2	[ ] 2	Incorporated *and* Principal Place of Business In Another State	[ ] 5	[ ] 5
Citizen or Subject of a Foreign Country	[ ] 3	[ ] 3	Foreign Nation	[ ] 6	[ ] 6

IV. NATURE OF SUIT *(Place an "X" in One Box Only)* Click here for: Nature of Suit Code Descriptions.

CONTRACT
- [ ] 110 Insurance
- [ ] 120 Marine
- [ ] 130 Miller Act
- [ ] 140 Negotiable Instrument
- [ ] 150 Recovery of Overpayment & Enforcement of Judgment
- [ ] 151 Medicare Act
- [ ] 152 Recovery of Defaulted Student Loans (Excludes Veterans)
- [ ] 153 Recovery of Overpayment of Veteran's Benefits
- [ ] 160 Stockholders' Suits
- [ ] 190 Other Contract
- [ ] 195 Contract Product Liability
- [ ] 196 Franchise

REAL PROPERTY
- [ ] 210 Land Condemnation
- [ ] 220 Foreclosure
- [ ] 230 Rent Lease & Ejectment
- [ ] 240 Torts to Land
- [ ] 245 Tort Product Liability
- [ ] 290 All Other Real Property

TORTS

PERSONAL INJURY
- [ ] 310 Airplane
- [ ] 315 Airplane Product Liability
- [ ] 320 Assault, Libel & Slander
- [ ] 330 Federal Employers' Liability
- [ ] 340 Marine
- [ ] 345 Marine Product Liability
- [ ] 350 Motor Vehicle
- [ ] 355 Motor Vehicle Product Liability
- [ ] 360 Other Personal Injury
- [ ] 362 Personal Injury - Medical Malpractice

PERSONAL INJURY
- [ ] 365 Personal Injury - Product Liability
- [ ] 367 Health Care/ Pharmaceutical Personal Injury Product Liability
- [ ] 368 Asbestos Personal Injury Product Liability

PERSONAL PROPERTY
- [ ] 370 Other Fraud
- [ ] 371 Truth in Lending
- [ ] 380 Other Personal Property Damage
- [ ] 385 Property Damage Product Liability

CIVIL RIGHTS
- [ ] 440 Other Civil Rights
- [ ] 441 Voting
- [ ] 442 Employment
- [ ] 443 Housing/ Accommodations
- [ ] 445 Amer. w/Disabilities - Employment
- [ ] 446 Amer. w/Disabilities - Other
- [ ] 448 Education

PRISONER PETITIONS

Habeas Corpus:
- [ ] 463 Alien Detainee
- [ ] 510 Motions to Vacate Sentence
- [ ] 530 General
- [ ] 535 Death Penalty

Other:
- [ ] 540 Mandamus & Other
- [ ] 550 Civil Rights
- [ ] 555 Prison Condition
- [ ] 560 Civil Detainee - Conditions of Confinement

FORFEITURE/PENALTY
- [ ] 625 Drug Related Seizure of Property 21 USC 881
- [ ] 690 Other

LABOR
- [ ] 710 Fair Labor Standards Act
- [ ] 720 Labor/Management Relations
- [ ] 740 Railway Labor Act
- [ ] 751 Family and Medical Leave Act
- [ ] 790 Other Labor Litigation
- [ ] 791 Employee Retirement Income Security Act

IMMIGRATION
- [ ] 462 Naturalization Application
- [ ] 465 Other Immigration Actions

BANKRUPTCY
- [ ] 422 Appeal 28 USC 158
- [ ] 423 Withdrawal 28 USC 157

PROPERTY RIGHTS
- [ ] 820 Copyrights
- [x] 830 Patent
- [ ] 835 Patent - Abbreviated New Drug Application
- [ ] 840 Trademark
- [ ] 880 Defend Trade Secrets Act of 2016

SOCIAL SECURITY
- [ ] 861 HIA (1395ff)
- [ ] 862 Black Lung (923)
- [ ] 863 DIWC/DIWW (405(g))
- [ ] 864 SSID Title XVI
- [ ] 865 RSI (405(g))

FEDERAL TAX SUITS
- [ ] 870 Taxes (U.S. Plaintiff or Defendant)
- [ ] 871 IRS—Third Party 26 USC 7609

OTHER STATUTES
- [ ] 375 False Claims Act
- [ ] 376 Qui Tam (31 USC 3729(a))
- [ ] 400 State Reapportionment
- [ ] 410 Antitrust
- [ ] 430 Banks and Banking
- [ ] 450 Commerce
- [ ] 460 Deportation
- [ ] 470 Racketeer Influenced and Corrupt Organizations
- [ ] 480 Consumer Credit (15 USC 1681 or 1692)
- [ ] 485 Telephone Consumer Protection Act
- [ ] 490 Cable/Sat TV
- [ ] 850 Securities/Commodities/ Exchange
- [ ] 890 Other Statutory Actions
- [ ] 891 Agricultural Acts
- [ ] 893 Environmental Matters
- [ ] 895 Freedom of Information Act
- [ ] 896 Arbitration
- [ ] 899 Administrative Procedure Act/Review or Appeal of Agency Decision
- [ ] 950 Constitutionality of State Statutes

V. ORIGIN *(Place an "X" in One Box Only)*

- [x] 1 Original Proceeding
- [ ] 2 Removed from State Court
- [ ] 3 Remanded from Appellate Court
- [ ] 4 Reinstated or Reopened
- [ ] 5 Transferred from Another District *(specify)*
- [ ] 6 Multidistrict Litigation - Transfer
- [ ] 8 Multidistrict Litigation - Direct File

VI. CAUSE OF ACTION

Cite the U.S. Civil Statute under which you are filing *(Do not cite jurisdictional statutes unless diversity)*:
35 U.S.C. § 100, et seq., § 271, § 283, § 284, § 285.

Brief description of cause:
Action for patent infringement

VII. REQUESTED IN COMPLAINT:

[ ] CHECK IF THIS IS A CLASS ACTION UNDER RULE 23, F.R.Cv.P.

DEMAND $

CHECK YES only if demanded in complaint:
JURY DEMAND: [6] Yes [ ] No

VIII. RELATED CASE(S) IF ANY *(See instructions)*:

JUDGE _____ DOCKET NUMBER _____

DATE 02/23/2024

SIGNATURE OF ATTORNEY OF RECORD /s/ Michael Bunis

FOR OFFICE USE ONLY

RECEIPT # _____ AMOUNT _____ APPLYING IFP _____ JUDGE _____ MAG. JUDGE _____

UNITED STATES DISTRICT COURT
DISTRICT OF MASSACHUSETTS

1. Title of case (name of first party on each side only) Progenics Pharmaceuticals, Inc. v. MIM Software Inc.

2. Category in which the case belongs based upon the numbered nature of suit code listed on the civil cover sheet. (See local rule 40.1(a)(1)).

☑ I. 160, 400, 410, 441, 535, 830*, 835*, 850, 880, 891, 893, R.23, REGARDLESS OF NATURE OF SUIT.

☐ II. 110, 130, 190, 196, 370, 375, 376, 440, 442, 443, 445, 446, 448, 470, 751, 820*, 840*, 895, 896, 899.

☐ III. 120, 140, 150, 151, 152, 153, 195, 210, 220, 230, 240, 245, 290, 310, 315, 320, 330, 340, 345, 350, 355, 360, 362, 365, 367, 368, 371, 380, 385, 422, 423, 430, 450, 460, 462, 463, 465, 480, 485, 490, 510, 530, 540, 550, 555, 560, 625, 690, 710, 720, 740, 790, 791, 861-865, 870, 871, 890, 950.
*Also complete AO 120 or AO 121. for patent, trademark or copyright cases.

3. Title and number, if any, of related cases. (See local rule 40.1(g)). If more than one prior related case has been filed in this district please indicate the title and number of the first filed case in this court.

N/A

4. Has a prior action between the same parties and based on the same claim ever been filed in this court?

YES ☐ NO ☑

5. Does the complaint in this case question the constitutionality of an act of congress affecting the public interest? (See 28 USC §2403)

YES ☐ NO ☑

If so, is the U.S.A. or an officer, agent or employee of the U.S. a party?

YES ☐ NO ☐

6. Is this case required to be heard and determined by a district court of three judges pursuant to title 28 USC §2284?

YES ☐ NO ☑

7. Do all of the parties in this action, excluding governmental agencies of the United States and the Commonwealth of Massachusetts ("governmental agencies"), residing in Massachusetts reside in the same division? - (See Local Rule 40.1(d)).

YES ☑ NO ☐

A. If yes, in which division do all of the non-governmental parties reside?

Eastern Division ☑ Central Division ☐ Western Division ☐

B. If no, in which division do the majority of the plaintiffs or the only parties, excluding governmental agencies, residing in Massachusetts reside?

Eastern Division ☐ Central Division ☐ Western Division ☐

8. If filing a Notice of Removal - are there any motions pending in the state court requiring the attention of this Court? (If yes, submit a separate sheet identifying the motions)

YES ☐ NO ☐

(PLEASE TYPE OR PRINT)

ATTORNEY'S NAME Michael Bunis

ADDRESS Choate, Hall & Stewart LLP, 2 International Place, Boston, MA 02110

TELEPHONE NO. 617-248-4030

(CategoryForm11-2020.wpd)